

Higher order QED corrections in Z physics

S.C. van der Marck

Higher order QED corrections in Z physics

De plechtigheid zal plaats vinden in het Groot
Auditorium van het Academiegebouw,
Rapenburg 73, Leiden.

Receptie na afloop van de promotie in het
Academiegebouw.

N.B. Met tijdrovende parkeerproblemen bij het
Academiegebouw moet rekening worden
gehouden.

Higher order QED corrections in Z physics

Proefschrift

ter verkrijging van de graad van Doctor aan de
Rijksuniversiteit te Leiden, op gezag van de Rec-
tor Magnificus Dr. L. Leertouwer, hoogleraar in
de faculteit der godgeleerdheid, volgens besluit
van het college van dekanen te verdedigen op
woensdag 24 april 1991 te klokke 14.15 uur

door

Steven Cees van der Marck

geboren te Roermond in 1964

Promotiecommissie:

Promotor: prof.dr. F.A. Berends

Referent: dr. W.L. van Neerven

Overige leden: prof.dr. P. Duinker

prof.dr. C.J.N. van den Meijdenberg

prof.dr. R.H. Terwiel

Contents

1	Motivation and outline	1
2	The Z line shape	4
2.1	Introduction	4
2.2	Total cross section with non-photonic corrections	5
2.2.1	Input parameters and $\sin^2 \vartheta_W$	5
2.2.2	Lowest order widths and cross sections	6
2.2.3	The corrected partial and total widths	8
2.2.4	Total cross section with electroweak corrections	10
2.2.5	Approximate expressions	12
2.3	The photonic or QED corrections	14
2.3.1	The relevance of various QED contributions	14
2.3.2	Initial state photon radiation	15
2.3.3	Final state photon radiation	17
2.3.4	Numerical results	18
2.3.5	Approximate analytical results	21
3	Large angle Bhabha scattering	26
3.1	Introduction	26
3.2	The structure function method and a simple toy model	28
3.3	Incorporating cuts in the LL calculation	34
3.4	Incorporating an acollinearity cut	40
3.5	The non-log terms for the initial state	42
3.6	The non-log terms for the final state	47
3.7	Bhabha scattering	49
3.8	Results and discussion	56
3.A	The first order virtual and soft QED corrections	64
4	The forward backward asymmetry	68
5	Small angle Bhabha scattering	76
5.1	Introduction	76
5.2	Numerical results	79

5.3	Analytical formulae	83
5.4	Conclusions	86
6	Two photon bremsstrahlung	89
6.1	Introduction	89
6.2	Matrix elements	91
6.3	Generating events	101
6.4	Numerical results	106
6.5	Conclusions	110
6.A	Spinor techniques	110
6.B	Collinear factors	113
6.C	The approximate total cross sections	114
7	Event generator techniques	119
7.1	Introduction	119
7.2	Fixed order Monte Carlos and the k_0 -problem	120
7.3	YFS exponentiation	122
7.3.1	Introduction	122
7.3.2	The distribution that has to be generated	122
7.3.3	Generating the 0-th order exponentiated distribution	126
7.3.4	The IR finite QED corrections	129
7.4	The structure function based approach	131
7.5	Advantages and drawbacks	134
	Samenvatting	137
	Curriculum vitae	140
	List of publications	141

*„Alle Wahrheit ist einfach“ – Ist das nicht zwiefach eine Lüge? –
F.W. Nietzsche*

Chapter 1

Motivation and outline

In recent years one of the main topics of high energy physics has been the study of the properties of the Z boson, called Z physics. The obvious reason for this is the fact that in 1989 SLC at Stanford, USA and LEP at Geneva, Switzerland began operating. Both these e^+e^- accelerators can run at energies around 91 GeV, where a Z boson can be produced almost at rest in the laboratory frame. The cross section for this production has a sharp resonance peak at this energy. Although the Z itself decays before it can be detected, the properties of the Z can be studied in great detail with LEP and SLC, by examining the decay products. It is for the first time that any of the bosons associated with the weak interaction can be studied with high accuracy. Already it has led to more precise measurements of some of the standard model parameters (notably M_Z , the mass of the Z) and to a high precision test of the standard model in comparing its predictions with measurements (e.g. Γ_Z , the width of the Z).

It is clear that one wants to compare theory with experiment at a level of precision that is given by the highest precision the experiments can reach. In order to achieve this one has to evaluate the theoretical predictions for measurable quantities with at least the experimental accuracy. Before LEP and SLC began running there were e^+e^- accelerators operating at lower energies. For the measurements at those accelerators it sufficed to evaluate the theoretical predictions perturbatively up to first order in the fine structure constant α , which at those energies had an estimated precision of a few percent. There are two main reasons why the same evaluations applied to LEP/SLC are less precise. Combined with the slightly higher statistics expected for LEP, compared to previous e^+e^- machines, this implies that due to the advent of accelerators like LEP and SLC the evaluations of the theoretical predictions had to be improved upon.

The first reason why the aforementioned evaluations at lower energies become less precise at LEP/SLC energies is that in the latter case the loop corrections due to the weak interaction start to play an important rôle, since the typical weak interaction energy scale has been reached. While previously these corrections could be neglected, they now have to be calculated in first order. The second reason is that the first order corrections due to quantum electrodynamics (QED) are larger at LEP/SLC than at e.g. PETRA. This is illustrated in fig. 1.1, where the total cross section for $e^+e^- \rightarrow \mu^+\mu^-$ is shown.

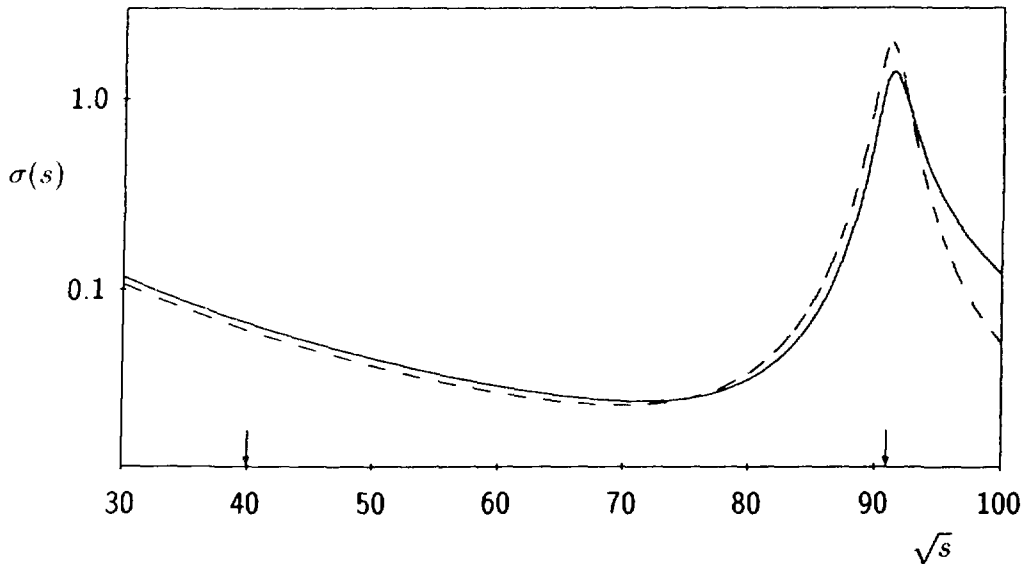


Fig. 1.1. The total cross section for muon pair production. The dashed curve corresponds to the Born result, whereas the solid curve shows the first order QED corrected result. The arrows indicate roughly the positions of PETRA (left) and LEP (right). The cross section is given in nanobarn, the energy in GeV. A cut on the invariant mass squared (s') of the muon pair of $0.2s$ was applied.

The lowest order cross section and the first order QED corrected cross section are plotted over a range of energies that includes both PETRA and LEP/SLC. The first order QED correction at PETRA is about +10%, whereas at the Z resonance it is roughly -35%. The implication of this is that one has to take higher order QED corrections into account at LEP/SLC, since the first order correction is -35% and the precision aimed for is below 1%.

The weak corrections have been calculated analytically by a number of groups, all agreeing on the results, a review of which is given in [1]. The reason that these calculations can be done analytically is that the weak corrections are loop corrections only, i.e. there is no contribution from the production of an extra final state particle. Hence the kinematics of the process under consideration are not changed, in contrast to QED corrections, where a part of the correction is given by the emission of one or more photons. The influence of this so-called bremsstrahlung on the kinematics is very complicated. One has to integrate over all situations where the extra photons remain undetected. These phase space integrations for the QED corrections are in general very difficult to perform analytically. Moreover the kinematics will be different for every experiment. Thus one has to resort to numerical integration for the QED corrections.

In the literature two approaches to the problem of calculating QED corrections are in use. One way is to calculate as many steps (integrations) analytically as is possible and to do the rest numerically. This is known as the semi-analytical method. In most cases only

the last integration is done numerically. A large part of this thesis, up to and including chapter 5, deals with this approach. The other approach is to calculate all integrations numerically. Since this involves multi-dimensional integration this is usually done using Monte Carlo techniques. The last part of this thesis is devoted to these methods.

In this thesis a number of calculations of higher order QED corrections are presented. The calculations all apply to the standard LEP/SLC processes

$$e^+ e^- \longrightarrow \bar{f} f,$$

where f stands for any fermion. Perhaps the most typical cases are the ones where $f \neq e^-, \nu_e$. In such cases the above process is only possible via annihilation of the incoming e^+e^- pair. At LEP/SLC this mainly occurs via the production and the subsequent decay of a Z boson, i.e. the cross section is heavily dominated by the Z resonance. These processes and the corrections to them, treated in the semi-analytical way, are discussed in chapter 2. The case $f = e^-$ ('Bhabha scattering') is a more difficult one, because that process can also occur via the exchange of a virtual photon in the t-channel. In fact the latter contribution is dominant at small scattering angles. Therefore one has to exclude the lower scattering angles if one is interested in Z physics. Having excluded that region one has to recalculate all QED corrections, which is done in chapter 3. The techniques introduced there enable us to calculate the difference between forward and backward scattering, the forward-backward asymmetry, for the cases $f \neq e^-, \nu_e$, which is the subject of chapter 4. In chapter 5 we return to the case $f = e^-$. At small scattering angles, where Bhabha scattering is dominated by photon exchange in the t-channel, this process is used in experiments to determine the luminosity of the e^+e^- accelerator. Hence an accurate theoretical description of this process at small angles is of vital interest to the overall normalization of all measurements at LEP/SLC. Chapter 5 gives such a description in a semi-analytical way. The last two chapters discuss Monte Carlo techniques that are used for the cases $f \neq e^-, \nu_e$. Chapter 6 describes the simulation of two photon bremsstrahlung, which is a second order QED correction effect. The results are compared with results of the semi-analytical treatment in chapter 2. Finally chapter 7 reviews several techniques that have been used to simulate higher order QED corrections for the cases $f \neq e^-, \nu_e$.

Several authors have contributed to the field of higher order QED calculations. Many contributions are reviewed in [1]. Throughout this thesis the results will be compared with other theoretical evaluations wherever possible.

Reference

- [1] "Z Physics at LEP 1", CERN 89-08, 3 volumes,
eds. G. Altarelli, R. Kleiss and C. Verzegnassi.

Chapter 2

The Z line shape

2.1 Introduction

The purpose of this chapter is to review the evaluation of the Z line shape. The aim is to obtain a theoretical accuracy of about 10 MeV in the position and width of the peak. Moreover the normalization for the prediction of the total cross section should be accurate within 0.3%.

For the total cross sections we are interested in the following channels

$$e^+e^- \longrightarrow f\bar{f}, \quad f \neq e^-, \nu_e. \quad (2.1.1)$$

From the measurement of these total cross sections information on the Z mass and on the partial and total widths of the Z should be obtained. The neutrino pair production cross section is indirectly measured in the neutrino counting experiment. Moreover, it is the simplest channel and as such a good illustration for the corrections. We focus on total cross sections. We assume that the experiments can make corrections like for acceptance such that the total cross section can be obtained. The question of the influence of cuts on the total cross sections should be answered by Monte Carlo studies. On the other hand the results presented in this chapter can serve as a particular test case for the event generators.

For the calculations in the Standard Model we use the on-shell (OS) renormalization scheme. The results depend on the following parameters: M_Z, m_{top}, M_H and α_s . The lepton masses are known experimentally. The quark masses represent a suitable parametrization of the dispersion relation results for the hadronic vacuum polarization. The values used in this thesis are (in GeV)

$$m_u = m_d = 0.041, \quad m_c = 1.5, \quad m_s = 0.15, \quad m_b = 4.5. \quad (2.1.2)$$

In the calculations we also need M_W , which is calculated from the input parameter G_μ , the muon decay constant, through the quantity Δr .

In this chapter we consider three main topics:

- A. Total cross section with non-photonic (electroweak) corrections.
- B. Inclusion of photonic (QED) corrections.
- C. Approximate analytic formulae, applicable to topics A and B.

Topic A is treated in section 2.2, together with the part of topic C that applies to it. In several subsections the following points will be discussed: the lowest order predictions and some qualitative features; total and partial widths of the Z; total cross sections including vertex, self energy, γZ mixing corrections and finally simple parametrizations of the electroweak corrected cross sections. In section 2.3 the various possible QED corrections are discussed. After that the most important one, i.e. initial state photon radiation, is considered. A short comment on the inclusion of final state radiation is made and numerical results are presented. Finally approximate analytical results are obtained.

It should be stressed that almost all the calculations presented in this chapter have been done by several groups and that agreement exists between the different computer programs [1]. Here we present one of these calculations.

2.2 Total cross section with non-photonic corrections

2.2.1 Input parameters and $\sin^2 \vartheta_W$

As mentioned in section 2.1 the input parameters in the actual calculations are M_Z, m_{top}, M_H and α_s . From the muon decay constant G_μ or from

$$A = \frac{\pi\alpha}{\sqrt{2} G_\mu} = (37.281 \text{ GeV})^2 \quad (2.2.1)$$

one determines M_W . In lowest order the relation reads

$$M_W^2 \sin^2 \vartheta_W = A. \quad (2.2.2)$$

Here we have introduced the quantity $\sin^2 \vartheta_W$, which in the on-shell renormalization scheme [2] is given to all orders by

$$\sin^2 \vartheta_W = 1 - \frac{M_W^2}{M_Z^2}. \quad (2.2.3)$$

Inserting this relation in eq.(2.2.2) yields an equation that is quadratic in $\sin^2 \vartheta_W$. Both roots of this equation lie in $[0, 1]$ and are therefore acceptable. One has to compare theory and experiment for another quantity, in order to decide between the two possibilities. For instance the scattering process

$$\nu_\mu + e^- \rightarrow \nu_\mu + e^- \quad (2.2.4)$$

is a candidate for such a comparison [3]. This singles out the root

$$\sin^2 \vartheta_W = \frac{1}{2} - \frac{1}{2} \sqrt{1 - \frac{4A}{M_Z^2}}, \quad (2.2.5)$$

which expresses $\sin^2 \vartheta_W$ in terms of the input parameters of the theory. From this equation the sign of $\sin \vartheta_W$ is still not determined. However this sign is irrelevant.

The inclusion of electroweak radiative corrections in muon decay modifies eq.(2.2.2) to

$$M_W^2 \sin^2 \vartheta_W = \frac{A}{1 - \Delta r}. \quad (2.2.6)$$

The quantity Δr and its dependence on the parameters of the theory have been discussed many times. A review is given in [4]. Here it suffices to say that Δr also depends on $\sin^2 \vartheta_W$. Since this dependence is non-trivial it is not feasible any more to solve eq.(2.2.6) for $\sin^2 \vartheta_W$ analytically. Therefore one usually writes

$$\sin^2 \vartheta_W = \frac{1}{2} - \frac{1}{2} \sqrt{1 - \frac{4A}{M_Z^2} \frac{1}{1 - \Delta r}} \quad (2.2.7)$$

and solves this equation iteratively for $\sin^2 \vartheta_W$.

The leading higher order effects due to a large top mass are not included in any of the calculations presented here, since these calculations are based on [5]. The leading m_t effects can be incorporated using ref. [6]. These effects are only noticeable for $m_t > 150$ GeV, and are small even then.

2.2.2 Lowest order widths and cross sections

In lowest order the partial width of a Z decaying into a fermion pair is given by

$$\Gamma_{Z \rightarrow ff}^{(0)} = \frac{\alpha}{6} N_c M_Z \left(1 - \frac{4m_f^2}{M_Z^2}\right)^{1/2} \left((g_f^-)^2 + (g_f^+)^2 + \frac{m_f^2}{M_Z^2} (6g_f^- g_f^+ - (g_f^-)^2 - (g_f^+)^2) \right), \quad (2.2.8)$$

with

$$\begin{aligned} g_f^- &= (I_f^3 - Q_f \sin^2 \vartheta_W) / (\sin \vartheta_W \cos \vartheta_W) \\ g_f^+ &= -Q_f \sin^2 \vartheta_W / (\sin \vartheta_W \cos \vartheta_W) \end{aligned} \quad (2.2.9)$$

and N_c representing the number of colors.

Making use of the tree level relation (2.2.2) and eqs.(2.2.1),(2.2.3) the lowest order width can also be written in terms of G_μ

$$\Gamma_{Z \rightarrow ff}^{(0)} = N_c \frac{G_\mu M_Z^3}{24\pi\sqrt{2}} \left(1 - \frac{4m_f^2}{M_Z^2}\right)^{1/2} \left(1 - \frac{4m_f^2}{M_Z^2} + (2I_f^3 - 4Q_f s_W^2)^2 \left(1 + \frac{2m_f^2}{M_Z^2}\right)\right). \quad (2.2.10)$$

At tree level, when $\sin^2 \vartheta_W$ and hence M_W are determined using eq.(2.2.5), this representation gives the same results as eq.(2.2.8). In higher order however, determining $\sin^2 \vartheta_W$ with eq.(2.2.7), the results from the two representations differ. We shall come back to these two representations later on.

The total width is given by

$$\Gamma_Z^{(0)} = \sum_f \Gamma_{Z \rightarrow \bar{f}f}^{(0)}. \quad (2.2.11)$$

It should be noted that in the massless fermion case the partial width (2.2.8) reduces to

$$\Gamma_{Z \rightarrow \bar{f}f}^{(0)} = \Gamma_- + \Gamma_+ = \frac{\alpha}{6} N_c M_Z \left(|g_f^-|^2 + |g_f^+|^2 \right) \quad (2.2.12)$$

where the $-$, $+$ sign refers to the helicity of f , the helicity of \bar{f} being opposite.

The total cross section in lowest order for reaction (2.1.1) with massless fermions reads

$$\sigma_0(s) = \frac{4\pi\alpha^2}{3s} \frac{N_c s^2}{4} \sum_{\lambda_e, \lambda_f = -1, 1} \left| \frac{g_e^{\lambda_e} g_f^{\lambda_f}}{s - M_Z^2 + iM_Z \Gamma_Z} + \frac{Q_e Q_f}{s} \right|^2. \quad (2.2.13)$$

The λ_e, λ_f term in the cross section corresponds to the helicity combination $-\lambda_e, \lambda_e, -\lambda_f, \lambda_f$ for e^+, e^-, \bar{f} and f . It is clear that in the neutrino case only the $\lambda_\nu = -1$ terms contribute. For Γ_Z we take in lowest order $\Gamma_Z^{(0)}$ from eq.(2.2.11). Using the definition (2.2.12) for decay widths into specific helicity states we can rewrite the total cross section in terms of widths and partial widths:

$$\sigma_0(s) = \frac{N_c s}{48\pi} \sum_{\lambda_e, \lambda_f = -1, 1} \left| \frac{R_{\lambda_e \lambda_f}}{s - M_Z^2 + iM_Z \Gamma_Z} + \frac{Q_e Q_f e^2}{s} \right|^2, \quad (2.2.14)$$

where

$$R_{\lambda_e \lambda_f} = \pm \lambda_e \lambda_f \frac{24\pi \Gamma_{\lambda_e}^{\frac{1}{2}} \Gamma_{\lambda_f}^{\frac{1}{2}}}{N_c^{\frac{1}{2}} M_Z}. \quad (2.2.15)$$

Here the \pm sign corresponds to $J_f^3 = \mp \frac{1}{2}$ of the final state. The partial and total widths are the lowest order expressions of eqs.(2.2.8) and (2.2.11). Carrying out the summations one finds

$$\sigma_0(s) = \frac{1}{(1 - M_Z^2/s)^2 + M_Z^2 \Gamma_Z^2/s^2} \left[\frac{C_R}{s} + \frac{C_I}{s} \left(1 - \frac{M_Z^2}{s} \right) \right] + \frac{C_Q}{s}, \quad (2.2.16)$$

with

$$\begin{aligned} C_R &= \frac{12\pi \Gamma_e \Gamma_f}{M_Z^2}, \\ C_I &= \mp \frac{4\pi Q_f \alpha (M_Z^2)}{M_Z} \left(\Gamma_+^{\frac{1}{2}}(e) - \Gamma_-^{\frac{1}{2}}(e) \right) \left(\Gamma_+^{\frac{1}{2}}(f) - \Gamma_-^{\frac{1}{2}}(f) \right) N_c^{1/2}, \\ C_Q &= \frac{4\pi\alpha^2}{3} Q_f^2 N_c. \end{aligned} \quad (2.2.17)$$

The first term in eq.(2.2.16) is the Breit-Wigner form for a spin 1 resonance, the last term is the pure QED cross section. The constant C_I in front of the interference term is positive for realistic $\sin^2 \vartheta_W$ values and is smallest for muon pair production.

The representation (2.2.16) for the total cross section is introduced for two reasons. Firstly the parameters have a direct physical meaning and secondly it will lead to a good approximative formula for the electroweak corrected expression. At the moment all the widths are still lowest order expressions.

At this point some qualitative features of eq.(2.2.16) may be noticed. Considering M_Z , Γ_Z , C_R , C_I and C_Q as parameters, the peak height (σ_{max}) and the positions of the maximum ($\sqrt{s_{max}}$) and the half maxima ($\sqrt{s_{\pm}}$) can be obtained by considering $\sigma_0(s)$ in a small region around $s = M_Z^2$. In the calculation one can expand in parameter combinations

$$\gamma = \Gamma_Z/M_Z, \quad (2.2.18)$$

and C_I/C_R and $\gamma^2 C_Q/C_R$, all of which are small. The higher order terms in these combinations can be neglected. The results are

$$\sigma_{max} = \frac{C_R}{\Gamma_Z^2} \left[1 + \frac{1}{4}\gamma^2 + \gamma^2(1 - \gamma^2)\frac{C_Q}{C_R} \right], \quad (2.2.19)$$

$$\sqrt{s_{max}} = M_Z \left[1 + \frac{1}{4}\gamma^2 + \frac{1}{4}\gamma^2\frac{C_I}{C_R} - \frac{1}{4}\gamma^4\frac{C_Q}{C_R} \right], \quad (2.2.20)$$

$$\begin{aligned} \sqrt{s_{\pm}} &= M_Z \left[1 + \frac{3}{8}\gamma^2 + \frac{1}{2}\gamma^2\frac{C_I}{C_R} - \frac{3}{4}\gamma^4\frac{C_Q}{C_R} \right] \\ &\pm \frac{\Gamma_Z}{2} \left[1 - \frac{1}{8}\gamma^2 + \gamma^2(1 + \frac{1}{4}\gamma^2)\frac{C_Q}{C_R} + \frac{1}{2} \left(\gamma^2\frac{C_Q}{C_R} \right)^2 \right]. \end{aligned} \quad (2.2.21)$$

Consider first the neutrino case, where $C_I = C_Q = 0$. The peak position is shifted to the right by $\frac{1}{4}\gamma^2 M_Z$, compared to a pure Breit-Wigner resonance, where the peak is located at $\sqrt{s_{max}} = M_Z$. The shift is caused by an extra factor s in the numerator. The average of $\sqrt{s_+}$ and $\sqrt{s_-}$ is shifted somewhat more, namely $\frac{3}{8}\gamma^2 M_Z$. Furthermore the apparent width $\sqrt{s_+} - \sqrt{s_-}$ is decreased by $\frac{1}{8}\gamma^2 \Gamma_Z$.

For the other fermion channels the one photon exchange is present. This increases the distance between the half maxima since the pure QED term only marginally changes over half a width but contributes to the peak value. Since the relative importance of the QED term is largest for muon pair production this effect will there be most noticeable.

2.2.3 The corrected partial and total widths

As it will become clear in the next subsection we need the first order corrections to $\Gamma_{Z \rightarrow f\bar{f}}^{(0)}$. These can be divided into four classes:

1. Non-photonic loop corrections
2. Photonic loop corrections and radiative decay

m_{top}	M_H	$\sin^2 \vartheta_W$	Γ_Z	$\Gamma_{Z \rightarrow \nu\bar{\nu}}$	$\Gamma_{Z \rightarrow e^+e^-}$	$\Gamma_{Z \rightarrow u\bar{u}}$	$\Gamma_{Z \rightarrow d\bar{d}}$	$\Gamma_{Z \rightarrow b\bar{b}}$
90	10	0.2300	2480	165.9	83.2	295.7	381.7	378.6
	100	0.2316	2483	166.2	83.4	295.9	382.0	378.9
	1000	0.2347	2475	165.9	83.2	294.6	380.6	377.5
130	10	0.2254	2488	166.3	83.5	297.2	383.3	378.2
	100	0.2270	2491	166.7	83.6	297.3	383.7	378.5
	1000	0.2303	2483	166.4	83.4	296.1	382.3	377.2
170	10	0.2200	2498	166.9	83.8	299.1	385.5	377.5
	100	0.2217	2501	167.3	84.0	299.2	385.9	377.9
	1000	0.2250	2493	167.0	83.8	298.0	384.5	376.6

Table 2.1. Results for total and partial widths of the Z including all corrections. The Z mass was taken to be 91.17 GeV. All widths are in MeV, the masses are in GeV.

3. QCD corrections

4. Decay into three or more particles

In refs. [7, 8, 9] the non-photonic corrections in the OS scheme have been discussed extensively. The calculations use different gauge choices and field renormalizations, but the results for the physical quantities are the same. A conclusion that can be drawn is that the results for $\bar{\Gamma}_{Z \rightarrow f\bar{f}}^{(0)}$ given by eq.(2.2.10) is in general much closer to the one loop corrected result than the result given by eq.(2.2.8). In fact eq.(2.2.10) in general is a good approximation for the width, at least for $m_{top} < 120$ GeV.

The photonic corrections give a multiplicative factor $(1 + \delta_{QED})$, where

$$\delta_{QED} = \frac{3\alpha}{4\pi} Q_f^2, \quad (2.2.22)$$

which is Q_f^2 times 0.17%. It should be noted that although we discuss the QED corrections to the cross sections in section 2.3, we include here the QED correction to the width. The reason is that it will have an effect on the propagator, as we will see in the next subsection.

The QCD corrections are obtained by multiplying the quark decays by the factor $(1 + \delta_{QCD})$. Its measured value [10] is

$$\delta_{QCD} \left((34 \text{ GeV})^2 \right) = 0.047 \pm 0.009. \quad (2.2.23)$$

From the running of the coupling constant α , one then obtains for our purposes

$$\delta_{QCD} \left((92 \text{ GeV})^2 \right) = 0.040 \pm 0.007, \quad (2.2.24)$$

m_{top}	$\sin^2 \vartheta_W$	Γ_Z	σ_{max}	$\sqrt{s_{max}}$	$\sqrt{s_-}$	$\sqrt{s_+}$
90	0.2316	2.483	1.997	91.153	89.914	92.410
130	0.2270	2.491	1.998	91.153	89.910	92.414
170	0.2217	2.501	2.000	91.153	89.904	92.419
90	0.2316	2.483	41.398	91.154	89.921	92.406
130	0.2270	2.491	41.417	91.154	89.918	92.410
170	0.2217	2.501	41.452	91.154	89.913	92.415

Table 2.2. Results for the peak cross section and the peak positions for muon production (upper half) and hadron production (lower half) including only electroweak corrections. The Z and Higgs masses were fixed at 91.17 and 100 GeV resp. All energies are in GeV and cross sections in nanobarn.

or $\alpha_s = 0.12$. For the $\bar{b}b$ channel the mass dependent QCD correction [11] is actually used. In practice δ_{QCD} in eq.(2.2.24) then takes the value 0.045 ± 0.007 . The error on the total width induced by the error on δ_{QCD} is about 10 MeV.

Besides the non-photonic loop corrections also decays into three or more particles represent corrections to the lowest order width. Two types were already treated above in the form of QED and QCD corrections. Of the other possible decays only the decay (calculated from the expressions in ref. [12])

$$Z \rightarrow H \bar{f} f \quad (2.2.25)$$

is of relevance, but only when $M_H \leq 10$ GeV. The other decays are negligible [13].

In table 2.1 results for the total and partial widths of the Z are listed for a range of top masses. The results are obtained with the program ZSHAPE [14]. The differences for the various values for m_{top} are quite noticeable. The Higgs mass is kept fixed, since the differences due to variation in M_H can only be seen if M_H is varied in a very large range.

2.2.4 Total cross section with electroweak corrections

The lowest order total cross section for massless fermions is given in eq.(2.2.13). The cross section is of order α^2 except at the resonance position where it is of order α^0 . As stressed in ref. [15] one should therefore consider the $\mathcal{O}(\alpha)$ corrections to Γ_Z . Since Γ_Z is related to the imaginary part of the self-energy it means that the one loop corrections to the propagator are not sufficient but that two loop corrections should be taken into account in the resonance region.

Besides the modifications of coupling constants by vertex corrections and the introduction of very small box diagrams, the electroweak corrections amount to the replace-

ments [5]

$$\frac{1}{s} \rightarrow \frac{1}{s + \Sigma_\gamma(s)}, \quad (2.2.26)$$

$$\frac{1}{s - M_Z^2 + iM_Z\Gamma_Z} \rightarrow \frac{1}{s - M_Z^2 + \Sigma_Z(s)}, \quad (2.2.27)$$

where

$$\Sigma_\gamma(s) = \Sigma_{\gamma\gamma}(s) - \frac{\Sigma_{\gamma Z}^2(s)}{s - M_Z^2 + \Sigma_Z(s)}, \quad (2.2.28)$$

$$\Sigma_Z(s) = \Sigma_{ZZ}(s) - \frac{\Sigma_{\gamma Z}^2(s)}{s + \Sigma_\gamma(s)}. \quad (2.2.29)$$

These expressions are obtained from a Dyson series summation involving the renormalized one particle irreducible self-energies $\Sigma_{\gamma\gamma}$, Σ_{ZZ} and $\Sigma_{\gamma Z}$. Besides the above propagators one has also to include a γZ mixing propagator, which takes the form

$$D_{\gamma Z}(s) = \frac{-\Sigma_{\gamma Z}(s)}{s[s - M_Z^2 + \Sigma_Z(s)]}. \quad (2.2.30)$$

In these expressions the real parts of Σ_γ and Σ_Z are taken in first order. The imaginary part of Σ_Z is considered up to second order. That is, also the imaginary part of Σ_{ZZ} should be evaluated in second order. This is done by the following approximation

$$\text{Im} \Sigma_{ZZ}^{(2)}(s) = \frac{s}{M_Z^2} \text{Im} \Sigma_{ZZ}^{(2)}(M_Z^2), \quad (2.2.31)$$

where the latter expression is related to the first order corrections to the width. All corrections to the width contribute to eq.(2.2.31) except for the wave function renormalization of the Z and γZ mixing contributions. This can be seen by expanding (2.2.27) in the resonance region

$$\frac{1}{s - M_Z^2 + \Sigma_Z(s)} = \frac{1}{1 + \Pi_Z(M_Z^2)} \frac{1}{s - M_Z^2 + \frac{i \text{Im} \Sigma_Z(s)}{1 + \Pi_Z(M_Z^2)}}, \quad (2.2.32)$$

where

$$\Pi_Z(M_Z^2) = \frac{\partial \text{Re} \Sigma_Z}{\partial s}(M_Z^2) \quad (2.2.33)$$

and

$$M_Z\Gamma_Z = \frac{\text{Im} \Sigma_Z(M_Z^2)}{1 + \Pi_Z(M_Z^2)}. \quad (2.2.34)$$

The denominator in eq.(2.2.34) represents the wave function renormalization of the Z. It gives a first order correction to Γ_Z . When one also considers the real part of the second

term in eq.(2.2.29) one effectively takes a part of the second order correction of the real part of Σ_Z into account. The effect of this has been discussed in [5]. For high top masses ($m_{top} \geq 150$ GeV) slight deviations from the results presented here occur. It should be stressed that for a conclusive discussion of this effect the full second order calculation of $\text{Re } \Sigma_Z$ should be performed.

In the replacement (2.2.27) it is not only of importance that corrections to Γ_Z or equivalently to $\Sigma_Z(s)$ are taken into account. Also the energy dependence of $\text{Im } \Sigma_Z(s)$ is crucial. It shifts the peak position with -35 MeV with respect to a constant width formula [16, 17]. In a qualitative discussion below we come back to this point.

Besides the propagator effects vertex corrections replace the couplings $g_{\bar{f}}$ and g_f^\dagger by s -dependent form factors. The overall normalization is affected by these corrections. The box diagrams turn out to be very small in the Feynman-'t Hooft gauge and can therefore be neglected in this gauge when calculating the total cross section.

In table 2.2 we give results for the electroweak corrected cross section for muon pair production and for hadron production. In the table the quantities σ_{max} , $\sqrt{s_{max}}$ and $\sqrt{s_{\pm}}$ are listed.

2.2.5 Approximate expressions

As mentioned in the previous subsection the modification of the total cross section (2.2.13) due to electroweak corrections is in essence due to an introduction of s -dependent form factors which replace the coupling constants g^\pm , and the changes (2.2.26), (2.2.27) and (2.2.30) of the propagators. Thus in several places in the original formula s -dependent quantities replace the original constant ones. Also the values for $s = M_Z^2$ are different from the lowest order quantities.

in the region of the resonance the s -dependence of $\Sigma_Z(s)$ in eq.(2.2.27) is crucial, the other s -dependences have a small influence. The s -dependence of $\text{Im } \Sigma_Z(s)$ near the resonance can be well approximated by the replacement

$$\begin{aligned} \frac{1}{s - M_Z^2 + iM_Z\Gamma_Z} &\rightarrow \frac{1}{s - M_Z^2 + is\Gamma_Z/M_Z} \\ &= \frac{1}{1 + i\gamma} \frac{1}{s - \widetilde{M}_Z^2 + i\widetilde{M}_Z\widetilde{\Gamma}_Z}, \end{aligned} \quad (2.2.35)$$

where we have introduced

$$\begin{aligned} \widetilde{M}_Z &= M_Z/\sqrt{1 + \gamma^2}, \\ \widetilde{\Gamma}_Z &= \Gamma_Z/\sqrt{1 + \gamma^2}. \end{aligned} \quad (2.2.36)$$

The other s -dependent corrections can be taken at $s = M_Z^2$. Effectively we get new coupling constants $g^\pm(M_Z^2)$ and

$$e^2(M_Z^2) = \frac{e^2}{1 + \Pi_\gamma(M_Z^2)}, \quad (2.2.37)$$

where

$$\Pi_\gamma(s) = \frac{\text{Re} \Sigma_{\gamma\gamma}(s)}{s} . \quad (2.2.38)$$

In the constants $g^\pm(M_Z^2)$ also form factor effects are incorporated. This is not done for the coupling to the photons. The imaginary parts of the form factors and Σ_γ are neglected at this point.

We now end up with the following approximation for the electroweak corrected total cross section for massless fermions.

$$\sigma(s) = \frac{1}{(1 - \tilde{M}_Z^2/s)^2 + \tilde{M}_Z^2 \tilde{\Gamma}_Z^2/s^2} \left[\frac{C_R}{s} + \frac{C_I}{s} \left(1 - \frac{M_Z^2}{s} \right) \right] + \frac{C_Q}{s} , \quad (2.2.39)$$

where now

$$\begin{aligned} C_R &= \frac{12\pi\Gamma_e\Gamma_f}{M_Z^2(1+\gamma^2)} , \\ C_I &= \mp \frac{4\pi Q_f \alpha(M_Z^2)}{M_Z(1+\gamma^2)} \left(\Gamma_+^{\frac{1}{2}}(e) - \Gamma_-^{\frac{1}{2}}(e) \right) \left(\Gamma_+^{\frac{1}{2}}(f) - \Gamma_-^{\frac{1}{2}}(f) \right) N_c^{1/2} , \\ C_Q &= \frac{4}{3}\pi Q_f^2 \alpha^2(M_Z^2) N_c . \end{aligned} \quad (2.2.40)$$

In this case Γ_e , Γ_f and Γ_\pm are the electroweak corrected partial widths without QED and QCD corrections. For b quarks the pure QED part now becomes the massive QED part, but in C_I we use the massless approximation.

The approximation (2.2.39) describes the exact electroweak corrected cross section within 0.2% in the range $[M_Z - \Gamma_Z, M_Z + \Gamma_Z]$. The values for maxima and half maxima obtained from (2.2.39) are within 1 MeV from the values in the tables.

Also for the approximate formula (2.2.39) one can derive expressions for the quantities σ_{max} , $\sqrt{s_{max}}$, $\sqrt{s_\pm}$:

$$\sigma_{max} = \frac{C_R}{\tilde{\Gamma}_Z^2} \left[1 + \frac{1}{4}\gamma^2 + \gamma^2(1 - \gamma^2) \frac{C_Q}{C_R} \right] , \quad (2.2.41)$$

$$\sqrt{s_{max}} = M_Z \left[1 - \frac{1}{4}\gamma^2 + \frac{1}{4}\gamma^2 \frac{C_I}{C_R} - \frac{1}{4}\gamma^4 \frac{C_Q}{C_R} \right] , \quad (2.2.42)$$

$$\begin{aligned} \sqrt{s_\pm} &= M_Z \left[1 - \frac{1}{8}\gamma^2 + \frac{1}{2}\gamma^2 \frac{C_I}{C_R} - \frac{3}{4}\gamma^4 \frac{C_Q}{C_R} \right] \\ &\pm \frac{\Gamma_Z}{2} \left[1 - \frac{5}{8}\gamma^2 + \gamma^2 \frac{C_Q}{C_R} + \frac{1}{2} \left(\gamma^2 \frac{C_Q}{C_R} \right)^2 \right] . \end{aligned} \quad (2.2.43)$$

Most of the changes with respect to eqs.(2.2.19)-(2.2.21) are due to the replacement (2.2.35), which can be accounted for by $M_Z, \Gamma_Z \rightarrow \tilde{M}_Z, \tilde{\Gamma}_Z$. The resulting peak position is now $\frac{1}{4}\gamma^2 M_Z$ below M_Z , whereas before the replacement (2.2.35) it was $\frac{1}{4}\gamma^2 M_Z$ above M_Z . Also it is apparent that the distance between the half maxima has decreased. The effects due to the one photon exchange have hardly changed, as these effects themselves are rather small and almost all corrections to them can be neglected.

2.3 The photonic or QED corrections

2.3.1 The relevance of various QED contributions

When one considers the full first order QED correction to the line shape, one finds a contribution from initial state radiation, final state radiation and from the interference between initial and final state radiation. When no cuts on the outgoing fermions are imposed the final state radiative correction is just eq.(2.2.22) and is therefore small. When a stringent cut on the fermion pair invariant mass is applied the correction can become negative and large. This is discussed in subsection 2.3.3. The size of the interference contribution to the total cross section is negligible [19, 20, 21]. Thus mainly the initial state radiative corrections remain. They are sizable due to the occurrence of large logarithms of the type

$$L = \log \frac{s}{m_e^2} . \quad (2.3.1)$$

It is clear from the large first order corrections found in refs. [19, 22] that higher order QED corrections are required for the description of the line shape. Let us list all initial state corrections up to and including order α^2 for muon pair production:

$$e^+e^- \rightarrow \mu^+\mu^- , \quad (2.3.2)$$

$$e^+e^- \rightarrow \mu^+\mu^-\gamma , \quad (2.3.3)$$

$$e^+e^- \rightarrow \mu^+\mu^-\gamma\gamma , \quad (2.3.4)$$

$$e^+e^- \rightarrow \mu^+\mu^-\bar{f}f . \quad (2.3.5)$$

The cross section for the first of these reactions is required with first and second order loop corrections. For the second process one loop corrections have to be calculated, whereas the last two reactions themselves give rise to $\mathcal{O}(\alpha^3)$ corrections to the first one. For the last process the case $f = e^-$ is dominant, hence we will only discuss that case.

When we consider e^+e^- scattering at a laboratory energy \sqrt{s} , the above reactions (2.3.3) – (2.3.5) give rise to differential cross sections $d\sigma/ds'$ with s' the square of the muon pair invariant mass. Their contribution to the total muon pair cross section is obtained by integration over s' . The relative sizes of $d\sigma/ds'$ make it possible to neglect the contribution of (2.3.5). This is based on the following considerations. Reaction (2.3.5) consists of four different parts:

- A. Bremsstrahlung of an e^+e^- pair from the initial e^+e^- states;
- B. Bremsstrahlung of a $\mu^+\mu^-$ pair from Bhabha scattering;
- C. The interference between the diagrams of A and B;
- D. The two photon reaction producing a muon pair.

The formulae and relative sizes are discussed in [23, 24]. In the region $s'/s > 0.2$ the cross sections $d\sigma/ds'$ from (2.3.3) and (2.3.4) dominate the contributions from A, B, C by more than 2 orders of magnitude. This is also true for D but in a more restricted region. In fact $d\sigma/ds'$ from D becomes greater than $d\sigma/ds'$ from photon emission for $s'/s < 0.3$. So if one wants to study muon pair production through the formation of a Z, the two photon initiated muon pairs should be removed from the data. One way is to apply a cut on s' . In that case the QED corrections given below should also involve this cut. This is not a problem, but one should then also take into account the effect of this cut on the final state radiative correction, which is not any more eq.(2.2.22), but a δ_{QED} depending on s' and the minimum value of s' . It is easy to incorporate this factor in the convolution to be discussed below. The inclusion of the final state QED corrections in this way is treated in subsection 2.3.3. In the following discussion we ignore the two-photon initiated muon pairs and consider the reactions (2.3.3) and (2.3.4) as the dominant contributions and do not restrict the allowed s' range. Thus we are left with initial state photon radiation.

2.3.2 Initial state photon radiation

One way to consider initial state photon radiation is to perform a standard but involved second order calculation for the initial state. One has to calculate double bremsstrahlung, the one-loop corrections to single bremsstrahlung and the two-loop vertex corrections. The result can be written in the form

$$\sigma(s) = \int_{z_0}^1 dz G(z) \sigma_w(sz) , \quad (2.3.6)$$

where the cross section including weak corrections is denoted by $\sigma_w(sz)$, i.e. the result of section 2.2.4. The invariant mass of the produced fermion pair is given by

$$s' = sz , \quad (2.3.7)$$

where

$$\frac{4m_f^2}{s} \leq z_0 \leq z \leq 1 , \quad (2.3.8)$$

Unless specified differently the cut-off invariant mass z_0s will be $4m_f^2$. In general $G(z)$ has the following expansion

$$\begin{aligned} G(z) = & \delta(1-z) + \frac{\alpha}{\pi} (a_{11}L + a_{10}) + \left(\frac{\alpha}{\pi}\right)^2 (a_{22}L^2 + a_{21}L + a_{20}) \\ & + \dots + \left(\frac{\alpha}{\pi}\right)^n \sum_{i=0}^n a_{ni}L^i + \dots \end{aligned} \quad (2.3.9)$$

Here the large logarithm (2.3.1) has been made explicit, which at LEP energies (~ 100 GeV) approximately has the value 24. The quantities a_{ij} are divided into two parts. One

part is proportional to $\delta(1-z)$ and contains only virtual and soft photon corrections such that s' remains greater than $s(1-\varepsilon)$. The other part proportional to $\vartheta(1-z-\varepsilon)$ contains hard bremsstrahlung, possibly accompanied by virtual and soft photon corrections. The $\delta(1-z)$ term involves logarithms

$$\ell = \log \varepsilon, \quad (2.3.10)$$

which in the convolution (2.3.6) will cancel similar terms arising from the $\vartheta(1-z-\varepsilon)$ terms. In the full second order calculation the coefficients $a_{1i}, i = 0, 1$ and $a_{2i}, i = 0, 1, 2$ are obtained. Instead of performing the explicit second order QED calculation one may apply the QCD structure function approach to QED problems. This has been advocated in refs. [25, 26, 27, 28]. Usually this method is used to obtain the leading logarithms, i.e., the terms

$$\left(\frac{\alpha}{\pi}\right)^n a_{nn} L^n \quad (2.3.11)$$

in eq.(2.3.9) up to a certain n .

When a number of terms of the form (2.3.11) has been obtained, certain parts of a_{nn} generalize to higher n values. Then it is often possible to carry out the summation over n in eq.(2.3.9) for those parts of the terms a_{nn} that are related to soft photons. The latter represents a specific exponentiation of some terms in the first order result.

We now discuss the present knowledge of the terms a_{ni} . The first order terms have been known for quite some time (e.g. refs. [19] and [22]), the explicit second order calculation [23, 29] gives all a_{2i} . In the structure function approach the coefficient a_{22} is obtained [25, 26, 27, 28] and agrees with the explicit second order calculation. It is also possible to get the complete subleading logarithms in the structure function approach. This has been done in ref. [23], where the coefficient a_{21} was found to be in agreement with the explicit $\mathcal{O}(\alpha^2)$ calculation. For a_{20} there is only the explicit way of calculation possible.

From the results of these calculations it becomes clear that certain terms can be resummed, and the division in $\delta(1-z)$ and $\vartheta(1-z-\varepsilon)$ terms is not necessary any more. The result of one particular way of doing this reads [23]

$$G(z) = \beta(1-z)^{\beta-1} \delta^{V+S} + \delta^H, \quad (2.3.12)$$

with

$$\begin{aligned} \beta &= \frac{2\alpha}{\pi}(L-1), \\ \delta^{V+S} &= 1 + \delta_1^{V+S} + \delta_2^{V+S}, \\ \delta^H &= \delta_1^H + \delta_2^H, \\ \delta_1^{V+S} &= \frac{\alpha}{\pi} \left(\frac{3}{2}L + 2\zeta(2) - 2 \right), \\ \delta_2^{V+S} &= \left(\frac{\alpha}{\pi} \right)^2 \left[\left(\frac{9}{8} - 2\zeta(2) \right) L^2 + \left(-\frac{45}{16} + \frac{11}{2}\zeta(2) + 3\zeta(3) \right) L \right] \end{aligned} \quad (2.3.13)$$

$$\begin{aligned}
& -\frac{6}{5}\zeta(2)^2 - \frac{9}{2}\zeta(3) - 6\zeta(2)\log 2 + \frac{3}{8}\zeta(2) + \frac{19}{4} \Big], \\
\delta_1^H &= -\frac{\alpha}{\pi}(1+z)(L-1), \\
\delta_2^H &= \left(\frac{\alpha}{\pi}\right)^2 \left\{ X - (1+z) \left[2\log(1-z)(L-1)^2 \right. \right. \\
&\quad \left. \left. + (L-1) \left(\frac{3}{2}L + 2\zeta(2) - 2 \right) \right] \right\}, \\
X &= \left(-\frac{1+z^2}{1-z} \log z + (1+z) \frac{1}{2} \log z + z - 1 \right) L^2 \\
&+ \left[\frac{1+z^2}{1-z} \left(\text{Li}_2(1-z) + \log z \log(1-z) + \frac{7}{2} \log z - \frac{1}{2} \log^2 z \right) \right. \\
&+ (1+z) \frac{1}{4} \log^2 z - \log z + \frac{7}{2} - 3z \Big] L \\
&+ \frac{1+z^2}{1-z} \left(-\frac{1}{6} \log^3 z + \frac{1}{2} \log z \text{Li}_2(1-z) + \frac{1}{2} \log^2 z \log(1-z) \right. \\
&- \frac{3}{2} \text{Li}_2(1-z) - \frac{3}{2} \log z \log(1-z) + \zeta(2) \log z - \frac{17}{6} \log z - \log^2 z \Big) \\
&+ (1+z) \left(\frac{3}{2} \text{Li}_3(1-z) - 2S_{1,2}(1-z) - \log(1-z) \text{Li}_2(1-z) - \frac{1}{2} \right) \\
&- \frac{1}{4} (1-5z) \log^2(1-z) + \frac{1}{2} (1-7z) \log z \log(1-z) - \frac{25}{6} z \text{Li}_2(1-z) \\
&+ \left(-1 + \frac{13}{3} z \right) \zeta(2) + \left(\frac{3}{2} - z \right) \log(1-z) + \frac{1}{6} (11+10z) \log z \\
&+ \frac{2}{(1-z)^2} \log^2 z - \frac{25}{11} z \log^2 z - \frac{2}{3} \frac{z}{1-z} \left(1 + \frac{2}{1-z} \log z + \frac{1}{(1-z)^2} \log^2 z \right).
\end{aligned} \tag{2.3.14}$$

In these definitions the polylogarithms $\text{Li}_n(x)$ and $S_{n,p}(x)$ have been introduced (cf. refs. [30] and [31]) and the Riemann zeta function $\zeta(2) = \pi^2/6$ and $\zeta(3) \approx 1.2020569$.

The terms δ_1^{V+S} , δ_2^{V+S} originate from first and second order virtual and soft photon corrections. Similarly δ_1^H and δ_2^H originate from single and double hard bremsstrahlung.

When $G(z)$ is expanded up to order $(\alpha/\pi)^2$ we find the complete second order result of ref. [23]. The form $G(z)$ contains however all higher order terms related to soft photon emission.

2.3.3 Final state photon radiation

The final state QED corrections can be formulated in such a way that they can be incorporated in an integral of the form (2.3.6). In fact all that need be done is to multiply the integrand by

$$F(z) = 1 + \frac{\alpha Q_f^2}{\pi} \left[\log \frac{s}{m_f^2} \left(2 \log \left(1 - \frac{z_0}{z} \right) + \frac{z_0}{z} \left(1 + \frac{1}{2} \frac{z_0}{z} \right) \right) + \frac{3}{4} + \right.$$

$$\begin{aligned}
& -2\frac{z_0}{z} - \frac{3}{4}\left(\frac{z_0}{z}\right)^2 - 2\log\left(1 - \frac{z_0}{z}\right) - 2\text{Li}_2\left(1 - \frac{z_0}{z}\right) + \\
& + \frac{z_0}{z}\left(1 + \frac{1}{2}\frac{z_0}{z}\right)\log\frac{z_0}{z} + 2\zeta(2) \Big] . \tag{2.3.15}
\end{aligned}$$

Here $z_0 = s_{\min}/s$ is the lower bound on the square of the final state fermion pair mass divided by s . It therefore also is the lower bound on the integration variable z . The large logarithm $\log(s/m_f^2)$ appearing here contains the mass m_f of the final state fermions, in contrast to m_e for initial state corrections. Furthermore it is clear that for $z_0 \ll z$ this factor reduces to $(1 + \delta_{QED})$. If on the other hand $z_0 \lesssim z$, the coefficient of $\log(s/m_f^2)$ does not vanish and hence the final state corrections are significantly larger than $(1 + \delta_{QED})$. In fact they will become negative in this case.

One can also exponentiate the soft photon contributions to $F(z)$, which results in

$$\begin{aligned}
F(z) = & \left(1 - \frac{z_0}{z}\right)^{\beta_f} \left[1 + \frac{\alpha Q_f^2}{\pi} \left(\frac{3}{2} \log \frac{s}{m_f^2} + 2\zeta(2) - 2 \right) \right] + \\
& - \frac{\alpha Q_f^2}{\pi} \left(\log \frac{s}{m_f^2} - 1 \right) \left(\frac{3}{2} - \frac{z_0}{z} - \frac{1}{2} \left(\frac{z_0}{z} \right)^2 \right) + \\
& \frac{2\alpha Q_f^2}{\pi} \left(-\text{Li}_2\left(1 - \frac{z_0}{z}\right) + \frac{5}{8} + \right. \\
& \left. + \frac{1}{2} \frac{z_0}{z} \left(1 + \frac{1}{2} \frac{z_0}{z} \right) \log \frac{z_0}{z} + -\frac{1}{2} \frac{z_0}{z} \left(1 + \frac{1}{4} \frac{z_0}{z} \right) \right) . \tag{2.3.16}
\end{aligned}$$

The exponent is defined as

$$\beta_f = \frac{2\alpha Q_f^2}{\pi} \left(\log \frac{s}{m_f^2} - 1 \right) . \tag{2.3.17}$$

2.3.4 Numerical results

The total cross section with electroweak corrections as listed in table 2.2 is now corrected for QED effects with eqs.(2.3.6) and (2.3.12). The results are in table 2.3.

The main features are a reduction ρ of the peak height, shifts $\Delta\sqrt{s_{max}}$, $\Delta\sqrt{s_{\pm}}$ of the peak and half peak positions. Considering hadron production we find approximately

$$\begin{aligned}
\rho & = 0.739 \pm 0.001 , \\
\Delta\sqrt{s_{max}} & = 109 \pm 1 \text{ MeV} , \\
\Delta\sqrt{s_-} & = 57 \pm 1 \text{ MeV} , \\
\Delta\sqrt{s_+} & = 419 \pm 2 \text{ MeV} . \tag{2.3.18}
\end{aligned}$$

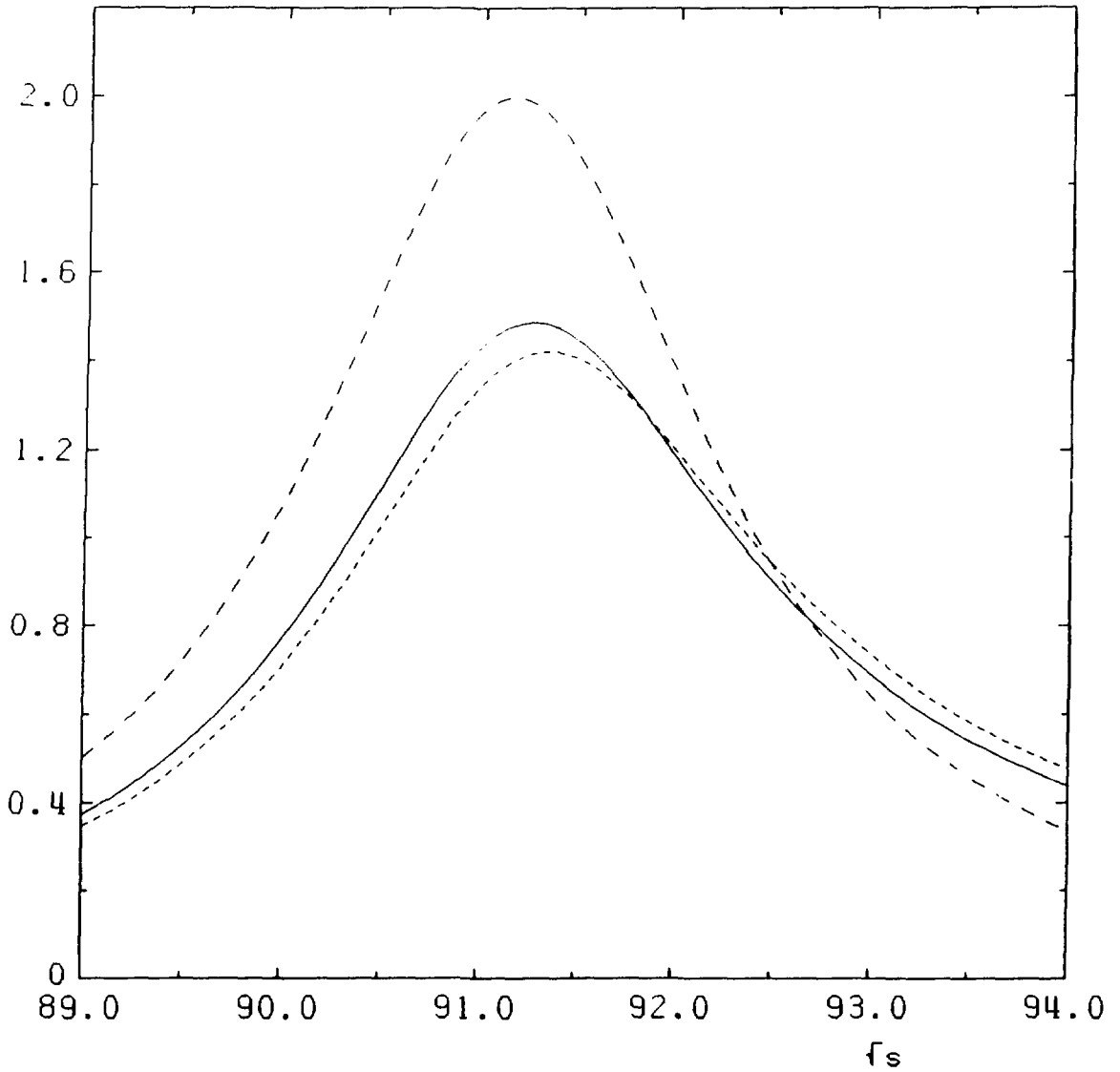


Fig. 2.1. Muon pair line shape curves including successive stages of corrections: only non-photonic corrections (fine dashed line), first order QED corrections applied to the previous one (dashed line) and second order exponentiated corrections applied to the first curve (solid line). The masses are $M_Z = 91.17$, $M_H = 100$ and $m_{top} = 130$ GeV and the minimum s' value used is $4m_\mu^2$.

m_{top}	$\sin^2 \vartheta_W$	Γ_Z	σ_{max}	$\sqrt{s_{max}}$	$\sqrt{s_-}$	$\sqrt{s_+}$
90	0.2316	2.483	1.487	91.261	89.962	92.841
130	0.2270	2.491	1.488	91.261	89.958	92.846
170	0.2217	2.501	1.490	91.262	89.953	92.853
90	0.2316	2.483	30.584	91.262	89.978	92.823
130	0.2270	2.491	30.607	91.263	89.975	92.829
170	0.2217	2.501	30.646	91.263	89.970	92.836

Table 2.3. Results for the peak cross section and the peak positions for muon pair production (upper half) and hadron production (lower half) including all corrections. The Z and Higgs masses were fixed at 91.17 and 100 GeV resp. All energies are in GeV and cross sections in nanobarn. The minimum s' value used is $4m_\mu^2$ for muons and $(10 \text{ GeV})^2$ for hadrons.

The indicated errors represent the spread in the table. For muon pairs we find

$$\begin{aligned}
\rho &= 0.745 \pm 0.001, \\
\Delta\sqrt{s_{max}} &= 108 \pm 1 \text{ MeV}, \\
\Delta\sqrt{s_-} &= 48 \pm 1 \text{ MeV}, \\
\Delta\sqrt{s_+} &= 432 \pm 2 \text{ MeV}.
\end{aligned} \tag{2.3.19}$$

We see that the distance between the half peak positions increase since $\Delta\sqrt{s_+}$ is much larger than $\Delta\sqrt{s_-}$. When we define the ratio τ as the ratio between the distances after and before the convolution, i.e.,

$$\tau = \frac{(\sqrt{s_+} - \sqrt{s_-})_{after}}{(\sqrt{s_+} - \sqrt{s_-})_{before}}, \tag{2.3.20}$$

we find throughout the table approximately

$$\begin{aligned}
\tau &\simeq 1.145 && \text{for hadrons,} \\
\tau &\simeq 1.153 && \text{for muons.}
\end{aligned} \tag{2.3.21}$$

For τ four decimals are given in order to see the difference between the hadron and muon channels. The differences between the muon pair case and the hadron case can be attributed to the pure QED term in the electroweak corrected cross section, i.e. the last term in (2.2.39). This term contributes about 0.5% to the peak value before convolution and is not decreased, but increased by the convolution. Typical for the first order correction is an increase of 60% [32]. This explains the somewhat larger factors ρ and τ and the different values for $\Delta\sqrt{s_\pm}$. The neutrino case is in all these respects very similar to the hadron case.

In figure 2.1 we illustrate the effects of the QED radiative corrections for muon pairs. The electroweak corrected cross section is depicted (fine dashed line) together with the

first order QED corrected (dashed line) and the second order exponentiated QED corrected cross section (solid line). This curve is evaluated according to eqs.(2.3.6) and (2.3.12), whereas the first order QED corrected one uses (2.3.6) and (2.3.9) up to the order α term. It is clear that the first order correction overestimates the effects and that the second order exponentiated form pushes the line shape slightly back to the non-QED corrected one. The minimum s' value used is $4m_\mu^2$.

2.3.5 Approximate analytical results

In order to obtain analytical formulae for the line shape including non-photonic and photonic corrections one necessarily has to make a number of approximations. The first approximation is to use eq.(2.2.39) for the electroweak corrected cross section $\sigma_w(s')$ in the convolution (2.3.6). However since we now want to include final state QED and QCD corrections, the constants appearing in eq.(2.2.39) are now taken to be

$$\begin{aligned}
 C_R &= \frac{12\pi\Gamma_e\Gamma_f}{M_Z^2(1+\gamma^2)}(1+\delta_{QED}), \\
 C_I &= \mp \frac{4\pi Q_f\alpha(M_Z^2)}{M_Z(1+\gamma^2)} \left(\Gamma_+^{\frac{1}{2}}(e) - \Gamma_-^{\frac{1}{2}}(e) \right) \left(\Gamma_+^{\frac{1}{2}}(f) - \Gamma_-^{\frac{1}{2}}(f) \right) \\
 &\quad \times N_c^{1/2}(1+\delta_{QED})(1+\delta_{QCD})^{1/2}, \\
 C_Q &= \frac{4}{3}\pi Q_f^2\alpha^2(M_Z^2)N_c(1+\delta_{QED})(1+\delta_{QCD}).
 \end{aligned} \tag{2.3.22}$$

The partial width Γ_f contains electroweak and QCD corrections, but not the QED corrections. The latter is included as overall factor in all three constants C_R , C_I and C_Q . We use the integration variable x , defined by $s' = s(1-x)$, so that one part of the integrand is given by $\sigma_w(s(1-x))$.

As second approximation the function $G(1-x)$ in eq.(2.3.6) is taken in the first order exponentiated form, which means that δ_2^{V+S} and δ_2^H are omitted. For the convolution of the pure QED term even the exponentiation can be omitted and the first order result [32] is used.

Thirdly, the integration region for the exponential part of G is extended to $[0, \infty]$, for the other part of G the region $[0, 1]$ is used and for the QED part the original integration region is kept. Due to the transformation (2.2.35) we can directly use some results of ref. [33]. One has the integrals

$$J_\beta = \beta \int_0^\infty dx \frac{x^{\beta-1}}{x^2 - 2\eta x \cos \zeta + \eta^2} = \eta^{\beta-2} \phi(\cos \zeta, \beta), \tag{2.3.23}$$

with

$$\phi(\cos \zeta, \beta) = \frac{\pi\beta \sin[(1-\beta)\zeta]}{\sin \pi\beta \sin \zeta},$$

$$\begin{aligned}\eta &= \sqrt{a^2 + b^2}, \quad \cos \zeta = a/\eta, \\ a &= \widetilde{M}_Z^2/s - 1, \quad b = \widetilde{M}_Z \widetilde{\Gamma}_Z/s,\end{aligned}\tag{2.3.24}$$

and from the δ_1^H part

$$\begin{aligned}J_1 &= \int_0^1 dx \frac{2-x}{(x+a)^2 + b^2} = \frac{2+a}{b} A - \frac{B}{2}, \\ J_2 &= \int_0^1 dx \frac{x(2-x)}{(x+a)^2 + b^2} = -\frac{a^2 + 2a - b^2}{b} A + (1+a)B - 1,\end{aligned}\tag{2.3.25}$$

with

$$\begin{aligned}A &= \arctan \frac{a+1}{b} - \arctan \frac{a}{b}, \\ B &= \log \frac{2a+1+a^2+b^2}{a^2+b^2}.\end{aligned}\tag{2.3.26}$$

The analytic approximate cross section is represented in terms of these integrals

$$\begin{aligned}\sigma(s) &= \left(\frac{C_R + C_I}{s} - \frac{\widetilde{M}_Z^2 + \widetilde{\Gamma}_Z^2}{s^2} C_I \right) \left(\eta^{\beta-2} \phi(\cos \zeta, \beta) (1 + \delta_1^{V+S}) - \frac{\beta}{2} J_1 \right) \\ &\quad - \frac{C_R + C_I}{s} \left(\frac{\beta}{\beta+1} \eta^{\beta-1} \phi(\cos \zeta, \beta+1) (1 + \delta_1^{V+S}) - \frac{\beta}{2} J_2 \right) \\ &\quad + \frac{C'_Q}{s},\end{aligned}\tag{2.3.27}$$

with

$$\begin{aligned}C'_Q &= C_Q \left[1 + \frac{\alpha}{\pi} \log \frac{s}{m_e^2} \left(2 \log \left(1 - \frac{s_{\min}}{s} \right) - \log \frac{s_{\min}}{s} + \frac{1}{2} + \frac{s_{\min}}{s} \right) \right. \\ &\quad \left. + \frac{\alpha}{\pi} \left(\frac{\pi^2}{3} - 1 - 2 \log \left(1 - \frac{s_{\min}}{s} \right) + \log \frac{s_{\min}}{s} - \frac{s_{\min}}{s} \right) \right].\end{aligned}\tag{2.3.28}$$

The expression (2.3.27) is within 0.4% a good approximation to the line shape in the region $[M_Z - 3\Gamma_Z, M_Z + \Gamma_Z]$. It applies to the lepton and quark channels.

From the approximate formula (2.3.27) one can derive expressions for σ_{\max} , $\sqrt{s_{\max}}$ and $\sqrt{s_{\pm}}$. One finds [35]

$$\sigma_{\max} = \frac{C_R}{\widetilde{M}_Z^2 \gamma^2} \gamma^\beta (1 + \delta_1^{V+S}) \left\{ 1 + \frac{5}{48} \pi^2 \beta^2 - \frac{3}{4} \pi \beta \gamma + \frac{\gamma^{(2-\beta)} C'_Q}{C_R (1 + \delta_1^{V+S})} \right\},\tag{2.3.29}$$

$$\sqrt{s_{\max}} = M_Z \left[1 - \frac{1}{4} \gamma^2 + \frac{1}{8} \pi \beta \gamma \right],\tag{2.3.30}$$

$$\begin{aligned} \sqrt{s_{\pm}} &= M_Z \left[1 + \frac{1}{4} \pi \beta \gamma \left(1 + \beta - \frac{5}{4} \gamma + \frac{\gamma^{(2-\beta)} C'_Q}{C_R(1 + \delta_1^{V+S})} \right) \right] \\ &\pm \frac{\Gamma_Z}{2} \left[1 + \left(1 + \beta + \frac{1}{4} \pi \beta \right) \left(\frac{1}{4} \pi \beta + \frac{\gamma^{(2-\beta)} C'_Q}{C_R(1 + \delta_1^{V+S})} \right) + \frac{\beta}{2} \left(1 + \frac{\pi \beta}{4} \right) \log(2) \right]. \end{aligned} \quad (2.3.31)$$

An important feature of the above formulae is the enhanced importance of the one photon exchange diagram, on the one hand because the resonance peak is lowered by a factor γ^β and on the other hand because the one photon exchange diagram is enhanced by a factor C'_Q/C_Q ($= 1.657$ for muons). The cause for the former effect is the soft photon radiation, which is dominant when near resonance. The cause for the latter effect is the hard photon radiation, probing the $1/s$ photon propagator, present in the one photon exchange diagram. Also the photon radiation distorts the peak in such a way that below the maximum the slope of the peak becomes steeper, while at the same time above the maximum the cross section does not decrease as rapidly as before, as it becomes favorable to emit radiation. This in turn means that the influence of adding the one photon exchange diagram on $\sqrt{s_+}$ is considerably larger after convolution (i.e. $\sqrt{s_+}$ shifts more to the right), whereas the shift of $\sqrt{s_-}$ to the left, due to the QED channel, is reduced. This results in a shift of the average of $\sqrt{s_-}$ and $\sqrt{s_+}$ to the right and an increase of the distance between these half maximum positions.

References

- [1] D.Y. Bardin et al. in "Z physics at LEP 1", CERN 89-08, Vol 1, p.89, eds. G. Altarelli, R. Kleiss and C. Verzegnassi.
- [2] D.A. Ross, J.C. Taylor, Nucl. Phys. B51 (1973) 25;
G. Passarino and M. Veltman, Nucl. Phys. B160 (1979) 151;
A. Sirlin, Phys. Rev. D22 (1980) 2695.
- [3] G. 't Hooft, Phys. Lett. B37 (1971) 195.
F.J. Hasert et al., Phys. Lett. B46 (1973) 121.
- [4] G. Burgers and F. Jegerlehner in "Z Physics at LEP 1", CERN 89-08, Vol 1, p.55, eds. G. Altarelli, R. Kleiss and C. Verzegnassi.
- [5] W. Hollik, Fortschr. Phys. 38 (1990) 165.
- [6] M. Consoli, W. Hollik and F. Jegerlehner, Phys. Lett. B227 (1989) 167.
- [7] W. Beenakker and W. Hollik, Z. f. Phys. C40 (1988) 141.
- [8] A.A. Akhundov, D.Y. Bardin and T. Riemann, Nucl. Phys. B276 (1986) 1;
D.Y. Bardin, M.S. Bilenky, G. Mitselmakher, T. Riemann and M. Sachwitz, Z. f. Phys. C44 (1989) 493.

- [9] D.C. Kennedy, B.W. Lynn, C.J.-C. Im, R.G. Stuart, Nucl. Phys. B321 (1989) 83.
- [10] W. de Boer, 10th Warsaw Symposium on Elementary Particles, Kazimierz (1987).
- [11] T.H. Chang, K.J.F. Gaemers and W.L. van Neerven, Nucl. Phys. B202 (1982) 407.
- [12] F.A. Berends and R. Kleiss, Nucl. Phys. B260 (1985) 32.
- [13] P. Kalyniak, J.N. Ng and P. Zakarauskas, Phys. Rev. D29 (1984) 502; D30 (1984) 123;
E. Franco in Physics at LEP, CERN 86-02, p. 187, ed. by J. Ellis and R. Peccei.
- [14] ZSHAPE, authors W. Beenakker, F.A. Berends and S.C. van der Marck.
- [15] W. Wetzel, Nucl. Phys. B227 (1983) 1; Yellow Report CERN 86-02 (1986), 40.
- [16] F.A. Berends, G. Burgers, W. Hollik and W.L. van Neerven, Phys. Lett. B203 (1988) 177.
- [17] D.Y. Bardin, A. Leike, T. Riemann and M. Sachwitz, Phys. Lett. B206 (1988) 539.
- [18] A. Borrelli, M. Consoli, L. Maiani, R. Sisto, Nucl. Phys. B333 (1990) 357.
- [19] F.A. Berends, R. Kleiss and S. Jadach, Nucl. Phys. B202 (1982) 63.
- [20] D.Y. Bardin, O.M. Fedorenko, T. Riemann, Dubna preprint E2-87-663 (1987);
D.Y. Bardin, M.S. Bilenky, O.M. Fedorenko and T. Riemann, Dubna preprint E2-88-324 (1988).
- [21] S. Jadach, J.H. Kühn, R.G. Stuart and Z. Was, Z. Phys. C38 (1988) 609.
- [22] M. Greco, G. Pancheri-Srivastava and Y. Srivastava, Nucl. Phys. B171 (1980) 118;
E B197 (1982) 54²
- [23] F.A. Berends, G. Burgers and W.L. van Neerven, Nucl. Phys. B297 (1988) 429; E
Nucl. Phys. B304 (1988) 921.
- [24] G. Burgers in Polarization at LEP, CERN 88-06, p. 121, edited by G. Alexander, G. Altarelli, A. Blondel, G. Coignet, E. Keil, D.E. Plane and D. Treille.
- [25] E.A. Kuraev and V.S. Fadin, Sov. J. Nucl. Phys. 41 (1985) 466.
- [26] G. Altarelli and G. Martinelli, Yellow Report CERN 86-02 (1986) 47.
- [27] O. Nicrosini and L. Trentadue, Phys. Lett. B196 (1987) 551.
- [28] V.S. Fadin and V.S. Khoze, Sov. J. Nucl. Phys. 47 (1988) 1073.
- [29] F.A. Berends, G. Burgers and W.L. van Neerven, Phys. Lett. B177 (1986) 191.

- [30] R. Barbieri, J.A. Mignaco and E. Remiddi, *Nuovo Cim.* 11A (1972) 824, 865.
- [31] A. Devoto and D.W. Duke, *Riv. Nuovo Cim.* 7, No. 6 (1984).
- [32] F.A. Berends and R. Kleiss, *Nucl. Phys.* B177 (1981) 237.
- [33] R.N. Cahn, *Phys. Rev.* D36 (1987) 2666.
- [34] F. Aversa and M. Greco, *Phys. Lett.* B228 (1989) 134.
- [35] W. Beenakker, F.A. Berends and S.C. van der Marck, *Z. f. Phys.* C46 (1990) 687.

Chapter 3

Large angle Bhabha scattering

3.1 Introduction

Ever since electron positron collisions were studied Bhabha scattering has been measured. The purpose was twofold: to determine the luminosity from small angle scattering and to test QED from large angle scattering. Even at PETRA energies the electroweak contributions were still small. Generally speaking the radiative corrections were not exceeding the 10% level for standard experimental cuts on energy and acollinearity of the detected particles. First order radiative corrections were adequate.

At LEP/SLC energies Bhabha scattering again serves as a luminosity monitor at small angles and as a test of the electroweak theory at large angles. One may also be interested in it as a background for other physics signals. As an example, radiative Bhabha scattering may give rise to a single photon in a neutrino counting set-up. For all these different purposes different parts of the Bhabha scattering cross section play a dominant role and may get considerable contributions from radiative corrections.

For small angle Bhabha scattering the one photon t-channel contribution is the most dominant part. As far as the radiative corrections are concerned they are expected to be similar to those at lower energies. When experimental cuts are not too tight the corrections should be smaller than 10%. Complete first order calculations for LEP/SLC energies, also incorporating first order weak corrections, are available [1]. A priori the second order correction is not expected to be sizable, but the required experimental accuracy may force the theoretical calculations to be at the 0.5% level. In that case some studies of second order corrections are needed to assess the precision of first order corrections.

For large angle Bhabha scattering the s-channel Z exchange is dominant. This part certainly requires initial state second order QED corrections and higher order soft photon corrections. Also the weak corrections should be incorporated: in first order in the vertex corrections and up to and including second order in the imaginary part of the Z-self energy. This has been extensively discussed in line shape studies, see e.g. ref. [2]. For large angle Bhabha scattering the s-channel is mainly Z exchange and the t-channel mainly one photon exchange. So one has a resonance and a background term. This background

term is sizable and is not necessarily corrected in the same way as the resonance. One knows from μ pair production that the resonance undergoes a large negative correction, whereas the background (being here one photon exchange in the s -channel) gets a sizable positive correction. Since the background in Bhabha scattering is far more important than in μ pair production a detailed study of second order corrections to the whole Bhabha process is necessary. A required accuracy of 0.5% would bring the treatment of Bhabha scattering much closer to the line shape evaluations of other fermion processes. That is the main goal of this chapter. It means that the standard model can be tested in Bhabha scattering, or in other words, information on the Z partial width Γ_{ee} can be extracted with about the same accuracy as in the case of the other partial widths.

There are many ways to obtain some idea of the corrected Bhabha cross section. One may apply a first order event generator like in ref [1], or for small angle Bhabha scattering an event generator with multiple photon emission [3]. To first order calculations one may add some higher order effects from soft photons [4] like has been done for the J/ψ [5]. It is however hard to claim that those approaches reach an accuracy of 0.5% or even 1%, since they all make some unwanted approximations, e.g. not treating the electroweak corrections to the required accuracy or omitting $\mathcal{O}(\alpha^2)$ hard bremsstrahlung.

So we have to establish a strategy which goes beyond the previous evaluations. The most ideal solution would be to develop an event generator which takes into account the relevant weak corrections and generates events with many soft and at least two hard photons. It should also ideally generate these events in a large section of phase space so that it can be applied to small and large angle Bhabha scattering and to neutrino counting background calculations. Since the relevant peaking of radiative Bhabha scattering is quite different for those different applications it is a very demanding task to generate all these structures in one multipurpose event generator. Therefore we adopt a more modest strategy, which can give at least relevant results for some realistic situations.

Our main objective is to get a description of the Z -line shape in Bhabha scattering with an accuracy of 0.5%. The evaluation should incorporate reasonably realistic experimental cuts, like an angular range, a minimum energy of the detected particles and a maximum acollinearity between them. These cuts make the treatment of the Z -line shape in Bhabha scattering different and more complicated than in μ pair production. A semi analytical procedure, i.e. partly analytical partly numerical, should give a total Bhabha scattering cross section with these cuts. The evaluation should achieve the following goals. The weak corrections should be incorporated as in ref. [2], i.e. improving on the results of [1]. A complete first order QED correction should be implemented. Second order QED corrections should be included in the leading log approximation. Some soft photon effects should be taken into account in all orders. Both the second order QED corrections and the higher order soft photon ones are mainly relevant for initial state corrections. Note that in $\mathcal{O}(\alpha^2)$ the subleading logarithms are not taken into account in contrast to the pure s -channel total cross section evaluations of refs. [2] and [6]. Of course the QED corrections are dependent on the imposed cuts. The methods and input we employ are the following. For the weak corrections we rely on refs. [7, 8]. For the QED corrections we

use the structure function method for differential cross sections. For the implementation of cuts this is necessary. Although the structure function method has been applied to total s-channel cross sections in QED [9, 10, 11, 6], the application to differential cross sections has been far less studied. This chapter can be considered as a considerable extension of ref. [12] where corrections to some differential cross sections were discussed. A very large fraction of the chapter is devoted to this. Since we want to clarify what assumptions go into the calculations many details are given. With some simple changes the formalism can also be applied to the forward-backward asymmetry in $\mu\mu$ pairs and to small angle Bhabha scattering. These questions will be addressed in chapters 4 and 5.

The actual outline of this chapter is as follows. Section 3.2 presents the general formalism of the structure function method for multidifferential cross sections and exemplifies some difficulties in Bhabha scattering. Section 3.3 uses this formalism and shows how the specific experimental cuts can be implemented in the method. The addition of an acollinearity cut is discussed in section 3.4. Whereas so far only leading log terms were treated sections 3.5 and 3.6 discuss non log terms from the initial and final state radiation. Section 3.7 gives the specific details for the case of Bhabha scattering, whereas the results are discussed in section 3.8. Some relevant formulae are collected in an appendix.

3.2 The structure function method and a simple toy model

In this section we will review the steps that lead to the formulae for the total and some differential cross sections for $2 \rightarrow 2$ processes in the leading logarithm approximation (LLA) for QED corrections. Next we will discuss a way to impose certain specific cuts on the momenta of the two outgoing particles.

First we have to define the kinematics of the process at the Born level in a form suitable for higher order corrections. At a later point we will discuss how to calculate the QED corrections to that process. Consider therefore a purely fermionic $2 \rightarrow 2$ process and call the momenta of the two incoming particles p_1, p_2 and the momenta of the two outgoing particles p_3 and p_4 . Obviously energy-momentum conservation then takes on the form

$$p_1 + p_2 = p_3 + p_4 . \quad (3.2.1)$$

We will assume throughout this chapter that all four particles may be considered massless, except if this would give rise to collinear divergences:

$$p_i^2 = 0 \quad (i = 1, \dots, 4) . \quad (3.2.2)$$

In the center of mass frame of the incoming particles we can write

$$\begin{aligned} p_1^\mu &= \frac{1}{2}\sqrt{s}(1, 0, 0, 1) , \\ p_2^\mu &= \frac{1}{2}\sqrt{s}(1, 0, 0, -1) , \end{aligned} \quad (3.2.3)$$

where we defined $s = (p_1 + p_2)^2$, the energy of the incoming particles squared. Defining furthermore E_3 as the energy of p_3 in this frame, ϑ_3 as the angle between \vec{p}_3 and \vec{p}_1 , φ_3 as the azimuthal angle of \vec{p}_3 and likewise for p_4 , we have

$$\begin{aligned} p_3^\mu &= E_3 (1, \cos \varphi_3 \sin \vartheta_3, \sin \varphi_3 \sin \vartheta_3, \cos \vartheta_3) , \\ p_4^\mu &= E_4 (1, \cos \varphi_4 \sin \vartheta_4, \sin \varphi_4 \sin \vartheta_4, \cos \vartheta_4) . \end{aligned} \quad (3.2.4)$$

The ranges for these angles are $\vartheta_i \in [0, \pi]$ and $\varphi_i \in [0, 2\pi]$. The two particle phase space reads

$$\begin{aligned} dPS_2 &\equiv \frac{1}{(2\pi)^2} \frac{d^3\vec{p}_3}{2E_3} \frac{d^3\vec{p}_4}{2E_4} \delta^{(4)}(p_1 + p_2 - p_3 - p_4) = \\ &= \frac{E_3}{4(2\pi)^2 |\sin \vartheta_4 \sin \varphi_4|} dE_3 dE_4 d\cos \vartheta_3 d\cos \vartheta_4 d\varphi_3 d\varphi_4 \times \\ &\quad \delta\left(\varphi_4 - \arccos \frac{E_3 \sin \vartheta_3 \cos \varphi_3}{-E_4 \sin \vartheta_4}\right) \delta(\sqrt{s} - E_3 - E_4) \times \\ &\quad \delta(E_3 \sin \vartheta_3 \sin \varphi_3 + E_4 \sin \vartheta_4 \sin \varphi_4) \delta(E_3 \cos \vartheta_3 + E_4 \cos \vartheta_4) . \end{aligned} \quad (3.2.5)$$

In this equation we have defined the arccosine to be double valued, i.e. to have values in $[0, 2\pi]$. Integrating over the two azimuthal angles φ_3 and φ_4 using the cylindrical symmetry (choose e.g. $\varphi_3 = \pi/2$) and one of the δ -functions respectively (which determines φ_4 then to be $3\pi/2$), we arrive at

$$\begin{aligned} dPS_2 &= \frac{\pi E_3}{2(2\pi)^2 \sin \vartheta_4} dE_3 dE_4 d\cos \vartheta_3 d\cos \vartheta_4 \times \\ &\quad \delta(\sqrt{s} - E_3 - E_4) \delta(E_3 \sin \vartheta_3 - E_4 \sin \vartheta_4) \delta(E_3 \cos \vartheta_3 + E_4 \cos \vartheta_4) . \end{aligned} \quad (3.2.6)$$

Introducing the Mandelstam variables

$$\begin{aligned} t_1 &\equiv (p_1 - p_3)^2 = -E_3 \sqrt{s} (1 - \cos \vartheta_3) , \\ u_1 &\equiv (p_2 - p_3)^2 = -E_3 \sqrt{s} (1 + \cos \vartheta_3) , \\ t_2 &\equiv (p_2 - p_4)^2 = -E_4 \sqrt{s} (1 + \cos \vartheta_4) , \\ u_2 &\equiv (p_1 - p_4)^2 = -E_4 \sqrt{s} (1 - \cos \vartheta_4) , \end{aligned} \quad (3.2.7)$$

we can re-write dPS_2 in terms of these invariants:

$$dPS_2 = \frac{1}{8\pi s} dt_1 du_1 dt_2 du_2 \delta(s + t_1 + u_1) \delta(t_1 - t_2) \delta(u_1 - u_2) . \quad (3.2.8)$$

Incorporating the spin averaged square of the (Born) matrix element $|\mathcal{M}|^2$ corresponding to the particular process and the flux factor $1/(2s)$, the differential cross section (at Born level) becomes

$$\frac{d^4\sigma}{dt_1 du_1 dt_2 du_2} = \frac{1}{16\pi s^2} |\mathcal{M}|^2 \delta(s + t_1 + u_1) \delta(t_1 - t_2) \delta(u_1 - u_2) . \quad (3.2.9)$$

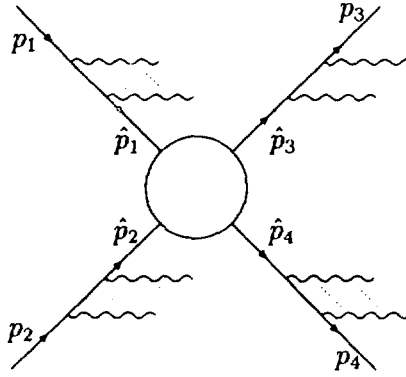


Fig. 3.1. A picturization of the mass factorization. The central circle denotes the hard scattering process.

This result coincides with the result given in [12], when we integrate over t_2 and u_2 (assuming they can have any value that is kinematically allowed, i.e. assuming we impose no cuts on the momentum p_4^μ), and when we identify $|\mathcal{M}|^2/(16\pi)$ with the σ_B occurring there.

So far we have only dealt with the $2 \rightarrow 2$ process. The question is how to calculate the QED corrections to eq.(3.2.9) in the LLA. This is done by allowing energy to be radiated off each of the 'external' momenta p_1, \dots, p_4 . The rate at which this happens is governed by the splitting functions. The splitting functions are related to the collinear divergences (or 'mass singularities') present in perturbative quantum field theories [13, 14]. These divergences take on the form

$$L_m = \log \frac{Q^2}{m^2} \quad , \quad Q^2 \gg m^2, \quad (3.2.10)$$

the so-called large logarithm of the scale Q^2 divided by the square of the mass m of the radiating particle. Because of the universality of the collinear divergences, the splitting functions are process independent. In this chapter we will only be concerned with those cases where the radiated energy is carried by photons, so that the particles that correspond to the external momenta do not change (i.e. we concern ourselves with diagonal splitting functions only).

This mechanism is illustrated by figure 3.1, where the circle in the center of the picture denotes the hard scattering $2 \rightarrow 2$ process, with modified momenta. These 'internal momenta' are given by

$$\begin{aligned} \hat{p}_i &= x_i p_i & i &= 1, 2 \\ \hat{p}_i &= \frac{1}{x_i} p_i & i &= 3, 4. \end{aligned} \quad (3.2.11)$$

The fractions x_i determine how much energy is lost. We will have to integrate over these fractions. One can also define invariants using the \hat{p}_i , which are related to the previous ones by

$$\begin{aligned}\hat{s} &= x_1 x_2 s , \\ \hat{t}_1 &= \frac{x_1}{x_3} t_1 , \quad \hat{u}_1 = \frac{x_2}{x_3} u_1 , \\ \hat{t}_2 &= \frac{x_2}{x_4} t_2 , \quad \hat{u}_2 = \frac{x_1}{x_4} u_2 .\end{aligned}\tag{3.2.12}$$

The mass factorization theorem then states [15]

$$\frac{s^4 d^4 \sigma}{dt_1 du_1 dt_2 du_2} = \int_0^1 \frac{dx_1}{x_1^2} \int_0^1 \frac{dx_2}{x_2^2} \int_0^1 \frac{dx_3}{x_3^2} \int_0^1 \frac{dx_4}{x_4^2} \Gamma(x_1) \Gamma(x_2) \mathcal{D}(x_3) \mathcal{D}(x_4) \frac{\hat{s}^4 d^4 \hat{\sigma}}{d\hat{t}_1 d\hat{u}_1 d\hat{t}_2 d\hat{u}_2}.\tag{3.2.13}$$

The $\Gamma(x_i)$ are the splitting functions, used for the initial state radiation, the $\mathcal{D}(x_i)$ are the fragmentation functions, used for the final state radiation. The $\hat{\sigma}$ stands for the so-called reduced cross section, which is free of collinear divergences and hence does not contain the logarithm L_m . This reduced cross section in general contains ϑ -functions reflecting kinematical constraints to make the process possible. These ϑ -functions can yield restrictions on the x_i .

This method is taken over from QCD, where $\hat{\sigma}$ is the 'mass factorized' cross section, which does not contain any collinear poles (for these are absorbed in the splitting functions), but which does depend on the mass factorization scale Q^2 . We now apply the inverse of the mass factorization method to predict the large logarithms for the QED corrected cross section σ . For the generic form of the splitting functions we refer to [12]. Here we restrict ourselves to the LLA, which means that for $\mathcal{O}(\alpha^i)$ corrections in the final result for σ we only consider the terms proportional to L_m^i . This implies that in the LLA the reduced cross section $\hat{\sigma}$ should not contain QED corrections and therefore is identical to the Born approximation. Moreover, in the LLA the $\Gamma(x_i)$ and the $\mathcal{D}(x_i)$ are identical. Up to second order in α , the form of the diagonal part of Γ is, in the LLA

$$\Gamma(x) = \delta(1-x) + \frac{\alpha Q_f^2}{2\pi} P_{ff}(x) L_m + \frac{1}{2} \left(\frac{\alpha Q_f^2}{2\pi} \right)^2 (P_{ff} \otimes P_{ff})(x) L_m^2.\tag{3.2.14}$$

Here L_m is the large logarithm as in eq.(3.2.10) and Q_f is the fractional charge of the radiating light fermion (which we will leave out when considering electrons or muons, since then $Q_f^2 = 1$). The choice of the scale Q^2 in L_m is a non-trivial one, the justification of which can be found in an exact calculation. For numerical studies the applied scale need not be identical to the one that is justified this way, thus mimicking non-leading log effects. This might bring the numerical result of a LL calculation closer to the result of

an exact calculation. The function P_{ff} is the Altarelli-Parisi splitting function [16] and has the form

$$P_{ff}(x) = \delta(1-x) \left[\frac{3}{2} + 2 \log \varepsilon \right] + \vartheta(1-x-\varepsilon) \frac{1+x^2}{1-x}. \quad (3.2.15)$$

The first term represents the virtual and soft photon corrections, whereas the second term is due to hard photon emission. The variable ε is the soft photon cut-off, which drops out in the end result. The convolution symbol \otimes is defined by

$$(f \otimes g)(x) \equiv \int_0^1 dx_1 \int_0^1 dx_2 f(x_1)g(x_2) \delta(x - x_1 x_2). \quad (3.2.16)$$

For the hard $2 \rightarrow 2$ process we can use eq.(3.2.9), with all invariants replaced by their 'hatted' counterparts. Using eq.(3.2.12) to eliminate the 'hats', one finds

$$\frac{\hat{s}^4 d^4 \hat{\sigma}}{d\hat{t}_1 d\hat{u}_1 d\hat{t}_2 d\hat{u}_2} = \frac{s^2}{16\pi} |\widehat{\mathcal{M}}|^2 x_1^2 x_2^2 x_3^2 x_4^2 \times \delta(x_1 x_2 x_3 s + x_1 t_1 + x_2 u_1) \delta(x_1 x_4 t_1 - x_2 x_3 t_2) \delta(x_2 x_4 u_1 - x_1 x_3 u_2). \quad (3.2.17)$$

Inserting this in eq.(3.2.13) results in

$$\frac{s^4 d^4 \sigma}{dt_1 du_1 dt_2 du_2} = \int_0^1 dx_1 \int_0^1 dx_2 \int_0^1 dx_3 \int_0^1 dx_4 \Gamma(x_1) \Gamma(x_2) \mathcal{D}(x_3) \mathcal{D}(x_4) \frac{x_3 s^2}{16\pi} |\widehat{\mathcal{M}}|^2 \times \delta(x_1 x_2 x_3 s + x_1 t_1 + x_2 u_1) \delta(x_1 x_4 t_1 - x_2 x_3 t_2) \delta(x_2 x_4 u_1 - x_1 x_3 u_2). \quad (3.2.18)$$

In this formula it is implicitly understood that the matrix element $\widehat{\mathcal{M}}$ describes the hard scattering process $\hat{p}_1, \hat{p}_2 \rightarrow \hat{p}_3, \hat{p}_4$. Using energy-momentum conservation for these momenta one can write $|\widehat{\mathcal{M}}|^2$ as a function of \hat{s} and \hat{t}_1 only.

Equation (3.2.18) can be used as a starting point for a number of different kinds of calculations. As an introduction let us consider the situation where we are interested in the one-particle inclusive differential cross section with respect to $\cos \vartheta_3$, i.e. $d\sigma/d \cos \vartheta_3$, where all other variables have been integrated over, imposing no cuts. The fact that we impose no cut on the energies of the outgoing particles implies that we can take $\mathcal{D}(x) = \delta(1-x)$, for the integral of $\mathcal{D}(x)$ over the full x range will yield unity anyway, as one should expect on the basis of the KLN theorem [14]. On top of that we can integrate over the variables t_2 and u_2 using two of the δ -functions. We obtain, maintaining the fragmentation function for p_3 for the moment

$$\frac{s^2 d^2 \sigma}{dt_1 du_1} = \int_0^1 \frac{dx_1}{x_1} \int_0^1 \frac{dx_2}{x_2} \int_0^1 \frac{dx_3}{x_3} \Gamma(x_1) \Gamma(x_2) \mathcal{D}(x_3) \frac{1}{16\pi} |\widehat{\mathcal{M}}|^2 \delta(x_1 x_2 x_3 s + x_1 t_1 + x_2 u_1). \quad (3.2.19)$$

Changing the variables back to E_3 and $\cos \vartheta_3$ we get

$$\frac{d^2\sigma}{dE_3 d\cos\vartheta_3} = \int_0^1 \frac{dx_1}{x_1} \int_0^1 \frac{dx_2}{x_2} \int_0^1 \frac{dx_3}{x_3} \Gamma(x_1)\Gamma(x_2)\mathcal{D}(x_3) \frac{E_3}{8\pi s} |\widehat{\mathcal{M}}|^2 \quad (3.2.20)$$

$$\times \delta\left(x_1 x_2 x_3 s - E_3 \sqrt{s} [x_1(1 - \cos\vartheta_3) + x_2(1 + \cos\vartheta_3)]\right),$$

so that, having integrated over the full E_3 range using the one remaining δ -function and setting $\mathcal{D}(x_3) = \delta(1 - x_3)$

$$\frac{d\sigma}{d\cos\vartheta_3} = \int_0^1 dx_1 \int_0^1 dx_2 \Gamma(x_1)\Gamma(x_2) \frac{1}{[x_1(1 - \cos\vartheta_3) + x_2(1 + \cos\vartheta_3)]^2} \frac{|\widehat{\mathcal{M}}|^2}{8\pi s}. \quad (3.2.21)$$

Having written $|\widehat{\mathcal{M}}|^2$ in terms of \hat{s} and \hat{t}_1 , we note from the δ -function in eq.(3.2.20), that \hat{t}_1 can be expressed in our integration variables as

$$\hat{t}_1 = \frac{x_1 t_1}{x_3} = \frac{-x_1^2 x_2 s (1 - \cos\vartheta_3)}{x_1(1 - \cos\vartheta_3) + x_2(1 + \cos\vartheta_3)}. \quad (3.2.22)$$

Since we intend to calculate corrections to Bhabha scattering we want to investigate the corrections to the pure t channel, as a toy model. Set therefore $|\widehat{\mathcal{M}}|^2 = 64\pi^2 \alpha^2 \hat{s}^2 / \hat{t}_1^2 \vartheta(\hat{s} - 4m_e^2)$. We are left with the integral

$$\frac{d\sigma}{d\cos\vartheta_3} = \frac{8\pi\alpha^2}{s} \frac{1}{(1 - \cos\vartheta_3)^2} \int_0^1 dx_1 \int_0^1 dx_2 \Gamma(x_1)\Gamma(x_2) \frac{1}{x_1^2} \vartheta(x_1 x_2 s - 4m_e^2). \quad (3.2.23)$$

Calculating this integral to one order in α , one finds

$$\frac{d\sigma}{d\cos\vartheta_3} = \frac{8\pi\alpha^2}{s} \frac{1}{(1 - \cos\vartheta_3)^2} \left[1 + \frac{\alpha}{2\pi} L_m \left(4 \log(1 - x_{min}) - \log x_{min} + \frac{1}{2} + \frac{1}{x_{min}} + x_{min} + \frac{1}{2} x_{min}^2 \right) \right]. \quad (3.2.24)$$

Here x_{min} is the lower bound on the integration variables x_1 and x_2 . Without any cuts (except possibly on $\cos\vartheta_3$, that we still may or may not integrate over), this lower bound is given by $4m_e^2/s$. For specific values of $\cos\vartheta_3$ however, the lower bound can get of the order m_e/\sqrt{s} . The corrections in eq.(3.2.24) will diverge as $1/x_{min}$, which at least is of the order \sqrt{s}/m_e ! This is significantly more severe than a logarithmic divergence, which one knows to be present in such cases. Therefore something will have to be changed to remove this behavior, which renders the calculation useless. As will become clear in the remainder of this chapter, the $1/x$ divergence is avoided by requiring the other particle to have a non-vanishing angle with the incoming beams as well. That is, the $1/x$ behavior can be seen as a remainder of the $1/(1 + \cos\vartheta_4)^2$ pole of the matrix element

squared, which we integrated over (by integrating over the full range of t_2 and u_2). This means that we have to impose an angular cut on both outgoing particles at the same time, when calculating the radiative corrections to a process with (photonic) t-channel scattering. Therefore our calculation for Bhabha scattering requires cuts on both the outgoing particles.

3.3 Incorporating cuts in the LL calculation

In the previous section we argued that we need cuts on the momenta of both outgoing particles, so in this section we present a way to do this for the structure function method. The applied cuts are symmetric in two ways: we apply the same cuts for either particle and we require the same *minimum* angular separation with either of the incoming beams. To be specific we demand

$$\begin{cases} E_{3,4} > E_0, \\ |\cos \vartheta_{3,4}| < c_m = \cos \vartheta_{min}. \end{cases} \quad (3.3.1)$$

The quantity E_0 is the minimum energy of the outgoing particles and ϑ_{min} their minimum separation angle with the beam axis. In terms of the invariants this means at least

$$-\frac{1}{2}s(1+c_m) < t_{1,2}, u_{1,2} < -E_0\sqrt{s}(1-c_m). \quad (3.3.2)$$

However this is not the full story. Due to the relations between the invariants, the allowed region for e.g. u_1 will depend on the value for t_1 . It is easy to deduce that

$$\max\left(-s-t_1, t_1 \frac{1+c_m}{1-c_m}\right) < u_1 < \min\left(-2E_0\sqrt{s}-t_1, t_1 \frac{1-c_m}{1+c_m}\right). \quad (3.3.3)$$

The calculation of the total cross section starts from the multi-differential one given by eq.(3.2.18). Cuts are incorporated by setting the integrand to zero if one or more of the invariants lie outside the above intervals. This we do by multiplying the integrand with ϑ -functions:

$$\begin{aligned} & \vartheta(s+t_1+u_1) \vartheta\left(u_1-t_1 \frac{1+c_m}{1-c_m}\right) \times \\ & \vartheta(-u_1-t_1-2E_0\sqrt{s}) \vartheta\left(-u_1+t_1 \frac{1-c_m}{1+c_m}\right) \end{aligned} \quad (3.3.4)$$

and similarly for t_2, u_2 . We now have a multi-dimensional integral over a rather non-trivial integration volume. There are of course many ways to solve this problem, one of which we describe in this section. The order of integration can make a lot of difference. We discuss one particular order, in which the integration volume is most easily expressed. The discussion of this integration will unavoidably be technical.

This specific order is only suited to calculate the total cross section, though up to this point all results are suited to calculate differential cross sections as well. We integrate over u_1 , t_2 and u_2 , using the three δ -functions. Note to this end that

$$x_3 \delta(x_1 x_2 x_3 s + x_1 t_1 + x_2 u_1) \delta(x_1 x_4 t_1 - x_2 x_3 t_2) \delta(x_2 x_4 u_1 - x_1 x_3 u_2) = \frac{1}{x_1 x_2^2 x_3} \delta\left(u_1 - \left[-x_1 x_3 s - \frac{x_1}{x_2} t_1\right]\right) \delta\left(t_2 - \left[\frac{x_1 x_4}{x_2 x_3} t_1\right]\right) \times \delta\left(u_2 - \left[-x_2 x_4 s - \frac{x_4}{x_3} t_1\right]\right), \quad (3.3.5)$$

from which the expressions for u_1 , t_2 and u_2 in terms of the remaining integration variables can be read off. Care has to be given to the ϑ -functions. The difference with the situation before the integration is that in the ϑ -functions we have replaced u_1 , t_2 and u_2 by the expressions given by eq.(3.3.5).

The ϑ -functions in (3.3.4) and the ones for t_2 and u_2 , give 8 ϑ -functions in our integrand, whereas we have only 5 integration variables. This might suggest that there are a few obsolete ones. This depends on the integration order. The choice is first to integrate over x_3 and x_4 (the relative order of these two not being relevant), then over \hat{t}_1 and finally over x_1 and x_2 . The boundaries on those integration variables are, defining $\hat{E}_0 = E_0 / (\frac{1}{2}\sqrt{s})$

$$x_{3,min} = \frac{\hat{E}_0}{x_1 - \frac{\hat{t}_1}{s} \frac{1 - x_1/x_2}{x_1}}, \quad x_{4,min} = \frac{\hat{E}_0}{x_2 + \frac{\hat{t}_1}{s} \frac{1 - x_1/x_2}{x_1}}. \quad (3.3.6)$$

The lower boundaries on x_3 and x_4 therefore depend on \hat{t}_1 , which is possible, because we integrate over \hat{t}_1 later. The boundaries for \hat{t}_1 in turn depend on the values of x_1 and x_2 :

$$\hat{t}_{1,min} = \begin{cases} \max\left(\frac{-x_1 x_2 s}{1 + \frac{x_1}{x_2} \frac{1 - c_m}{1 + c_m}}, x_1 s \frac{x_1 - \hat{E}_0}{1 - x_1/x_2}\right) & \text{for } x_1 > x_2, \\ \max\left(\frac{-x_1^2 s}{\frac{x_1}{x_2} + \frac{1 - c_m}{1 + c_m}}, -x_1 s \frac{x_2 - \hat{E}_0}{1 - x_1/x_2}\right) & \text{for } x_1 < x_2, \end{cases} \quad (3.3.7)$$

$$\hat{t}_{1,max} = \begin{cases} \min\left(\frac{-x_1^2 s}{\frac{x_1}{x_2} + \frac{1 + c_m}{1 - c_m}}, -x_1 s \frac{x_2 - \hat{E}_0}{1 - x_1/x_2}\right) & \text{for } x_1 > x_2, \\ \min\left(\frac{-x_1 x_2 s}{1 + \frac{x_1}{x_2} \frac{1 + c_m}{1 - c_m}}, x_1 s \frac{x_1 - \hat{E}_0}{1 - x_1/x_2}\right) & \text{for } x_1 < x_2. \end{cases}$$

The integration over x_1 and x_2 therefore separates into two distinct regions, which are related by the interchange $x_1 \leftrightarrow x_2$. Also the lower boundaries for x_3 and x_4 interchange under $x_1 \leftrightarrow x_2$. Furthermore it can be shown that given the values for x_1 and x_2 either the first or the second 'column' in eq.(3.3.7) yields the most restrictive boundaries for both $\hat{t}_{1,\min}$ and $\hat{t}_{1,\max}$. The boundaries on x_1 and x_2 are given by the requirements

$$\begin{aligned} \frac{x_{1,2}}{x_{2,1}} &> \frac{1 - c_m}{1 + c_m} \quad , \\ x_1 + x_2 &> 2\hat{E}_0 \quad , \end{aligned} \quad (3.3.8)$$

$$\text{implying} \quad x_{1,2} > \hat{E}_0(1 - c_m) \quad .$$

This results in the following general expression for a total cross section under the specified cuts:

$$\begin{aligned} \sigma = \frac{1}{s^2} \int_{x_{1,\min}}^1 \frac{dx_1}{x_1^2} \int_{x_{2,\min}}^1 \frac{dx_2}{x_2^2} \Gamma(x_1)\Gamma(x_2) \int_{\hat{t}_{1,\min}}^{\hat{t}_{1,\max}} d\hat{t}_1 \frac{|\mathcal{M}|^2(x_1 x_2 s, \hat{t}_1)}{16\pi} \\ \times \int_{x_{3,\min}}^1 dx_3 \mathcal{D}(x_3) \int_{x_{4,\min}}^1 dx_4 \mathcal{D}(x_4) \quad . \end{aligned} \quad (3.3.9)$$

Here we have written the result as compactly as possible, but it needs an additional remark. As all the integration boundaries stem from the ϑ -functions, the integrals have to be defined to be zero as soon as the lower boundary is larger than the upper boundary, since then the product of the two ϑ -functions vanishes. That is, the more correct way to write the integrals would be

$$\int_{-\hat{s}}^0 d\hat{t}_1 \vartheta(\hat{t}_1 - \hat{t}_{1,\min}) \vartheta(-\hat{t}_1 + \hat{t}_{1,\max}) \quad \text{instead of} \quad \int_{\hat{t}_{1,\min}}^{\hat{t}_{1,\max}} d\hat{t}_1 \quad . \quad (3.3.10)$$

Furthermore in eq.(3.3.9) we have explicitly indicated in terms of which variables the matrix element squared has to be written in order to use this equation.

Using this result we can come back to the toy model of the previous section, i.e. a matrix element squared $|\widehat{\mathcal{M}}|^2 = 64\pi^2\alpha^2\hat{s}^2/\hat{t}_1^2$. As in the previous section we will impose no cut on the energy of the outgoing particles, so we will leave out the final state radiation. Also the boundaries for \hat{t}_1 in eq.(3.3.7) simplify by taking $E_0 = 0$. In first order in α , when at least $x_1 = 1$ or $x_2 = 1$ we can combine the x_1 and the x_2 integral into one integral over x

$$\sigma = \frac{1}{s^2} \int_{x_{\min}}^1 \frac{dx}{x^2} \left[\delta(1-x) + \frac{\alpha L_m}{\pi} P_{ee}(x) \right] \int_{\hat{t}_{1,\min}}^{\hat{t}_{1,\max}} d\hat{t}_1 4\pi\alpha^2 \frac{x^2 s^2}{\hat{t}_1^2} \quad (3.3.11)$$

$$= 4\pi\alpha^2 \int_{x_{min}}^1 dx \left[\delta(1-x) + \frac{\alpha L_m}{\pi} P_{ee}(x) \right] \left(\frac{1+x\frac{1+c_m}{1-c_m}}{xs} - \frac{x+\frac{1-c_m}{1+c_m}}{x^2s} \right).$$

In the last line we carried out the \hat{t}_1 integration and used its boundaries for $E_0 = 0$. The integral over x yields

$$\sigma = \frac{4\pi\alpha^2}{s} \left\{ \frac{4c_m}{1-c_m^2} + \frac{\alpha L_m}{\pi} \left[\frac{8c_m}{1-c_m^2} \log(1-x_{min}) + \frac{1+c_m}{1-c_m} \left(x_{min} + \frac{1}{2}x_{min}^2 \right) + \frac{1-c_m}{1+c_m} \left(-\frac{1}{2} - \frac{1}{x_{min}} + \log x_{min} \right) \right] \right\}. \quad (3.3.12)$$

The Born term here obviously is the one in eq.(3.2.24), integrated over $\cos\vartheta_3$ from $-c_m$ to c_m . In the first order corrections we again have a term $1/x_{min}$. But fortunately there is a significant difference in the way this term appears compared to eq.(3.2.24) and in the value x_{min} now has. Both differences are due to the one extra cut we imposed: that also the vector \vec{p}_4 has an angle with the beam axis between ϑ_{min} and $180^\circ - \vartheta_{min}$. The difference in the $1/x_{min}$ term is the factor $(1-c_m)/(1+c_m)$ in front. Moreover the value for x_{min} can be obtained from eqs.(3.3.8), knowing that either $x_1 = 1$ or $x_2 = 1$ (and using $E_0 = 0$). We find

$$x_{min} = \frac{1-c_m}{1+c_m}. \quad (3.3.13)$$

Hence the incorporation of cuts automatically leads to a lower bound on x at $\mathcal{O}(\alpha)$. Therefore the $\vartheta(\hat{s} - 4m_e^2)$ that was used in section 3.2 is not needed here.

The $1/x_{min}$ term now is of order unity times $\alpha L_m/\pi$ and therefore does not pose a problem any more. Of course the limit $c_m \rightarrow 1$ cannot be taken, but that is a characteristic of photonic t-channel scattering, already at the Born level.

At this point we address the question how to use eq.(3.3.9) in a practical situation for numerical results for a total cross section. Generally speaking the problem is that we still have 5 integrations. Doing all 5 analytically would be very hard, if only for the difficulties the boundaries present. Performing them numerically also poses many problems, especially because the order of integration is so important, in connection with the form of the integration boundaries. This makes this formulation rather unfit for a 5-dimensional Monte Carlo integration, unless one is able to map the variables more conveniently. Therefore a combination of analytical and numerical integrations is probably the best solution.

Thus the first integration to do analytically is the integration over x_3 and x_4 . It has to be decided then to which order in α we want to calculate the leading log final state corrections. We will calculate the first and second order corrections. The first order corrections have to be convoluted with the initial state corrections and hence have to be calculated for arbitrary x_1 and x_2 values. For the second order corrections it is sufficient to convolute without initial state corrections. Therefore these corrections can be calculated

for $x_1 = x_2 = 1$. Calculating the first order final state corrections for arbitrary x_1 and x_2 we have

$$\int_{x_{3,\min}}^1 dx_3 \mathcal{D}(x_3) \int_{x_{4,\min}}^1 dx_4 \mathcal{D}(x_4) = 1 + \frac{\alpha}{2\pi} L_m \left[2 \log(1 - x_{3,\min}) + 2 \log(1 - x_{4,\min}) + x_{3,\min} + x_{4,\min} + \frac{1}{2} x_{3,\min}^2 + \frac{1}{2} x_{4,\min}^2 \right]. \quad (3.3.14)$$

The lower boundaries $x_{3,\min}$ and $x_{4,\min}$ are given by eqs.(3.3.6). From the dependence on \hat{t}_1 in these boundaries it is immediately clear that the integral over \hat{t}_1 will be more involved when including these first order final state corrections. If however we set the energy cut E_0 to zero, we have $x_{3,\min} = x_{4,\min} = 0$ and hence all first order final state corrections vanish. This property holds to all orders in a LL calculation, as is guaranteed by the KLN theorem [14].

The second order final state corrections for $x_1 = x_2 = 1$ have the form

$$\frac{1}{2} \left(\frac{\alpha L_m}{\pi} \right)^2 \left[-2\zeta(2) + 2\text{Li}_2(1 - \hat{E}_0) + 2\hat{E}_0(2 + \hat{E}_0) \log(1 - \hat{E}_0) + 4 \log^2(1 - \hat{E}_0) - \frac{3}{4} \hat{E}_0(2 + \hat{E}_0) \log \hat{E}_0 + \hat{E}_0 + \frac{5}{8} \hat{E}_0^2 + \frac{1}{2} \hat{E}_0^3 + \frac{1}{8} \hat{E}_0^4 \right] \quad (3.3.15)$$

times the Born cross section. For $\hat{E}_0 = 0$ the KLN result is recovered. For realistic \hat{E}_0 values these corrections are tiny, e.g. for $\hat{E}_0 = \frac{1}{2}$ we find -0.1% times the Born cross section.

We want to postpone the discussion of the \hat{t}_1 -integration, for this depends strongly on the matrix element squared for the process at hand. It suffices to say here that we will opt to do this integration analytically. The last integrations are the ones over x_1 and x_2 . These we will do numerically. Again we have to decide to what order we want to calculate the corrections, for this is independent from our choice for the final state corrections. Again however we will discuss the possibilities to calculate second order corrections, because in some cases the initial state corrections are very large [2]. Moreover as in some of these cases these corrections mainly come from soft photon radiation, we will discuss soft photon exponentiation as well.

The integral over x_1 and x_2 has an integrand that is a function of x_1 and x_2 separately. Note that in the matrix element squared the dependence is only on $x_1 x_2$, but that in the integration boundaries for \hat{t}_1 , x_3 and x_4 , see eqs.(3.3.6) and (3.3.7), x_1 and x_2 do occur separately, though it is arranged in such a way that the integrand is symmetric under $x_1 \leftrightarrow x_2$ (due to a property of the integration boundaries that was noted before). As will become clear this is a disadvantage when calculating these integrals. Therefore we will separate the integral into a part that includes the dominant part of the corrections and that is a function of $x_1 x_2$ only and a part that includes the rest. That is, we write

$$\int_0^1 dx_1 \int_0^1 dx_2 \Gamma(x_1) \Gamma(x_2) f(x_1, x_2) = \int_0^1 dx_1 \int_0^1 dx_2 \Gamma(x_1) \Gamma(x_2) [f(x_1 x_2, 1) +$$

$$f(x_1, x_2) - f(x_1 x_2, 1)]. \quad (3.3.16)$$

The integration over the fractions $x_{1,2}$ is over the full range from 0 to 1, because the ϑ -function constraints are included in the function f . The first term in eq.(3.3.16) is the dominant part. The last terms cancel when $x_1 = 1$ or $x_2 = 1$ or both, and thus contributes only to the second and higher order hard photon corrections. The first term can be written as a one-dimensional integral

$$\int_0^1 dx_1 \int_0^1 dx_2 \Gamma(x_1) \Gamma(x_2) f(x_1 x_2, 1) = \int_0^1 dz \varphi(z) f(z, 1), \quad (3.3.17)$$

where we defined (having an e^+e^- initial state)

$$\begin{aligned} \varphi(z) &\equiv \int_0^1 dx_1 \int_0^1 dx_2 \Gamma(x_1) \Gamma(x_2) \delta(z - x_1 x_2) \\ &= \delta(1 - z) + \frac{\alpha}{\pi} P_{ee}(z) L_m + \frac{1}{2} \left(\frac{\alpha}{\pi} \right)^2 (P_{ee} \otimes P_{ee})(z) L_m^2. \end{aligned} \quad (3.3.18)$$

Again we only considered the diagonal splitting functions up to and including order α^2 . It is this dominant part where soft photon exponentiation can be carried out. This can be done by using the following form for $\varphi(z)$:

$$\begin{aligned} \varphi_{e\text{expon}}(z) &= \frac{\exp\left(\frac{3\alpha}{2\pi} L_m\right) \exp(-\beta\gamma E)}{\Gamma(1 + \beta)} \beta(1 - z)^{-1 + \beta} \\ &\quad + \frac{\alpha}{\pi} \delta_1^H(z) + \left(\frac{\alpha}{\pi} \right)^2 \delta_2^H(z) \\ &= \beta(1 - z)^{-1 + \beta} \left[1 + \frac{\alpha}{\pi} \delta_1^{VS} + \left(\frac{\alpha}{\pi} \right)^2 \delta_2^{VS} \right] \\ &\quad + \frac{\alpha}{\pi} \delta_1^H(z) + \left(\frac{\alpha}{\pi} \right)^2 \delta_2^H(z), \end{aligned} \quad (3.3.19)$$

with

$$\begin{aligned} \delta_1^{VS} &= \frac{3}{2} L_m, \\ \delta_2^{VS} &= \left(\frac{9}{8} - \frac{\pi^2}{3} \right) L_m^2, \\ \delta_1^H &= -(1 + z) L_m, \\ \delta_2^H &= \left(-\frac{1 + z^2}{1 - z} \log z + (1 + z) \left[-2 \log(1 - z) + \frac{1}{2} \log z \right] - \frac{1}{2} z - \frac{5}{2} \right) L_m^2, \\ \beta &= \frac{2\alpha}{\pi} L_m. \end{aligned} \quad (3.3.20)$$

Expanding the first form of eq.(3.3.19) yields the second one, which starts to deviate in $\mathcal{O}(\alpha^3)$. In the first form the $\Gamma(1 + \beta)$ stands for the Γ -function, not for a splitting function. To avoid any confusion we will not use the Γ -function in the remainder. Notice that the form $(1 - z)^{-1+\beta}$ contains a tail into the hard photon part. Therefore this is the soft photon distribution extended over all photon energies.

The part with $f(x_1, x_2) - f(x_1 x_2, 1)$ is a 2-dimensional integral that cannot be reduced to a 1-dimensional one. Therefore exponentiation in terms of one variable is not possible for this term. But for this term it is not needed either, since it exhibits no soft photon peaking behavior that needs to be resummed. If therefore soft photon exponentiation has to be performed for a specific problem, it is sufficient to perform it for the term on the first line of eq.(3.3.16).

This completes our general discussion on the calculation of the LL corrections for a total cross section applying the cuts specified in eq.(3.3.1). We can summarize the result as follows. The first step is to calculate, preferably analytically, the \hat{t}_1 -integral of the square of the (process dependent) matrix element times the (universal) factor given by (3.3.14). A final result then arises from performing (e.g. numerically) a one-dimensional integral of this intermediate result times a 'flux function' ($\varphi(z)$). If higher order corrections on the initial state are needed, one has to calculate a two-dimensional integral as well, though over a non-dominant hard photon part. Soft photon exponentiation is possible. This method is applicable to photonic t-channel scattering processes, for which cuts are essential. For a specific process one now has to specify the matrix element and the scale Q^2 appearing in the logarithm L_m .

In the following section we will treat the question of incorporating an additional cut, namely on the acollinearity, within the framework of this type of LL calculation.

3.4 Incorporating an acollinearity cut

It is possible to incorporate yet another cut in the calculation of the LL correction: a cut on the acollinearity of the final state fermions. Though the treatment of this cut is rigorous, as is the treatment of the cuts on the angles and the energies, it is dealt with in a different way. Therefore we devote a separate section to it.

First let us define the acollinearity ζ

$$\zeta \equiv |\pi - \angle(\vec{p}_3, \vec{p}_4)| . \quad (3.4.1)$$

The variables in which this quantity can be expressed in the LLA are the angles of \vec{p}_3 and \vec{p}_4 with the beam axis. The cosines of these angles depend on our integration variables:

$$\begin{aligned} \cos \vartheta_3 &= 1 - 2 \left[1 - \frac{x_1}{x_2} - \frac{x_1^2 s}{\hat{t}_1} \right]^{-1} , \\ \cos \vartheta_4 &= -1 + 2 \left[1 - \frac{x_2}{x_1} - \frac{x_2^2 s}{\hat{t}_1} \right]^{-1} . \end{aligned} \quad (3.4.2)$$

The difference in sign is due to the fact that both angles are defined with respect to the same direction (i.e. \vec{p}_1) and that \vec{p}_3 and \vec{p}_4 have to lie back to back at Born level. The acollinearity is then given, in this LL approach, by

$$\zeta = |\zeta'|, \quad \zeta' \equiv \pi - \vartheta_3 - \vartheta_4. \quad (3.4.3)$$

The angles $\vartheta_{3,4}$ lying in the interval $[0, \pi]$, the acollinearity has its values in $[0, \pi]$ as well. The azimuthal angles do not play a rôle here because that information is lost in the leading log approach. Although we in principle have an analytical formula for the acollinearity in terms of the integration variables, using eqs.(3.4.2) and (3.4.3), the sum of two arccosines in that formula makes it impossible to invert that relation straightaway. In the actual numerical calculation the inversion will be done numerically. For the discussion it is useful to introduce the quantity

$$\Delta c \equiv \cos \vartheta_3 + \cos \vartheta_4,$$

that obviously will not contain these arccosines:

$$\Delta c = 2 \frac{(x_2 - x_1)(x_1 + x_2)}{x_1 x_2} \frac{\hat{t}_1}{(1 - x_1/x_2 - x_2/x_1)\hat{t}_1 + x_1 x_2 s + \hat{t}_1^2 / (\hat{t}_1 + x_1 x_2 s)}. \quad (3.4.4)$$

The method to incorporate a cut on the acollinearity hinges on the fact that the variable ζ' is a monotonously increasing function of the quantity Δc . This enables us to determine the maxima and minima of ζ' by determining the ones of Δc . This we do by considering the derivative of Δc with respect to \hat{t}_1 , at fixed x_1 and x_2 . The minima and maxima of ζ' give the ones for the acollinearity ζ . Together with the zeroes of ζ , that correspond to the zeroes of Δc , we have all the ingredients we need. First a few remarks on the expression for Δc are in order.

In the LL approach the incoming particles with momenta p_1 and p_2 radiate off some energy and retain only $x_1 p_1$ and $x_2 p_2$ of their momenta. Then the particles, having these reduced momenta, scatter. In the center of mass frame in which this 'hard' scattering takes place, the final state particle momenta \hat{p}_3 and \hat{p}_4 are produced back to back. In order to go back to the laboratory frame one has to boost these momenta (this boost is zero if $x_1 = x_2$, since in that case these two frames coincide). Finally the particles with momenta \hat{p}_3 and \hat{p}_4 radiate off some energy and retain only the fractions x_3 and x_4 of their original momenta, ending up with p_3 and p_4 . The radiation off the initial state and the final state is collinear with the momentum of the particle from which it is emitted. The difference between the laboratory frame and the center of mass frame of the 'hard' scattering is due to initial state radiation only. The boost between these two frames is collinear with the incoming momenta, i.e. along the direction of the beam axis. It is only this boost that causes a non-zero acollinearity. With this picture in mind one notices a few features of the above form for Δc .

- Δc does not depend on x_3 or x_4 . This is because the final state radiation is collinear with the particle emitting it.

- Δc vanishes if $x_1 - x_2 \rightarrow 0$, for in that limiting case the two frames mentioned above coincide, and the two particles are produced back to back in the laboratory frame.
- Δc vanishes if $\hat{t}_1 \rightarrow 0$ or if $\hat{u}_1 \equiv -\hat{t}_1 - x_1 x_2 s \rightarrow 0$. For $\hat{t}_1 = 0$ and for $\hat{u}_1 = 0$ all momenta are directed along the beam axis. So the boost is collinear with the outgoing momenta themselves, and cannot introduce an acollinearity between them.

We want to know at what values for \hat{t}_1 the quantity Δc has a maximum or a minimum. Therefore we calculate the derivative with respect to \hat{t}_1 and find

$$\frac{\partial \Delta c}{\partial \hat{t}_1} \sim \hat{t}_1 + \frac{1}{2} x_1 x_2 s . \quad (3.4.5)$$

The proportionality factors can only give zero if $x_1 x_2 (x_2 - x_1) = 0$. The case $x_1 x_2 = 0$ is taken to be excluded by our previously defined cuts on $\cos \vartheta_{3,4}$ and on $E_{3,4}$ (see eqs.(3.3.8)). For $x_1 - x_2 = 0$ we already know from the above discussion that the acollinearity is zero, independent of the value of \hat{t}_1 . The conclusion is then that the quantity $|\Delta c|$, and hence also the acollinearity, has a maximum at $\hat{t}_1 = -\frac{1}{2} x_1 x_2 s$. Using the cuts as defined by eq.(3.3.1), leading to the \hat{t}_1 integration boundaries (3.3.7), one can check that this value for \hat{t}_1 is always between these integration boundaries. In other words, the maximum acollinearity for given x_1 and x_2 is always present in the integration over \hat{t}_1 . Having found no other zeroes for $\partial \Delta c / \partial \hat{t}_1$, the minima for the acollinearity are then obtained at the integration boundaries for \hat{t}_1 .

We now focus on the numerical implementation of the acollinearity cut. The cut on the acollinearity leads to three possible situations. The first possibility is that the maximum allowed value for the acollinearity is larger than all those that can be obtained within the \hat{t}_1 -interval. In that case the \hat{t}_1 integration can be carried out as before. The second possibility is that this maximum value is smaller than all those that can be obtained within the \hat{t}_1 -interval. In that case the integral over \hat{t}_1 has to be set to zero. The most awkward situation however is when within the \hat{t}_1 interval one can have values both above and below the maximum acollinearity. In that case one has to find the two values for \hat{t}_1 , let us call them \hat{t}_a and \hat{t}_b , where this maximum acollinearity is obtained. Because it is very hard to do this analytically, we will do this numerically. This can be implemented using standard search routines, without taking too much CPU time. The only thing we have to do then is to calculate the \hat{t}_1 integral over two separate intervals, namely from $\hat{t}_{1,min}$ to \hat{t}_a and from \hat{t}_b to $\hat{t}_{1,max}$ (unless of course one of these intervals turns out to be empty, which still is a possible outcome).

3.5 The non-log terms for the initial state

In this section we discuss the non log terms arising from initial state radiation, whereas in the next section those of the final state will be considered. We deal only with the terms

first order in α . The reason is twofold. The required precision of the radiative corrections often calls for the complete $\mathcal{O}(\alpha)$ corrections. Nevertheless the separation of the complete $\mathcal{O}(\alpha)$ correction into a LL and a non log part is essential for the following reason. When the non log term is small compared to the LL part, it justifies the scale chosen in the LL part. In such a case the second order LL term is expected to be far more important than the second order subleading terms and those can therefore be neglected. In the explicit numerical calculations for large angle Bhabha scattering we shall use $Q^2 = s$ and shall justify this by showing that the non-log terms are indeed small. This is the subject of section 3.8.

The way in which we shall calculate the $\mathcal{O}(\alpha)$ non log term should incorporate the experimental cuts. This can most easily be done numerically. However a numerically stable procedure should be adopted. A full $\mathcal{O}(\alpha)$ calculation from which the LL calculation of the preceding sections is subtracted is numerically rather difficult since one has to integrate a strongly peaked cross section. Instead of this we integrate the difference of two cross sections which both peak similarly. The first one being the exact one and the second one a modified collinear approximation. The last one is chosen to lead to the $\mathcal{O}(\alpha)$ LL expression of the last sections. The integration deals with that part of the cross section where the photon is harder than $\varepsilon \frac{1}{2} \sqrt{s}$. Below this value, for a suitably small ε , the $\mathcal{O}(\alpha)$ correction is just a factor times the Born cross section. The contribution to the total cross section from this part comes from a one dimensional integral over t . The factor contains $\mathcal{O}(\alpha)$ virtual and soft corrections. Since we are interested in the non log terms one should remove the LL terms from the known analytical expressions. In appendix 3.A we give some details.

It should be noted that although we only explicitly mention here non log terms from the initial state and in the next section from the final state, we shall also include terms due to the interference between initial and final state and box diagrams. They are not LL terms and should be included in the exact $\mathcal{O}(\alpha)$ corrected matrix elements squared to get the full $\mathcal{O}(\alpha)$ correction in the end result.

The rest of the section is devoted to the derivation of the approximate hard bremsstrahlung cross section which leads exclusively to the $\mathcal{O}(\alpha)$ LL result of the previous sections. The expression will take the form of a universal factor times a specific process dependent reduced cross section. Although an expression like eq.(3.2.13) is well known, the approximate collinear bremsstrahlung cross section leading to it is not discussed in detail. It is this approximate cross section that we need. The main point about its derivation is to obtain the procedure to go from the five momenta p_1, \dots, p_4, k to the four momenta $\hat{p}_1, \dots, \hat{p}_4$, such that both $p_1^\mu + p_2^\mu - p_3^\mu - p_4^\mu - k^\mu = 0$ and $\hat{p}_1^\mu + \hat{p}_2^\mu - \hat{p}_3^\mu - \hat{p}_4^\mu = 0$ is preserved throughout.

Let us start by writing down the phase space for the three outgoing particles in terms of the variables we want to use:

$$dPS_3 \equiv \frac{1}{(2\pi)^5} \frac{d^3\vec{p}_3}{2E_3} \frac{d^3\vec{p}_4}{2E_4} \frac{d^3\vec{k}}{2k_0} \delta^{(4)}(p_1 + p_2 - p_3 - p_4 - k) \quad (3.5.1)$$

$$= \frac{1}{8(2\pi)^5} dk_0 d\Omega_k dE_3 d\Omega_3 \delta \left(\cos \angle(\vec{p}_3, \vec{k}) - \frac{E_3 k_0 + \sqrt{s} \left(\frac{1}{2} \sqrt{s} - E_3 - k_0 \right)}{E_3 k_0 \sqrt{1 - m_f^2/E_3^2}} \right).$$

We have defined $E_3, \Omega_3 (k_0, \Omega_k)$ to be the energy and solid angle of $p_3^\mu (k^\mu)$. All variables are defined in the $p_1 + p_2$ CM frame. Furthermore we defined

$$\begin{aligned} m_f^2 &= p_3^2 = p_4^2, \\ m_i^2 &= p_1^2 = p_2^2, \end{aligned} \quad (3.5.2)$$

not to be neglected at this moment, as we will hit collinear singularities otherwise. For convenience the charge of the fermions is taken to be $\pm e$. The angles of \vec{k} and \vec{p}_3 are taken with respect to \vec{p}_1 . The δ -function is left, because our objective is to integrate over the photon angles and end up with a Born-like phase space plus an integral over some fraction x that is related to the photon energy k_0 . In the Born-like phase space we will need some δ -function to relate E_3 and the angle of \vec{p}_3 (with respect to whatever we will choose then) through the fraction x .

We now specify the approximate matrix element in two steps. First we take

$$|\mathcal{M}_{1\gamma}(p_1, p_2, p_3, p_4, k)|^2 = e^2 \left[\frac{1+x^2}{x(1-x)} \frac{1}{(p_1 \cdot k)} - \frac{m_i^2}{(p_1 \cdot k)^2} \right] |\mathcal{M}_{0\gamma}(p_1 - k, p_2, p_3, p_4)|^2, \quad (3.5.3)$$

with the definition $x = 1 - k_0/(\frac{1}{2}\sqrt{s})$. This matrix element squared is a good approximation for the full hard photon matrix element squared in those cases where p_1 and k are collinear [17]. We shall use it also outside the collinear situation: in fact we are going to integrate over the full range of the photon angles. This can be done as it leads to a good prescription yielding the structure function method. It is clear that taking this form for the matrix element, we only hope to produce the structure function formula for the corrections on the p_1 line. The p_2 line can be treated analogously, the final state momenta will be treated in the next section. Another point we want to stress is that in the way eq.(3.5.3) is written down, the four momenta that go into the Born-like matrix element $\mathcal{M}_{0\gamma}$ do preserve energy momentum conservation.

As a second step also $\mathcal{M}_{0\gamma}$ and the phase space undergo an approximation. Since $p_1^\mu - k^\mu$ depends on the photon angles an integration over the photon variables in eq.(3.5.3) would not lead to a factorized form. Therefore we fix the photon angles in $\mathcal{M}_{0\gamma}$ to the collinear case. In other words: fix $p_1^\mu - k^\mu$ to be $p_1^\mu (1 - k_0/(\frac{1}{2}\sqrt{s})) = x p_1^\mu$, within $\mathcal{M}_{0\gamma}$ only. However we are still confronted with a dependence on the photon angles in the relation between Ω_3 and E_3 , defined by the δ -function in the phase space defined by eq.(3.5.1). Also for this relation we take the typical Ω_k -values, where \vec{k} is collinear with \vec{p}_1 . With these two changes we have

$$dPS_3 |\mathcal{M}_{1\gamma}|^2 = \frac{1}{8(2\pi)^5} dk_0 d\Omega_k e^2 \left[\frac{1+x^2}{x(1-x)} \frac{1}{(p_1 \cdot k)} - \frac{m_i^2}{(p_1 \cdot k)^2} \right] \times$$

$$dE_3 d\Omega_3 \delta \left(\cos \vartheta_3 - \frac{E_3 k_0 + \sqrt{s} \left(\frac{1}{2} \sqrt{s} - E_3 - k_0 \right)}{E_3 k_0 \sqrt{1 - m_f^2/E_3^2}} \right) \times |\mathcal{M}_{0\gamma}(xp_1, p_2, ?, ?)|^2. \quad (3.5.4)$$

We can observe two features. Firstly the integral over the photon angles can now be done, regardless of the form of $\mathcal{M}_{0\gamma}$. Secondly we have a problem with the momenta that we have to insert in $\mathcal{M}_{0\gamma}$. Taking the momentum xp_1 follows from the above discussion, and taking p_2 is obvious since it is a fixed incoming momentum. However taking p_3 and p_4 to complete the set of four momenta is clearly wrong, for this would violate energy-momentum conservation.

From what we have done so far it can be deduced what we have to do. We still have one δ -function to fix one of the integration variables. Let us say, for argument's sake, we choose as integration variables $\cos \vartheta_3$ and φ_3 (and of course x). Then from the δ -function in eq.(3.5.4) the value for E_3 follows. Using the mass relation $p_3^2 = m_f^2$, the whole momentum p_3^μ is then known. However since this is not the same momentum p_3^μ as the one we started with (the one we would have built using the original momentum k^μ), we will denote the new one by \hat{p}_3^μ . Analogously we define $\hat{p}_1^\mu = xp_1^\mu$ and $\hat{p}_2^\mu = p_2^\mu$. The last momentum \hat{p}_4^μ now follows from energy-momentum conservation. It will now be shown that the above approximate matrix element actually leads to the results of the structure function method. First the angular photon integration is performed

$$\begin{aligned} \int d\Omega_k \left[\frac{1+x^2}{x(1-x)} \frac{1}{(p_1 \cdot k)} - \frac{m_i^2}{(p_1 \cdot k)^2} \right] &= \\ &= 2\pi \left[\frac{1+x^2}{x(1-x)} \frac{2}{k_0 \sqrt{s}} \frac{1}{\sqrt{1-4m_i^2/s}} \log \frac{s(1+\sqrt{1-4m_i^2/s})^2}{4m_i^2} - \frac{2}{k_0^2} \right] \\ &= 2\pi \frac{4}{s} \left[\frac{1+x^2}{x(1-x)^2} \log \frac{s}{m_i^2} - \frac{2}{(1-x)^2} \right], \end{aligned} \quad (3.5.5)$$

where in the last line we expressed k_0 in terms of x and took the small mass limit $m_i^2 \ll s$. Inserting this in eq.(3.5.4) we get

$$\begin{aligned} \int dPS_3 |\mathcal{M}_{1\gamma}|^2 &= \frac{1}{(2\pi)^2} \frac{1}{2\sqrt{s}} \int dx dE_3 d\Omega_3 \times \\ &\quad \delta \left(\cos \vartheta_3 - \frac{\frac{1}{2}(1-x)E_3\sqrt{s} + \sqrt{s} \left(\frac{1}{2}x\sqrt{s} - E_3 \right)}{\frac{1}{2}(1-x)E_3\sqrt{s}\sqrt{1 - m_f^2/E_3^2}} \right) \times \\ &\quad \frac{\alpha}{2\pi} \left[\frac{1+x^2}{x(1-x)^2} \log \frac{s}{m_i^2} - \frac{2}{(1-x)^2} \right] |\mathcal{M}_{0\gamma}(\hat{p}_1, \hat{p}_2, \hat{p}_3, \hat{p}_4)|^2 \\ &= \frac{1}{(2\pi)^2} \int dE_3 \frac{1}{2} E_3 \sqrt{1 - m_f^2/E_3^2} d\Omega_3 \times \end{aligned} \quad (3.5.6)$$

$$\int \frac{dx}{x} \delta \left((1-x)\sqrt{s}\sqrt{E_3^2 - m_f^2} \cos \vartheta_3 - xs + (1+x)E_3\sqrt{s} \right) \times \\ \frac{\alpha}{2\pi} \left[\frac{1+x^2}{1-x} \log \frac{s}{m_f^2} - \frac{2x}{1-x} \right] |\mathcal{M}_{0\gamma}(\hat{p}_1, \hat{p}_2, \hat{p}_3, \hat{p}_4)|^2 .$$

In the last step we re-arranged the argument of the δ -function and changed the order of integrations. In this final result we recognize on the first line a familiar form of the 2-particle phase space, if we add to it the δ -function of the second line with $x = 1$, which is

$$\delta \left(s - 2E_3\sqrt{s} \right) .$$

The third line is the integral over the hard part of the first order LL splitting function (plus a non-log part stemming from the mass term in (3.5.3)) times a Born-like matrix element. We have also indicated explicitly the momenta $\hat{p}_1, \dots, \hat{p}_4$. Note furthermore that an explicit argument for the logarithm has emerged, quite independently of the specifics of the matrix elements. Finally we can make the correspondence with previous sections more evident. Eq.(3.5.6) can be compared to eq.(3.2.20) when integrating over φ_3 , yielding a factor 2π , and including the flux factor $1/(2s)$ and neglecting m_f where possible. In fact, if we do this and change variables to t_1 and u_1 , instead of E_3 and $\cos \vartheta_3$, we find

$$\frac{1}{2s} \int dPS_3 |\mathcal{M}_{1\gamma}|^2 = \frac{1}{16\pi s^2} \int dt_1 du_1 \int \frac{dx}{x} \delta(xs + xt_1 + u_1) \times \quad (3.5.7) \\ \frac{\alpha}{2\pi} \left[\frac{1+x^2}{1-x} \log \frac{s}{m_f^2} - \frac{2x}{1-x} \right] |\mathcal{M}_{0\gamma}(\hat{p}_1, \hat{p}_2, \hat{p}_3, \hat{p}_4)|^2 .$$

When we compare this result to eq.(3.2.19), (3.2.14) and (3.2.15) we see that the correct LL term is reproduced with scale $Q^2 = s$ and in addition a non log term. The last term originates from the second term in eq.(3.5.3), i.e. a term proportional to m_f^2 . Thus the first term of eq.(3.5.3) together with the modified $\mathcal{M}_{0\gamma}$ and phase space gives the LL term. Although we now have obtained the answer for our approximate matrix element squared we have found more, i.e. an additional term proportional to $2x/(1-x)$. This term arises naturally from the collinear approximation and makes the residue of the soft photon pole $L_m - 1$ instead of L_m . Since soft photons constitute a sizable part in the corrections it is necessary to replace $\beta = 2\alpha L_m/\pi$ in eq.(3.3.20) by

$$\beta = \frac{2\alpha}{\pi} (L_m - 1) . \quad (3.5.8)$$

When doing so, one should replace m_f^2 in eq.(3.5.3) by m_f^2/x in order to obtain $2/(1-x)$ in eq.(3.5.7). Thus we have defined an approximate cross section which leads to the LL expression with β given by eq.(3.5.8).

The numerical integration of the difference of the exact and four approximate cross sections over the phase space allowed by the cuts is most easily done by Monte Carlo

integration techniques. The approximate cross sections contain the collinear radiation from the incoming and outgoing particles. One generates for an incoming p_1 and p_2 the momenta p_3, p_4 and k , where p_3 and p_4 are required to satisfy the cuts. From this set one constructs four other sets of momenta e.g. the set $\hat{p}_1, \hat{p}_2, \hat{p}_3, \hat{p}_4$ and fraction x_1 corresponding to initial state collinear radiation from the particle with momentum p_1 . The other sets correspond to collinear radiation from the other particles. This is discussed in the next section for final state radiation. The combination of matrix elements is smooth enough to obtain a reliable non log result by a Monte Carlo integration technique.

3.6 The non-log terms for the final state

In the previous section we discussed a method to obtain the non-log terms for the initial state corrections, in this section we want to do the same for the final state corrections. Most of it is analogous to the initial state corrections. The approximate matrix element squared is however not quite the same. We start again by writing down the phase space

$$dPS_3 = \frac{1}{4(2\pi)^5} k_0 dk_0 d\Omega_k dE_3 d\Omega_3 \sqrt{E_3^2 - m_f^2} \times \delta\left(s - 2\sqrt{s}k_0 - 2\sqrt{s}E_3 + 2E_3k_0 \left[1 - \cos\angle(\vec{p}_3, \vec{k})\sqrt{1 - m_f^2/E_3^2}\right]\right). \quad (3.6.1)$$

We defined $E_3, \Omega_3 (k_0, \Omega_k)$ as the energy and solid angle of $p_3^\mu (k^\mu)$. All variables are defined in the $p_1 + p_2$ CM frame and all angles are taken with respect to \vec{p}_1 . Again we will keep the δ -function. The approximate matrix element squared we start with reads

$$|\mathcal{M}_{1\gamma}(p_1, p_2, p_3, p_4, k)|^2 = e^2 \left[\frac{1+x^2}{1-x} \frac{1}{(p_3 \cdot k)} - \frac{m_f^2}{(p_3 \cdot k)^2} \right] |\mathcal{M}_{0\gamma}(p_1, p_2, p_3+k, p_4)|^2, \quad (3.6.2)$$

with the definition $x = E_3/(E_3 + k_0)$. It is a good approximation to the exact matrix element in those cases where \vec{p}_3 is collinear with \vec{k} . Note that the momenta going into $\mathcal{M}_{0\gamma}$ in eq.(3.6.2) obey energy-momentum conservation. Just as in the previous section we fix the direction of \vec{k} in $\mathcal{M}_{0\gamma}$ and the δ -function to be collinear with \vec{p}_3 . This results in

$$dPS_3 |\mathcal{M}_{1\gamma}|^2 = \frac{1}{4(2\pi)^5} k_0 dk_0 d\Omega_k e^2 \left[\frac{1+x^2}{1-x} \frac{1}{(p_3 \cdot k)} - \frac{m_f^2}{(p_3 \cdot k)^2} \right] dE_3 d\Omega_3 \times \sqrt{E_3^2 - m_f^2} \delta\left(s - 2\sqrt{s}k_0 - 2\sqrt{s}E_3 + 2E_3k_0 \left[1 - \sqrt{1 - m_f^2/E_3^2}\right]\right) \times |\mathcal{M}_{0\gamma}(p_1, p_2, ?, ?)|^2. \quad (3.6.3)$$

Once more we have created a form where we can easily do the integration over the photon angles, but where we have to be careful which momenta to insert in $\mathcal{M}_{0\gamma}$. We choose as integration variables $\cos\vartheta_3$ and φ_3 . Having chosen those, E_3 follows from the δ -function

in eq.(3.6.3). Using the mass relation $p_3^2 = m_f^2$ we then know all components of the altered version of p_3^μ , which we will call \hat{p}_3^μ . The incoming momenta are fixed beam momenta, so define $\hat{p}_1 = p_1$, $\hat{p}_2 = p_2$. Having fixed three out of four momenta we have $\hat{p}_4 = \hat{p}_1 + \hat{p}_2 - \hat{p}_3$.

The next thing to do is to integrate over the photon angles, which yields

$$\begin{aligned}
\int d\Omega_k \left[\frac{1+x^2}{1-x} \frac{1}{(p_3 \cdot k)} - \frac{m_f^2}{(p_3 \cdot k)^2} \right] &= \\
&= 2\pi \left[\frac{1+x^2}{1-x} \frac{1}{E_3 k_0} \frac{1}{\sqrt{1-m_f^2/E_3^2}} \log \frac{E_3^2(1+\sqrt{1-m_f^2/E_3^2})^2}{m_f^2} - \frac{2}{k_0^2} \right] \\
&= 2\pi \frac{x^2}{E_3^2} \left[\frac{1+x^2}{x(1-x)^2} \log \frac{4E_3^2}{m_f^2} - \frac{2}{(1-x)^2} \right]. \tag{3.6.4}
\end{aligned}$$

In the last line we expressed k_0 in terms of x and E_3 and assumed that $m_f^2 \ll E_3^2$. We can insert this in eq.(3.6.3), setting m_f to zero where possible. We change the integration over k_0 into one over x and obtain

$$\begin{aligned}
\int dPS_3 |\mathcal{M}_{1\gamma}|^2 &= \frac{1}{(2\pi)^2} \int dE_3 \frac{1}{2} E_3 d\Omega_3 \int \frac{dx}{x} \delta(xs - 2\sqrt{s}E_3) \times \\
&\quad \frac{\alpha}{2\pi} \left[\frac{1+x^2}{1-x} \log \frac{4E_3^2}{m_f^2} - \frac{2x}{1-x} \right] |\mathcal{M}_{0\gamma}(\hat{p}_1, \hat{p}_2, \hat{p}_3, \hat{p}_4)|^2. \tag{3.6.5}
\end{aligned}$$

Also here we recognize on the first line a familiar form for the 2-particle phase space, in combination with the δ -function if it were taken at $x = 1$. The rest is the integral over the hard part of the first order fragmentation function (plus a non-log part coming from the mass term in the matrix element) times a Born-like matrix element. In order to make the relation to the previous sections more evident, we have to include the flux factor $1/(2s)$ and integrate over the angle φ_3 in order to compare to eq.(3.2.20). We furthermore change variables from E_3 and $\cos\vartheta_3$ to t_1 and u_1 . This results in

$$\begin{aligned}
\frac{1}{2s} \int dPS_3 |\mathcal{M}_{1\gamma}|^2 &= \frac{1}{16\pi s^2} \int dt_1 du_1 \int \frac{dx}{x} \delta(xs + t_1 + u_1) \times \\
&\quad \frac{\alpha}{2\pi} \left[\frac{1+x^2}{1-x} \log \frac{x^2 s}{m_f^2} - \frac{2x}{1-x} \right] |\mathcal{M}_{0\gamma}(\hat{p}_1, \hat{p}_2, \hat{p}_3, \hat{p}_4)|^2, \tag{3.6.6}
\end{aligned}$$

to be compared with eq.(3.2.19). Once again, as we noted below eq.(3.5.7), we see that the residue of the soft photon pole is $L_m - 1$ rather than L_m .

There is however an important difference between this result and the one obtained in the previous section for the initial state: the argument of the logarithm is not a constant here. In this argument E_3 or x , one of our integration variables, appears. Nevertheless we usually assume, when calculating the LL corrections along the lines of section 3.2,

that the scale Q^2 is independent of the integration variables. We can solve this problem by taking a collinear factor that integrates to a logarithm with a scale Q^2 that does not depend on any of the integration variables. In principle we are free to do this, as long as we also calculate the other part of the corrections, i.e. the non-log terms. Keeping in mind that that was exactly what we were setting out to do, we can take another collinear factor. By changing the collinear factor we are merely shifting contributions from the LL part to the non-log part and vice versa. Our choice will be to take a modified collinear factor in eq.(3.6.3), namely

$$e^2 \left[\frac{1+x^2}{1-x} \frac{1}{E_3 k_0 (1 - \cos \angle(\vec{p}_3, \vec{k}) \sqrt{1 - 4m_f^2/s})} - \frac{m_f^2}{(p_3 \cdot k)^2} \right]. \quad (3.6.7)$$

It can easily be shown that after integration this yields the same result as in eq.(3.6.4), but with the argument $4E_3^2/m_f^2$ of the logarithm replaced by s/m_f^2 , which indeed is independent of all other integration variables. Also the convergence of the numerical Monte Carlo integration is still sufficient with this approximation instead of the one of eq.(3.6.3).

Finally we want to comment on the mass m_f in the case of final state corrections. After eq.(3.6.4) we have neglected it wherever possible, but in principle this is not necessary for the derivation. However, if m_f were comparable with E_3 , the argument of the logarithm in eq.(3.6.4) would be close to unity and hence the logarithm would not be large, let alone leading. Therefore there is not much sense in allowing m_f to become rather large and still only do a 'leading log' calculation. Having said this we will now turn to Bhabha scattering, with $m_f = m_e$, i.e. m_f is very small.

3.7 Bhabha scattering

In this section we want to discuss the specifics of Bhabha scattering when implementing the methods of the previous sections. Since we consider the matrix elements squared for the processes $e^+e^- \rightarrow e^+e^-(\gamma)$ as well known [18], both in terms of dot products and in terms of spinor products, we can implement the calculation of the non-log terms using the methods of sections 3.5 and 3.6 (and using the FORTRAN program VEGAS to do the Monte Carlo integration [19]) without much further discussion. The only point we want to come back to at the end of this section is what variables we want to choose as the integration variables. For the LL calculation, on the other hand, we need to write the matrix element squared for $e^+(p_1)e^-(p_2) \rightarrow e^+(p_3)e^-(p_4)$ in terms of the invariants s and t only, in accordance with the discussion at the end of section 3.3. Furthermore we will have to integrate this matrix element squared times the final state correction factor given by eq.(3.3.14) over the invariant t . Finally, in order to complete the calculation, we will have to include the pure weak (non-QED) corrections at some point. In this section we will give the desired form of the matrix element squared in terms of s and t , in which

the weak corrections can be incorporated and we will give the ingredients for carrying out the integration over t .

The Born matrix element squared for the process $e^+e^- \rightarrow e^+e^-$ can be written as

$$|\mathcal{M}_{Born}|^2(s, t) = (4\pi\alpha)^2 \sum_{i=1}^8 W_i I_i, \quad (3.7.1)$$

where

$$\begin{aligned} I_1 &= \frac{t^2 + u^2}{s^2}, & I_2 &= \frac{t - u}{s}, & I_3 &= \frac{t}{s}, & I_4 &= 1, \\ I_5 &= \frac{s}{t}, & I_6 &= \frac{s}{t - M_Z^2}, & I_7 &= \frac{s^2}{t^2}, & I_8 &= \frac{s^2}{(t - M_Z^2)^2}, \end{aligned} \quad (3.7.2)$$

and where the W_i are constants at Born-level. $I_1(I_2)$ is the (anti)symmetric part of the s -channel squared contributions, for

$$\begin{aligned} \frac{t^2 + u^2}{s^2} &= \frac{1}{2}(1 + \cos^2 \vartheta), \\ \frac{t - u}{s} &= \cos \vartheta, \end{aligned}$$

with ϑ the angle between say the incoming e^+ and the outgoing e^+ . As we want to use the methods of sections 2 and 3, we have to write this in terms of s and t only, as we have indicated already in eq.(3.7.1) (in order to use this in eq.(3.3.9), s and t then have to be replaced by $x_1 x_2 s$ and t_1 respectively). Using $s + t + u = 0$ we therefore eliminate u :

$$I_1 = 2\frac{t^2}{s^2} + 2I_3 + I_4, \quad I_2 = 2I_3 + I_4.$$

The W_i are mainly combinations of coupling constants and s -channel propagators, but they can be written in a way that enables the inclusion of first order pure weak (non-QED) corrections.

$$\begin{aligned} W_1 &= \frac{1}{2} (|p_{s,+}|^2 + |p_{s,-}|^2)^2 + \text{Re} (p_{s,+} z_{s,+}^* + p_{s,-} z_{s,-}^*)^2 + \frac{1}{2} (|z_{s,+}|^2 + |z_{s,-}|^2)^2, \\ W_2 &= \frac{1}{2} (|p_{s,+}|^2 - |p_{s,-}|^2)^2 + \text{Re} (p_{s,+} z_{s,+}^* - p_{s,-} z_{s,-}^*)^2 + \frac{1}{2} (|z_{s,+}|^2 - |z_{s,-}|^2)^2, \\ W_3 &= V_1 + V_2, \\ W_4 &= (p_{t,+}^2 + z_{t,+}^2)^2 + (p_{t,-}^2 + z_{t,-}^2)^2 + 2V_1 + \left(2 + \frac{M_Z^2}{s}\right) V_2, \\ W_5 &= 2(p_{t,+}^4 + p_{t,-}^4) - \frac{2s}{M_Z^2} (p_{t,+} z_{t,+} + p_{t,-} z_{t,-})^2 + V_1, \\ W_6 &= \frac{2s}{M_Z^2} (p_{t,+} z_{t,+} + p_{t,-} z_{t,-})^2 + 2 \left(2 + \frac{M_Z^2}{s}\right) (p_{t,+}^2 z_{t,+}^2 + p_{t,-}^2 z_{t,-}^2) \end{aligned}$$

$$\begin{aligned}
& +2 \left(1 + \frac{M_Z^2}{s}\right) (z_{i,+}^4 + z_{i,-}^4) + \left(1 + \frac{M_Z^2}{s}\right)^2 V_2, \\
W_7 &= (p_{i,+}^2 + p_{i,-}^2)^2, \\
W_8 &= (z_{i,+}^2 + z_{i,-}^2)^2 + \frac{M_Z^2}{s} \left(2 + \frac{M_Z^2}{s}\right) (z_{i,+}^4 + z_{i,-}^4). \tag{3.7.3}
\end{aligned}$$

The contributions $V_{1,2}$ come from the interference between the s- and the t-channel and are given by

$$\begin{aligned}
V_1 &= 2 \operatorname{Re} \left[p_{s,+}^2 p_{i,+}^2 + p_{s,-}^2 p_{i,-}^2 + p_{i,+}^2 z_{s,+}^2 + p_{i,-}^2 z_{s,-}^2 \right], \\
V_2 &= 2 \operatorname{Re} \left[p_{s,+}^2 z_{i,+}^2 + p_{s,-}^2 z_{i,-}^2 + z_{s,+}^2 z_{i,+}^2 + z_{s,-}^2 z_{i,-}^2 \right]. \tag{3.7.4}
\end{aligned}$$

Here we have defined

$$\begin{aligned}
p_{s,\lambda} &= - \left[(Q_e + F_{\gamma,e}^V(s)) - \lambda F_{\gamma,e}^A(s) \right] [\chi_\gamma(s)]^{1/2}, \tag{3.7.5} \\
z_{s,\lambda} &= \left[\left(v_e + F_{Z,e}^V(s) + Q_e \frac{\hat{\Sigma}_{\gamma Z}(s)}{s} \right) - \lambda (a_e + F_{Z,e}^A(s)) \right] [\chi_Z(s)]^{1/2},
\end{aligned}$$

where $\chi_{\gamma(Z)}(s)$ is the renormalized $\gamma(Z)$ propagator function as a function of the momentum transfer s and $F_{Z,f}^{V(A)}$ is the (axial-)vector form factor for the $Z\bar{f}f$ vertex due to pure weak (non QED) vertex corrections, as is $F_{\gamma,f}^{V(A)}$ for the $\gamma\bar{f}f$ vertex. For the t-channel quantities we defined

$$\begin{aligned}
p_{t,\lambda} &= - \left[(Q_e + F_{\gamma,e}^V(t)) - \lambda F_{\gamma,e}^A(t) \right] \left[\frac{t}{t + \hat{\Sigma}_\gamma(t)} \right]^{1/2}, \tag{3.7.6} \\
z_{t,\lambda} &= \left[\left(v_e + F_{Z,e}^V(t) + Q_e \frac{\hat{\Sigma}_{\gamma Z}(t)}{t} \right) - \lambda (a_e + F_{Z,e}^A(t)) \right] \left[\frac{t - M_Z^2}{t - M_Z^2 + \hat{\Sigma}_Z(t)} \right]^{1/2},
\end{aligned}$$

where $\hat{\Sigma}_{\gamma(Z)}(t)$ is the renormalized self energy of the $\gamma(Z)$ as a function of the momentum transfer t and $\hat{\Sigma}_{\gamma Z}(t)$ is the γ - Z mixing. The square roots in eqs.(3.7.5),(3.7.6) are implicitly understood to be complex valued ones, defined on the same Riemann sheet as the logarithm (independent of the choice of the particular Riemann sheet). For the explicit form of the quantities $\chi_{\gamma,Z}$ and $\hat{\Sigma}_{\gamma,Z,\gamma Z}$ and $F_{\gamma(Z),f}^{V(A)}$ we refer to [7, 8] (in [8] however the $F_\gamma^{V(A)}$ are defined with the opposite sign). From these explicit expressions one can see that $p_{s,\lambda}$, $z_{s,\lambda}$ are complex valued whereas $p_{t,\lambda}$, $z_{t,\lambda}$ are real. We will leave out the contributions from the ZZ and WW boxes, for we have checked that on resonance these contributions do not exceed 0.1%, whereas off resonance (i.e. at $\sqrt{s} = 120$ GeV) they are at most 0.2%.

Taking the expressions from the above references means that we follow the renormalization scheme outlined there. Here we only want to remind the reader that in this

scheme e.g. the masses of the Z, the Higgs boson and the top quark are input parameters, whereas e.g. the mass of the W, the width of the Z and $\sin^2 \vartheta_W$ are calculated parameters (from the muon decay constant G_μ). Finally we should remark that we calculate the light quark contributions to the vacuum polarization in the t-channel ($\hat{\Sigma}_\gamma(t)/t$) using a parametrization of the dispersion integral over the hadronic total cross section in e^+e^- collisions. Motivation to do so can be found in [20], together with the exact procedure.

Thus by suitably defining $p_{s,\lambda}$ and $z_{s,\lambda}$ etc. one can incorporate the self-energy corrections and the pure weak vertex corrections in the above form for $|\mathcal{M}|^2$. However it is obvious from eq.(3.7.6) that $p_{t,\lambda}$ and $z_{t,\lambda}$ depend on t through the one loop corrections. This prohibits one to integrate the I_i over t , considering the W_i as constants. Nevertheless we do need to calculate this integral, as indicated by eq.(3.3.9). To do this integral analytically with t -dependent W_i is too cumbersome. Performing it numerically would be possible but would add one more numerical integration slowing down the whole calculation. A practical solution to this problem is the following. For the contributions without QED corrections (i.e. the contributions with $\Gamma(x_i) = \mathcal{D}(x_i) = \delta(1 - x_i)$ in eq.(3.3.9)) one can do this integration numerically, for in this case it is a one dimensional integration over a smooth function. For the rest of the contributions it is sufficient to approximate the pure weak corrections by calculating them only at one particular value of t and assume that they are the same at all other values of t . In fact it turns out that this is a rather good approximation if this particular t is chosen to be

$$t = -2s \frac{1 - c_m}{1 + x_1 x_2 - c_m(1 - x_1 x_2)}.$$

(c_m is the cosine of the minimum separation angle ϑ_{min} as defined in eq.(3.3.1).) Some motivation for this choice can be given, since it has to do with the value for t as occurring in eq.(3.2.22). But the real requirement is to minimize the deviations from the exact calculation. This can only be checked a posteriori. Combined with the fact that the approximation is made for the QED correction terms only, we have checked that the deviations from the exact calculation are of the order of 0.1% and hence that they are of no experimental relevance.

Having done this, the integration over t for these contributions can be done by integrating the very simple integrands I_i . Using the results of section 3.3 however, we want to include final state radiation at this point, by including the factor given by eq.(3.3.14) in our integrand. Apart from the trivial integrals for the lowest order term, we now have integrands of the form

$$I_i f(a, b, t) \equiv I_i \left[\log \left(1 - \frac{1}{a + bt} \right) + \frac{1}{2} \frac{1}{a + bt} + \frac{1}{4} \frac{1}{(a + bt)^2} \right].$$

The values for a and b follow from the lower boundaries of x_3 and x_4 as given by

eqs.(3.3.6):

$$\begin{cases} a = \frac{x_1}{\dot{E}_0} & , & b = -\frac{1-x_1/x_2}{x_1\dot{E}_0s} & \text{(from } x_3), \\ a = \frac{x_2}{\dot{E}_0} & , & b = \frac{1-x_1/x_2}{x_1\dot{E}_0s} & \text{(from } x_4). \end{cases} \quad (3.7.7)$$

Written in this way we cannot take $E_0 = 0$ any more, but we have to remember that in that case we know the final state LL corrections to vanish anyway. However for non-vanishing E_0 we have

$$\begin{aligned} \int dt t^2 f(a, b, t) &= \frac{1}{3} \left(t^3 + \frac{a^3}{b^3} \right) \log \left(1 - \frac{1}{a+bt} \right) + \frac{-3a^2 + 3a - 1}{3b^3} \log(a-1+bt) \\ &\quad - \frac{t^2}{6b} - \frac{t}{3b^2}(-2a+1) + \frac{1}{2b} \left(\frac{1}{2}t^2 - \frac{a}{b}t + \frac{a^2}{b^2} \log(a+bt) \right) \\ &\quad + \frac{1}{4b^2} \left(t - 2\frac{a}{b} \log(a+bt) - \frac{a^2}{b} \frac{1}{a+bt} \right), \\ \int dt t f(a, b, t) &= \frac{1}{2} \left(t^2 - \frac{a^2}{b^2} \right) \log \left(1 - \frac{1}{a+bt} \right) - \frac{-2a+1}{2b^2} \log(a-1+bt) \\ &\quad - \frac{t}{2b} + \frac{1}{2b} \left(t - \frac{a}{b} \log(a+bt) \right) + \frac{1}{4b^2} \left(\log(a+bt) + \frac{a}{a+bt} \right), \\ \int dt f(a, b, t) &= \left(t + \frac{a}{b} \right) \log \left(1 - \frac{1}{a+bt} \right) - \frac{1}{b} \log(a-1+bt) \\ &\quad + \frac{1}{2b} \log(a+bt) - \frac{1}{4b} \frac{1}{a+bt}, \\ \int dt \frac{1}{t} f(a, b, t) &= \log \frac{a-1}{a} \log t - \text{Li}_2 \left(-\frac{bt}{a-1} \right) + \text{Li}_2 \left(-\frac{bt}{a} \right) \\ &\quad - \frac{1}{2a} \left(1 + \frac{1}{2a} \right) \log \frac{a+bt}{t} + \frac{1}{4a} \frac{1}{a+bt}, \\ \int dt \frac{1}{t^2} f(a, b, t) &= - \left(\frac{1}{t} + \frac{b}{a-1} \right) \log \left(1 - \frac{1}{a+bt} \right) + \frac{b}{a(a-1)} \log \frac{t}{a+bt} \\ &\quad + \frac{1}{2a} \left(1 + \frac{1}{a} \right) \frac{b}{a} \log \frac{a+bt}{t} - \frac{1}{2a} \left(1 + \frac{1}{2a} \right) \frac{1}{t} \\ &\quad - \frac{1}{4a^2} \frac{b}{a+bt}. \end{aligned} \quad (3.7.8)$$

The expressions for the integrals

$$\int dt \frac{1}{t - M_Z^2} f(a, b, t) \quad \text{and} \quad \int dt \frac{1}{(t - M_Z^2)^2} f(a, b, t)$$

can be obtained from the last two in eq.(3.7.8) by means of the substitution

$$t \rightarrow t - M_Z^2 \quad \text{and} \quad a \rightarrow a + bM_Z^2.$$

Several arguments of logarithms will become negative in these expressions. Therefore these are implicitly understood to be complex valued. A check on the results is that the imaginary parts should vanish in the end, as we started with real valued integrands.

The above expressions appear to have singularities if either $b \rightarrow 0$ or $a \rightarrow 1$. These two limits can be taken using expansions for the integrals when necessary:

$$\begin{aligned}
 \int dt t^2 f(a, b, t) &= \frac{1}{3} t^3 \left[\log \frac{a-1}{a} + \frac{1}{2a} \left(1 + \frac{1}{2a} \right) \right] - \frac{b}{8a^2} \left(1 + \frac{1}{a} \right) t^4 \\
 &\quad + \frac{1}{4} \frac{bt^4}{a(a-1)} + \mathcal{O}(b^2), \\
 \int dt t f(a, b, t) &= \frac{1}{2} t^2 \left[\log \frac{a-1}{a} + \frac{1}{2a} \left(1 + \frac{1}{2a} \right) \right] - \frac{b}{6a^2} \left(1 + \frac{1}{a} \right) t^3 \\
 &\quad + \frac{1}{3} \frac{bt^3}{a(a-1)} + \mathcal{O}(b^2), \\
 \int dt f(a, b, t) &= t \left[\log \frac{a-1}{a} + \frac{1}{2a} \left(1 + \frac{1}{2a} \right) \right] - \frac{b}{4a^2} \left(1 + \frac{1}{a} \right) t^2 \\
 &\quad + \frac{1}{2} \frac{bt^2}{a(a-1)} + \mathcal{O}(b^2), \\
 \int dt \frac{1}{t} f(a, b, t) &= \frac{1}{2} \log^2(bt) + \text{Li}_2(-bt) - \frac{3}{4} \log \frac{1+bt}{t} + \frac{1}{4} \frac{1}{1+bt} + \mathcal{O}(a-1), \\
 \int dt \frac{1}{t^2} f(a, b, t) &= -\frac{1}{t} \left(1 + \log \left(\frac{bt}{1+bt} \right) \right) - 2b \log \frac{bt}{1+bt} - \frac{3}{4t} \\
 &\quad - \frac{1}{4} \frac{b}{1+bt} + \mathcal{O}(a-1). \tag{3.7.9}
 \end{aligned}$$

From these expressions it is clear that the limits $b \rightarrow 0$ and $a \rightarrow 1$ are incompatible: they can not be taken both at the same time. However $a = 1$ and $b = 0$ only occurs if $x_1 = x_2 = \hat{E}_0$. As can be seen from eq.(3.3.8) this is at the very edge of the phase space. It can be checked that though the above expressions yield a singularity in the integrand at $x_1 = x_2 = \hat{E}_0$, the integral over x_1 and x_2 over a finite area remains finite.

Summarizing the results so far, we have the following situation. We can substitute the explicit form of the integrals for the I_i . These are then functions only of a , b , t_{\min} and t_{\max} , and hence, using eqs.(3.3.7) and (3.7.7), only of x_1 and x_2 (and of the fixed parameters c_m and E_0). This means that from this point onwards we can do the integrations, i.e. the ones over x_1 and x_2 , numerically.

At this point we can improve our results for the higher order corrections in a very straightforward way, by making the following observation. As has been known for a long time [21], and as has been mentioned in sections 5 and 6, not only the terms $1/(p \cdot k)$ are of a universal nature: also the terms $-m^2/(p \cdot k)^2$ are. This means that it is the factor

$\frac{2\alpha}{\pi}(L_e - 1) = \beta$ that becomes the exponent, rather than $\frac{2\alpha}{\pi}L_e$, when performing soft photon exponentiation (see [21]). Therefore we can improve the higher order corrections by taking this expression for β in eq.(3.3.19). Doing so one cannot claim to have taken all next to leading log terms into account, but one has accounted for the most important ones. A measure for how well this works can be obtained from the first order corrections, by comparing the LL result with the full $\mathcal{O}(\alpha)$ result. In the next section we will come back to this point.

In the remainder of this section we want to focus on the Monte Carlo integration to calculate the first order non-log terms. As stated at the beginning of this section we use the integration routine VEGAS. The pseudo-random number generator we use is called RANMAR and is introduced and discussed in [22]. The matrix elements we use are well known in the literature, so the only problem left is the choice of variables. We have a 5-dimensional integral at hand and we use a general purpose integration routine. Hence it is best to choose those variables in which the integrand varies most steeply. We will choose k_0 , the energy of the photon, $\cos \vartheta_k$ and φ_k , the angles of the photon with respect to the incoming e^+ , and $\cos \vartheta_3$ and φ_3 , the angles of the outgoing e^+ with respect to the photon. Notice that by choosing $\cos \vartheta_k$ both the peaks arising when the photon gets collinear with either incoming particle are easily localized, i.e. at $\cos \vartheta_k = \pm 1$. By choosing $\cos \vartheta_3$ the same can be said for the situation where the photon is collinear with the outgoing e^+ ($\cos \vartheta_3 = 1$). So we are left with the situation where the photon is collinear with the outgoing e^- . But in that case the outgoing e^+ has to lie back to back with the photon and the outgoing e^- . Hence this peak is easily localized at $\cos \vartheta_3 = -1$. Moreover the peaking towards soft photons is localized at the lower end of the k_0 integration. Thus every peak in the integrand is localized in terms of only one of our integration variables. This is important for a program like VEGAS to work smoothly.

Having motivated our choice we will now give the expression for the phase space in terms of the chosen variables, together with the algorithm to construct events.

$$dPS_3 = \frac{1}{4(2\pi)^5} \frac{E_3}{2\sqrt{s} - 2k_0(1 - \cos \vartheta_3)} k_0 dk_0 d\cos \vartheta_k d\varphi_k d\cos \vartheta_3 d\varphi_3. \quad (3.7.10)$$

The energy of p_3 is given in terms of the basic 5 variables by

$$E_3 = \frac{s(1 - 2k_0/\sqrt{s})}{2\sqrt{s} - 2k_0(1 - \cos \vartheta_3)}. \quad (3.7.11)$$

Using the basic integration variables and E_3 we can construct k^μ and p_3^μ . In doing so we have to rotate \vec{p}_3 , for its angles were defined with respect to \vec{k} . The momentum p_4^μ then follows from energy-momentum conservation.

In the above we have neglected the electron mass m_e . We are allowed to do so because the integrand does not have any collinear divergences anymore: for we have subtracted the four collinear matrix elements from the full one. The resulting integrand therefore is finite in all parts of the phase space, even when taking $m_e = 0$ (but of course only as long as we have $k_0 > \varepsilon \frac{1}{2}\sqrt{s}$, where $\varepsilon \frac{1}{2}\sqrt{s}$ is the soft photon cut-off).

The integration variables are assigned values in the following ranges

$$\begin{aligned} k_0 &\in \left[\varepsilon \frac{1}{2} \sqrt{s}, \frac{1}{2} \sqrt{s} (1 - 4m_e^2/s) \right], \\ \cos \vartheta_k, \cos \vartheta_3 &\in [-1, 1], \\ \varphi_k, \varphi_3 &\in [0, 2\pi]. \end{aligned}$$

For the upper bound on k_0 we maintained the electron mass to ensure that the invariant mass of the final state e^+e^- pair does not become lower than $4m_e^2$. We remind the reader that in the numerical non log calculation also the interference between initial and final state radiation is taken into account as has been discussed in section 3.5.

3.8 Results and discussion

We have implemented all that has been discussed in the previous sections in a FORTRAN program. In this section we want to check its results against other more limited calculations by omitting parts of the full calculation. Moreover we present the new results of the full calculation. Although the second order final state corrections of eq.(3.3.16) are included in this program, the results presented in this section do not contain these corrections because they are very small ($\sim 0.1\%$). Furthermore all the results have been obtained using the scale choice $Q^2 = s$, a justification of which can be found in the fact that the non-log terms turn out to be small.

The main check that is available is to compare with the program BABAMC [1]. In BABAMC all pure weak and all QED corrections are calculated to one order in α . Therefore this can serve as a check on our first order corrections. Since BABAMC is an event generator, we can apply cuts on both angle and energy of the outgoing particles, and therefore we can also check the way we implemented those cuts in our calculation. Unfortunately the treatment of the pure weak corrections in BABAMC is very different from what has become customary since BABAMC was made, so in order to check our program we had to make a version where this treatment of the pure weak corrections was taken over from BABAMC. Moreover we took the value for the Z width that BABAMC uses (if the user does not specify otherwise), which was 2.27 GeV. For the input parameters we used $M_Z = 91.1$ GeV, $M_H = 100$ GeV and $m_{top} = 100$ GeV. We calculated the total cross section at four points for the total center of mass energy: three points around the Z peak and one point away from it. At each point we imposed four different sets of cuts, namely

$$\begin{aligned} 1 : & \quad \vartheta_m = 10^\circ & E_0 = 0 \\ 2 : & \quad \vartheta_m = 10^\circ & E_0 = \frac{1}{2} \times \frac{1}{2} \sqrt{s} \\ 3 : & \quad \vartheta_m = 42^\circ & E_0 = 0 \\ 4 : & \quad \vartheta_m = 42^\circ & E_0 = \frac{1}{2} \times \frac{1}{2} \sqrt{s} \end{aligned} \tag{3.8.1}$$

\sqrt{s}	'Born'	BABAMC	LL $\mathcal{O}(\alpha)$	$\mathcal{O}(\alpha)$	$\mathcal{O}(\alpha^2)$	$\mathcal{O}(\alpha^2)+\text{exp.}$
89.1	5628.	5275. \pm 6.	5281.	5269. \pm 5.	5358. \pm 5.	5352. \pm 5.
		4990. \pm 6.	4939.	4974. \pm 5.	5025. \pm 5.	5010. \pm 5.
	700.6	545. \pm 2.	543.7	544.9 \pm .1	565.0 \pm .1	556.2 \pm .1
		522. \pm 2.	517.9	520.2 \pm .1	539.8 \pm .1	531.0 \pm .1
91.1	6199.	5741. \pm 9.	5744.	5742. \pm 5.	5833. \pm 5.	5860. \pm 5.
		5433. \pm 9.	5377.	5415. \pm 5.	5469. \pm 5.	5497. \pm 5.
	1516.	1125. \pm 3.	1120.	1128. \pm 1.	1178. \pm 1.	1177. \pm 1.
		1070. \pm 3.	1057.	1069. \pm 1.	1119. \pm 1.	1118. \pm 1.
93.1	3841.	4168. \pm 3.	4176.	4171. \pm 4.	4143. \pm 4.	4158. \pm 4.
		3946. \pm 3.	3911.	3938. \pm 4.	3875. \pm 4.	3892. \pm 4.
	336.3	464. \pm 1.	462.4	464.5 \pm .1	428.9 \pm .1	440.7 \pm .1
		452. \pm 1.	449.6	452.0 \pm .1	415.7 \pm .1	427.5 \pm .1
120.0	2354.	2349. \pm 6.	2353.	2351. \pm 2.	2382. \pm 2.	2382. \pm 2.
		2211. \pm 6.	2188.	2210. \pm 2.	2218. \pm 2.	2219. \pm 2.
	70.7	76.4 \pm .1	76.2	76.1 \pm .1	77.1 \pm .1	77.0 \pm .1
		73.5 \pm .1	73.5	73.2 \pm .1	73.9 \pm .1	73.8 \pm .1

Table 3.1. Results for the total cross section compared with BABAMC. The four lines per value for \sqrt{s} (GeV) correspond to the four sets of cuts defined in eq.(3.8.1). All cross sections are in picobarn. Here LL $\mathcal{O}(\alpha)$ means the result including leading log first order corrections, whereas $\mathcal{O}(\alpha)$ stands for the exact first order corrected result. The $\mathcal{O}(\alpha^2)$ entry then furthermore includes second order leading log corrections and the rightmost column then includes soft photon exponentiation on top of that.

We have listed the results in table 3.1. The entry listed under 'Born' is the total cross section in Born approximation, but including the pure weak corrections at $\mathcal{O}(\alpha)$. All entries to the right then list the cross sections when including QED corrections at several levels. A number of remarks can be made on the basis of this table.

- The full $\mathcal{O}(\alpha)$ corrected result agrees with BABAMC, as indeed it should.
- The leading log result already is very near to the full $\mathcal{O}(\alpha)$ corrected result. The differences are almost negligible for $E_0 = 0$ and are of the order of 1% for $E_0 = \frac{1}{2} \times \frac{1}{2} \sqrt{s}$. This we take to be the a posteriori justification for not calculating non leading log effects in higher orders.
- The $\mathcal{O}(\alpha^2)$ corrected results differ appreciably from the $\mathcal{O}(\alpha)$ corrected ones. Especially on resonance these differences are large, larger in fact than the difference between the LL $\mathcal{O}(\alpha)$ and the full $\mathcal{O}(\alpha)$ results. This of course is the reason for

\sqrt{s}	'Born'	FPAIR	LL $\mathcal{O}(\alpha^2)$	$\mathcal{O}(\alpha^2)$	$\mathcal{O}(\alpha^2)+\text{exp.}$
89.1	548.2	403±1	400.1	404.1±.7	400.6±.7
		394±1	389.3	394.2±.1	390.8±.1
	370.2	268±1	268.2	270.2±.1	267.8±.1
		264±1	262.2	265.0±.1	262.7±.1
91.1	1956.	1448±5	1437.	1452.±.1.	1447.±.1.
		1420±5	1403.	1421.±.1.	1416.±.1.
	1321.	969±3	967.5	973.4±1.7	969.8±1.7
		954±3	946.0	956.1±.3	952.6±.3
93.1	552.5	600±1	594.4	599.4±.2	607.7±.2
		587±1	579.2	584.9±.1	693.1±.1
	373.0	399±1	397.6	400.0±.1	405.6±.1
		392±1	388.6	391.6±.2	397.1±.2
120.1	11.37	29.0±.1	28.8	29.2±.1	29.0±.1
		27.1±.1	26.6	26.7±.1	26.6±.1
	7.67	16.6±.1	16.2	16.5±.1	16.4±.1
		16.1±.1	15.7	15.8±.1	15.7±.1

Table 3.2. Results for the total cross section compared with FPAIR. The four lines per value for \sqrt{s} (GeV) correspond to the four sets of cuts defined in eq.(3.8.1). All cross sections are in picobarn.

calculating these higher order corrections. The calculation is completed by exponentiating the soft photon contributions, which is important when slightly off resonance (i.c. at 89.1 and 93.1 GeV), where the cross section is rapidly varying as a function of s and where hence soft photon corrections are dominant.

- Away from the resonance (i.c. at 120 GeV) the $\mathcal{O}(\alpha^2)$ may still be important, but soft photon exponentiation is not interesting any more. This is due to the fact that soft photon corrections are not the dominant ones here.

In comparing with BABAMC we have checked our $\mathcal{O}(\alpha)$ corrections. It would be nice also to have a check on the higher order ones. For the t-channel contributions there is no program available to compare the higher order corrections with. For the s-channel however there is. We will compare with the program FPAIR [17], which is a Monte Carlo program including $\mathcal{O}(\alpha^2)$ initial state corrections and $\mathcal{O}(\alpha)$ final state corrections. We did a number of runs at the same points in energy as we took when comparing with BABAMC, but now we calculated the s-channel contributions only, with muons as the final state fermions. In comparing we now could take the version of the pure weak corrections that was discussed in section 3.7. An entirely different problem however was that we had to leave out the interference between initial and final state QED corrections and the QED

ζ_{max}	BABAMC	LL $\mathcal{O}(\alpha)$	$\mathcal{O}(\alpha)$	$\mathcal{O}(\alpha^2)$	$\mathcal{O}(\alpha^2)+exp.$
180°	5750.±5.	5744.	5749.±7.	5838.±7.	5865.±7.
20°	5619.±5.	5633.	5629.±7.	5725.±7.	5753.±7.
10°	5505.±5.	5534.	5506.±7.	5611.±7.	5640.±7.
5°	5329.±5.	5380.	5336.±8.	5461.±8.	5492.±8.
180°	1127.±2.	1120.	1127.±1.	1180.±1.	1179.±1.
20°	1108.±2.	1112.	1109.±1.	1163.±1.	1162.±1.
10°	1087.±2.	1104.	1089.±1.	1144.±1.	1143.±1.
5°	1056.±2.	1090.	1057.±1.	1115.±1.	1114.±1.

Table 3.3. Results for the total cross section (in picobarn) using an acollinearity cut, compared with BABAMC. All entries are calculated at $\sqrt{s} = 91.1$ GeV. The upper half of the table is for an angular cut of 10°, the lower half for an angular cut of 42°.

box diagrams. Having done that the results of the two programs could be compared. The results for the same set of cuts as used for table 3.1 are listed in table 3.2. In this table the third and fifth column from the left can be compared. From table 3.2 we conclude that our calculation agrees with FPAIR and hence that our $\mathcal{O}(\alpha^2)$ corrections are in good shape. As in the case of the comparison with BABAMC we observe that the result of the LL calculation comes close to the result of the full calculation. Also again we see an influence of the soft photon exponentiation when around the Z resonance, but not away from it.

Having compared with BABAMC and with FPAIR we know the $\mathcal{O}(\alpha)$ and $\mathcal{O}(\alpha^2)$ corrections to be correct. Also we know that the cuts on the energies and angles of the outgoing particles have been incorporated correctly. The correctness of the cut on the acollinearity can be deduced from table 3.3. Once again the full $\mathcal{O}(\alpha)$ corrected results coincide with the BABAMC results. Differences with table 3.1 for $\zeta_{max} = 180^\circ$ are merely statistical fluctuations. It is also clear from the table that in the LLA the result for the total cross section deviates a little more from the fully corrected result, once a rather stringent cut is applied on the acollinearity. The fact that this effect is compensated when adding the non-log contributions is another check of the program.

Next we want to investigate the implications of the higher order corrections for some physics results. Experiments at LEP/SLC are already well on their way in measuring, among other things, large angle Bhabha scattering [23]. As a typical angular region we will consider scattering between 42° and 138°. In this region the s-channel contributions dominate. Nevertheless there is a still sizable t-channel contribution (about 13% for the Born approximation) that will turn out to have a noticeable effect on the influence of higher order corrections. Despite that, one can still consider quantities that are of interest in pure s-channel processes, such as the peak height of the Z resonance (σ_{max}), the peak

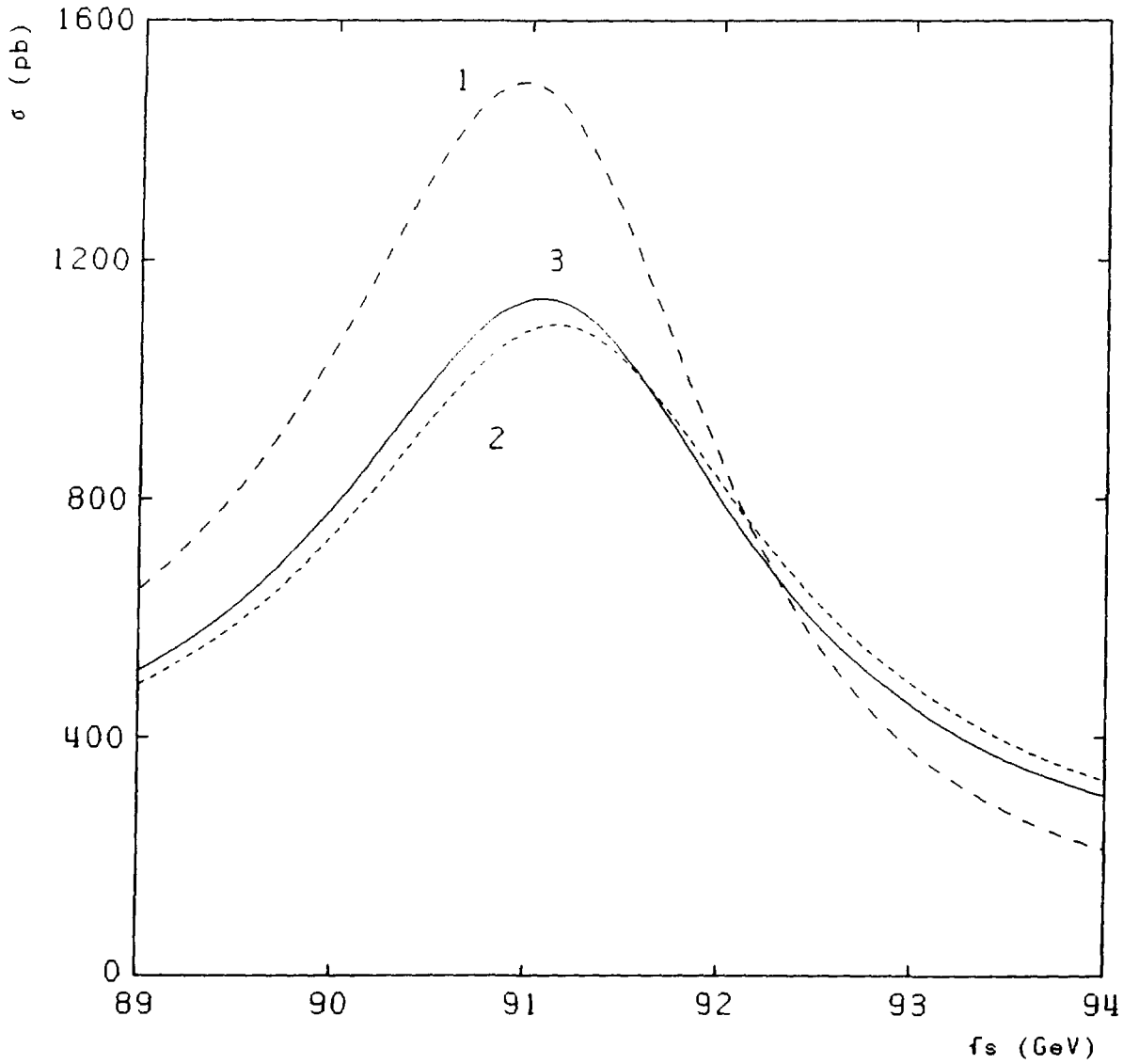


Fig. 3.2. The total cross section as a function of the energy, using an angular cut of 42° and an energy cut of 10 GeV. The first curve (long dash) corresponds to the Born result, including pure weak corrections, the second curve (short dash) includes first order LL QED corrections and the third line (solid line) has second order exponentiated LL QED corrections.

$\sqrt{s_{max}}$	$\sqrt{s_-}$	$\sqrt{s_+}$	$\sqrt{s_+} - \sqrt{s_-}$	$\sigma_{max}(\text{pb})$
91.16	89.91	92.41	2.50	1318.
90.96	89.32	92.17	2.85	1495.
91.14	89.30	92.77	3.47	1094.
91.06	89.28	92.57	3.29	1136.

Table 3.4. Peak height and positions for Bhabha scattering with $M_Z = 91.17$ GeV. The first line corresponds to only s -channel contributions at Born level, including weak corrections. Lines 2-4 correspond to lines 1-3 of figure 3.2, so the second line in this table is for Born s - and t -channel, including pure weak corrections, the third line includes first order LL QED corrections and the last line has second order exponentiated LL QED corrections. All positions are in GeV.

position ($\sqrt{s_{max}}$) and the two positions where the peak is reduced to half its peak height ($\sqrt{s_{\pm}}$). In figure 3.2 we have plotted three curves to demonstrate the effects on these quantities. For the input parameters we took $M_Z = 91.17$ GeV, $M_H = 100$ GeV and $m_{top} = 100$ GeV. We required a minimum energy for the outgoing particles of 10 GeV, but imposed no cut on the acollinearity. The first line corresponds to the Born result including pure weak corrections. The second line then includes LL $\mathcal{O}(\alpha)$ QED corrections, whereas the third line includes LL $\mathcal{O}(\alpha^2)$ exponentiated QED corrections. In table 3.4 the values for the above mentioned quantities are listed together with the result for s -channel scattering only (at Born level). Especially interesting are the differences between the last two lines in this table, as they show the need for calculating higher order corrections once more. Particularly noteworthy are also the differences between the values for $\sqrt{s_+} - \sqrt{s_-}$, which may be seen as the apparent width of the Z resonance. Table 3.4 shows that upon including the t -channel contributions, this quantity increases with respect to the apparent width from the s -channel.

A similar picture can be made when calculating the total cross section in the angular region from 10° to 170° . Because of the dominance of the t -channel contributions in this region, the Z resonance is not as significant any more. In particular there is no sense any more in looking for the positions where the peak is at half its maximum height. The curves for the total cross section with and without QED corrections are given in figure 3.3. Notice that in this figure the differences between the first order and the higher order corrected curves is still apparent. In other words, although the result is dominated by the t -channel contributions, the higher order corrections are still needed. This gives rise to the question whether these higher order corrections would still be needed if the s -channel contributions were entirely negligible. Therefore we have calculated the t -channel contributions and their corrections separately. We have listed the results in table 3.5. Here we have included results from an $\mathcal{O}(\alpha)$ calculation with an exponentiation of soft photons. We see that such an approximation is not reliable. The $\mathcal{O}(\alpha^2)$ hard bremsstrahlung still

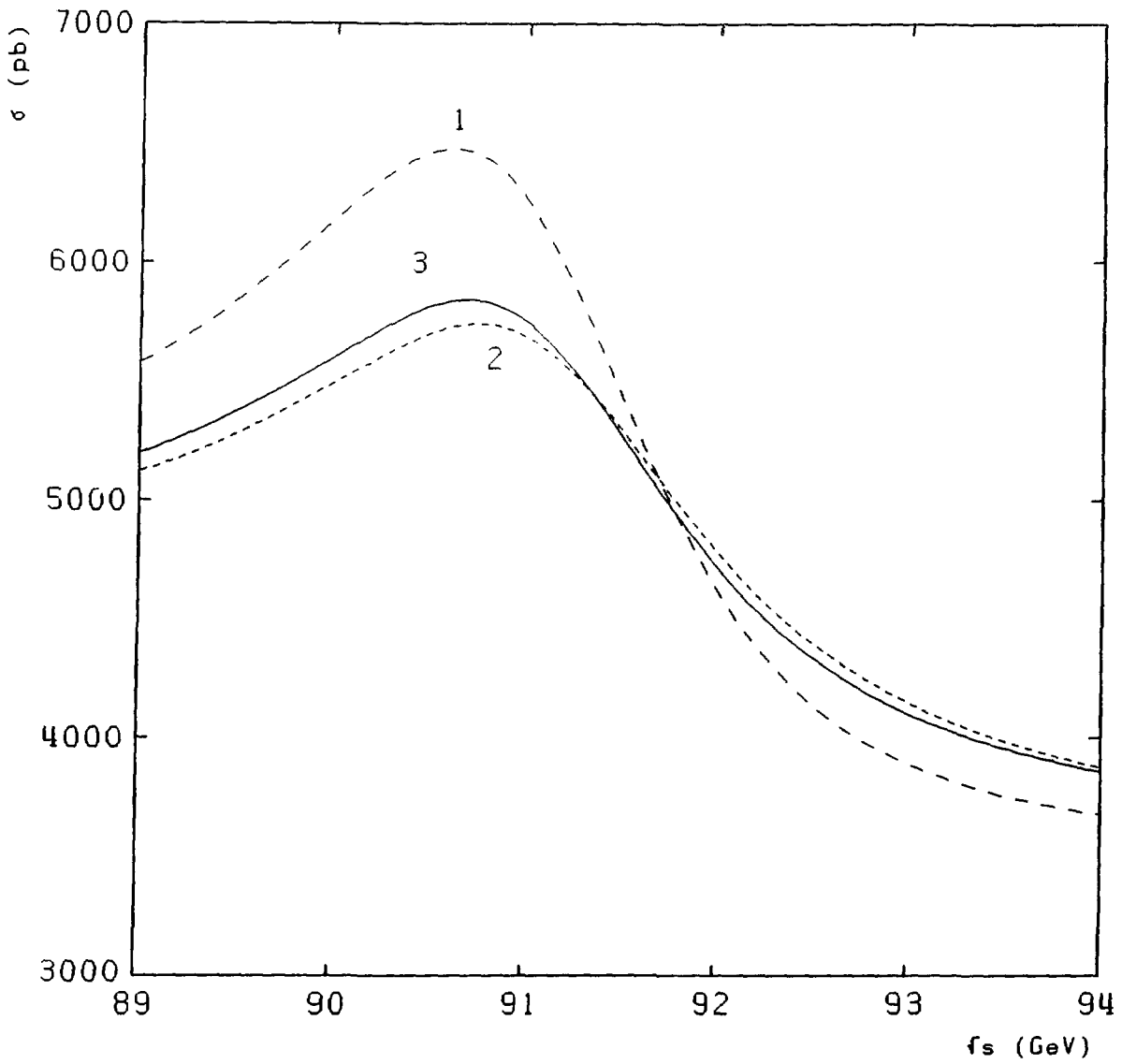


Fig. 3.3. The total cross section as a function of the energy, using an angular cut of 10° and an energy cut of 10 GeV. The conventions are the same as in figure 3.2.

\sqrt{s}	'Born'	LL $\mathcal{O}(\alpha)$	$\mathcal{O}(\alpha)$	$\mathcal{O}(\alpha)+\text{exp.}$	$\mathcal{O}(\alpha^2)$	$\mathcal{O}(\alpha^2)+\text{exp.}$
89.1	4475.	4453.	4427.±16.	4425.±16.	4487.±16.	4489.±16.
		4126.	4116.±21.	4104.±21.	4135.±21.	4139.±21.
	177.6	172.4	170.8±.2	170.6±.2	172.4±.2	172.6±.2
		165.1	163.8±.2	163.6±.2	164.8±.2	164.9±.2
91.1	4286.	4264.	4224.±18.	4223.±18.	4282.±18.	4284.±18.
		3951.	3936.±18.	3925.±18.	3910.±18.	3914.±18.
	170.8	165.8	164.7±.2	164.5±.2	166.3±.2	166.4±.2
		158.8	157.0±.2	156.8±.2	157.9±.2	158.1±.2
93.1	4104.	4083.	4044.±18.	4043.±18.	4100.±18.	4102.±18.
		3783.	3792.±16.	3781.±16.	3809.±16.	3812.±16.
	162.9	158.1	156.9±.2	156.8±.2	158.4±.2	158.5±.2
		151.4	149.8±.2	149.6±.2	150.7±.2	150.8±.2
120.1	2477.	2464.	2450.±9.	2449.±9.	2484.±9.	2486.±9.
		2278.	2288.±9.	2281.±9.	2299.±9.	2301.±9.
	96.57	93.60	92.8±.1	92.7±.1	94.7±.1	94.8±.1
		89.50	88.6±.1	88.5±.1	90.2±.1	90.2±.1

Table 3.5. The t-channel contributions and their corrections. The four lines per value for \sqrt{s} (GeV) correspond to the four sets of cuts defined in eq.(3.8.1). All cross sections are in picobarn.

gives a surprisingly large contribution. This can be explained as follows. The part of the Born matrix element squared that is given by $|\widehat{\mathcal{M}}|^2 = 64\pi^2\alpha^2\hat{s}^2/t_1^2$ is by far the dominant part. The second order initial state leading log corrections to this part can be calculated for $E_0 = 0$ to be

$$\begin{aligned}
\Delta\sigma = \frac{4\pi\alpha^2}{s} \left(\frac{\alpha L_m}{\pi}\right)^2 & \left\{ \frac{4c_m}{1-c_m^2} \left[-\frac{1}{2}c_m \log x_{min} + \zeta(2) + \frac{13}{64c_m}(1+c_m)^2 \right. \right. \\
& \left. \left. - \log \frac{1-c_m}{1+c_m} \log \frac{2c_m}{1+c_m} + 2 \log^2 \frac{2c_m}{1+c_m} \right] \right. \\
& + \frac{1-c_m}{1+c_m} \left[-\frac{1}{8} \log \frac{1-c_m}{1+c_m} - \frac{1}{8} \log^2 \frac{1-c_m}{1+c_m} + \frac{3}{16} \right. \\
& \left. \left. - 2 \text{Li}_2 \left(\frac{1-c_m}{1+c_m} \right) + 2\zeta(2) \right] - \frac{3}{2} \log \frac{1-c_m}{1+c_m} - 1 \right\}. \quad (3.8.2)
\end{aligned}$$

It can be seen that for c_m values close to unity the above expression contains terms proportional to $1/(1-c_m)$, just like the Born term. This in contrast to the first order corrections given by eq.(3.3.12). Therefore the $\mathcal{O}(\alpha)$ LL corrections are suppressed with a factor $(1-c_m)$ with respect to the Born term, whereas the $\mathcal{O}(\alpha)$ non-log terms and the $\mathcal{O}(\alpha^2)$ LL corrections are not. This explains why in tabel 3.5 the $\mathcal{O}(\alpha^2)$ LL corrections

can get of the order of the $\mathcal{O}(\alpha)$ LL corrections.

In eq.(3.8.2) x_{min} is an ad hoc lower bound on the fractions $x_{1,2}$, introduced for argument's sake. In the above example this lower bound is assumed to be small. If no cuts on energies or acollinearity are imposed, x_{min} is of the order of m_e/\sqrt{s} . Since in the LL approach masses have been neglected wherever possible, the exact mass dependence of this lower bound cannot be determined here. In a realistic calculation it is therefore better to introduce an energy cut $E_0 \gg m_e$ to avoid problems with mass terms.

Finally it should be noted that we have checked that the suppression factor $(1 - c_m)$ for the $\mathcal{O}(\alpha)$ LL corrections is a consequence of taking symmetric angular cuts, i.e. integrating from ϑ_{min} to $180 - \vartheta_{min}$. This means that for luminosity type of calculations this suppression factor is not present.

Appendix 3.A: The first order virtual and soft QED corrections

For completeness we list here the form of the first order virtual and soft QED corrections in a way that is suited for application to both s- and t-channel diagrams.

The QED vertex corrections to the s-channel diagrams can be incorporated by adding a contribution that is a factor times the lowest order diagrams, the factor being

$$\frac{\alpha}{2\pi} Q_e^2 \Lambda_1(s, m_e) = \frac{\alpha}{2\pi} Q_e^2 \left\{ \left[2 \log \frac{\lambda^2}{-s - i\epsilon} + \log \frac{-s - i\epsilon}{m_e^2} \right] \left[\log \frac{-s - i\epsilon}{m_e^2} - 1 \right] + 2 \log \frac{-s - i\epsilon}{m_e^2} + 4 \left(\frac{\pi^2}{12} - 1 \right) \right\}. \quad (3.A.1)$$

For the t-channel diagrams one merely has to replace s by t . In this formula the photon mass λ is the IR regulator that has to cancel in any physics result and ϵ is a small offset to fix the analytical continuation.

For the box contributions we find that we can write their contribution as factors times the lowest order diagrams (having one virtual photon less), provided we do so per helicity combination of the particles involved. We define λ_1 to be minus the helicity of the outgoing positron and λ_2 as the helicity of the incoming electron (this choice is made irrespective of the particular channel). One of course has to sum the result over helicities explicitly, since usually only the sum is desired. For a specific helicity combination however the $\gamma\gamma$ boxes in the s-channel yield the following factor times the lowest order s-channel photon exchange matrix element

$$Q_e^2 \{ V^\gamma(s, t) + \lambda_1 \lambda_2 A^\gamma(s, t) \}, \quad (3.A.2)$$

with

$$A^\gamma(s, t) = \frac{\alpha}{2\pi} [G(s, t) + G(s, u)],$$

$$V^{\gamma\gamma}(s,t) = \frac{\alpha}{2\pi} \left[G(s,t) - G(s,u) + 2 \log \frac{\lambda^2}{-s-i\epsilon} \log \frac{t+i\epsilon}{u} \right], \quad (3.A.3)$$

$$G(s,t) = \frac{s}{2(s+t)} \log \frac{t}{s+i\epsilon} - \frac{s(s+2t)}{4(s+t)^2} \left[\log^2 \frac{t}{s+i\epsilon} + \pi^2 \right].$$

The t-channel analogues can be obtained by $s \leftrightarrow t$. The contribution from the γZ boxes in the s-channel can be written in a similar way:

$$Q_e^2 \{ V^{\gamma Z}(s,t) + \lambda_1 \lambda_2 A^{\gamma Z}(s,t) \}, \quad (3.A.4)$$

with

$$A^{\gamma Z}(s,t) = \frac{\alpha}{2\pi} [A(s,t) + A(s,u)],$$

$$V^{\gamma Z}(s,t) = \frac{\alpha}{2\pi} \left[A(s,t) - A(s,u) + 2 \text{Li}_2 \left(1 + \frac{M^2}{t+i\epsilon} \right) - 2 \text{Li}_2 \left(1 + \frac{M^2}{u} \right) + 4 \log \frac{M\lambda}{M^2-s} \log \frac{t+i\epsilon}{u} \right], \quad (3.A.5)$$

$$A(s,t) = \frac{s-M^2}{s+t} \left\{ \log \frac{t+i\epsilon}{s-M^2} + \frac{M^2}{s} \log \left(1 - \frac{s}{M^2} \right) + \frac{s+2t+M^2}{s+t} \left[\log \left(-\frac{t+i\epsilon}{M^2} \right) \log \frac{M^2-s}{M^2+t} + \text{Li}_2 \left(\frac{s}{M^2} \right) - \text{Li}_2 \left(-\frac{t}{M^2} \right) \right] \right\},$$

using the shorthand notation

$$M^2 \equiv \begin{cases} M_Z^2 - iM_Z\Gamma_Z & \text{(s channel boxes)} \\ M_Z^2 & \text{(t channel boxes)} \end{cases}.$$

Γ_Z is the $\mathcal{O}(\alpha)$ corrected total width of the Z, expressions for which can e.g. be found in [24]. Again the t-channel analogues are obvious. Finally the soft photon contributions are given by the soft factor S times the lowest order matrix element squared, S being

$$S = \frac{\alpha}{\pi} Q_e^2 \left\{ \left(2 \log \epsilon - \log \frac{\lambda^2}{s} \right) (2B_e + B_{int}) - \frac{2}{3} \pi^2 + 1 - B_e^2 - 2 \text{Li}_2 \left(1 + \frac{s}{t} \right) + 2 \text{Li}_2 \left(1 + \frac{s}{u} \right) \right\}. \quad (3.A.6)$$

Here we have defined ϵ to be the soft photon cut-off in units of $\frac{1}{2}\sqrt{s}$ and furthermore

$$B_e = \log \frac{s}{m_e^2} - 1, \\ B_{int} = 2 \log \frac{t}{u}.$$

The dilogarithm function is defined by

$$\text{Li}_2(z) \equiv - \int_0^1 \frac{\log(1-zt)}{t} dt ,$$

for complex z values that do not lie on the dilogarithmic cut.

References

- [1] M. Böhm, A. Denner and W. Hollik, Nucl. Phys. B304 (1988) 687.
F.A. Berends, R. Kleiss and W. Hollik, Nucl. Phys. B304 (1988) 712.
- [2] D.Y. Bardin et al., in "Z Physics at LEP 1", CERN 89-08, Vol.1, p.89, eds. G. Altarelli, R. Kleiss and C. Verzegnassi.
- [3] S. Jadach and B.F.L. Ward, Phys. Rev. D38 (1988) 2897 (E: D39 (1989) 1471);
Contr. to Proceedings of the Workshop on "electroweak Radiative Corrections", Ringberg Castle (FRG), 1989, ed. J. H. Kühn;
Contr. to Proceedings of the NATO Conference on Radiative Corrections, Brighton, 1989, to be published.
- [4] M. Caffo, E. Remiddi and F. Semeria in "Z Physics at LEP 1", CERN 89-08, Vol.1, p.171, eds. G. Altarelli, R. Kleiss and C. Verzegnassi.
M. Greco, La Riv. Nuovo Cim. 11 (1988) 1.
- [5] F.A. Berends and G. Komen, Nucl. Phys. B115 (1976) 114.
- [6] F.A. Berends, G.J.H. Burgers and W.L. van Neerven, Nucl. Phys. B297 (1988) 429.
- [7] W. Hollik, Fortschr. Physik. 38 (1990) 165.
- [8] W. Beenakker, thesis University of Leiden (1989).
- [9] E.A. Kuraev and V.S. Fadin, Sov. J. Nucl. Phys. 41 (1985) 466.
- [10] G. Altarelli and G. Martinelli, Yellow Report, CERN 86-02 (1986) 47.
- [11] O. Nicosini and L. Trentadue, Phys. Lett. B196 (1987) 551.
- [12] W. Beenakker, F.A. Berends and W.L. van Neerven, in Proceedings of the Workshop on "electroweak Radiative Corrections", Ringberg Castle (FRG), 1989, ed. J. H. Kühn.
- [13] N. Nakanishi, Progr. Theor. Phys. 19 (1958) 159

- [14] T. Kinoshita, *J. Math. Phys.* **3** (1962) 650.
T.D. Lee and M. Nauenberg, *Phys. Rev.* **B133** (1964) 1549.
- [15] J.C. Collins and G. Sterman, *Nucl. Phys.* **B185** (1982) 172.
J.C. Collins, D.E. Soper and G. Sterman, *Phys. Lett* **B134** (1984) 263; *Nucl. Phys.* **B261** (1985) 104.
G.T. Bodwin, *Phys. Rev.* **D31** (1985) 2616 and references therein.
- [16] V.N. Gribov and L.N. Lipatov, *Sov. J. Nucl. Phys.* **15** (1972) 438, 675.
G. Altarelli and G. Parisi, *Nucl. Phys.* **B126** (1977) 298.
E.G. Floratos, D.A. Ross and C.T. Sachrajda, *Nucl. Phys.* **B129** (1977) 66; *E: B139* (1978) 545.
A. González-Arroyo, C. López and F.J. Ynduráin, *Nucl. Phys.* **B153** (1979) 161.
A. González-Arroyo and C. López, *Nucl. Phys.* **B166** (1980) 429.
E.G. Floratos, C. Kounnas and R. Lacaze, *Phys. Lett.* **B98** (1981) 89,285.
- [17] R. Kleiss and S.C. van der Marck, *Nucl. Phys.* **B342** (1990) 61,
see also chapter 6 of this thesis.
- [18] F.A. Berends, R. Kleiss, P. de Causmaecker, R. Gastmans, W. Troost and T.T. Wu, *Nucl. Phys.* **B206** (1982) 61.
R. Kleiss, *Z. f. Phys.* **C33** (1987) 433.
F.A. Berends, R. Kleiss and W. Hollik, *Nucl. Phys.* **B304** (1988) 712.
- [19] G.P. Lepage, *J. Comp. Phys.* **27** (1978) 192.
G.P. Lepage, Cornell preprint CLNS-80/447 (1980).
- [20] H. Burkhardt, F. Jegerlehner, G. Penso and C. Verzegnassi, *Z. f. Phys.* **C43** (1989) 497.
H. Burkhardt, in *Proceedings of the Workshop on "electroweak Radiative Corrections"*, Ringberg Castle (FRG), 1989, ed. J. H. Kühn.
H. Burkhardt, in *Proceedings of the NATO Conference on Radiative Corrections*, Brighton, 1989, to be published.
- [21] D.R. Yennie, S.C. Frautschi and H. Suura, *Ann. Phys.* **13** (1961) 379.
- [22] G. Marsaglia and A. Zaman, Florida State University Report FSU-SCRI-87-50 (1987).
F. James, CERN preprint DD 88-22 (1988).
- [23] ALEPH collaboration, *Phys. Lett.* **B235** (1990) 399,
DELPHI collaboration, *Phys. Lett.* **B241** (1990) 425,
L3 collaboration, *Phys. Lett.* **B238** (1990) 122,
OPAL collaboration, *Phys. Lett.* **B240** (1990) 497,
MARK II collaboration, *Phys. Rev. Lett.* **63** (1989) 2780.
- [24] W. Beenakker and W. Hollik, *Z. f. Phys.* **C40** (1988) 141.

Chapter 4

The forward backward asymmetry

The precision experiments at LEP require an accurate knowledge of radiative corrections. For the Z line shape accurate evaluations are available [1]. For Bhabha scattering the situation has recently been improved [2]. The resonance shape for a total Bhabha cross section restricted with respect to the angles and energies of the e^+ and e^- in the final state has been evaluated with high precision. To be specific, as to the photonic corrections the $\mathcal{O}(\alpha)$ correction has been included exactly, the $\mathcal{O}(\alpha^2)$ is evaluated in the leading log (LL) approximation, whereas the soft photons have been resummed. The weak corrections are taken in $\mathcal{O}(\alpha)$ except in the propagators which contain some $\mathcal{O}(\alpha^2)$ effects [1]. The technique of that evaluation can also be applied to the forward-backward asymmetry A_{FB} in muon pair production. This technique is based on the structure function approach for *differential* cross sections, which was discussed for QED corrections in ref.[3].

It is worthwhile to apply the method to A_{FB} . The present situation for A_{FB} is summarized in ref.[4]. In particular various A_{FB} calculations [3, 5, 6, 7, 8] are compared. From the review it is clear that there is room for improvement. The weak corrections have been calculated by a number of groups [9, 10] and agree. The differences arise in the photonic corrections. There are several $\mathcal{O}(\alpha)$ calculations, but the situation for the $\mathcal{O}(\alpha^2)$ corrections is less established. Some calculations take $\mathcal{O}(\alpha^2)$ in LL into account, but only one evaluation does this with the correct flux function. Others use for A_{FB} the same flux function as for total cross sections, whereas in ref.[3] it has been shown that for hard photons this is not correct. There is however another serious problem with all semi analytical calculations reviewed in [4]. None of them incorporates energy and/or acollinearity cuts, so that the results cannot be applied to realistic situations.

The present calculation wants to improve on the above sketched situation by including these cuts and wants to avoid incorrect flux function procedures. The latter is achieved by the structure function approach for *differential* cross sections. It is closely related to that of ref.[2], except that the angular ranges are different. We shall indicate below how this affects the integration boundaries. We also discuss two possible definitions of A_{FB} which arise naturally.

The forward-backward asymmetry can be defined in a number of ways, all of which are equivalent in the Born approximation. We will consider two definitions. In both definitions

the asymmetry is defined as the difference of forward scattering and backward scattering divided by the sum of these two:

$$A_{FB} = \frac{\sigma_F - \sigma_B}{\sigma_F + \sigma_B} . \quad (4.1)$$

However the ingredients σ_F and σ_B differ for the two definitions we want to consider. Define

$$\begin{aligned} c_+ &\equiv \cos \vartheta_+ \equiv \cos \angle (e^+, \bar{f}) \equiv \cos \angle (\vec{p}_1, \vec{p}_3) , \\ c_- &\equiv \cos \vartheta_- \equiv \cos \angle (e^-, f) \equiv \cos \angle (\vec{p}_2, \vec{p}_4) . \end{aligned} \quad (4.2)$$

The definition for σ_F and σ_B that is commonly used for theoretical calculations is

$$\begin{aligned} \sigma_{F,1} &: c_- > 0 \quad c_+ \text{ arbitrary}, \\ \sigma_{B,1} &: c_- < 0 \quad c_+ \text{ arbitrary}. \end{aligned} \quad (4.3)$$

that is, one looks at one particle only. We will refer to this definition and its associated A_{FB} as definition 1. Since in experiments one usually detects the other particle, it makes sense to take as a second definition

$$\begin{aligned} \sigma_{F,2} &: c_+, c_- > 0 , \\ \sigma_{B,2} &: c_+, c_- < 0 . \end{aligned} \quad (4.4)$$

Only events with a large acollinearity between f and \bar{f} can contribute to the difference between these two definitions. Hence the definitions coincide at the Born level. Moreover in general the difference can be reduced by imposing an acollinearity cut. In the remainder the method is sketched to calculate the asymmetry according to both definitions. Numerical results are presented and compared with the literature.

The starting point is to calculate the cross section for specific angular and energy cuts. Moreover an acollinearity cut can be applied. The precise cuts that are imposed are defined by

$$\begin{aligned} \vartheta_{m+} &< \vartheta_+ < \vartheta_{M+} , \\ \vartheta_{m-} &< \vartheta_- < \vartheta_{M-} , \\ E_f &> \hat{E}_0^+ \times \frac{1}{2} \sqrt{s} , \\ E_f &> \hat{E}_0^- \times \frac{1}{2} \sqrt{s} , \\ \zeta &< \zeta_{max} . \end{aligned} \quad (4.5)$$

In the leading log approximation (LLA) the cross section including QED and weak corrections can then be written as

$$\begin{aligned} \sigma = \frac{1}{s^2} \int_{x_{1,min}}^1 \frac{dx_1}{x_1^2} \int_{x_{2,min}}^1 \frac{dx_2}{x_2^2} \Gamma(x_1) \Gamma(x_2) \int_{\hat{t}_{1,min}}^{\hat{t}_{1,max}} d\hat{t}_1 \frac{\sum |\mathcal{M}|^2(x_1 x_2 s, \hat{t}_1)}{64\pi} \\ \times \int_{x_{3,min}}^1 dx_3 \mathcal{D}(x_3) \int_{x_{4,min}}^1 dx_4 \mathcal{D}(x_4) . \end{aligned} \quad (4.6)$$

This formula was derived in [2] for a somewhat more limited set of cuts. The notation and definitions are taken over from [2]. Although \hat{t}_1 is now an integration variable, it originates from $\hat{t}_1 = (x_1/x_3)(p_1 - p_3)^2$. The quantity $\frac{1}{4} \sum |\mathcal{M}|^2(s, t)$ is the spin averaged Born matrix element squared, including pure weak corrections, $\Gamma(x)$ is the splitting function and $\mathcal{D}(x)$ the fragmentation function. Both $\Gamma(x)$ and $\mathcal{D}(x)$ depend on a scale Q^2 and the initial state fermion mass m_e (Γ) or the final state fermion mass m_f (\mathcal{D}). We shall return to the matter of the scale choice later on. For the masses $m_{e,f}$ of the fermions the small mass limit is taken. The boundaries on the integration variables stem from the cuts that are imposed. Therefore if the lower bound on an integration variable becomes larger than the upper bound, the integration has to yield zero, since in that case the two cuts cannot be satisfied at the same time.

The boundaries on x_3 and x_4 are given by

$$\begin{aligned} x_{3,\min} &= \frac{\hat{E}_0^+}{x_1 - \frac{\hat{t}_1}{s} \frac{1 - x_1/x_2}{x_1}}, \\ x_{4,\min} &= \frac{\hat{E}_0^-}{x_2 + \frac{\hat{t}_1}{s} \frac{1 - x_1/x_2}{x_1}}. \end{aligned} \quad (4.7)$$

The lower boundaries on x_3 and x_4 therefore depend on \hat{t}_1 , which is possible, because we integrate over \hat{t}_1 later. The boundaries for \hat{t}_1 in turn depend on the values of x_1 and x_2 . Introducing the notation

$$\begin{aligned} c_{M+} &= \cos \vartheta_{m+} & c_{m+} &= \cos \vartheta_{M+}, \\ c_{M-} &= \cos \vartheta_{m-} & c_{m-} &= \cos \vartheta_{M-}. \end{aligned} \quad (4.8)$$

the \hat{t}_1 boundaries are

$$\hat{t}_{1,\min} = \begin{cases} \max \left(\frac{-x_1 x_2 s}{1 + \frac{x_1}{x_2} \frac{1 + c_{m-}}{1 - c_{m-}}}, \frac{-x_1 x_2 s}{1 + \frac{x_2}{x_1} \frac{1 + c_{m+}}{1 - c_{m+}}}, -x_2 s \frac{x_1 - \hat{E}_0^+}{1 - x_2/x_1} \right) & \text{for } x_1 > x_2, \\ \max \left(\frac{-x_1 x_2 s}{1 + \frac{x_1}{x_2} \frac{1 + c_{m-}}{1 - c_{m-}}}, \frac{-x_1 x_2 s}{1 + \frac{x_2}{x_1} \frac{1 + c_{m+}}{1 - c_{m+}}}, -x_1 s \frac{x_2 - \hat{E}_0^-}{1 - x_1/x_2} \right) & \text{for } x_1 < x_2, \end{cases} ,$$

$$\hat{t}_{1,\max} = \begin{cases} \min \left(\frac{-x_1 x_2 s}{1 + \frac{x_1}{x_2} \frac{1 + c_{M-}}{1 - c_{M-}}}, \frac{-x_1 x_2 s}{1 + \frac{x_2}{x_1} \frac{1 + c_{M+}}{1 - c_{M+}}}, -x_1 s \frac{x_2 - \hat{E}_0^-}{1 - x_1/x_2} \right) & \text{for } x_1 > x_2, \\ \min \left(\frac{-x_1 x_2 s}{1 + \frac{x_1}{x_2} \frac{1 + c_{M-}}{1 - c_{M-}}}, \frac{-x_1 x_2 s}{1 + \frac{x_2}{x_1} \frac{1 + c_{M+}}{1 - c_{M+}}}, -x_2 s \frac{x_1 - \hat{E}_0^+}{1 - x_2/x_1} \right) & \text{for } x_1 < x_2. \end{cases} \quad (4.9)$$

From the requirement that $\hat{t}_{1,min} < \hat{t}_{1,max}$ one can derive that

$$\begin{aligned} \frac{x_1}{x_2} &> \sqrt{\frac{1+c_{m+}}{1-c_{m+}} \frac{1-c_{M-}}{1+c_{M-}}} , \\ \frac{x_2}{x_1} &> \sqrt{\frac{1-c_{M+}}{1+c_{M+}} \frac{1+c_{m-}}{1-c_{m-}}} , \\ x_1 + x_2 &> \hat{E}_0^+ + \hat{E}_0^- . \end{aligned} \quad (4.10)$$

These restrictions on $x_{1,2}$ are not complete, but the full ones are rather complicated. However the full ones are all included in the requirement $\hat{t}_{1,min} < \hat{t}_{1,max}$, which can be easily implemented if the integrations over x_1 and x_2 are done numerically. The acollinearity cut can also be implemented in a numerical way, determining the allowed \hat{t}_1 region by a numerical search for the boundaries [2].

Equation (4.6) can be written as

$$\sigma = \int_0^1 dx_1 \int_0^1 dx_2 \Gamma(x_1) \Gamma(x_2) f(x_1, x_2) , \quad (4.11)$$

where the integration over the fractions $x_{1,2}$ is over the full range from 0 to 1, because the boundaries are included in the analytically evaluated function f using ϑ -functions. In general the function f is not symmetric in its arguments. However since the integration is a symmetric one, we only need the symmetric part of f :

$$f^{symm}(x_1, x_2) = \frac{1}{2} f(x_1, x_2) + \frac{1}{2} f(x_2, x_1) . \quad (4.12)$$

Using the function f^{symm} exponentiation can be carried out following the procedure outlined in [2]. It can furthermore be shown that if the same cuts are applied for both particles, i.e.

$$c_{m-} = c_{m+} \quad \text{and} \quad c_{M-} = c_{M+} \quad \text{and} \quad \hat{E}_0^+ = \hat{E}_0^- ,$$

the function f is automatically symmetric.

This completes our discussion of the LL calculation of the total cross section with cuts as defined in eq.(4.5). At first order the non-log QED contributions can be calculated in a numerical way, so that the first order corrections are complete. A discussion of this non-log calculation can be found in [2].

It is easy to see that using the cuts as defined in eq.(4.5) one can calculate the forward-backward asymmetry according to both definition 1 and definition 2. In principle one can even calculate the cross section for a small bin in the angle of one of the particles ('angular distribution'). However one must be careful choosing the scale Q^2 . The requirement on the choice is that the first order LL contributions are dominant over the non-log ones, which can be checked because we perform a complete first order calculation. This then justifies calculating only the LL corrections at higher orders.

\sqrt{s}	Forward				Backward			
	'Born'	LL $\mathcal{O}(\alpha)$	$\mathcal{O}(\alpha)$	$\mathcal{O}(\alpha^2)$	'Born'	LL $\mathcal{O}(\alpha)$	$\mathcal{O}(\alpha)$	$\mathcal{O}(\alpha^2)$
88.17	109.9	77.1	77.9(1)	84.2(1)	188.7	140.0	140.8(1)	148.7(3)
		73.4	73.6(1)	79.4(1)		136.3	136.6(1)	144.1(1)
89.17	234.0	154.3	155.7(1)	169.9(2)	330.6	230.8	232.3(1)	248.5(2)
		150.4	150.9(1)	164.7(1)		226.9	227.1(2)	243.5(1)
90.17	567.7	358.6	361.8(2)	398.3(2)	662.6	440.3	444.0(3)	479.9(3)
		354.5	356.2(2)	392.0(2)		436.1	437.6(3)	474.1(2)
91.17	1014.9	689.2	695.5(3)	741.4(5)	983.3	704.1	710.4(6)	744.3(5)
		684.3	687.6(4)	733.6(4)		699.3	701.5(4)	737.0(6)
92.17	668.1	583.1	587.6(3)	578.7(3)	540.5	518.4	522.6(4)	504.1(2)
		577.7	580.8(3)	571.9(4)		513.0	514.1(2)	497.1(2)
93.17	338.3	371.0	373.3(2)	352.9(2)	230.0	300.2	301.9(3)	277.7(2)
		365.3	367.0(1)	346.9(1)		294.6	295.2(1)	271.7(1)
94.17	195.8	251.9	253.2(2)	235.9(1)	112.7	190.8	191.6(1)	173.4(2)
		246.3	247.4(1)	230.1(1)		185.1	185.7(1)	167.5(1)

Table 4.1. The LL and non-log first order corrections to the forward and backward cross sections for muon pair production. The column under the heading LL $\mathcal{O}(\alpha)$ contains the cross sections with first order LL corrections, the column with $\mathcal{O}(\alpha)$ lists the fully corrected first order result. The column with $\mathcal{O}(\alpha^2)$ includes on top of that the second order LL corrections plus soft photon exponentiation. The numbers between brackets indicate the estimated numerical error in the last digit. For each energy the first line displays the results for definition 1 (see text) and the second line for definition 2. All cross sections are in picobarn, energies in GeV.

For the forward-backward asymmetry we have chosen $Q^2 = s$. To indicate that for this choice the LL corrections are dominant, we have listed the first order LL corrected results and the fully first order corrected results for both the forward and the backward cross section for muon pair production in table 4.1. The results have been obtained by an extended version of the analytical Bhabha program (ALIBABA) of [2]. In this case no energy or acollinearity cuts were applied. The input parameters were specified to be $M_Z = 91.17$, $M_H = 100$ and $m_{top} = 130$, all in GeV. The fact that in this table the LL corrections are dominant does not necessarily imply that the same scale works as well for angular distribution type of calculations. These calculations would therefore require additional careful study. However for the asymmetry we can conclude from table 4.1 that in higher order only the LL corrections are needed. Therefore we can now turn to the higher order corrected results.

The results are collected in tables 4.2-4.4. Table 4.2 presents results without energy and acollinearity cuts, whereas table 4.3 shows results with cuts on energy and acollinearity. For convenience the exact $\mathcal{O}(\alpha)$ results are given together with the full results, i.e. including LL $\mathcal{O}(\alpha^2)$ and exponentiation. It is clear that with an aimed experimental ac-

\sqrt{s}	'Born'	$\mathcal{O}(\alpha)$		ZFITTER	ALIBABA	
		def. 1	def. 2		def. 1	def. 2
88.17	-0.264	-0.288	-0.300	-0.279	-0.277	-0.289
88.67	-0.218	-0.244	-0.252	-0.235	-0.235	-0.242
89.17	-0.172	-0.198	-0.202	-0.189	-0.188	-0.193
89.67	-0.125	-0.150	-0.152	-0.141	-0.140	-0.144
90.17	-0.077	-0.102	-0.103	-0.093	-0.093	-0.095
90.67	-0.031	-0.053	-0.055	-0.046	-0.045	-0.046
91.17	0.016	-0.011	-0.010	-0.002	-0.002	-0.002
91.67	0.061	0.028	0.028	0.037	0.037	0.037
92.17	0.106	0.059	0.061	0.069	0.069	0.070
92.67	0.149	0.085	0.087	0.096	0.097	0.099
93.17	0.191	0.106	0.108	0.118	0.119	0.122
93.67	0.231	0.124	0.127	0.137	0.138	0.141
94.17	0.269	0.138	0.142	0.152	0.153	0.157
94.67	0.306	0.152	0.157	0.165	0.166	0.171

Table 4.2. The forward-backward asymmetry for m_{μ} pair production without any cuts. The rightmost two columns show the result for the two definitions of the asymmetry, corrected at $\mathcal{O}(\alpha^2)$ (plus exponentiation).

\sqrt{s}	'Born'	$\mathcal{O}(\alpha)$		ZFITTER	ALIBABA	
		def. 1	def. 2		def. 1	def. 2
88.17	-0.264	-0.295	-0.296	-0.289	-0.285	-0.286
88.67	-0.218	-0.248	-0.248	-0.240	-0.238	-0.239
89.17	-0.172	-0.199	-0.200	-0.191	-0.190	-0.190
89.67	-0.125	-0.149	-0.150	-0.142	-0.141	-0.141
90.17	-0.077	-0.100	-0.101	-0.093	-0.093	-0.093
90.67	-0.031	-0.053	-0.054	-0.045	-0.046	-0.045
91.17	0.016	-0.010	-0.009	-0.001	-0.002	-0.002
91.67	0.061	0.028	0.029	0.038	0.038	0.037
92.17	0.106	0.059	0.060	0.071	0.071	0.071
92.67	0.149	0.086	0.086	0.099	0.098	0.099
93.17	0.191	0.106	0.108	0.122	0.121	0.123
93.67	0.231	0.125	0.127	0.142	0.141	0.143
94.17	0.269	0.142	0.143	0.159	0.158	0.160
94.67	0.306	0.157	0.159	0.174	0.173	0.175

Table 4.3. The forward-backward asymmetry for m_{μ} pair production using an energy cut of $\frac{1}{4}\sqrt{s}$ on both final state particles and an acollinearity cut of 10° . The rightmost two columns show the result for the two definitions of the asymmetry, corrected at $\mathcal{O}(\alpha^2)$ (plus exponentiation).

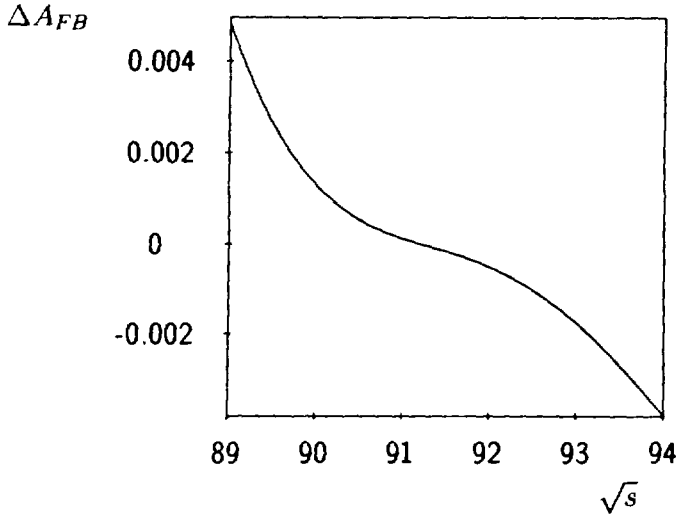


Fig. 4.1. The difference $\Delta A_{FB} = A_{FB,1} - A_{FB,2}$ between the two definitions of the asymmetry without cuts as a function of the energy.

\sqrt{s}	$m_{top} = 90$	$m_{top} = 130$	$m_{top} = 170$
88.17	-0.280	-0.277	-0.275
88.67	-0.236	-0.235	-0.233
89.17	-0.190	-0.188	-0.187
89.67	-0.142	-0.140	-0.140
90.17	-0.095	-0.093	-0.091
90.67	-0.048	-0.045	-0.045
91.17	-0.004	-0.002	-0.001
91.67	0.036	0.037	0.039
92.17	0.069	0.069	0.071
92.67	0.095	0.097	0.098
93.17	0.118	0.119	0.120
93.67	0.136	0.138	0.138
94.17	0.151	0.153	0.154
94.67	0.164	0.166	0.168

Table 4.4. The topmass dependence of the fully corrected asymmetry without cuts, using definition 1.

curacy $\delta A_{FB} = 0.0035$ [4] the corrections in $\mathcal{O}(\alpha^2)$ as considered in this chapter have to be taken into account. Also the influence of cuts is non negligible. The same holds for the difference in definitions for A_{FB} for the case of no cuts. The acollinearity cut clearly decreases the difference between the definitions. For convenience the difference is plotted

in fig 4.1.

In order to show in another way the relevance of the radiative corrections table 4.4 collects predictions for different top masses. The changes caused by varying the top mass are smaller than the changes caused by going from $\mathcal{O}(\alpha)$ to $\mathcal{O}(\alpha^2)$ corrections.

Finally, both tables 4.2 and 4.3 contain results of a new not yet published calculation by Bardin et al., which is an extension of [11]. The calculation uses definition 1 for A_{FB} , considers some $\mathcal{O}(\alpha^2)$ corrections and can implement energy and acollinearity cuts. Within the above mentioned experimental accuracy there is no difference between the two calculations. Therefore we conclude that the predictions for A_{FB} including higher order photonic corrections are now well under control even for realistic experimental cuts.

It is clear that the same program can be applied to the forward-backward asymmetry for quarks, as long as masses can be neglected.

References

- [1] D.Y. Bardin et al., in "Z Physics at LEP 1", CERN 89-08, Vol.1, p.89, eds. G. Altarelli, R. Kleiss and C. Verzegnassi.
- [2] W. Beenakker, F.A. Berends and S.C. van der Marck, Nucl. Phys. B349 (1991) 323, see also chapter 3.
- [3] W. Beenakker, F.A. Berends and W.L. van Neerven, in Proceedings of the Workshop on "electroweak Radiative Corrections", Ringberg Castle (FRG), 1989, ed. J. H. Kühn.
- [4] M. Böhm, W. Hollik et al., in "Z Physics at LEP 1", CERN 89-08, Vol.1, p.203, eds. G. Altarelli, R. Kleiss and C. Verzegnassi.
- [5] D.Y. Bardin et al., Phys. Lett. B229 (1989) 405.
- [6] Z. Was and S. Jadach, Phys. Rev. D 41 (1990) 1425.
- [7] G. Montagna, O. Nicrosini and L. Trentadue, Phys. Lett. B231 (1989) 492.
- [8] J.E. Campagne and R. Zitoun, Phys. Lett. B222 (1989) 497.
- [9] W.F.L. Hollik, Fort. Physik 38 (1990) 165.
- [10] D.Y. Bardin et al., Z. Phys. C44 (1989) 493.
- [11] D.Y. Bardin, M. Bilenky, A. Chizov, A. Sazonov, O. Fedorenko, T. Riemann and M. Sachwitz, Nucl. Phys. B351 (1991) 1.

Chapter 5

Small angle Bhabha scattering

5.1 Introduction

The accuracy with which one wants to measure the luminosity at LEP is higher than at previous electron positron machines. This requires a theoretical knowledge of the small angle Bhabha scattering cross section with a precision of at least 0.5%. Since at small angles Bhabha scattering is dominated by one photon exchange in the t-channel the high precision requirement is a demand on an accurate QED calculation. Although in principle it is straightforward to perform such a QED evaluation, in practice higher order QED corrections are complex and time consuming. The present paper wants to improve on the present knowledge of small angle Bhabha scattering and wants to provide a benchmark for future evaluations.

In order to appreciate the problem let us briefly summarize the present situation. Additional material can be found in ref.[1]. Suppose the idealized small angle Bhabha measurement determines the cross section for the scattering of a positron over an angle ϑ_+ , where the detected positron and electron have an acollinearity angle $\zeta < \zeta_{max}$ and have energies $E_{\pm} > E_{min}$. Theory has to provide $d\sigma/d\Omega_+$ as defined by these kinematical conditions or this cross section integrated over a small ϑ_+ range. When one wants to calculate this cross section in lowest order plus a complete order α correction, the procedure has been discussed at great length in ref. [2]. One has

$$\begin{aligned} \frac{d\sigma}{d\Omega_+} &= \frac{d\sigma^0}{d\Omega_+} (1 + \delta_V + \delta_S(k_1)) \\ &+ \int_{k_0 < k_1} \left(\frac{d\sigma^B}{d\Omega_+ d\Omega_\gamma dk_0} - \frac{d\sigma^S}{d\Omega_+ d\Omega_\gamma dk_0} \right) d\Omega_\gamma dk_0 \\ &+ \int_{k_0 > k_1} \left(\frac{d\sigma^B}{d\Omega_+ d\Omega_\gamma dk_0} \right) d\Omega_\gamma dk_0, \end{aligned} \quad (5.1.1)$$

where $d\Omega_\gamma dk_0$ describes the photon phase space. The $\mathcal{O}(\alpha)$ correction contains virtual corrections δ_V from loop diagrams and gets a contribution from real bremsstrahlung.

The exact bremsstrahlung cross section $d\sigma^B$ can be approximated for soft photons ($k_0 \ll E_{beam}$) by a simple factorized cross section $d\sigma^S$. When the photon phase space is isotropic up to some photon energy k_1 (not necessarily soft) the bremsstrahlung cross section approximated by $d\sigma^S$ and integrated up to the energy k_1 gives an analytic contribution $\delta_S(k_1) d\sigma^0/d\Omega_+$. Since the approximation of $d\sigma^B$ by $d\sigma^S$ may not be accurate enough the second term in eq.(5.1.1) corrects for this. The third term describes the emission of hard anisotropic bremsstrahlung. The acollinearity and energy conditions determine k_1 and the ϑ_γ integration range. The way in which eq.(5.1.1) is divided into various parts is convenient since the infrared divergences cancel explicitly in the analytical expression for $\delta_V + \delta_S(k_1)$. Moreover the integral over the difference of $d\sigma^B$ and $d\sigma^S$ is convergent since the infrared divergences cancel. The technical problem now is the precise evaluation of the third term. Due to a complex peaking structure of this cross section a numerical integration requires great care [2]. One could even perform this integral analytically [3], which gives an improvement in computational speed but is not required for the needed precision. It should be noted that the quantity k_1 can be varied to lower values, the only effect is that the last integral ($k_0 > k_1$) will also have an isotropic photon emission part. The final answer remains the same.

It should be stressed that the above procedure, based on eq.(5.1.1) is exact. Nothing is neglected. The method has been applied to Bhabha scattering in [4], even in the case where the J/ψ resonance is present [5]. Since the exact $d\sigma^B$ is rather complicated when all electron masses are kept, one can use high energy approximations as introduced in refs. [6] and [7], which are valid for $s, -t \gg m_e^2$. This will speed up the calculation.

So far we have considered an ideal measurement which can be described in terms of simple kinematical cuts. This is not a necessity but has only been done for convenience. More complicated cuts, like $E_\gamma + E_\pm > E_{min}$ or exclusion of certain azimuthal angle ranges can also be imposed on the numerical integration of the hard bremsstrahlung cross section (the last term in eq.(5.1.1)). Such things have in fact been done by experimentalists in the past. The calculation remains exact in order α .

To implement cuts it is however more convenient to have an event generator [8] which simulates at the same time radiative ($k_0 > k_1$) and non-radiative ($k_0 < k_1$) events. The soft photon energy k_1 should then be very small for two reasons. One is that the soft photon does not influence the kinematics of the hard particles and the other is that we can neglect the second term in eq.(5.1.1). The latter is required by the fact that we need positive probabilities to generate events. The last term in eq.(5.1.1) is positive since it is a cross section, the second is however a difference of cross sections. The first term should also be positive. Since we know from the analytic expressions that for very small k_1 the factor $1 + \delta_V + \delta_S(k_1)$ becomes negative, we find a lower limit for k_1 . Since k_1 cannot be made arbitrary small any more the omission of the second term in eq.(5.1.1) introduces necessarily an error in the event generator ("the k_0 problem", see also chapter 7). It is only because we want to generate events with weight one that we need a division of the cross section into positive parts. For Bhabha scattering a pure QED event generator was introduced in ref. [9] and one containing weak corrections in ref. [10]. In the literature

they are sometimes referred to as `OLDBAB` and `BABAMC`.

In summary, the $\mathcal{O}(\alpha)$ correction can be calculated exactly when we use eq.(5.1.1). Also weak corrections can be easily included. An event generator makes it easier to implement any kind of cuts, but will introduce some inaccuracy. While writing this paper we received a preprint [11], which compares an event generator to analytical results for a toy model of Bhabha scattering.

Thus the order α correction is not a problem, even for involved experimental cuts. The crucial question is whether higher order corrections are needed. For the previous electron positron machines they have not been used. As we shall see below the typical $\mathcal{O}(\alpha)$ correction is about -8% for the idealized small angle Bhabha measurement. This means that we could have to worry about the $\mathcal{O}(\alpha^2)$ correction when we require an accuracy of 0.5% .

The main objective of this paper is to argue that the $\mathcal{O}(\alpha^2)$ correction cannot be neglected. The most convincing way to show this is to perform an explicit exact $\mathcal{O}(\alpha^2)$ correction calculation. This has been possible for the mupair total cross section [12], since there one could restrict the calculation to initial state radiation and since the phase space integrations did not involve any cuts. For Bhabha scattering we do not have these simplifications, so one is faced with a much more involved second order calculation. It is doubtful whether such an evaluation will be carried out in the near future. Nevertheless one would like to answer the question whether $\mathcal{O}(\alpha^2)$ corrections are needed. This can be done by considering leading log (LL), i.e. $(\alpha L/\pi)^n$ parts of the radiative corrections, where $L = \log(Q^2/m^2)$, with Q^2 a suitable scale like s or t . For the total mupair cross section the LL contribution can be obtained by using the structure function method [13, 14] with scale s . A comparison with the explicit calculation [12] containing also the subleading and non-log terms gives further support to the relevance of the LL calculation.

In this paper we shall evaluate the $\mathcal{O}(\alpha^2)$ LL contributions to the small angle Bhabha cross section. We have to apply the structure function method to differential cross sections. For QED the method has been described in [15] and applied to large angle Bhabha scattering [16] and to the forward-backward asymmetry in mupair production [17].

The difference with the previous applications is the choice of scale. Since small angle Bhabha scattering is dominated by the t-channel one photon exchange diagram, whereas large angle Bhabha scattering is predominantly s-channel Z-exchange, it seems natural to choose t as scale.

An exact order α calculation should be compared with a LL calculation with scale t and when the LL part is dominant (80% or more) it makes sense to perform a LL calculation of order α^2 with the same scale t . The precise t value choice will be discussed below, but of course Q^2 should obey $Q^2 = -t \gg m_e^2$, otherwise there are no LL terms present.

The outline of what we shall do is as follows. In section 5.2 we define a set of cuts for an ideal luminosity measurement. Then we show the size of the exact $\mathcal{O}(\alpha)$ correction and the LL part. Moreover the $\mathcal{O}(\alpha)$ correction is compared to the event generator of ref. [10]. Also a comparison is made with a more general event generator `BHLUMI` [18] which avoids the k_0 problem by an exponentiation procedure for soft photons. It generates

only one hard photon but in principle many soft photons. It contains a part of the $\mathcal{O}(\alpha^2)$ corrections, but can also be run in the $\mathcal{O}(\alpha)$ approximation.

Then we evaluate the LL $\mathcal{O}(\alpha^2)$ correction plus an exponentiation of soft photons in even higher orders. This is also compared with the complete BHLUMI event generator. A marked difference arises. Our higher order correction has a different sign from the correction given by BHLUMI. In section 5.3 we investigate the origin of the discrepancy by performing analytical calculations. The conclusions are summarized in section 5.4.

5.2 Numerical results

The idealized small angle Bhabha measurement we will discuss is defined by the cuts

$$\begin{aligned} \vartheta_{\min} < \vartheta_{\pm} < \vartheta_{\max}, \\ E_{\pm} > E_{\min}. \end{aligned} \tag{5.2.1}$$

Here $\vartheta_{+(-)}$ is the angle of the outgoing positron (electron) with respect to the incoming positron (electron) and $E_{+(-)}$ is the energy of the outgoing positron (electron). For the numerical studies we will take $\vartheta_{\min} = 3^\circ$ and $\vartheta_{\max} = 8^\circ$ and $E_{\min} = \frac{1}{2}E_{\text{beam}}$. No other cuts will be imposed. Note however that the above ones imply among other things a maximum acollinearity and a maximum photon energy. The specific values for the angles are realistic for some current experiments. For other experiments slightly lower values are used. We have checked explicitly that this does not affect the qualitative features of our results.

For this idealized situation one can calculate the total cross section using the methods of refs. [16, 17] and the program ALIBABA. This means that the $\mathcal{O}(\alpha)$ corrections can be calculated exactly, whereas the higher order corrections are evaluated in the leading log approximation (LLA). It is therefore important which scale is chosen for this approximation. We will show that in $\mathcal{O}(\alpha)$ the choice

$$Q^2 = -t(\vartheta_{\max}) = \frac{1}{2}s(1 - \cos \vartheta_{\max}) \tag{5.2.2}$$

is a good choice. That is, with this choice the LL $\mathcal{O}(\alpha)$ corrections constitute $\gtrsim 90\%$ of the complete $\mathcal{O}(\alpha)$ QED correction. Therefore it is expected that with this choice also in higher order the LL corrections are dominant.

At $\mathcal{O}(\alpha)$ we can compare our results to results obtained with the event generators BABAMC and BHLUMI. Because the treatment of the weak corrections and of the hadronic contribution to the photon self-energy are different in the various programs, all programs were modified to reproduce the BABAMC treatment. This choice was not made because the BABAMC treatment is the best one, but because this was the most convenient solution to implement. Taking over the BABAMC treatment implies the following:

1. All corrections are strictly of $\mathcal{O}(\alpha)$, i.e. there is no convolution between for instance weak corrections and QED corrections.

\sqrt{s}	Born +weak	BABAMC	ALIBABA	
			$\mathcal{O}(\alpha)$	LL $\mathcal{O}(\alpha)$
87.17	45.48	42.07±0.04	41.94±0.09	42.17
89.17	43.64	40.30±0.04	40.34±0.09	40.43
91.17	41.39	38.38±0.04	38.33±0.08	38.47
93.17	39.25	36.42±0.04	36.47±0.09	36.49
95.17	37.75	34.98±0.04	34.91±0.12	35.03

Table 5.1. Results for the cross section corrected to $\mathcal{O}(\alpha)$, obtained with different programs. Born+weak stands for the Born cross section including weak corrections. The input parameters were $M_Z = 91.17$ GeV, $M_H = 100$ GeV and $m_{top} = 130$ GeV. All energies are in GeV, cross sections in nanobarn.

2. Propagator corrections are not resummed (i.e. no Dyson summation).
3. The hadronic contribution to the vacuum polarization is calculated from the analytical formulae (in contrast to calculating it as a dispersion integral over the total hadronic cross section).

With these modifications the results of the programs BABAMC and ALIBABA for the idealized luminosity measurement are shown in table 5.1. The entry Born+weak means a calculation of the Born cross section and the order α weak corrections. By our definition weak corrections mean non-photonic corrections. The QED corrections are the photonic corrections i.e. those due to real or virtual photons. In this terminology the photon vacuum polarization belongs to the weak corrections and is therefore in order α included in Born+weak. The other entries contain besides Born+weak also the order α QED corrections to the Born cross section and not to the weak corrections, i.e. strict $\mathcal{O}(\alpha)$. The completely order α corrected results are seen to agree within 0.2%, which is comparable to the standard deviation and which is better than the desired 0.5% accuracy. All first order QED corrections with respect to Born are roughly -7.8% . We also ran the program BHLUMI in the $\mathcal{O}(\alpha)$ mode. For the cross section at 87.17, 89.17 and 91.17 GeV agreement with the values in the table was found. For the other energies we were confronted with many events with negative weights. Even for $k_1 = 0.1 E_{beam}$ many events with negative weights occurred. Since this k_1 value is already very high and will lead to a non-negligible contribution from the second term in eq.(5.1.1), one has to conclude that there is no point in trying to choose k_1 even higher. Therefore we were not able to compare the $\mathcal{O}(\alpha)$ corrected cross section with BHLUMI for the energies 93.17 and 95.17 GeV. For the more interesting mode of BHLUMI with higher order corrections such problems are not present.

Concluding the discussion of the $\mathcal{O}(\alpha)$ corrections, it should be noted from table 5.1 that the LL $\mathcal{O}(\alpha)$ corrections, calculated with the scale (5.2.2) are dominant. In fact they

\sqrt{s}	Born +'weak'	' $\mathcal{O}(\alpha)$ '	BHLUMI	ALIBABA
87.17	45.41	41.69±0.08	41.39±0.04	41.88±0.08
89.17	43.57	39.95±0.08	39.80±0.04	40.14±0.08
91.17	41.33	38.06±0.07	37.62±0.04	38.21±0.07
93.17	39.20	36.07±0.07	35.70±0.04	36.23±0.07
95.17	37.70	34.78±0.08	34.34±0.04	34.94±0.08

Table 5.2. Results for the higher order corrected cross section. Note that the Born+'weak' and the ' $\mathcal{O}(\alpha)$ ' entry are defined differently from the corresponding ones in table 5.1 (see text). The input parameters were $M_Z = 91.17$ GeV, $M_H = 100$ GeV and $m_{top} = 130$ GeV. All energies are in GeV, cross sections in nanobarn.

give more than 90% of the $\mathcal{O}(\alpha)$ QED corrections.

Results for the higher order corrected cross section are shown in table 5.2. The results in this table were obtained by running BHLUMI and ALIBABA with all corrections included. For BHLUMI the parameters were KEYRAD=100 and EPSCM= 10^{-3} . For ALIBABA the options were IORDER=4, IFINAL=2 and NONLOG=1. Table 5.2 gives rise to the following remarks.

- A. The 'weak' corrections are defined differently than the ones in table 5.1.
- B. The ' $\mathcal{O}(\alpha)$ ' entry is defined differently from the $\mathcal{O}(\alpha)$ entry in table 5.1.
- C. BHLUMI and ALIBABA disagree by about 1.2% in the total result.
- D. ALIBABA gives a positive higher order correction with respect to the ' $\mathcal{O}(\alpha)$ ' result.

As to point A, the difference with table 5.1 is that a Dyson summation is made for the propagators and that the hadronic vacuum polarization has been calculated by means of a dispersion integral over the total hadronic cross section [20]. We thus have a dressed Born approximation in the first column. As to point B, the QED $\mathcal{O}(\alpha)$ evaluation now is a convolution over this dressed Born approximation. This means that the vacuum polarization effect in the photon t channel propagator is also convoluted by $\mathcal{O}(\alpha)$ QED effects, whereas in table 5.1 only the Born cross section without vacuum polarization effect is convoluted. In practice it means that an increased cross section gets a first order QED correction, which in itself is of the order of -8% . In the convolution this yields an order α corrected cross section which is smaller than the one of table 5.1. Concerning point C and D, a small difference of 0.2% can be understood from the Dyson summation in ALIBABA and its absence in BHLUMI. So there remains a difference of about 1%.

What is left are the pure QED higher order corrections. When compared with the ' $\mathcal{O}(\alpha)$ ' result BHLUMI gives a correction of about -0.8% . The program ALIBABA gives a

positive higher order correction of +0.4%. It is the purpose of the next section to explain this difference by performing some analytical calculations.

First however we want to clarify the situation by describing exactly which corrections are taken into account in the ALIBABA results. Schematically these results contain a number of terms:

$$\begin{aligned} \sigma = & \int dz I(z) \sigma_w(z, s) F(z) \\ & + \int dx_1 \int dx_2 I_2(x_1, x_2) \sigma_0(x_1, x_2, s) \\ & + F_2 \sigma_w(s) + N. \end{aligned} \quad (5.2.3)$$

The first term is an integral over a product of an initial state LL QED correction factor $I(z)$, a Born cross section including weak corrections, $\sigma_w(z, s)$, and a final state LL QED correction factor $F(z)$. The factor $I(z)$ contains initial state LL QED corrections up to and including second order in α , plus soft photon exponentiation. The factor $F(z)$ contains final state LL QED corrections up to and including first order. The second term in eq.(5.2.3) originates from the fact that at $\mathcal{O}(\alpha^2)$ not all initial state LL QED corrections can be written as a one-dimensional integral. Although this has been possible in the case of m upair production [12, 13, 14], this is not so for Bhabha scattering due to the cuts [16]. Therefore a two-dimensional integral is left for some of the $\mathcal{O}(\alpha^2)$ initial state LL QED corrections (see also next section). These corrections are again a convolution of an initial state factor ($I_2(x_1, x_2)$) times a Born cross section σ_0 . Since the corrections in I_2 are already of $\mathcal{O}(\alpha^2)$, the Born cross section appearing here is not corrected for weak effects. This is done to gain computational speed for the two-dimensional numerical integration. The $\mathcal{O}(\alpha^2)$ LL QED corrections are completed by including the $\mathcal{O}(\alpha^2)$ final state LL QED corrections, which can be written as a factor F_2 times the Born cross section $\sigma_w(s)$. This explains the third term.

Concluding from the above all leading log QED corrections up to and including $\mathcal{O}(\alpha^2)$ and including initial state soft photon exponentiation are incorporated in the first three terms in eq.(5.2.3). Almost all of these corrections are convoluted with the weak corrections. The only exception is $I_2(x_1, x_2)\sigma_0$, which is already of $\mathcal{O}(\alpha^2)$ and hence is small ($\sim 0.5\%$). Since the weak corrections are about 6%, leaving out the weak corrections when calculating the integral over $I_2(x_1, x_2)\sigma_0$ is well justified.

The last term in eq.(5.2.3), which is called N , includes the $\mathcal{O}(\alpha)$ QED non-log terms. These terms are calculated by numerical integrations, which for the hard photon part is a five-dimensional one. With our scale choice these terms contribute $\lesssim 10\%$ of the complete $\mathcal{O}(\alpha)$ QED correction or, equivalently, $\lesssim 1\%$ of the total result. Therefore these terms do not need to be convoluted with the weak corrections. Moreover it can be inferred that one can neglect the higher order non-LL QED corrections, which are expected to be about 10% of the complete $\mathcal{O}(\alpha^2)$ exponentiated QED corrections, i.e. roughly 0.05%.

It is amusing to note that the higher order results of ALIBABA in the special case of

table 5.2 lie closer to the BABAMC values in table 5.1 than to the BILUMI results. From the discussion above it is clear that this is a numerical accident.

5.3 Analytical formulae

The cross section for the luminosity measurement is heavily dominated by the part of the spin averaged matrix element squared that in Born approximation is given by

$$|\mathcal{M}|^2 = 64\pi^2\alpha^2\frac{s^2}{t^2}. \quad (5.3.1)$$

At Born level this is responsible for 99.7% of the total cross section, using the same cuts as before. Therefore taking this particular matrix element can serve as a toy model to try and understand some of the features of the higher order QED corrections. This is done in the following by analytically calculating the $\mathcal{O}(\alpha)$ and $\mathcal{O}(\alpha^2)$ leading log QED corrections to this matrix element. It is clear that some of the finer details will be lost in this toy model e.g. the effect of the vacuum polarization. We shall however be able to explain the negative $\mathcal{O}(\alpha)$ correction and the positive $\mathcal{O}(\alpha^2)$ correction.

The basis of the calculation is eq.(6) of ref. [17]. With an approximation in the second order terms coming from the convolution of $\mathcal{O}(\alpha)$ initial state corrections with $\mathcal{O}(\alpha)$ final state corrections, this leads, for the idealized small angle Bhabha cross section, to

$$\begin{aligned} \sigma &= \frac{4\pi\alpha^2}{s} \frac{1}{\sqrt{\eta_M\eta_m}} F(x_0) \int_0^1 dx_1 \Gamma_{ee}(x_1) \int_0^1 dx_2 \Gamma_{ee}(x_2) \\ &\times \left\{ \left(\frac{1}{\eta x_1^2} - \frac{\eta}{x_2^2} \right) \vartheta(x_2 - \eta x_1) \vartheta(x_2 - x_0) \vartheta(x_1 - x_2) + (x_1 \leftrightarrow x_2) \right\}. \end{aligned} \quad (5.3.2)$$

Here we defined

$$\begin{aligned} \eta_M &= \frac{1 - \cos \vartheta_{min}}{1 + \cos \vartheta_{min}}, \quad \eta_m = \frac{1 - \cos \vartheta_{max}}{1 + \cos \vartheta_{max}}, \quad \eta = \sqrt{\frac{\eta_M}{\eta_m}}, \\ F(x_0) &= \left[\int_{x_0}^1 dx \mathcal{D}_{ee}(x) \right]^2, \quad x_0 = \frac{E_{min}}{E_{beam}}. \end{aligned} \quad (5.3.3)$$

$\Gamma_{ee}(x)$ stands for the electron splitting function and $\mathcal{D}_{ee}(x)$ for the electron fragmentation function, which are equal in the LLA. The derivation of eq.(5.3.2) involves careful examination of the integration boundaries for x_1 and x_2 . The fact that $\eta_{M,m} \ll 1$ while $\eta \lesssim 1$ has been used.

Two different situations can arise, due to the ϑ -functions in eq.(5.3.2). The one situation is characterized by $x_0 \leq \eta$, the other by $x_0 \geq \eta$. If $x_0 \leq \eta$ all ϑ -functions are needed. If on the other hand $x_0 \geq \eta$, one can leave out the factor $\vartheta(x_2 - \eta x_1)$ and

hence the integration area is somewhat easier. For our idealized luminosity measurement we have $\vartheta_{\min} = 3^\circ$, $\vartheta_{\max} = 8^\circ$ and $E_{\min} = \frac{1}{2}E_{\text{beam}}$, yielding $\eta \approx 0.3745$ and $x_0 = \frac{1}{2}$. Therefore we will only discuss the case $x_0 \geq \eta$. Nevertheless we have calculated the other case too, of which it is worth mentioning that there the second order corrections become significantly larger for $x_0 \rightarrow 0$, because of the much larger phase space and the peaking behavior of the integrand. However $x_0 \rightarrow 0$ does not seem to be very realistic in view of the current experiments.

For $x_0 \geq \eta$ the expression for the cross section including LL $\mathcal{O}(\alpha)$ corrections is

$$\sigma = \frac{4\pi\alpha^2}{s} \frac{1}{\sqrt{\eta_M\eta_m}} \left\{ \frac{1}{\eta} - \eta + \beta \left[\left(\frac{1}{\eta} - \eta \right) \left(2 \log(1 - x_0) + \frac{1}{2}x_0(1 + \frac{1}{2}x_0) \right) + \frac{1}{2} \left(\frac{x_0}{\eta} - \frac{\eta}{x_0} \right) \left(1 + \frac{1}{2}x_0 \right) + \frac{1}{2}\eta \log x_0 \right] \right\}. \quad (5.3.4)$$

We use the notation $\beta = (2\alpha/\pi)(L - 1)$. This expression yields a LL $\mathcal{O}(\alpha)$ correction of about -8.1% for our cuts. This is a sufficiently good description of the $\mathcal{O}(\alpha)$ correction in table 5.2. For the LL $\mathcal{O}(\alpha^2)$ corrections we find, neglecting the convolution of $\mathcal{O}(\alpha)$ initial state corrections with $\mathcal{O}(\alpha)$ final state corrections altogether

$$\begin{aligned} \Delta\sigma = \frac{4\pi\alpha^2}{s} \frac{1}{\sqrt{\eta_M\eta_m}} \frac{1}{16} \beta^2 & \left\{ -\frac{1}{2}\eta \log^2 x_0 + \left(-\frac{12}{\eta} + 8\eta \right) \log x_0 \log(1 - x_0) \right. \\ & + \left[-\frac{2}{\eta} - \eta + \frac{\eta}{x_0} - 8\frac{x_0}{\eta} - 4\frac{x_0^2}{\eta} + 3\eta x_0 + \frac{3}{2}\eta x_0^2 \right] \log x_0 \\ & + \left[16\frac{x_0}{\eta} - 8\frac{\eta}{x_0} + 8\frac{x_0^2}{\eta} - 4\eta x_0^2 - 4\eta - 8\eta x_0 \right] \log(1 - x_0) \\ & - \frac{12}{\eta} \text{Li}_2(x_0) + \left(8\eta + \frac{4}{\eta} \right) \zeta(2) + \frac{13}{4\eta} - \eta + 16 \left(\frac{1}{\eta} - \eta \right) \log^2(1 - x_0) \\ & \left. + 3\frac{x_0}{\eta} - 5\eta x_0 + \frac{3}{2}\frac{x_0^2}{\eta} - \frac{7}{4}\eta x_0^2 + x_0^3 \left(\frac{1}{\eta} - \eta \right) \left(1 + \frac{1}{4}x_0 \right) \right\}. \quad (5.3.5) \end{aligned}$$

For the numerical example these terms add up to $+0.4\%$, in good agreement with table 5.2. Thus the results of ALIBABA are confirmed by the qualitative analytical calculations. Next we try to understand why BHLUMI appears to be so different.

The event generator BHLUMI includes higher order corrections via exponentiation of the soft photon distribution. This is done in a so-called exclusive way, which cannot be easily reproduced by a simple analytical formula. One can however compare with a formula for the first order exponentiated distribution for inclusive quantities. We take the first order exponentiated form of the distribution proposed in eq.(12) of ref. [19] in the expectation that it represents some of the features of BHLUMI. This results in

$$\sigma = \frac{4\pi\alpha^2}{s} \frac{1}{\sqrt{\eta_M\eta_m}} F(x_0) \frac{e^{-\gamma_E\beta}}{\Gamma(1 + \beta)} e^{\frac{1}{4}\beta} \quad (5.3.6)$$

$$\times \beta \int_{x_0}^1 dz (1-z)^{-1} + \beta \left[\frac{1}{2} + \frac{1}{2}\beta + \frac{1}{2}z^2 \right] \left[\frac{1}{\eta} - \frac{\eta}{z^2} \right]$$

as an alternative for eq.(5.3.2). Here Γ stands for the Γ -function, not for a splitting function. Also the final state corrections can be taken in the first order exponentiated form

$$F(x_0) = (1-x_0)^\beta \left(1 + \frac{3}{4}\beta \right) - \frac{1}{2}\beta \left(\frac{3}{2} - x_0 - \frac{1}{2}x_0^2 \right). \quad (5.3.7)$$

It can be checked easily that this form reproduces eq.(5.3.4) for the Born term and the first order LL corrections. The second order LL corrections calculated from this expression however are different:

$$\begin{aligned} \Delta\sigma = & \frac{4\pi\alpha^2}{s} \frac{1}{\sqrt{\eta_M\eta_m}} \frac{1}{16} \beta^2 \left\{ 32 \left(\frac{1}{\eta} - \eta \right) \log^2(1-x_0) + 8\eta \log x_0 \log(1-x_0) \right. \\ & + \left[-4\eta x_0^2 - 8\eta x_0 - 16 \frac{\eta}{x_0} - 20\eta + 12 \frac{x_0^2}{\eta} + 24 \frac{x_0}{\eta} + \frac{12}{\eta} \right] \log(1-x_0) \\ & + \left[2\eta x_0^2 + 4\eta x_0 + 2\eta \right] \log x_0 - 8\eta \text{Li}_2(x_0) - \eta x_0^2 - 4\eta x_0 - 10 \frac{\eta}{x_0} + \frac{7}{2}\eta \\ & \left. + \left(16\eta - \frac{8}{\eta} \right) \zeta(2) + \frac{x_0^4}{\eta} + 4 \frac{x_0^3}{\eta} + 3 \frac{x_0^2}{\eta} - 10 \frac{x_0}{\eta} + \frac{27}{2\eta} \right\}. \quad (5.3.8) \end{aligned}$$

This contributes -0.1% to the total cross section, in contrast to eq.(5.3.5).

To understand where the positive contributions leading to eq.(5.3.5) come from one can do the following. One can write eq.(5.3.2) as

$$\sigma = \int_0^1 dx_1 \int_0^1 dx_2 \Gamma(x_1)\Gamma(x_2) f(x_1, x_2), \quad (5.3.9)$$

by introducing $f(x_1, x_2)$. Since f is symmetric in its arguments the Born term and most of the corrections are contained in the part given by

$$\sigma_1 = \int_0^1 dx_1 \int_0^1 dx_2 \Gamma(x_1)\Gamma(x_2) f(x_1 x_2, 1). \quad (5.3.10)$$

More specifically σ_1 contains the Born term, the complete LL $\mathcal{O}(\alpha)$ correction and all higher order LL virtual and soft photon corrections from the initial state. For σ_1 the two integrations can be reduced to a one-dimensional integration [16]. The remaining terms are given by

$$\sigma_2 = \int_0^1 dx_1 \int_0^1 dx_2 \Gamma(x_1)\Gamma(x_2) [f(x_1, x_2) - f(x_1 x_2, 1)]. \quad (5.3.11)$$

The contribution from σ_2 starts at $\mathcal{O}(\alpha^2)$ and is due to two hard photons. In fact it turns out that for the idealized luminosity measurement the LL $\mathcal{O}(\alpha^2)$ corrections coming from σ_2 dominate the complete LL $\mathcal{O}(\alpha^2)$ correction. This can be demonstrated by neglecting σ_2 completely, in which case eq.(5.3.5) reduces to

$$\begin{aligned} \Delta\sigma = & \frac{4\pi\alpha^2}{s} \frac{1}{\sqrt{\eta_M\eta_m}} \frac{1}{16} \beta^2 \left\{ -8 \left(\frac{1}{\eta} - \eta \right) \log x_0 \log(1-x_0) - \eta \log^2 x_0 \right. \\ & + \left[2 \frac{\eta}{x_0} + 2\eta - 3 \frac{x_0^2}{\eta} - 6 \frac{x_0}{\eta} \right] \log x_0 + 8 \left(\frac{1}{\eta} - \eta \right) \log^2(1-x_0) \\ & + \left[-8 \frac{\eta}{x_0} - 4\eta + 4 \frac{x_0^2}{\eta} + 8 \frac{x_0}{\eta} \right] \log(1-x_0) \\ & \left. - \frac{8}{\eta} \text{Li}_2(x_0) + 8\eta\zeta(2) - \frac{9}{2}\eta + \frac{x_0^2}{2\eta} + 4 \frac{x_0}{\eta} \right\}. \end{aligned} \quad (5.3.12)$$

This would lead to a LL $\mathcal{O}(\alpha^2)$ contribution of -0.1% . Hence the contribution from σ_2 is 0.5% . Since all virtual and soft photon corrections are contained in σ_1 , this 0.5% is entirely coming from corrections due to two hard photons.

In ref.[18] it is stated that double hard bremsstrahlung is not included. Therefore 0.5% of the discrepancy can be traced back to this aspect of BHLUMI. The remaining 0.5% difference can come from different sources. As we have seen in the previous section some $\mathcal{O}(\alpha^i) \otimes \mathcal{O}(\alpha^j)$ ($i, j \leq 2$) effects can be neglected and others cannot. Moreover it is very well possible that the actual effective algorithm in BHLUMI is not accurately enough represented by eq.(5.3.6), which could account for the difference.

5.4 Conclusions

The demand of an accuracy of 0.5% in the theoretical prediction for small angle Bhabha scattering forces us to consider $\mathcal{O}(\alpha^2)$ corrections. For an idealized luminosity measurement both numerical and analytical evaluations show this necessity. Moreover, it is clear that double hard bremsstrahlung has to be taken into account. Also one has to justify where $\mathcal{O}(\alpha^i) \otimes \mathcal{O}(\alpha^j)$ ($i, j \leq 2$) corrections are kept and where they are omitted.

Although our evaluation gives an answer to a specific luminosity measurement, one prefers in general a higher order event generator. The only candidate to which we could compare (BHLUMI) gives a marked difference of 1.2% with our results. Part of the difference can be removed when two hard photons are included in the generator. We suspect that the remaining discrepancy can be removed when all the subtleties of products of corrections are taken into consideration. The results of the present paper can serve as a benchmark for future event generators, which include multiple photon emission.

Two additional comments should be made. In an actual luminosity measurement an event where a photon and an electron satisfy the selection criteria of a positron and electron may in practice be added to the luminosity sample. We want to note that this

contamination can be evaluated in the structure function approach (the unseen lepton going in the beam pipe). One needs the $\Gamma_{\gamma e}$ splitting function instead of Γ_{ee} and the Compton cross section instead of σ_w . An analytical evaluation gives a 0.01% contribution to the cross sections of table 5.2.

Another question is whether multiple bremsstrahlung is the only important $\mathcal{O}(\alpha^2)$ effect. In the case of the s-channel process lepton pair production was explicitly shown to be negligible in comparison to two photon emission [12]. Here we checked only the emission of an electron positron pair from an incoming electron by means of a $\Gamma_{\gamma e} \otimes \Gamma_{e\gamma}$ contribution. The contribution to the small angle Bhabha scattering is of the order of 0.01%. If in an actual luminosity measurement an event, where two electrons or two positrons satisfy the selection criteria of a positron and electron, is added to the luminosity sample, this contribution is multiplied by two. The emission of a virtual photon decaying into an e^+e^- pair and the corresponding electron loop insertion into the vertex correction [12] have not been calculated for Bhabha scattering, but are for muon pair production below 0.2%. The contribution from two-photon processes is negligible due to the cuts.

Keeping in mind the accuracy of the numerical calculation, the neglect of subleading $\mathcal{O}(\alpha^2)$ logarithms and the neglect of e^+e^- pair emission we expect our evaluation of the idealized luminosity measurement to have a precision of 0.5%.

References

- [1] M. Caffo et al., in "Z Physics at LEP 1", CERN 89-08, Vol.1, p.171, eds. G. Altarelli, R. Kleiss and C. Verzegnassi.
- [2] F.A. Berends, K.J.F. Gaemers and R. Gastmans, Nucl. Phys. B63 (1973) 381.
- [3] G. Passarino, Nucl. Phys. B204 (1982) 237.
- [4] F.A. Berends, K.J.F. Gaemers and R. Gastmans, Nucl. Phys. B68 (1974) 541.
- [5] F.A. Berends and G.J. Komen, Nucl. Phys. B115 (1976) 114.
- [6] F.A. Berends, R. Kleiss, P. de Causmaecker, R. Gastmans and T.T. Wu, Phys. Lett. B103 (1981) 124.
- [7] F.A. Berends, R. Kleiss, P. de Causmaecker, R. Gastmans, W. Troost and T.T. Wu, Nucl. Phys. B206 (1982) 61.
- [8] F.A. Berends and R. Kleiss, Nucl. Phys. B177 (1981) 237.
- [9] F.A. Berends and R. Kleiss, Nucl. Phys. B228 (1983) 537.
- [10] M. Böhm, A. Denner and W. Hollik, Nucl. Phys. B304 (1988) 687.
F.A. Berends, R. Kleiss and W. Hollik, Nucl. Phys. B304 (1988) 712.

- [11] S. Jadach, E. Richter-Was, B.F.L. Ward and Z. Wąs, Phys. Lett. B253 (1991) 469.
- [12] F.A. Berends, W.L. van Neerven and G.J.H. Burgers, Nucl. Phys. B297 (1988) 429; E Nucl. Phys. B304 (1988) 921.
- [13] E.A. Kuraev and V.S. Fadin, Sov. J. Nucl. Phys. 41 (1985) 466.
- [14] G. Altarelli and G. Martinelli, Yellow Report CERN 86-02 (1986) 47.
- [15] W. Beenakker, F.A. Berends and W.L. van Neerven, in Proceedings of the Workshop on "electroweak Radiative Corrections", Ringberg Castle (FRG), 1989, ed. J.H. Kühn.
- [16] W. Beenakker, F.A. Berends and S.C. van der Marck, Nucl. Phys. B349 (1991) 323, see also chapter 3.
- [17] W. Beenakker, F.A. Berends and S.C. van der Marck, Phys. Lett. B251 (1990) 299, see also chapter 4.
- [18] S. Jadach and B.F.L. Ward, Phys. Rev. D40 (1989) 3582.
- [19] S. Jadach, M. Skrzypek and B.F.L. Ward, CERN-TH.5858/90.
- [20] H. Burkhardt, F. Jegerlehner, G. Penso and C. Verzegnassi, Z. f. Phys. C43 (1989) 497.

Chapter 6

Two photon bremsstrahlung

6.1 Introduction

During the last years there has been considerable progress in the field of high precision phenomenology of the Standard Model. In particular the computation of radiative corrections for the muon/quark pair production process at LEP1, $e^+e^- \rightarrow \bar{f}f$, has been completely performed to the one loop, or $\mathcal{O}(\alpha)$, level [1]. These corrections can be divided into 'purely weak' ones and QED ones; the QED corrections can be described by all Feynman diagrams where a virtual or real photon has been added to the Born level graphs, while weak corrections consist of all other one loop diagrams. Due to the possibility of having additional particles (*i.e.* bremsstrahlung photons) in the final state, the QED effects are for practical applications best described with the use of Monte Carlo techniques (although extremely important and useful analytical results have also been obtained [2, 3]).

It is well known that, at least around the Z resonance, one loop corrections are in general not sufficient for a reliable and accurate phenomenological description, and higher order corrections have to be taken into account, at least in the QED sector. It has been established that the weak corrections are typically small, provided we express the Born level cross section in terms of judiciously chosen parameters; this results in the use of the so-called 'improved' or 'modified' Born formulae, for which many different forms have been proposed [4]. Assuming that we write the cross section with the one loop weak corrections in this way, the purely weak higher order corrections can be neglected at the level of accuracy aimed for in the LEP experiments. This leaves us with the problem of dealing with the higher order virtual photon and bremsstrahlung effects. The most important and well known way of treating these higher order QED effects is the so-called soft photon exponentiation. First treated in a consistent and thorough manner in the classical paper by Yennie, Frautschi and Suura (YFS) [5], this amounts to a resummation of the leading terms in all higher order virtual and real photon graphs, where the total amount of energy radiated off by the bremsstrahlung photons is restricted to be below some value $\Delta E \ll E_b$, where $E_b = \sqrt{s}/2$ is the beam energy.

While theoretically attractive, this approach to the radiative corrections can nowadays

not be considered adequate. The use of an energy cutoff ΔE is only an attempt to implement the influence of experimental cuts, however crudely: in typical experimental situations, ΔE is not a fixed number but may for instance depend on the production angles of the fermion pair*. Also, the bremsstrahlung photons cannot always be treated in the soft photon approximation: in particular when a photon is emitted close to the beam direction, or collinear with one of the produced fermions, its energy may be a quite sizable fraction of E_b under realistic experimental conditions. So, in the summation of the higher order effects, nonleading terms may become relevant, of which the precise exponentiation prescription is not at present known, although a number of promising Ansätze exists [6]. The last drawback in the use of YFS exponentiation is the fact that the formulae as they appear in [5] concern only *inclusive* cross sections, that is, cross sections in which integration has been performed over the photon momenta. If one is only interested in the total cross section σ or the fermion angular distribution $d\sigma/d\Omega_f$ this is of course desirable, but for a Monte Carlo treatment it is less adequate since in a Monte Carlo simulation (where every event must have a well defined, positive probability) we want to know the *exclusive*, multidifferential cross section $d\sigma/d\Omega_f dk_1 d\Omega_1 dk_2 d\Omega_2 \cdots dk_n d\Omega_n$ (where k_i and Ω_i denote the energy and solid angle of bremsstrahlung photon i), for arbitrary n .

In an extremely important and beautiful paper, Jadach and Ward [7] have shown that the YFS approach of [5] can in fact be transformed so as to give information on the above complete multidifferential distribution, and they have presented an algorithm for actually generating such distributions. Whereas in this way one of the main obstacles to 'exclusive exponentiation' has been overcome, a number of nontrivial issues remain to be settled. In the first place, the Jadach-Ward approach [7] is only valid at present for initial state radiation. The radiative corrections from the final state fermions as well as the interference between initial and final state radiation remains to be adequately implemented in a similar algorithm. In the second place, the use of exclusive exponentiation enables us to use the full matrix elements for each order in the QED perturbation series: however, in all existing implementations at most only the $\mathcal{O}(\alpha)$ level is treated exactly, and the higher order matrix elements are implemented only approximately.

It is the purpose of this chapter to describe the implementation of the two loop bremsstrahlung matrix element, that is, the matrix elements for $e^+e^- \rightarrow \bar{f}f\gamma\gamma$, where the photons are emitted from the initial state. For massless fermions and electrons, these matrix elements have been given by the CALKUL collaboration [8] for the case of photon exchange and are therefore not appropriate for LEP physics: we generalize this treatment to the case of photon and Z exchange. In addition, the CALKUL group has indicated how mass effects are to be taken into account [9]: however this treatment is not really suited to computer implementation, and we also extend and improve on that. An additional feature of our result is that we give separate helicity amplitudes so that the possibility of polarized e^+e^- beams is included.

The layout of this chapter is as follows. In section 6.2 we present all the necessary

*Here and in the following, 'fermion' stands for muon, tau lepton, their associated neutrino types, or any of the light quarks.

formulae for the matrix elements, based on the use of spinor techniques [10]. A good deal of the section is devoted to a discussion on how these formulae are to be used in an actual Monte Carlo program: in particular the question of how to compute the mass effects turns out to be far from trivial. In section 6.3 we describe the implementation of our results in the Monte Carlo program *FPAIR*. This program simulates carefully the emission of up to two hard bremsstrahlung photons from the initial state, and up to one from the final state. Not complete yet in the sense that we have not included exponentiation so far, its strength is rather in the precise description of explicitly hard photon events. We describe all algorithms leading to the full simulation. In section 6.4 we compare our results with some other formulae and algorithms present in the literature. In particular, we are in a good position to compare *FPAIR* with the Monte Carlo program *DYMU2* by Campagne and Zitoun [11]. Since *DYMU2* also generates up to 2 photons from the initial, and up to 1 from the final state, it is ideally suited to this kind of comparison. It should be noted that in *DYMU2* the alternative structure function approach [12] to the higher order QED effects has been adopted. This provides an interesting possibility of checking the structure function approach against a more exact treatment, which both have their advantages and drawbacks. Finally, in section 6.5 we draw our conclusions and indicate the directions of further development.

6.2 Matrix elements

In this section we present the matrix elements for the process

$$e^+(p_+, \lambda_+)e^-(p_-, \lambda_-) \rightarrow \bar{f}(q_2, \lambda_f)f(q_1, \lambda_f)\gamma(k_1, \lambda_1)\gamma(k_2, \lambda_2), \quad (6.2.1)$$

where the two photons are emitted from the initial state electron and positron. In eq.(6.2.1) we have indicated the momenta as well as the helicity indices $\lambda = \pm$ of the various particles. Since we are also going to consider collinear photon radiation, where the masses of the e^+e^- cannot be neglected, the helicities λ_+ and λ_- are to be taken as independent of each other: on the other hand, we shall take the final state fermions to be massless in this section, and helicity conservation along massless fermion lines implies that in our convention (which is described in detail in appendix A, but which differs from the convention used in chapter 2) the helicity indices for both f and \bar{f} must be equal. Since it will turn out that we also need the zero and one photon amplitudes we shall also give them: these have of course been given many times in the literature, but we include them for completeness and in order to be able to work in a consistent manner in the case of collinear radiation.

For computational tools we use the so-called spinor techniques which are described in great detail in [10]. We present a summary of the most important results in appendix A for completeness. The basic quantity is the so-called spinor product which we define as

$$s_{\lambda_1, \lambda_2}(p_1, p_2) = \bar{u}_{\lambda_1}(p_1)u_{\lambda_2}(p_2) \quad (6.2.2)$$

for massless fermions (i.e. $p_1^2 = p_2^2 = 0$) the product vanishes if $\lambda_1 = \lambda_2$ but if one or both momenta are massive it is also nonzero. Another point of importance is the choice of the polarization vector $\varepsilon_{\lambda_i}^\mu(k_i)$ of photon $i = 1, 2$. It turns out to be most convenient to use also a spinorial form:

$$\varepsilon_{\lambda_i}^\mu(k_i) = \frac{\lambda_i}{\sqrt{2}} \frac{\bar{u}_{\lambda_i}(k_i) \gamma^\mu u_{\lambda_i}(q_i)}{s_{-\lambda_i, \lambda_i}(k_i, q_i)}. \quad (6.2.3)$$

As demonstrated in [10], this satisfies the usual requirements for definite helicity states $(\varepsilon_\pm \cdot k_i) = 0$, $(\varepsilon_\pm \cdot \varepsilon_\pm) = 0$, $(\varepsilon_+ \cdot \varepsilon_-) = -1$ and $(\varepsilon_+^\mu)^* = \varepsilon_-^\mu$. The vector q_i^μ is an auxiliary massless vector with $(q_i \cdot k_i) \neq 0$, a choice of which fixes a gauge choice for the external photon i . The representation (6.2.3) also has the nice property that in each gauge invariant subset of diagrams q_i^μ can be chosen completely arbitrarily, without the need to take into account relative complex phases which plagued the original CALKUL results [8]. The freedom of choice of q_i^μ allows an optimization of the calculation, which we employ as follows. In initial state radiation, all bremsstrahlung photon lines are attached to the e^+e^- fermion line which starts with $\bar{u}_{\lambda_+}(p_+)$ and ends with $u_{\lambda_-}(p_-)$. In case one considers the electrons to be massless, one has to have $\lambda_+ = \lambda_- \equiv \lambda_e$. One can then make the following helicity dependent choice for q_i for photon i :

$$q_i^\mu = \begin{cases} p_-^\mu & \text{if } \lambda_i = \lambda_e, \\ p_+^\mu & \text{if } \lambda_i = -\lambda_e, \end{cases} \quad (6.2.4)$$

which leads to a considerable simplification of the calculation since many Feynman diagrams are made to vanish. A few remarks are in order here. In the first place, although this may not be completely obvious from the above formulation, the choice (6.2.4) is in fact equivalent to the original CALKUL gauge choice. There is however a difference due to the fact that the CALKUL group only considered Abelian gauge theories (i.e. QED) with all particles strictly massless, while the above definition is completely applicable to nonabelian bremsstrahlung (i.e. QCD) with arbitrary fermion masses as well. Secondly, it should be noted that we are allowed to make a choice for q_i for each bremsstrahlung photon independently, which is necessary to make the definition (6.2.4) workable for the case of more than one photon. In the last place, there is a price to be paid for the simplification of the calculation in the use of eq.(6.2.4): as can be seen from eq.(6.2.3), the polarization vector ε introduces an additional denominator into the matrix element, which goes like $\sqrt{(p_+ \cdot k)}$ or $\sqrt{(p_- \cdot k)}$. Hence when the photon becomes collinear with either p_+ or p_- the matrix element will superficially diverge more strongly than the expected $1/\sqrt{(p_\pm \cdot k)}$. Of course this is compensated for by cancellations in the denominator (as described in detail by the CALKUL group in [13]) but it indicates that in collinear situations the choice (6.2.4) is less adequate. Since anyway in such situations we cannot neglect the electron mass and therefore λ_+ and λ_- do not have to be equal, we shall employ a different choice for collinear photons:

$$q_i^\mu = \begin{cases} p_+^\mu & \text{if } k_i \text{ is collinear with } p_-, \\ p_-^\mu & \text{if } k_i \text{ is collinear with } p_+. \end{cases} \quad (6.2.5)$$

This way, the individual components of ε_i^μ will remain of order unity even in collinear situations. This implies that under this alternative choice (6.2.5) only those Feynman diagrams have to be taken into account in which the photon line is actually attached to the external leg of the fermion with which it is collinear [9]. With 'collinear' in the above we mean a kinematical configuration where, say, $(p_+ \cdot k)$ is much smaller than all the other momentum transfers in the problem, but *not* necessarily so small that it is comparable with m_e^2 , where m_e is the electron mass. In other words, our approach assumes that there is a possibility of kinematical configurations where the strong ordering $m_e^2 \ll (p_+ \cdot k_i) \ll s$ holds: in that case, the two gauge choices (6.2.4) and (6.2.5) will lead to results that are smoothly connected, although in the choice (6.2.4) we neglect all mass terms, and in the choice (6.2.5) we neglect many of the Feynman diagrams. Below, we will study this question in more detail and show that our approach is in fact possible at LEP energies.

Let us start with the no bremsstrahlung case. It turns out to be convenient to define the combination of Z and photon propagators and their associated couplings to the incoming and outgoing fermions as

$$(i_{\lambda_e, \lambda_f}(s) = \frac{Q_e Q_f}{s} + \frac{(v_e - \lambda_e a_e)(v_f - \lambda_f a_f)}{s - M_Z^2 + iM_Z \Gamma_Z} , \quad (6.2.6)$$

which is appropriate when the fermions are considered massless. Here, Q_e , v_e and a_e stand for the electron charge, vector and axial vector coupling, and similarly for Q_f , v_f and a_f . The $\lambda_{e,f}$ are the helicity indices of the electrons and fermions. Note the difference with eq.(2.2.14), due to the difference in helicity-convention. The argument s is the momentum transfer in the photon and Z propagator, and M_Z , Γ_Z are the mass and width of the Z. The above definition can of course be trivially extended to take into account the effects of the photon and Z self-energy correction effects as amply described in the literature [4].

The helicity amplitudes $\mathcal{M}_0(\lambda_+, \lambda_-; \lambda_f)$ for the no bremsstrahlung case and for massless e^+e^- , where λ_+ , λ_- and λ_f denote the helicity indices of the e^+ , e^- , and ff , respectively, can now be written quite simply as follows:

$$\begin{aligned} \mathcal{M}_0(\lambda, \lambda; \lambda_f) &= 2i(i_{\lambda, \lambda_f}(s) s_{\lambda, -\lambda}(p_+, r_1) s_{-\lambda, \lambda}(r_2, p_-)) \\ &= 2i(i_{\lambda, \lambda_f}(s) \frac{1}{s} s_{\lambda, -\lambda}(p_+, p_-) s_{\lambda, -\lambda}(r_1, r_2) \{s_{-\lambda, \lambda}(p_-, r_2)\}^2) \\ &= 2i(i_{\lambda, \lambda_f}(s) \frac{1}{s} s_{-\lambda, \lambda}(p_+, p_-) s_{-\lambda, \lambda}(r_1, r_2) \{s_{\lambda, -\lambda}(p_+, r_1)\}^2) , \\ \mathcal{M}_0(\lambda, -\lambda; \lambda_f) &= 0 , \end{aligned} \quad (6.2.7)$$

where helicity conservation along the electron line is explicitly indicated, and the set of vectors r_1^μ, r_2^μ is the following helicity dependent permutation of q_1^μ, q_2^μ :

$$(r_1, r_2) = \begin{cases} (q_1, q_2) & \text{if } \lambda_f = \lambda , \\ (q_2, q_1) & \text{if } \lambda_f = -\lambda . \end{cases} \quad (6.2.8)$$

In eq.(6.2.7) we have neglected an irrelevant overall complex phase. The three equivalent forms for $\mathcal{M}_0(\lambda, -\lambda; \lambda_f)$ follow immediately from the momentum conservation $p_+ + p_- = q_1 + q_2$: they are given here since we shall encounter them again in the bremsstrahlung case. The above formulation is obviously well suited for compact and easy-to-check computer implementation, and we shall put the results for single and double bremsstrahlung in the same form.

For single bremsstrahlung we have helicity amplitudes $\mathcal{M}_1(\lambda_+, \lambda_-; \lambda_f; \lambda_1)$ which now depend on the photon helicity as well. It turns out that the relevant index is not the helicity index λ_1 of photon 1 itself, but rather the helicity relative to that of the electrons. As before, the helicity amplitudes with $\lambda_+ \neq \lambda_-$ are zero: the 8 nonzero ones are given by

$$\begin{aligned}\mathcal{M}_1(\lambda, \lambda; \lambda_f; \lambda) &= -2iQ_e G_{\lambda, \lambda_f}(s') N_+(k_1) \times \\ &\quad s_{\lambda, -\lambda}(p_+, p_-) s_{\lambda, -\lambda}(r_1, r_2) \{s_{-\lambda, \lambda}(p_-, r_2)\}^2, \\ \mathcal{M}_1(\lambda, \lambda; \lambda_f; -\lambda) &= +2iQ_e G_{\lambda, \lambda_f}(s') N_-(k_1) \times \\ &\quad s_{-\lambda, \lambda}(p_+, p_-) s_{-\lambda, \lambda}(r_1, r_2) \{s_{\lambda, -\lambda}(p_+, r_1)\}^2, \quad (6.2.9)\end{aligned}$$

with

$$N_\lambda(k_1) = \frac{\lambda\sqrt{2}}{s_{-\lambda, \lambda}(k_1, p_+) s_{\lambda, -\lambda}(p_+, p_-) s_{-\lambda, \lambda}(p_-, k_1)}, \quad (6.2.10)$$

and $s' = (q_1 + q_2)^2$ is the invariant mass of the final state fermion pair.

For double bremsstrahlung we now have of course two photon helicities entering in the amplitude $\mathcal{M}_2(\lambda_+, \lambda_-; \lambda_f; \lambda_1, \lambda_2)$. Its 16 nonzero values are the following:

$$\begin{aligned}\mathcal{M}_2(\lambda, \lambda; \lambda_f; \lambda, \lambda) &= -2iQ_e s G_{\lambda, \lambda_f}(s') N_+(k_1) N_+(k_2) \times \\ &\quad s_{\lambda, -\lambda}(p_+, p_-) s_{\lambda, -\lambda}(r_1, r_2) \{s_{-\lambda, \lambda}(p_-, r_2)\}^2, \\ \mathcal{M}_2(\lambda, \lambda; \lambda_f; -\lambda, -\lambda) &= -2iQ_e s G_{\lambda, \lambda_f}(s') N_-(k_1) N_-(k_2) \times \\ &\quad s_{-\lambda, \lambda}(p_+, p_-) s_{-\lambda, \lambda}(r_1, r_2) \{s_{\lambda, -\lambda}(p_+, r_1)\}^2, \\ \mathcal{M}_2(\lambda, \lambda; \lambda_f; \lambda, -\lambda) &= -2iQ_e s G_{\lambda, \lambda_f}(s') N_+(k_1) N_-(k_2) \times \\ &\quad \left\{ \frac{1}{\Delta_+} s_{\lambda, -\lambda}(p_+, k_1) s_{-\lambda, \lambda}(k_1, p_-) s_{\lambda, -\lambda}(p_-, k_2) s_{-\lambda, \lambda}(r_2, p_-) \right. \\ &\quad \times (s_{-\lambda, \lambda}(k_2, p_+) s_{\lambda, -\lambda}(p_+, r_1) - s_{-\lambda, \lambda}(k_2, k_1) s_{\lambda, -\lambda}(k_1, r_1)) \\ &\quad + \frac{1}{\Delta_-} s_{\lambda, -\lambda}(p_+, r_1) s_{-\lambda, \lambda}(k_1, p_+) s_{\lambda, -\lambda}(p_+, k_2) s_{-\lambda, \lambda}(k_2, p_-) \\ &\quad \times (s_{-\lambda, \lambda}(r_2, p_-) s_{\lambda, -\lambda}(p_-, k_1) - s_{-\lambda, \lambda}(r_2, k_2) s_{\lambda, -\lambda}(k_2, k_1)) \\ &\quad - (s_{\lambda, -\lambda}(p_+, p_-) s_{-\lambda, \lambda}(p_-, r_2) - s_{\lambda, -\lambda}(p_+, k_2) s_{-\lambda, \lambda}(k_2, r_2)) \\ &\quad \left. \times (s_{\lambda, -\lambda}(r_1, p_+) s_{-\lambda, \lambda}(p_+, p_-) - s_{\lambda, -\lambda}(r_1, k_1) s_{-\lambda, \lambda}(k_1, p_-)) \right\}, \\ \mathcal{M}_2(\lambda, \lambda; \lambda_f; -\lambda, \lambda) &= \{\mathcal{M}_2(\lambda, \lambda; \lambda_f; \lambda, -\lambda)\}_{k_1 \leftrightarrow k_2}, \quad (6.2.11)\end{aligned}$$

with

$$\Delta_{\pm} = (p_{\pm} - k_1 - k_2)^2 . \quad (6.2.12)$$

It should be noted that if the photon helicities are equal the resulting amplitude has a quite simple form. It reduces as in the one photon case to the Born level amplitude, multiplied by two 'infrared factors' (as compared to one factor in the single bremsstrahlung case): note, however, that in the presence of bremsstrahlung the various 'Born type' forms that arise are no longer numerically equivalent. In fact this simplification has been shown by the CALKUL group to persist to arbitrary order for those helicity amplitudes where all photon helicities are equal [8]. The same is observed in QCD where a similar factorization for multigluon scattering for which the form of the amplitudes where two gluons have helicity opposite to all the other ones was first conjectured by Parke and Taylor in [15] and later proved rigorously by Berends and Giele [16]. For the cases where the photon helicities are opposite no such simplification is observed: in particular 'composite denominators' like Δ_+ are not wholly compensated by a combination of Dirac matrices in the numerator, whereas in the equal helicity case they are. As a consequence the behavior in the various collinear limits is more complicated in the opposite helicity cases: still, when $\Delta_+ \rightarrow 0$ the numerator also vanishes, as can be seen from the concurrence of the products $s_{\lambda, -\lambda}(p_+, k_1)$, $s_{-\lambda, \lambda}(k_2, p_+)$, and $s_{-\lambda, \lambda}(k_2, k_1)$ with $1/\Delta_+$, which go to zero if \vec{p}_+ , \vec{k}_1 and \vec{k}_2 are all collinear. This has a consequence for the case of *triple* bremsstrahlung which we shall discuss below.

We now turn to the issue of the mass effects. As mentioned above, mass effects become relevant when for instance $(p_+ \cdot k_1)$ becomes comparable to m_e^2 . In that case, $(p_+ \cdot k_1) \ll s$ and we are allowed to neglect many Feynman diagrams, namely those that do not contain $(p_+ \cdot k_1)^{-1}$ explicitly as a propagator. These considerations lead us to the following strategy for computing the mass effects. Let us consider a Feynman diagram where one or more photons are emitted collinearly with p_+^{μ} : all these diagrams start with the e^+ external leg, to which the collinear photons are attached. In this part of the relevant diagrams, *which is equal for all those diagrams that we have to take into account*, all occurring momentum transfers are comparable to each other and much smaller than the large momentum transfers like s (by our definition of collinearity). After this 'collinear' part of the diagrams, we encounter the first vertex where a large momentum transfer takes place. It can easily be seen that after this vertex, no more small denominators can occur in the electron propagator until we reach the other extreme end of the diagram, where a collinear part may occur due to those photons that are collinear with p_- . We see that the diagrams are decomposed naturally into collinear parts where all momentum transfers are small (and we may have to keep the electron mass), and a 'hard scattering' part where we have to take into account all diagrams but where we can certainly neglect the electron mass. It is obvious that this decomposition is not strictly gauge invariant and we therefore have to be careful in choosing the gauge of the collinear photons, for which as we have argued above the choice (6.2.5) is appropriate.

We shall now derive the expressions for collinear photon radiation. This is most simply

described by the following explicit example. Consider a process where a photon with momentum k_1^μ and helicity $+$ is radiated collinearly with the electron, with momentum p_-^μ and helicity $+$. As argued above, in the gauge of eq.(6.2.5) we only have to consider diagrams which contain the collinear part

$$C^{(-)}(p_-, +; k_1, +) \equiv \frac{1}{-2(p_- \cdot k_1)} (\not{p}_- - \not{k}_1 + m_e) \not{\epsilon}_+(k_1) u_+(p_-) , \quad (6.2.13)$$

By using the definition of $\not{\epsilon}$ of eq.(6.2.3) and the identities

$$\begin{aligned} \not{p}_- + m_e &= u_+(p_-) \bar{u}_+(p_-) + u_-(p_-) \bar{u}_-(p_-) , \\ \not{k}_1 &= u_+(k_1) \bar{u}_+(k_1) + u_-(k_1) \bar{u}_-(k_1) , \end{aligned} \quad (6.2.14)$$

we can immediately decompose the above collinear part to write

$$\begin{aligned} C^{(-)}(p_-, +; k_1, +) &= \frac{1}{\sqrt{2}(p_- \cdot k_1) s_{-,+}(k_1, q)} \\ &\quad \{ s_{+,+}(p_-, q) s_{+,+}(p_-, k_1) u_+(p_-) \\ &\quad - s_{+,-}(p_-, k_1) s_{-,+}(p_-, q) u_+(p_-) \\ &\quad + s_{-,+}(q, k_1) s_{+,+}(p_-, k_1) u_-(k_1) \} , \end{aligned} \quad (6.2.15)$$

where already 5 out of the 8 terms have dropped out because of the symmetry properties of the spinor products and the fact that the $s_{+,+}$ and $s_{-,+}$ vanish for two massless vectors. We will now further simplify eq.(6.2.15) by considering the order of magnitude of the various terms. In the collinear limit, the denominator is of order $\mathcal{O}(m_e^2)$ [†], and this would give rise to a cross section behaving like $\mathcal{O}(m_e^{-4})$. As is well known, however, the actual behavior of the cross section is rather $\mathcal{O}(m_e^{-2})$. Therefore, the numerator of eq.(6.2.15) has to exhibit cancellations that brings its peaking behavior down by $\mathcal{O}(m_e)$. Thus, we may expand the numerator of (6.2.15) and neglect terms that are of order $\mathcal{O}(m_e^2)$, which will not give a noticeable contribution to the cross section (in the same sense in which we neglect a number of Feynman diagrams in the collinear situation). We have the following orders of magnitude for the various quantities appearing in this numerator:

$$\begin{aligned} s_{+,\pm}(p_-, k_1) &= \mathcal{O}(m_e) , \\ s_{+,+}(p_-, q) &= \mathcal{O}(m_e) , \\ s_{+,-}(q, k_1) &= y_1 s_{+,-}(q, p_-) + \mathcal{O}(m_e) , \\ u_\pm(k_1) &= y_1 u_\pm(p_-) + \mathcal{O}(m_e) . \end{aligned} \quad (6.2.16)$$

Here we have introduced

$$y_i \equiv \sqrt{k_i^0/p_-^0} \sim \sqrt{(k_i \cdot q)/(p_- \cdot q)} . \quad (6.2.17)$$

[†]Note that, since we use the gauge choice (6.2.5), we take q^μ to be explicitly not collinear to p_-^μ or k_1^μ so that the product $s_{-,+}(k_1, q)$ remains of order $\mathcal{O}(1)$ in the collinear situation.

With this information we find that eq.(6.2.15) can be rewritten as follows, where we have dropped terms of order $\mathcal{O}(m_e^2)$ and higher in the numerator:

$$C^{(-)}(p_-, +; k_1, +) = \frac{1}{\sqrt{2}(p_- \cdot k_1) y_1} \times \left\{ s_{+,-}(p_-, k_1) u_+(p_-) + y_1^2 s_{+,+}(p_-, k_1) u_-(p_-) \right\}. \quad (6.2.18)$$

Note that the spinor products with q^μ as an argument have cancelled: this is in fact a proof that to the order in m_e that we are working in, our result is indeed gauge invariant. We see from eq.(6.2.18) that the effect of the collinear bremsstrahlung can be viewed as turning the definite helicity state $u_+(p_-)$ into a linear combination of two helicity states $u_+(p_-)$ and $u_-(p_-)$, each with a different weight. In fact, because we have argued that all mass effects have been properly taken into account and from this point on we can treat the remainder of the amplitude as describing the scattering of massless particles, we can assume that $(p_- - k_1)^\mu$ is a massless vector as well, and we have

$$u_\pm(p_-) \sim \frac{u_\pm(p_- - k_1)}{\sqrt{1 - y_1^2}}. \quad (6.2.19)$$

Hence we are allowed to use

$$C^{(-)}(p_-, +, k_1, +) = A_+^{(-)}(p_-, +, k_1, +) u_+(p_- - k_1) + A_-^{(-)}(p_-, +, k_1, +) u_-(p_- - k_1), \quad (6.2.20)$$

with

$$A_+^{(-)}(p_-, +, k_1, +) = \frac{s_{+,-}(p_-, k_1)}{\sqrt{2} y_1 \sqrt{1 - y_1^2} (p_- \cdot k_1)},$$

$$A_-^{(-)}(p_-, +, k_1, +) = \frac{m_e y_1^2}{\sqrt{2} \sqrt{1 - y_1^2} (p_- \cdot k_1)}. \quad (6.2.21)$$

Here we have used the explicit expression $s_{+,+}(p_-, k_1) = m_e y_1$ in order to illustrate the fact that for strictly massless electrons the coefficient $A_-^{(-)}(p_-, +, k_1, +)$ vanishes. It is of course straightforward to derive similar expressions for the other helicity cases, and for the case of collinear radiation from the positron as well. In general, we have

$$C^{(-)}(p_-, \lambda_-, k_1, \lambda_1) \equiv \frac{(\not{p}_- - \not{k}_1 + m_e) \not{\epsilon}_{\lambda_1}(k_1) u_{\lambda_-}(p_-)}{(p_- - k_1)^2 - m_e^2}$$

$$= A_+^{(-)}(p_-, \lambda_-, k_1, \lambda_1) u_+(p_- - k_1) + A_-^{(-)}(p_-, \lambda_-, k_1, \lambda_1) u_-(p_- - k_1),$$

$$C^{(+)}(p_+, \lambda_+, k_1, \lambda_1) \equiv \frac{\not{\epsilon}_{\lambda_+}(p_+) \not{\epsilon}_{\lambda_1}(k_1) (-\not{p}_+ + \not{k}_1 + m_e)}{(p_+ - k_1)^2 - m_e^2}$$

$$= A_+^{(+)}(p_+, \lambda_-, k_1, \lambda_1) \bar{v}_+(p_+ - k_1) + A_-^{(+)}(p_+, \lambda_-, k_1, \lambda_1) \bar{v}_-(p_+ - k_1). \quad (6.2.22)$$

The explicit expressions for $A_{\pm}^{(\pm)}$ are given in appendix B. The case of double collinear radiation can be treated in the same way: in this case, terms up to order $\mathcal{O}(m_e^2)$ in the numerator must be kept, and also we have to take into account two diagrams instead of only one. We have

$$\begin{aligned}
C^{(-)}(p_-, \lambda_-, k_1, \lambda_1, k_2, \lambda_2) &\equiv \\
&\equiv \frac{(\not{p}_- - \not{k}_1 - \not{k}_2 + m_e)\not{\epsilon}_{\lambda_2}(k_2)(\not{p}_- - \not{k}_1 + m_e)\not{\epsilon}_{\lambda_1}(k_1)u_{\lambda_-}(p_-)}{[(p_- - k_1)^2 - m_e^2][(p_- - k_1 - k_2)^2 - m_e^2]} + (k_1, \lambda_1 \leftrightarrow k_2, \lambda_2) \\
&= A_+^{(-)}(p_-, \lambda_-, k_1, \lambda_1, k_2, \lambda_2)u_+(p_- - k_1 - k_2) + \\
&\quad A_-^{(-)}(p_-, \lambda_-, k_1, \lambda_1, k_2, \lambda_2)u_-(p_- - k_1 - k_2) , \tag{6.2.23}
\end{aligned}$$

$$\begin{aligned}
C^{(+)}(p_+, \lambda_+, k_1, \lambda_1, k_2, \lambda_2) &\equiv \\
&\equiv \frac{\bar{v}_{\lambda_+}(p_+)\not{\epsilon}_{\lambda_1}(k_1)(-\not{p}_+ + \not{k}_1 + m_e)\not{\epsilon}_{\lambda_2}(k_2)(-\not{p}_+ + \not{k}_1 + \not{k}_2 + m_e)}{[(p_+ - k_1)^2 - m_e^2][(p_+ - k_1 - k_2)^2 - m_e^2]} + (k_1, \lambda_1 \leftrightarrow k_2, \lambda_2) \\
&= A_+^{(+)}(p_+, \lambda_+, k_1, \lambda_1, k_2, \lambda_2)\bar{v}_+(p_+ - k_1 - k_2) + \\
&\quad A_-^{(+)}(p_+, \lambda_+, k_1, \lambda_1, k_2, \lambda_2)\bar{v}_-(p_+ - k_1 - k_2) . \tag{6.2.24}
\end{aligned}$$

where again the explicit expressions are given in appendix B. We now turn to the implementation of these results in the computation of collinear amplitudes. In the case of single bremsstrahlung collinear with the incoming electron, it is clear that we can write the amplitude as

$$\begin{aligned}
\mathcal{M}_1(p_+, \lambda_+, p_-, \lambda_-, k_1, \lambda_1; q_1, q_2, \lambda_f) &= \\
&\quad \mathcal{M}_0(p_+, \lambda_+, p_- - k_1, +; q_1, q_2, \lambda_f)A_+^{(-)}(p_-, \lambda_-, k_1, \lambda_1) \\
&\quad + \mathcal{M}_0(p_+, \lambda_+, p_- - k_1, -; q_1, q_2, \lambda_f)A_-^{(-)}(p_-, \lambda_-, k_1, \lambda_1) \\
&= \mathcal{M}_0(p_+, \lambda_+, p_- - k_1, \lambda_+; q_1, q_2, \lambda_f)A_{\lambda_+}^{(-)}(p_-, \lambda_-, k_1, \lambda_1) , \tag{6.2.25}
\end{aligned}$$

where in the last line we have used the conservation of helicity along the massless electron-positron line in \mathcal{M}_0 . Note that the momentum argument p_-^μ in \mathcal{M}_0 now has changed into $p_-^\mu - k_1^\mu$. This is important for the following reason. In any physical amplitude or cross section, overall momentum conservation holds, and consequently there are infinitely many different ways to write the cross section as a function of the external momenta. If the actual arguments used in $\mathcal{M}_{0,1,2,\dots}$ do in fact satisfy momentum conservation, all these alternative formulations will give the same numerical value for the cross section: but if they do not satisfy momentum conservation differing formulations will lead to different results. In eq.(6.2.25), any of the equivalent formulations will give the same result: if we would have used $u(p_-)$ instead this would not be the case.

For single photon bremsstrahlung collinear with the incoming positron, we of course have

$$\mathcal{M}_1(p_+, \lambda_+, p_-, \lambda_-, k_1, \lambda_1; q_1, q_2, \lambda_f) =$$

$$\begin{aligned}
& \mathcal{M}_0(p_+ - k_1, +, p_-, \lambda_-; q_1, q_2, \lambda_f) A_+^{(+)}(p_+, \lambda_+, k_1, \lambda_1) \\
& + \mathcal{M}_0(p_+ - k_1, -, p_-, \lambda_-; q_1, q_2, \lambda_f) A_-^{(+)}(p_+, \lambda_+, k_1, \lambda_1) \\
& = \mathcal{M}_0(p_+ - k_1, \lambda_-, p_-, \lambda_-; q_1, q_2, \lambda_f) A_{\lambda_-}^{(-)}(p_+, \lambda_+, k_1, \lambda_1) . \quad (6.2.26)
\end{aligned}$$

In the case of double bremsstrahlung there are more possible collinear situations: we can have one photon collinear with one beam, two photons collinear with the same beam, or one photon collinear with one of the beams each. If only one of the photons, say k_1 is collinear with, say p_- , we can immediately write the extension of eq.(6.2.25):

$$\begin{aligned}
& \mathcal{M}_2(p_+, \lambda_+, p_-, \lambda_-, k_1, \lambda_{1,2}, \lambda_2; q_1, q_2, \lambda_f) = \\
& = \mathcal{M}_1(p_+, \lambda_+, p_- - k_1, \lambda_+, k_2, \lambda_2; q_1, q_2, \lambda_f) A_{\lambda_+}^{(-)}(p_-, \lambda_-, k_1, \lambda_1) , \quad (6.2.27)
\end{aligned}$$

with obvious changes for radiation collinear with the positron. In case the two photons are both collinear with the electron, we of course find

$$\begin{aligned}
& \mathcal{M}_2(p_+, \lambda_+, p_-, \lambda_-, k_1, \lambda_{1,2}, \lambda_2; q_1, q_2, \lambda_f) = \\
& = \mathcal{M}_1(p_+, \lambda_+, p_- - k_1 - k_2, \lambda_+; q_1, q_2, \lambda_f) A_{\lambda_+}^{(-)}(p_-, \lambda_-, k_1, \lambda_1, k_2, \lambda_2). \quad (6.2.28)
\end{aligned}$$

Note that as in the case of single bremsstrahlung, in eqs.(6.2.27) and (6.2.28) only one of the helicities survives in the final answer, since always either the positron or electron can be taken as massless. In the case where each of these has its own collinear photon this does no longer hold, and we have, when k_1 is collinear with p_- and k_2 with p_+ :

$$\begin{aligned}
& \mathcal{M}_2(p_+, \lambda_+, p_-, \lambda_-, k_1, \lambda_{1,2}, \lambda_2; q_1, q_2, \lambda_f) = \\
& = \mathcal{M}_0(p_+ - k_2, +, p_- - k_1, +; q_1, q_2, \lambda_f) \times A_+^{(+)}(p_+, \lambda_+, k_2, \lambda_2) A_+^{(-)}(p_-, \lambda_-, k_2, \lambda_2) \\
& + \mathcal{M}_0(p_+ - k_2, -, p_- - k_1, -; q_1, q_2, \lambda_f) \times A_-^{(+)}(p_+, \lambda_+, k_2, \lambda_2) A_-^{(-)}(p_-, \lambda_-, k_2, \lambda_2). \quad (6.2.29)
\end{aligned}$$

In this expression we have a coherent superposition of the two opposite helicity combinations of the incoming fermions: since we evaluate the cross section at the level of helicity amplitudes this is not a problem but if one would rather use the more standard techniques using traces in the squared matrix element extremely cumbersome expressions would arise. This can be easily seen from the fact that for instance the massless helicity amplitudes each contain either only G_{+, λ_f} or only G_{-, λ_f} , whereas in eq.(6.2.29) we have a nontrivial complex linear combination of G_{+, λ_f} and G_{-, λ_f} in every amplitude.

The above expressions suffice for a completely well defined algorithm to evaluate up to the two photon bremsstrahlung matrix elements in all possible kinematical configurations. The extension to the case of final state collinear radiation is of course straightforward. The only thing left for a computer implementation of the above formulae (in which we have indicated all arguments explicitly in order to show how the actual computer code looks in practice) is a way to determine, for a given event, whether or not to use the

massless expression, or any of the appropriate collinear ones. Obviously, we need to ensure a smooth transition from the noncollinear, massless case with all diagrams but fewer helicity combinations, and the collinear, massive case with fewer diagrams but all helicity combinations. Due to our definition of collinearity such a smooth transition is in fact possible: if we let a photon become more and more collinear with a beam the point where we can start neglecting diagrams comes *before* the point where we start having to account for m_e . Some experimentation has lead us to the following algorithm: for each photon i we define the quantity

$$f_i = \log \frac{(p_+ \cdot k_i)}{(p_- \cdot k_i)} , \quad (6.2.30)$$

which for massless electrons is just the rapidity of the photon. If for a given event (i.e. configuration of generated momenta) $f_1 > 15$ we call k_1 collinear with p_+ ; for $f_1 < -15$ we call it collinear with p_- . Note that for $f_1 = 15$ the angle between \vec{k}_1 and \vec{p}_+ is about 1 mrad, which is still a lot larger than m_e^2/E_b^2 . Next, if $|f_2| > 10$ we also call k_2 collinear (obviously, we also have to check this with k_1 and k_2 interchanged). The reason to relax the condition on the second photon is the following. If k_2 is only slightly less collinear than k_1 , say, $f_2 = 14.5$, one may run into problems: calling k_1 collinear and k_2 noncollinear, one would neglect terms like $(p_+ \cdot k_1)$ with respect to terms like $(p_+ \cdot k_2)$, which are in fact of comparable magnitude: so we would have to call both of them either collinear or noncollinear. This dilemma is best solved empirically: considering events with $15 < f_1 < 16$ and $10 < f_2 < 11$ we found that the 'collinear' and the 'noncollinear' treatment give results agreeing to within a fraction of 10^{-3} . This justifies the smoothness of the above procedure.

Before finishing this section we want to remark that of course eqs.(6.2.25) and (6.2.27) are of course not strictly necessary. Because only one helicity contribution is nonnegligible, we may of course also consider the squared form of the amplitude, implicitly summed over the spins: for instance if k_1 is collinear with p_- , this reads

$$|\mathcal{M}_1(p_+, p_-, k_1)|^2 = |\mathcal{M}_0(p_+, p_- - k_1)|^2 \times B(p_-, k_1) . \quad (6.2.31)$$

with

$$\begin{aligned} B(p_-, k_1) &= \sum_{\lambda_-, \lambda_1} \left| A_{\pm}^{(-)}(p_-, \lambda_-, k_1, \lambda_1) \right|^2 \\ &= \frac{1 + (1 - x_1)^2}{x_1 (p_- \cdot k_1)} - \frac{m_e^2 (1 - x_1)}{(p_- \cdot k_1)^2} , \end{aligned} \quad (6.2.32)$$

which is of course nothing but the well known Altarelli-Parisi type splitting function for massive fermions. For the double bremsstrahlung case the corresponding factor can be derived for the case of eq.(6.2.28) but, as already remarked above, not for the case of eq.(6.2.29). In both cases the amplitude level expressions are anyway simpler than the squared ones. However we have checked that we get equivalent results by squaring and

summing the explicit A 's in the double collinear case, or first squaring the matrix elements, and then working out the collinear situation (using, of course, the same axial gauge in both cases). That is, the following equality holds in the collinear limit up to terms of order m^3 :

$$\begin{aligned} \sum_{\lambda_-, \lambda_1, \lambda_2} \left| A_{\lambda}^{(-)}(p_-, \lambda_-, k_1, \lambda_1, k_2, \lambda_2) \right|^2 \not{p}_- &= \frac{1}{1 - x_1^2 - x_2^2} \times \quad (6.2.33) \\ &\times \left[\frac{\not{p}_- - \not{k}_1 - \not{k}_2 + m}{(p_- - k_1 - k_2)^2 - m^2} \gamma^\alpha \frac{\not{p}_- - \not{k}_1 + m}{(p_- - k_1)^2 - m^2} \gamma^\beta + (k_1 \leftrightarrow k_2) \right] (\not{p}_- + m) \\ &\times \left[\gamma^\nu \frac{\not{p}_- - \not{k}_1 + m}{(p_- - k_1)^2 - m^2} \gamma^\mu \frac{\not{p}_- - \not{k}_1 - \not{k}_2 + m}{(p_- - k_1 - k_2)^2 - m^2} + (k_1 \leftrightarrow k_2) \right] \\ &\times \left(-g_{\nu\beta} + \frac{k_{1\nu} q_\beta + k_{1\beta} q_\nu}{(k_1 \cdot q)} \right) \left(-g_{\mu\alpha} + \frac{k_{2\mu} q_\alpha + k_{2\alpha} q_\mu}{(k_2 \cdot q)} \right). \end{aligned}$$

Another remark is in order here. We have been able to express the collinear amplitudes for single bremsstrahlung in that for the nonradiative process, and the collinear one for double bremsstrahlung in that for the single bremsstrahlung process. Likewise, in the case of *triple* bremsstrahlung we might envisage reducing the collinear amplitude to the one for double bremsstrahlung with a collinear factor. However we think that at that point the quality of the approximation may start to deteriorate for the following reason. The nonradiative and single bremsstrahlung amplitudes can be written in a *robust* form, that is, the numerical result of their evaluation can be seen to be stable if the argument momenta p_+ or p_- are not strictly massless: therefore we are allowed to make the approximation that for instance $p_+ - k_1$ is proportional to p_+ if k_1 is sufficiently collinear with p_+ . As remarked above, in our expression for the double bremsstrahlung amplitude a number of numerical cancellations are still apparent in the numerator, cancelled by similar (but not identical!) ones in the denominator. Consequently we have less control over the stability of the final answer when photons become slightly collinear (but not collinear enough to warrant going over to the collinear expression). It is therefore not clear yet how such an expression will behave when we shall replace $p_+ - k_3$, say, by p_+ . It appears that it would be extremely useful if a simple and robust expression for the double bremsstrahlung cross section could be constructed. We doubt, however, that this is possible.

6.3 Generating events

In addition to expressions for the matrix elements, also algorithms to generate events distributed according to this matrix element are needed. Because this distribution peaks sharply, generating such events efficiently is not trivial when two bremsstrahlung photons occur.

Let us first discuss the phase space, PS_4 . For the four particle final state

$$\bar{f}(q_2) f(q_1) \gamma(k_1) \gamma(k_2)$$

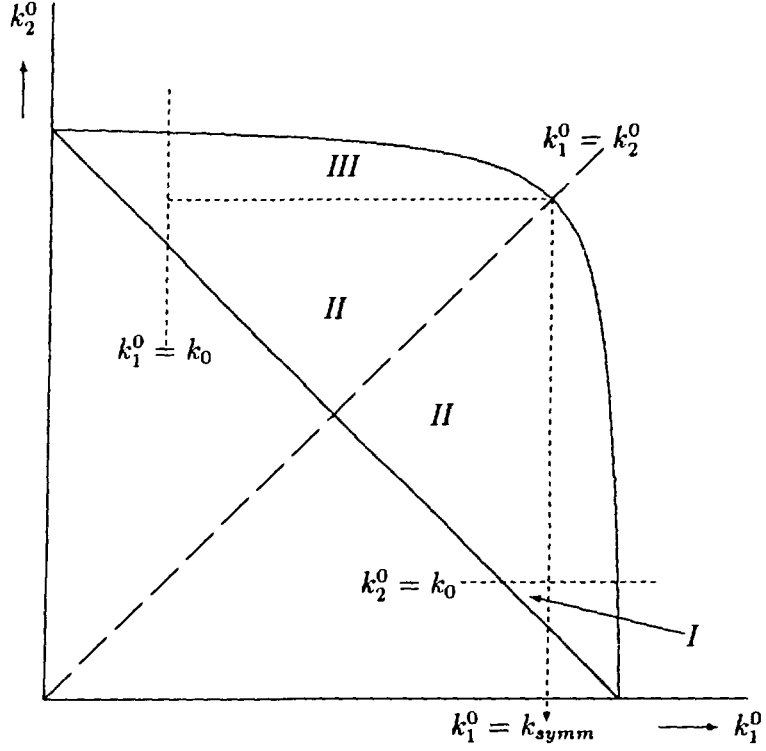


Fig. 6.1. A Dalitz plot for the $\bar{f}f\gamma\gamma$ phase space. Along the axes are the two photon energies.

one has

$$\begin{aligned}
 dPS_4 = & \frac{1}{2} \frac{1}{2s} \frac{1}{(2\pi)^8} d^4k_1 \delta^+(k_1^2) d^4k_2 \delta^+(k_2^2) \\
 & \times d^4q_2 \delta^+(q_2^2 - m_f^2) d^4q_1 \delta^+(q_1^2 - m_f^2) \\
 & \times \delta^{(4)}(p_+ + p_- - q_2 - q_1 - k_1 - k_2). \quad (6.3.1)
 \end{aligned}$$

The factor $\frac{1}{2}$ is the statistical factor for two identical bosons in the final state, whereas the factor $1/2s$ is the flux factor and $s = (p_+ + p_-)^2$ is the C.M. energy squared of the incoming particles. As basic variables we will choose $s' = (q_2 + q_1)^2$, the invariant mass squared of the final state fermion pair, k_1^0 , the energy of one of the photons, Ω_1 and Ω_2 , the solid angles of both the photons and Ω_f^* , the solid angle of q_2^* , where the * indicates that it is defined in the C.M. frame of the final state fermion pair. These variables have been chosen because the matrix element peaks in most of them. One then has

$$dPS_4 = \frac{1}{2} \frac{1}{2s} \frac{1}{(2\pi)^8} \frac{1}{2^5} \frac{k_1^0(k_2^0)^2}{s - s' - 2k_1^0\sqrt{s}} dk_1^0 d\Omega_1 d\Omega_2 \sqrt{1 - m_f^2/(q_2^0)^2} d\Omega_f^*, \quad (6.3.2)$$

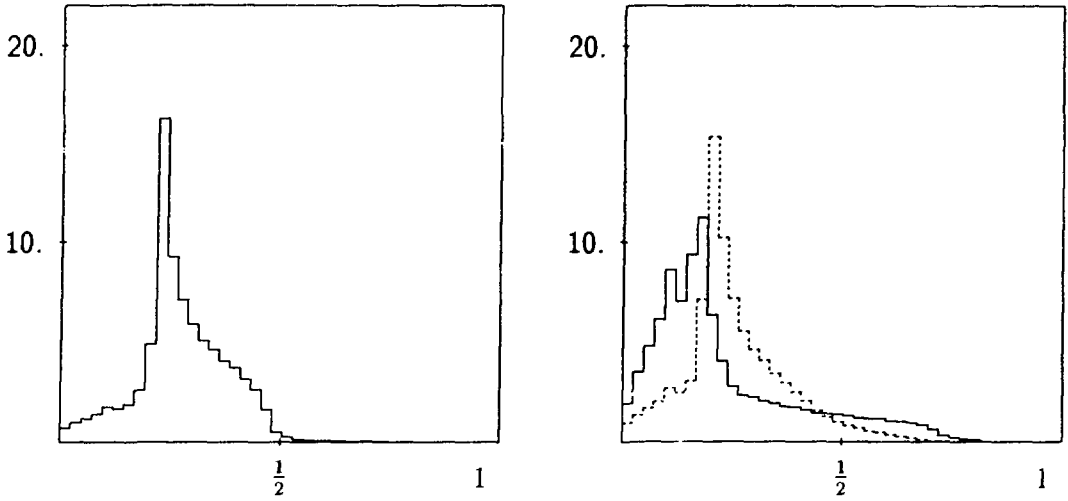


Fig. 6.2. The distribution of the weights (in units of 1000 events per bin) for double bremsstrahlung at $\sqrt{s} = 91.17$ GeV (left), 87.17 GeV (right, solid line) and 95.17 GeV (right, dashed line).

where

$$k_2^0 = \frac{s - s' - 2k_1^0 \sqrt{s}}{2\sqrt{s} - 2k_1^0(1 - \cos \angle(k_1, k_2))} . \quad (6.3.3)$$

The final state fermions will be treated as massless, $m_f = 0$, since this was also done for the matrix element. The square of the matrix element is approximated by

$$\frac{1}{4} \sum_{\lambda_j} |M|_{app}^2 = \frac{e^8 s^3 s' G(s')}{(p_+ \cdot k_1)(p_+ \cdot k_2)(p_- \cdot k_1)(p_- \cdot k_2)} , \quad (6.3.4)$$

where we used

$$G(s') = \sum_{\lambda_e, \lambda_f = -1, 1} |G_{\lambda, \lambda_f}(s')|^2 . \quad (6.3.5)$$

With the notation

$$d\Omega_i = dc_i d\varphi_i , \quad (6.3.6)$$

$$p = \frac{1}{\sqrt{1 - m^2/(p_+^0)^2}} , \quad (6.3.7)$$

one has for the approximant in terms of our basic variables:

$$\frac{1}{4} \sum_{\lambda_j} |M|_{app}^2 = \frac{2^{12} \pi^4 \alpha^4 s s' G(s')}{(k_1^0)^2 (k_2^0)^2 (p^2 - c_1^2)(p^2 - c_2^2)} \quad (6.3.8)$$

The integration over Ω_j^* is trivial. The next integral we perform is the k_1^0 integral, from $k_1^0 = k_0$ up to $k_1^0 = k_{max}$, where k_0 is the distinction between soft and hard photons and

$$k_{max} = \frac{s - s' - 2k_0\sqrt{s}}{2\sqrt{s} - 2k_0(1 - \cos \angle(k_1, k_2))}. \quad (6.3.9)$$

This upper boundary introduces an extra dependence on the angle between the two photons. Performing the integral with this boundary therefore would leave us with a distribution for the photon angles that we would not be able to generate. Instead, exploiting the $k_1 \leftrightarrow k_2$ symmetry of the problem, we integrate over k_1^0 from k_0 up to

$$k_{symm} = \frac{1}{2}(\sqrt{s} - \sqrt{s'})$$

and multiply by two. As can be seen from the Dalitz plot 5.1 we now have overestimated area *II* by a factor 2 and we have added a contribution from area *I*, which was not there before. We correct for this when generating k_1^0 values, by assigning a weight equal to 1 for events in area *III*, equal to $\frac{1}{2}$ for events in area *II* and equal to 0 for events in area *I*, and then applying weight rejection. This way one is able generate the distribution of eq. (6.3.4).

Having done the k_1^0 integration one has

$$\begin{aligned} \int dPS_4 \frac{1}{4} \sum_{\lambda_j} |M|_{app}^2 &= \frac{2^3 \alpha^4}{(2\pi)^3} \int d\Omega_1 d\Omega_2 ds' \frac{s' G(s')}{s - s'} \\ &\times \frac{1}{(p^2 - c_1^2)(p^2 - c_2^2)} \log \frac{s - s' - 2k_0\sqrt{s}}{2k_0\sqrt{s'}}. \end{aligned} \quad (6.3.10)$$

The advantage of the procedure followed so far is that the integration over Ω_1 and Ω_2 is now extremely simple, yielding

$$\int dPS_4 \frac{1}{4} \sum_{\lambda_j} |M|_{app}^2 = \frac{4\alpha^4}{\pi} \log^2 \frac{s}{m^2} \int ds' \frac{s' G(s')}{s - s'} \log \frac{s - s' - 2k_0\sqrt{s}}{2k_0\sqrt{s'}}. \quad (6.3.11)$$

The approximate total cross section resulting from the s' integration is given in appendix C for completeness. At this point we will assume that this s' distribution (6.3.11) can be generated in some way. As it still is a rather complicated distribution, due to the behavior of $G(s')$, we used a general purpose routine. The algorithm, then, is as follows.

1. Generate s' according to the distribution (6.3.11).
2. Generate c_1 according to $1/(p - c_1)$ and flip the sign in 50% of the cases. Generate φ according to a flat distribution. Repeat this procedure for Ω_2 .
3. Generate k_1^0 according to

$$\frac{1}{k_1^0} + \frac{1}{\frac{1}{2}\sqrt{s}(1 - s'/s) - k_1^0}$$

between the boundaries k_0 and $\frac{1}{2}(\sqrt{s} - \sqrt{s'})$. Notice that both terms are positive definite over this k_1^0 range. The energy of the other photon is then given by eq. (6.3.3).

4. Apply weight rejection with the following weight:

$$w = \begin{cases} 0 & \text{if } k_2^0 < k_0 \\ \frac{1}{2} & \text{if } k_0 < k_2^0 < k_{symm} \\ 1 & \text{if } k_2^0 > k_{symm} \end{cases}$$

5. Generate Ω_f^* , that is $\cos\vartheta^*$ and φ^* , both according to a flat distribution. The resulting momenta q_2^* and q_1^* have to be boosted to the lab frame.

6. Apply weight rejection with as weight

$$w = \frac{\sum_{\lambda_j} |M|^2}{\sum_{\lambda_j} |M|_{app}^2} . \quad (6.3.12)$$

The last step ensures that in the end one generates the distribution as given by the complete matrix element. Since it is clear that step 1 – 5 can be done very fast, the efficiency of this algorithm is determined by the efficiency of the last step. For reasonable efficiency one needs a weight distribution that is sharply peaked and bounded from above by a value not too far from the peak. For a typical set of values for the input parameters ($M_Z = 91.17$ GeV, $\sin^2\vartheta_w = 0.2270$) we show the result for this weight distribution in figure 6.2. From these histograms it appears the weight rejection is in fact quite efficient at all energies.

Being able to generate events with two hard photons (with $k_i^0 > k_0$), in order to have an event generator that is complete up to and including order α^2 , one also needs events with one hard photon or even no hard photon at all. From the Monte Carlo point of view these are not very difficult to generate. The only difficulty is including the two loop virtual and soft photon corrections. But since these have been calculated analytically [2], one can simply use those results. We employ the following algorithm.

- Approximate the no hard photon distribution by

$$\frac{1}{4} \sum_{\lambda_j} |M^{0\gamma}|_{app}^2 = (1 + \delta^{VS}) 2 e^4 s^2 G(s) , \quad (6.3.13)$$

which can be generated trivially, and weigh this with the full lowest matrix element, divided by the above approximation. The factor δ^{VS} contains the complete order α and order α^2 virtual and soft photon corrections as calculated in [2]. The above approximation gives rise to an approximate total cross section

$$\sigma_{app}^{0\gamma} = (1 + \delta^{VS}) 2 \pi \alpha^2 s G(s) , \quad (6.3.14)$$

which will be modified to the exact cross section for this type of events by multiplying by the average of the weights.

- Approximate the 1 hard photon distribution by

$$\frac{1}{4} \sum_{\lambda_j} |M^{1\gamma}|_{app}^2 = \frac{e^6}{3} \frac{1}{(p_+ \cdot k_1)} \left(2 \frac{p_+^0}{k_1^0} + \frac{p_+^0}{p_+^0 - k_1^0} \right) s'^2 G(s') + (p_+ \leftrightarrow p_-), \quad (6.3.15)$$

which leads to an approximate total cross section of

$$\sigma_{app}^{1\gamma} = \frac{\alpha^3}{3s} \log \frac{s}{m^2} \int ds' \left(\frac{2}{s-s'} + \frac{1}{s'} \right) s'^2 G(s'). \quad (6.3.16)$$

The result when integrated over s' has been listed in appendix C as well, for completeness. The distribution (6.3.15) can be generated, assuming once more one has a way of generating the resulting $d\sigma_{app}/ds'$ distribution. One then has to weigh the events with the complete matrix element, where one loop virtual and soft photon corrections have been included. To make the approximation (6.3.15) better one can include e.g. a factor

$$1 + \frac{\alpha}{\pi} \left(2 \log k_0 \left(\log \frac{s}{m^2} - 1 \right) + \frac{3}{2} \log \frac{s}{m^2} + \frac{\pi^2}{3} - 2 \right) \quad (6.3.17)$$

to take into account part of the virtual and soft photon corrections already. This makes the weight rejection step more efficient. The complete one loop virtual and soft photon corrections can once again be taken from [2]. It should be noted however that if one does so, one lacks the $\cos \vartheta^*$ dependence of the virtual photon corrections to the single hard bremsstrahlung matrix element. Also another remark is in order here. Because the one hard photon contribution is the only one where virtual and soft photon corrections appear up to one loop, this is the only contribution that can become negative when including such corrections and lowering the value of k_0 . The restriction that this contribution remains positive turns out to restrict k_0 to $k_0 > 10^{-4} p_+^0$. This seems to be low enough for all practical purposes.

We have implemented the generation of the no photon distribution and the one hard photon distribution as well. In the next section we will present some numerical results.

6.4 Numerical results

In the Monte Carlo program *FPAIR* we have implemented up to double photon bremsstrahlung from the initial state using the methods described in the previous sections. Weak corrections have been included by using the library of the program *ZSHAPE* (see [6]). We also incorporated one loop final state QED corrections using a somewhat modified version of the techniques described in [23]. In this section some results are presented.

\sqrt{s}	ZSHAPE	FPAIR		DYMU2	
		no cuts	cuts	no cuts	cuts
81.17	38.2	38.1±0.1	32.9±0.1	38.0±0.1	33.4±0.1
83.17	49.8	49.8±0.1	43.9±0.1	49.7±0.1	44.4±0.1
85.17	74.9	74.8±0.1	67.3±0.1	74.9±0.1	68.2±0.1
87.17	142.0	141.7±0.2	130.0±0.2	142.3±0.2	131.8±0.1
89.17	411.5	410.7±0.4	381.1±0.4	412.2±0.4	385.9±0.4
91.17	1471.1	1471.4±1.5	1372.7±1.5	1473.3±1.5	1375.4±1.5
93.17	611.6	612.1±0.6	568.4±0.6	617.8±0.6	574.6±0.6
95.17	283.6	283.8±0.3	261.0±0.3	285.3±0.3	263.2±0.3
97.17	175.9	176.0±0.2	158.8±0.2	176.1±0.2	159.4±0.2
99.17	125.5	125.4±0.1	107.3±0.1	125.4±0.1	107.0±0.1
101.17	96.9	96.9±0.1	71.7±0.1	96.7±0.1	70.3±0.1

Table 6.1. Monte Carlo and semianalytical results for the total cross section. Input parameters and cuts are given in the text.

\sqrt{s}	MUCUT	FPAIR		DYMU2	
		no cuts	cuts	no cuts	cuts
81.17	-0.699	-0.676	-0.695	-0.674	-0.691
83.17	-0.631	-0.623	-0.631	-0.617	-0.623
85.17	-0.519	-0.522	-0.521	-0.513	-0.511
87.17	-0.364	-0.369	-0.364	-0.366	-0.359
89.17	-0.180	-0.187	-0.184	-0.180	-0.175
91.17	0.007	0.003	0.001	0.005	0.006
93.17	0.127	0.126	0.125	0.128	0.129
95.17	0.189	0.185	0.189	0.185	0.191
97.17	0.232	0.220	0.233	0.220	0.235
99.17	0.272	0.242	0.275	0.245	0.285
101.17	0.343	0.257	0.344	0.260	0.358

Table 6.2. Monte Carlo and semianalytical results for the forward-backward asymmetry. The Monte Carlo estimate for the standard deviation of these results is 2 in the last digit. The flags used in MUCUT were igs=1, iexp1=1, iexpf=0, interf=0, ifinal=1, inorm=1, isoft2=1, delta=0.2. Input parameters and cuts are given in the text.

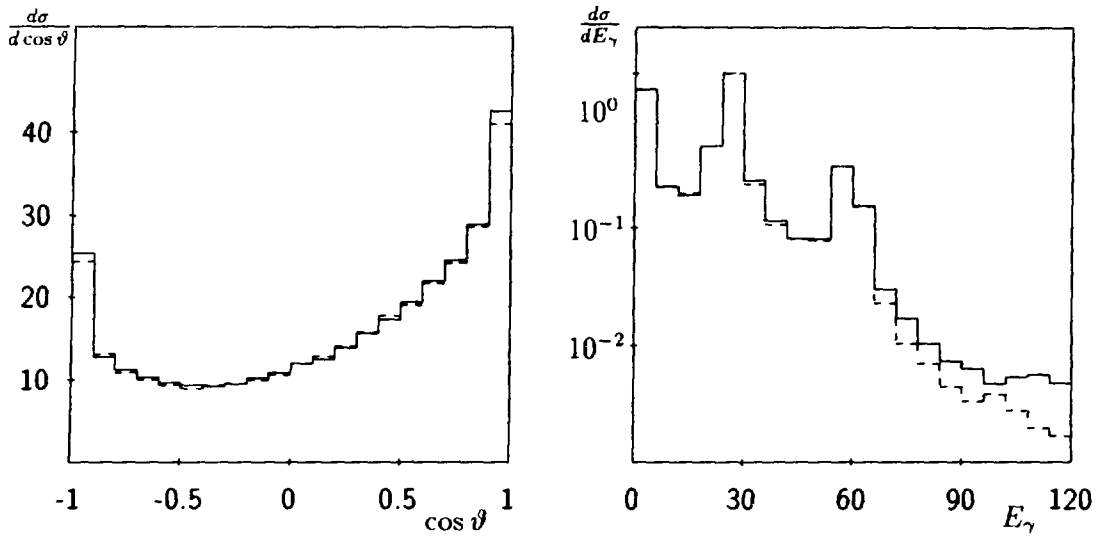


Fig. 6.3. The $\cos \vartheta$ (left) and E_γ (right) distributions at $\sqrt{s} = 120$ GeV. No cuts are applied. The distributions are given by DYMU2 (dashed line) and FPAIR (solid line).

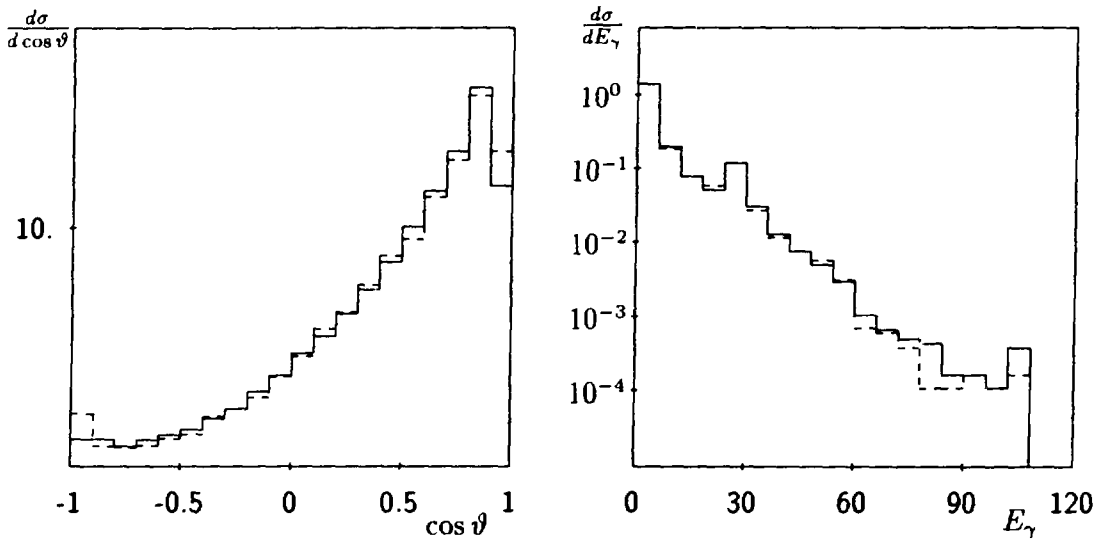


Fig. 6.4. The $\cos \vartheta$ (left) and E_γ (right) distributions at $\sqrt{s} = 120$ GeV. Canonical cuts are applied. The distributions are given by DYMU2 (dashed line) and FPAIR (solid line).

As the input parameters we use $f = \mu^-$, $M_Z = 91.17$ GeV, $M_H = 100$ GeV, $m_{top} = 130$ GeV, which leads to $\sin^2 \vartheta_w = 0.2270$ and $\Gamma_Z = 2.491$ GeV. We will consider the distributions of $\cos \vartheta = \cos \angle(q_2, p_+)$, the angle between e^+ and μ^+ , and $E_\gamma = \sum_i k_i^0$, the total energy carried away by photons. There are several calculations that can be compared to our results. In the first place, there is the analytical result

incorporated in ZSHAPE, which computes the total cross section to high precision and serves as a benchmark for Monte Carlo event generators. For the $\cos\vartheta$ distribution there is the semianalytical program MUCUT presented in [3], which also gives the forward-backward asymmetry. In this program the weak corrections are approximated by using the so called G_μ representation, which should be well enough for our purposes. Finally, we have compared to the Monte Carlo DYMU2 of [11], which is ideally suited to our purposes since it also generates up to 2 photons from the initial, and up to 1 from the final state. Throughout we impose the cut $s' > 0.2s$. This is meant to be more or less realistic: indeed, in [2] it was shown that such a strict cut would be necessary to suppress the background from two photon processes such as $e^+e^- \rightarrow e^+e^-\mu^+\mu^-$. Requiring $s' > 0.2s$ allows us to treat the muons as massless for all events, thus avoiding the region at $s' \sim 0$ where all calculations are known to differ. In spite of this cut on s' we will refer to the case where we impose no other cuts as the case with 'no cuts'. We can also imagine an additional set of 'canonical cuts', which are slightly more realistic. These we choose to be

$$\begin{aligned} 15^\circ < \vartheta_{1,2} < 165^\circ, \\ 180^\circ - \angle(q_1, q_2) < 10^\circ, \\ s' > 0.2s. \end{aligned} \tag{6.4.1}$$

The results for the total cross section from the runs with and without canonical cuts are given in table 6.1, for a number of different values for the CM energy \sqrt{s} . In table 6.2 the analogous results for the forward-backward asymmetry are given. The agreement of FPAIR and DYMU2 with the analytical results from ZSHAPE (with its exponentiation option turned off!) is seen to be quite good: the line shape is well reproduced. It is however strange to note that the result of MUCUT agrees with the case where cuts are applied, where it should agree with the case without cuts. This could suggest that a cut or approximation is made implicitly in MUCUT. For the residual effects of exponentiation in the line shape we refer to [6]. The influence of the cuts is similar in both FPAIR and DYMU2.

Next, we plot the $\cos\vartheta$ and E_γ distributions when no canonical cuts are applied. For the E_γ -plot the cut on s' was lowered to 1 GeV^2 , in order to have a large hard photon tail. The results are shown in figure 6.3. As far as can be seen from these histograms, there is agreement between the two results. Only in the E_γ distribution the two Monte Carlo programs differ slightly in the hard photon area. This need not to be a surprise since it was the motivation for calculating two hard photon bremsstrahlung explicitly. Note that here we have taken $\sqrt{s} = 120 \text{ GeV}$, that is, well above the Z peak. In that case, hard bremsstrahlung is one of the dominant effects, so that a comparison between FPAIR and DYMU2 really informs us about the behavior of the programs when generating bremsstrahlung, not just about the behavior of back-to-back events which dominate around the peak. The results after canonical cuts are shown in figure 6.4. Again the results of the two programs compare well, but for the hard photon part in the E_γ distribution.

6.5 Conclusions

In this chapter we have described how the matrix elements for double bremsstrahlung from the initial state can be computed. The use of spinor techniques ensures quick and compact evaluation, even in the case where photons are emitted close to the beams. The extension to bremsstrahlung from the produced fermions is of course straightforward. Special care is necessary in the transition region between collinear and noncollinear radiation to ensure smooth behavior of the numerical result: due to the fact that a strong ordering of the type $m_e^2 \ll (p \cdot k_1) \ll (p \cdot k_2) \ll s$ is kinematically possible: if this were not the case then probably the complete set of diagrams, including a nonzero electron mass throughout, would be necessary. We have outlined an algorithm for generating double bremsstrahlung events according to the exact distribution. Here a careful study of the structure of phase space for two soft photons is necessary: by employing the symmetry in the photon momenta an efficient algorithm can be constructed. We have presented some results from the corresponding program `FPAIR`, and compared these to other results known in the literature. The program is seen to do as well as can be expected. To finish, we want to stress again that of course a two loop treatment is not the final answer, even if the results for the total cross section coincide with those of analytical exponentiated programs like `ZSHAPE`. For one, there is still the so-called k_0 -problem, that is one cannot put k_0 lower than a given value without having events with negative weights. Only a fully exponentiated Monte Carlo can circumvent this problem. Secondly, final state radiation is only included up to one loop, and interference between initial and final state radiation is not treated at all. Fortunately, these effects are small at the Z resonance but a good all-round Monte Carlo will at some time have to be constructed that does include them and will allow detailed studies of off-resonance phenomena. Such a Monte Carlo will unavoidably have to include two loop effects as described in this chapter. The present study can be seen as a step towards this goal.

Appendix 6.A: Spinor techniques

In this appendix we shall present the relevant formulae necessary for the evaluation of the bremsstrahlung matrix elements using spinor techniques. More details can for instance be found in [10]. We start with two four-vectors k_0^μ and k_1^μ which satisfy

$$(k_0 \cdot k_0) = (k_0 \cdot k_1) = 0 \quad , \quad (k_1 \cdot k_1) = -1 \quad , \quad (6.A.1)$$

and two spinors $u_-(k_0)$ and $u_+(k_0)$ defined by

$$\begin{aligned} u_-(k_0)\bar{u}_-(k_0) &= \frac{1}{2}(1 - \gamma^5)\not{k}_0 \\ u_+(k_0) &\equiv \not{k}_1 u_-(k_0) \quad . \end{aligned} \quad (6.A.2)$$

We now define a spinor for any (massive or massless) fermion momentum p_i^μ as follows:

$$u_\lambda(p_i) = \frac{1}{\sqrt{2(p \cdot k_0)}} (\not{p}_i + m_i) u_{-\lambda}(k_0) , \quad (6.A.3)$$

where $(p_i \cdot p_i) = m_i^2$: for particles, m_i is positive, while for antiparticles m_i is negative. The limit $m_i \rightarrow 0$ is smooth and leads to fermion states with definite helicity:

$$\lim_{m_i \rightarrow 0} u_\lambda(p_i) \bar{u}_\lambda(p_i) = \frac{1}{2} (1 + \lambda \gamma^5) \not{p}_i , \quad (6.A.4)$$

while for $m_i \neq 0$ (when the helicity is not a Lorentz invariant concept) we have the usual form

$$u_\lambda(p_i) \bar{u}_\lambda(p_i) = \frac{1}{2} (\not{p}_i + m_i) (1 + \gamma^5 \not{f}_i) , \quad (6.A.5)$$

where the fermion spin polarization s_i^μ is given by

$$s_i^\mu = \frac{1}{m_i} \left(p_i^\mu - \frac{m_i^2}{(p_i \cdot k_0)} k_0^\mu \right) . \quad (6.A.6)$$

The spinor products can now be computed using the well known trace techniques: for instance, we have

$$s_{+,-}(p_1, p_2) = \frac{\text{Tr} [(1 - \gamma^5) \not{k}_0 (\not{p}_1 + m_1) (\not{p}_2 + m_2) \not{k}_1]}{4\sqrt{(p_1 \cdot k_0)(p_2 \cdot k_0)}} . \quad (6.A.7)$$

Explicit expressions for the spinor products are obtained by taking explicit forms for k_0^μ and k_1^μ : using

$$\begin{aligned} (k_0^0, k_0^x, k_0^y, k_0^z) &= (1, 1, 0, 0) , \\ (k_1^0, k_1^x, k_1^y, k_1^z) &= (0, 0, 1, 0) , \end{aligned} \quad (6.A.8)$$

we obtain the following formulae:

$$\begin{aligned} s_{+,-}(p_1, p_2) &= (p_1^y + ip_1^z) \left[\frac{p_2^0 - p_2^x}{p_1^0 - p_1^x} \right]^{\frac{1}{2}} - (p_1 \leftrightarrow p_2) , \\ s_{+,-}(p_2, p_1) &= -s_{+,-}(p_1, p_2) , \\ s_{-,+}(p_1, p_2) &= -s_{+,-}(p_1, p_2)^* , \\ s_{+,+}(p_1, p_2) &= m_1 \left[\frac{p_2^0 - p_2^x}{p_1^0 - p_1^x} \right]^{\frac{1}{2}} + (p_1 \leftrightarrow p_2) , \\ s_{+,+}(p_2, p_1) &= s_{+,+}(p_1, p_2) , \\ s_{-,-}(p_1, p_2) &= s_{+,+}(p_1, p_2) . \end{aligned} \quad (6.A.9)$$

Note that $s_{+,-}$ and $s_{-,+}$ are antisymmetric, and $s_{+,+}$ and $s_{-,-}$ are symmetric in p_1^μ and p_2^μ . Moreover, in the ultra-relativistic limit $m_1, m_2 \rightarrow 0$ $s_{+,+}$ and $s_{-,-}$ vanish, whereas in the nonrelativistic limit $\vec{p}_1, \vec{p}_2 \rightarrow 0$ the $s_{+,-}$ and $s_{-,+}$ go to zero. There is an interesting relation between the spinor products and the more familiar vector products. In the general massive case we are considering here it reads

$$\frac{1}{4} \sum_{\lambda_1, \lambda_2 = \pm} |s_{\lambda_1, \lambda_2}(p_1, p_2)|^2 = (p_1 \cdot p_2) + m_1 m_2 \quad , \quad (6.A.10)$$

which in fact turns out to be about the most (numerically) stable way of computing the vector product $(p_1 \cdot p_2)$, especially when the masses are zero or small. A few other useful relations exist, which we give here without derivation: again we refer to [10] for details. First, for any string S of Dirac matrices, we have the reversion identity:

$$\bar{u}_{\lambda_1}(p_1) S u_{\lambda_2}(p_2) = \lambda_1 \lambda_2 \bar{u}_{-\lambda_2}(p_2) S^R u_{-\lambda_1}(p_1) \quad , \quad (6.A.11)$$

where S^R is the string S written in reversed order. Then, there is the Chisholm identity:

$$[\bar{u}_+(q_1) \gamma^\mu u_+(q_2)] \gamma_\mu = 2 \{ u_+(q_2) \bar{u}_+(q_1) + u_-(q_1) \bar{u}_-(q_2) \} \quad , \quad (6.A.12)$$

which holds for *massless* q_1^μ and q_2^μ . The so-called two dimensional Schouten identity leads to the formula

$$\begin{aligned} s_{+,-}(p_1, p_2) s_{+,-}(p_3, p_4) &+ \\ s_{+,-}(p_2, p_3) s_{+,-}(p_1, p_4) &+ \\ s_{+,-}(p_3, p_1) s_{+,-}(p_2, p_4) &= 0 \quad , \end{aligned} \quad (6.A.13)$$

where the momenta $p_{1,2,3,4}^\mu$ may have any mass. We want to stress that the result (6.A.13) is new in the sense that it is also seen to hold for massive momenta: to our knowledge this has not been established before. Note that in the Weyl spinor formulation constructed by Berends and Giele [14], which is completely equivalent to our spinor techniques for *massless* fermions, this relation follows immediately from the fact that their spinors have two components: in our case, it is derived most trivially by writing out the explicit definition of $s_{+,-}$ as given in eq.(6.A.9). It follows that eq.(6.A.13) also holds if we restrict the products $s_{+,-}$ to their real or imaginary parts only. Finally, another amusing identity is

$$s_{+,-}(p_1, p_2) = \frac{1}{m_3} (s_{+,+}(p_3, p_1) s_{+,-}(p_3, p_2) - s_{+,+}(p_3, p_2) s_{+,-}(p_3, p_1)) \quad , \quad (6.A.14)$$

which for instance turns out to be handy in the case of collinear double bremsstrahlung: again, here p_1^μ and p_2^μ may have any mass, and m_3 is of course the mass associated with p_3 . This finishes our review of spinor formulae: with the above tools, the matrix elements presented in section 6.2 can be derived immediately.

Appendix 6.B: Collinear factors

Here we give the collinear factors A discussed in section 6.2. It is immediately clear that upon flipping all helicities in any A we obtain the same result with only the replacement $s_{+,-} \leftrightarrow s_{-,+}$, so we only list half of them. For single collinear radiation we have

$$\begin{aligned}
 A_+^{(-)}(p_-, +, k_1, +) &= D_1 s_{+,-}(p_-, k_1) , \\
 A_+^{(-)}(p_-, +, k_1, -) &= -D_1 s_{-,+}(p_-, k_1)(1 - y_1^2) , \\
 A_+^{(-)}(p_-, -, k_1, +) &= 0 , \\
 A_+^{(-)}(p_-, -, k_1, -) &= -D_1 m_e y_1^3 ,
 \end{aligned} \tag{6.B.1}$$

with

$$D_1 = \frac{1}{\sqrt{2}y_1\sqrt{1-y_1^2}(p_- \cdot k_1)} . \tag{6.B.2}$$

Similarly,

$$\begin{aligned}
 A_+^{(+)}(p_+, +, k_1, +) &= -D_2 s_{+,-}(p_+, k_1)(1 - y_1^2) , \\
 A_+^{(+)}(p_+, +, k_1, -) &= D_2 s_{-,+}(p_+, k_1) , \\
 A_+^{(+)}(p_+, -, k_1, +) &= D_2 m_e y_1^3 , \\
 A_+^{(+)}(p_+, -, k_1, -) &= 0 ,
 \end{aligned} \tag{6.B.3}$$

with

$$D_2 = \frac{1}{\sqrt{2}y_1\sqrt{1-y_1^2}(p_+ \cdot k_1)} . \tag{6.B.4}$$

Note that since $p_+^0 = p_-^0 = E_b$ the value of y_1 is the same whether defined using p_- or p_+ : for final state radiation this is of course no longer true. For double collinear radiation we have to take into account two diagrams, leading to

$$\begin{aligned}
 A_\lambda^{(-)}(p_-, \lambda_-, k_1, \lambda_1, k_2, \lambda_2) &= F_\lambda^{(-)}(p_-, \lambda_-, k_1, \lambda_1, k_2, \lambda_2) \\
 &\quad + F_\lambda^{(-)}(p_-, \lambda_-, k_2, \lambda_2, k_1, \lambda_1) , \\
 F_+^{(-)}(p_-, +, k_1, +, k_2, +) &= D_3 s_{+,-}(p_-, k_1) (s_{+,-}(p_-, k_1) y_1 y_2 \\
 &\quad + s_{+,-}(p_-, k_2)(1 - y_1^2)) , \\
 F_+^{(-)}(p_-, +, k_1, +, k_2, -) &= -D_3 (m_e^2 y_1^3 y_2 + s_{+,-}(p_-, k_1) s_{-,+}(p_-, k_2)(1 - y_1^2 - y_2^2)) , \\
 F_+^{(-)}(p_-, +, k_1, -, k_2, +) &= -D_3 s_{-,+}(p_-, k_1) (s_{+,-}(p_-, k_1) y_1 y_2 (1 - y_1^2) \\
 &\quad + s_{+,-}(p_-, k_2)(1 - y_1^2)^2) , \\
 F_+^{(-)}(p_-, +, k_1, -, k_2, -) &= D_3 s_{-,+}(p_-, k_1) (s_{-,+}(p_-, k_1) y_1 y_2 (1 - y_1^2 - y_2^2) \\
 &\quad + s_{-,+}(p_-, k_2)(1 - y_1^2)(1 - y_1^2 - y_2^2)) ,
 \end{aligned}$$

$$\begin{aligned}
F_-^{(-)}(p_-, +, k_1, +, k_2, +) &= D_3 m_e \left(s_{+,-}(p_-, k_1) y_2 (y_1^4 + y_2^2 + y_1^2 y_2^2) \right. \\
&\quad \left. + s_{+,-}(p_-, k_2) y_1^3 (1 - y_1^2 - y_2^2) \right) , \\
F_-^{(-)}(p_-, +, k_1, +, k_2, -) &= -D_3 m_e y_1^3 \left(s_{-,+}(p_-, k_1) y_1 y_2 + s_{-,+}(p_-, k_2) (1 - y_2^2) \right) , \\
F_-^{(-)}(p_-, +, k_1, -, k_2, +) &= -D_3 m_e y_2^3 s_{-,+}(p_-, k_1) , \\
F_-^{(-)}(p_-, +, k_1, -, k_2, -) &= 0 , \tag{6.B.5}
\end{aligned}$$

with

$$D_3 = \frac{1}{2y_1 y_2 \sqrt{1 - y_1^2 - y_2^2} (p_- \cdot k_1) [(p_- \cdot k_1) + (p_- \cdot k_2) - (k_1 \cdot k_2)]} . \tag{6.B.6}$$

Finally, for double collinear radiation from the positron we have

$$\begin{aligned}
A_\lambda^{(+)}(p_+, \lambda_+, k_1, \lambda_1, k_2, \lambda_2) &= F_\lambda^{(+)}(p_+, \lambda_+, k_1, \lambda_1, k_2, \lambda_2) \\
&\quad + F_\lambda^{(+)}(p_+, \lambda_+, k_2, \lambda_2, k_1, \lambda_1) , , \\
F_+^{(+)}(p_+, +, k_1, +, k_2, +) &= D_4 s_{+,-}(p_+, k_1) \left(s_{+,-}(p_+, k_1) y_1 y_2 (1 - y_1^2 - y_2^2) \right. \\
&\quad \left. + s_{+,-}(p_+, k_2) (1 - y_1^2) (1 - y_1^2 - y_2^2) \right) , \\
F_+^{(+)}(p_+, +, k_1, +, k_2, -) &= -D_4 s_{+,-}(p_+, k_1) \left(s_{-,+}(p_+, k_1) y_1 y_2 (1 - y_1^2) \right. \\
&\quad \left. + s_{-,+}(p_+, k_2) (1 - y_1^2)^2 \right) , \\
F_+^{(+)}(p_+, +, k_1, -, k_2, +) &= -D_4 \left(m_e^2 y_1^3 y_2 + s_{-,+}(p_+, k_1) s_{+,-}(p_+, k_2) (1 - y_1^2 - y_2^2) \right) , \\
F_+^{(+)}(p_+, +, k_1, -, k_2, -) &= D_4 s_{-,+}(p_+, k_1) \left(s_{-,+}(p_+, k_1) y_1 y_2 \right. \\
&\quad \left. + s_{-,+}(p_+, k_2) (1 - y_1^2) \right) , \\
F_-^{(+)}(p_+, +, k_1, +, k_2, +) &= 0 , \\
F_-^{(+)}(p_+, +, k_1, +, k_2, -) &= D_4 m_e y_2^3 s_{+,-}(p_+, k_1) , \\
F_-^{(+)}(p_+, +, k_1, -, k_2, +) &= D_4 m_e y_1^3 \left(s_{+,-}(p_+, k_1) y_1 y_2 + s_{+,-}(p_+, k_2) (1 - y_1^2) \right) , \\
F_-^{(+)}(p_+, +, k_1, -, k_2, -) &= -D_4 m_e \left(s_{-,+}(p_+, k_1) y_2 (y_1^4 + y_2^2 + y_1^2 y_2^2) \right. \\
&\quad \left. + s_{-,+}(p_+, k_2) y_1^3 (1 - y_1^2 - y_2^2) \right) , \tag{6.B.7}
\end{aligned}$$

with

$$D_4 = \frac{1}{2y_1 y_2 \sqrt{1 - y_1^2 - y_2^2} (p_+ \cdot k_1) ((p_+ \cdot k_1) + (p_+ \cdot k_2) - (k_1 \cdot k_2))} . \tag{6.B.8}$$

Appendix 6.C: The approximate total cross sections

For completeness we list our results for the approximate total cross sections corresponding with the one hard photon contribution and the two hard photons contribution respectively.

These expressions can be obtained by integrating eq. (6.3.16) and (6.3.11) over s' . It must be stressed that these are not 'approximate cross sections' in the sense that their result should coincide with the exact one to some acceptable degree of accuracy, but rather that they just serve to normalize the event weights: indeed, $\sigma_{app}^{1\gamma}$ and $\sigma_{app}^{2\gamma}$ coincide with their exact counterparts only up to a factor $\langle w \rangle$ (the mean weight) which can differ appreciably from 1.

$$\sigma_{app}^{1\gamma} = \frac{\alpha^3}{3s} \log \frac{s}{m^2} \left[s(B_1 I_1 + 2B_2 I_2) + (B_3 + B_4(s + M_Z^2)) I_4 + (B_3(s + M_Z^2) - M_Z^2 \Gamma_Z^2 B_4) I_3 \right], \quad (6.C.1)$$

$$\sigma_{app}^{2\gamma} = \frac{4\alpha^4}{\pi} \log^2 \frac{s}{m^2} \left[-\log(2k_0)(B_1 I_1 + B_2 I_2 + B_3 I_3 + B_4 I_4) + B_1 \left(-\frac{1}{2} I_5 + I_6 \right) + B_2 \left(-\frac{1}{2} I_7 + I_8 \right) + B_4 \operatorname{Re} \left(-\frac{1}{2} I_9 + I_{10} \right) - \frac{B_3}{M_Z \Gamma_Z} \operatorname{Im} \left(-\frac{1}{2} I_9 + I_{10} \right) \right]. \quad (6.C.2)$$

If one has included a factor like the one in eq. (6.3.17) in the approximation (6.3.15) for the one hard photon distribution, one should multiply $\sigma_{app}^{1\gamma}$ by the same factor.

We have defined the following integrals

$$I_1 = \log \frac{s'_{max}}{s'_{min}},$$

$$I_2 = \log \frac{s - s'_{min}}{s - s'_{max}},$$

$$I_3 = \frac{1}{M_Z \Gamma_Z} \left(\arctan \frac{s'_{max} - M_Z^2}{M_Z \Gamma_Z} - \arctan \frac{s'_{min} - M_Z^2}{M_Z \Gamma_Z} \right),$$

$$I_4 = \frac{1}{2} \log \frac{(s'_{max} - M_Z^2)^2 + M_Z^2 \Gamma_Z^2}{(s'_{min} - M_Z^2)^2 + M_Z^2 \Gamma_Z^2},$$

$$I_5 = \frac{1}{2} \log^2 s'_{max} - \frac{1}{2} \log^2 s'_{min},$$

$$I_6 = \log(s - 2k_0\sqrt{s}) \log \frac{s'_{max}}{s'_{min}} - \operatorname{Li}_2 \left(\frac{s'_{max}}{s - 2k_0\sqrt{s}} \right) + \operatorname{Li}_2 \left(\frac{s'_{min}}{s - 2k_0\sqrt{s}} \right),$$

$$I_7 = \log s \log \frac{s - s'_{min}}{s - s'_{max}} + \operatorname{Li}_2(1 - s'_{max}/s) - \operatorname{Li}_2(1 - s'_{min}/s),$$

$$I_8 = -\frac{1}{2} \log^2(s - s'_{max}) - \operatorname{Li}_2 \left(\frac{2k_0\sqrt{s}}{s - s'_{max}} \right) + \frac{1}{2} \log^2(s - s'_{min}) + \operatorname{Li}_2 \left(\frac{2k_0\sqrt{s}}{s - s'_{min}} \right),$$

$$\begin{aligned}
I_9 &= +\log(s'_{max} - M_Z^2 + iM_Z\Gamma_Z) \log s'_{max} - \frac{1}{2} \log^2 s'_{max} - \text{Li}_2\left(\frac{M_Z^2 - iM_Z\Gamma_Z}{s'_{max}}\right) \\
&\quad - \log(s'_{min} - M_Z^2 + iM_Z\Gamma_Z) \log s'_{min} + \frac{1}{2} \log^2 s'_{min} + \text{Li}_2\left(\frac{M_Z^2 - iM_Z\Gamma_Z}{s'_{min}}\right), \\
I_{10} &= +\log(s - 2k_0\sqrt{s} - M_Z^2 + iM_Z\Gamma_Z) \log(s'_{max} - M_Z^2 + iM_Z\Gamma_Z) \\
&\quad - \log(s - 2k_0\sqrt{s} - M_Z^2 + iM_Z\Gamma_Z) \log(s'_{min} - M_Z^2 + iM_Z\Gamma_Z) \\
&\quad - \text{Li}_2\left(\frac{s'_{max} - M_Z^2 + iM_Z\Gamma_Z}{s - 2k_0\sqrt{s} - M_Z^2 + iM_Z\Gamma_Z}\right) + \text{Li}_2\left(\frac{s'_{min} - M_Z^2 + iM_Z\Gamma_Z}{s - 2k_0\sqrt{s} - M_Z^2 + iM_Z\Gamma_Z}\right),
\end{aligned}$$

and the following constants

$$\begin{aligned}
B_1 &= \frac{4Q_e Q_f}{s}, \\
B_2 &= B_1 + \frac{4Q_e Q_f s + 8Q_e Q_f v_e v_f (s - M_Z^2)}{(s - M_Z^2)^2 + M_Z^2 \Gamma_Z^2}, \\
B_3 &= \frac{4(v_e^2 + a_e^2)(v_f^2 + a_f^2) M_Z^2 (s - M_Z^2 - \Gamma_Z^2) - 8Q_e Q_f v_e v_f M_Z^2 \Gamma_Z^2}{(s - M_Z^2)^2 + M_Z^2 \Gamma_Z^2}, \\
B_4 &= B_2 - B_1.
\end{aligned}$$

The value for the lower bound on the invariant mass squared of the final state fermion pair as dictated by the phase space is $4m_f^2$. But in the given procedure this value can be set arbitrarily, with $4m_f^2$ as the minimum possible value. The upper boundary s'_{max} is determined by how 'soft' hard photons can become and by the number of hard photons. To be precise, for one hard photon one has

$$s'_{max} = s \left(1 - \frac{k_0}{p_+^0}\right), \quad (6.C.3)$$

whereas for two hard photons

$$s'_{max} = s \left(1 - \frac{k_0}{p_+^0}\right)^2. \quad (6.C.4)$$

References

- [1] See, for instance, M. Böhm, W. Hollik and H. Spiesberger, *Z.f.Phys.* **C27** (1985) 523; *Fortschr.Phys.* **34** (1986) 687;
M. Consoli, W. Hollik, and F. Jegerlehner, in "Z physics at LEP 1", CERN Yellow report 89-08, Vol.1 (G. Altarelli, R. Kleiss and C. Verzegnassi, eds.).
- [2] F.A. Berends, G.J.H. Burgers and W.L. van Neerven, *Nucl. Phys.* **B297** (1988) 429.

- [3] D. Bardin, L. Vertogradov, Yu. Sedykh and T. Riemann, CERN preprint TH.5434/89.
- [4] A. Borelli, M. Consoli, L. Maiani and R. Sisto, Nucl. Phys. B333 (1990) 357.
- [5] D.R. Yennie, S.C. Frautschi and H. Suura, Ann. Phys. 13 (1961) 379.
- [6] F.A. Berends et al., in 'Z physics at LEP 1', CERN Yellow report 89-08, Vol.1 (G. Altarelli, R. Kleiss and C. Verzegnassi, eds.).
- [7] S. Jadach and B.F.L. Ward, Phys. Rev. D38 (1988) 2897 (E:D39 (1989) 1471); Contr. to Proceedings of the Workshop on "electroweak Radiative Corrections", Ringberg Castle (FRG), 1989, ed. J. H. Kühn; Contr. to Proceedings of the NATO Conference on Radiative Corrections, Brighton, 1989, to be published.
- [8] The CALKUL collaboration, Nucl. Phys. B264 (1986) 243; B264 (1986) 265.
- [9] The CALKUL collaboration, Nucl. Phys. B239 (1984) 382.
- [10] R. Kleiss, Nucl. Phys. B241 (1984) 61;
R. Kleiss and W.J. Stirling, Nucl. Phys. B262 (1985) 235.
- [11] J.-E. Campagne and R. Zitoun, Phys. Lett. B222 (1989) 497;
Z. Phys. C43 (1989) 469;
J.-E. Campagne, Ph.D. thesis, Paris, LPNHEP 89.02.
- [12] E.A. Kuraev and V.S. Fadin, Yad. Fiz. 41 (1985) 753 (Sov. J. Nucl. Phys. 1 (1985) 466);
G. Altarelli and G. Martinelli, in 'Physics at LEP', J. Ellis and R. Peccei, eds., CERN Yellow Report 86-02;
V. Baier, V.S. Fadin and V.A. Khoze, Nucl. Phys. B65 (1973) 381;
L. Lipatov, Yad. Fiz. 20 (1974) 181 (Sov. J. Nucl. Phys. 20 (1975) 94);
O. Nicosini and L. Trentadue, Phys. Lett. B196 (1987) 551.
- [13] The CALKUL collaboration, Phys. Lett. 103B (1981) 124; Nucl. Phys. B206 (1982) 61.
- [14] F.A. Berends and W. Giele, Nucl. Phys. B294 (1987) 700.
- [15] S.J. Parke and T.R. Taylor, Phys. Rev. D35 (1987) 313.
- [16] F.A. Berends and W. Giele, Nucl. Phys. B306 (1988) 759;
F.A. Berends, W. Giele and H. Kuijf, Phys. Lett. B232 (1989) 266.
- [17] W.J.P. Beenakker and W. Hollik, ECFA workshop on LEP 200, CERN 87-08 p. 185, W. Hollik, Fortschr. Physik. 38 (1990) 165.

- [18] A.A. Akhundov, D.Y. Bardin and T. Riemann, Nucl. Phys. B276 (1986) 1.
- [19] D.R. Yennie, S.C. Frautschi and H. Suura, Ann. Phys. 13 (1961) 379.
- [20] R. Kleiss, CERN preprint TH.5439/89.
- [21] T. Kinoshita, J. Math. Phys. 3 (1962) 650.
T.D. Lee and M. Nauenberg, Phys. Rev. B133 (1964) 1549.
- [22] R. Kleiss, Z. Phys. C33 (1987) 433.
- [23] R. Kleiss, Phys. Lett. B180 (1986) 400.

Chapter 7

Event generator techniques

7.1 Introduction

In this chapter a number of Monte Carlo techniques is discussed. The methods all are designed to generate explicitly the momenta of a fermion pair and of a number of photons. One important restriction is imposed: only initial state radiation is considered for s-channel processes of the type

$$e^+e^- \longrightarrow \bar{f}f, \quad f \neq e^-, \nu_e. \quad (7.1.1)$$

The reasons to review the techniques that are used in the literature to write Monte Carlo programs for these processes are the following. First of all the techniques are quite different; having seen one of them is not having seen them all. Moreover the presentations of the techniques are done in very different manners and notations. This has resulted in a situation where most people have a good understanding of at most one of the methods. The immediate implication is that there has been a lot of confusion over the question where the results of the various techniques should compare well and where they are expected to deviate from each other. Another consequence is that there is no place in the literature, so far, where the advantages and drawbacks of each method have been discussed in an unbiased way. The aim of this chapter is twofold. We want to give explicit descriptions of a number of methods, including detailed algorithms for the generation of events. Secondly, having described the methods in all their technical detail, we are in a position to list the positive and the negative features of each of them.

Implicit in the discussion of this chapter is the hope that in acquiring a better understanding of the Monte Carlo methods used for the s-channel processes (7.1.1), one might develop better ideas for techniques that could be applied to other processes, most importantly to Bhabha scattering. At this moment the level of accuracy of the Monte Carlo programs that exist for Bhabha scattering is not thought to be sufficient [1]. Improving on these programs has however turned out to be very difficult. Reviewing the techniques that are applied to the s-channel may serve as a first step towards the construction of better techniques for Bhabha scattering.

In subsequent sections three methods are discussed. First the case where the QED corrections are taken into account up to a fixed order in α is treated (section 7.2). Next, a technique to sum up all the so-called infra-red divergent QED corrections is described in detail (section 7.3). This technique is due to Jadach and Ward [2] and is based on the work of Yennie, Frautschi and Suura [3]. The third and last method discussed here is based on the structure function approach. The treatment given in section 7.4 is rather closely related to the one by Bonvicini and Trentadue [4]. Finally in section 7.5 the advantages and drawbacks of all these techniques are discussed.

7.2 Fixed order Monte Carlo and the k_0 -problem

The type of Monte Carlo programs, that was first introduced for the purpose of calculating cross sections for (7.1.1), and that has been used most extensively, is the type where the QED corrections are calculated up to a fixed order in α . The calculation in chapter 6 is only one of the many examples of this type. Because chapter 6 gives explicit expressions and algorithms, we will restrict ourselves here to merely discussing a very general feature of this type of Monte Carlo. This feature is usually referred to as "the k_0 -problem" and has been mentioned already in chapter 5. The k_0 -problem has recently been discussed in detail in [5].

Let us consider, without loss of generality, a Monte Carlo program that includes the initial state QED corrections, up to and including first order in α , for the process (7.1.1). As is discussed in chapter 5, the total cross section gets contributions from three different parts: a part corresponding to virtual photons, a part corresponding to real photons, with energy $k_0 \leq k_1$ (soft photons) and a part corresponding to real photons, with energy $k_0 > k_1$ (hard photons). The first two contributions both can be written in a factorized form and hence they can be combined easily into one virtual/soft part, written as a factor times the lowest order cross section $\sigma_0(s)$:

$$\sigma_{VS}(s, k_1) = [1 + \delta_{VS}(k_1)] \sigma_0(s). \quad (7.2.1)$$

Here the term 1 corresponds to the lowest order contribution and δ_{VS} to the virtual/soft corrections to that. In first order the form of δ_{VS} is

$$\delta_{VS}(k_1) = \frac{\alpha}{\pi} \left[2(L-1) \log \frac{k_1}{E} + \frac{3}{2}L + 2\zeta(2) - 2 \right], \quad (7.2.2)$$

where E is the beam energy, $L = \log(s/m_e^2)$ and $s = 4E^2$. Note that lowering k_1 can result in $1 + \delta_{VS}(k_1) < 0$. This observation will prove to be the key issue for the implementation of these corrections in a Monte Carlo program.

The third and last contribution, corresponding to hard photons, in general does not factorize. We will denote this contribution by $\sigma_H(s, k_1)$, which consists of a difficult integral over a three particle phase space. This term also depends on k_1 , because the

photon phase space is integrated only over the part where $k_0 > k_1$, k_0 being the photon energy, k_1 a fixed small energy. Upon lowering k_1 , $\sigma_H(s, k_1)$ will increase, since the photon phase space is enlarged. Further, one should realize that σ_H necessarily has to be positive, for it corresponds to (in principle) detectable $e^+e^- \rightarrow \bar{f}f\gamma$ events.

There is a clear connection with the discussion in chapter 5. The term $\sigma_{VS}(s, k_1)$ corresponds to the first line of eq.(5.1.1), whereas the contribution $\sigma_H(s, k_1)$ corresponds to the third line. We have *assumed* that k_1 is small enough, so that the contribution from the second line in eq.(5.1.1) vanishes. In that case the k_1 dependence of σ_{VS} is cancelled by the k_1 dependence of σ_H , reflecting the fact that k_1 is an arbitrary parameter, as long as it is small enough. As stated in chapter 5, all these contributions can be calculated exactly, albeit sometimes at the expense of considerable amounts of CPU time. However, making a Monte Carlo on the basis of the two contributions σ_{VS} and σ_H may pose an extra problem.

Suppose one wants to generate events according to the combined distribution for virtual/soft/no photons on the one hand and hard photons on the other hand. The first thing one has to do is to decide whether the next event will have a hard photon or not. This is done in a probabilistic way, with the chance

$$P(k_1) = \frac{\sigma_H(s, k_1)}{\sigma_H(s, k_1) + \sigma_{VS}(s, k_1)} \quad (7.2.3)$$

that the next event will have a hard photon. The fact that the ratio P is interpreted as a probability and hence has to lie within $[0, 1]$, yields an extra restriction: $\sigma_{VS}(s, k_1) \geq 0$, or, equivalently, $1 + \delta_{VS}(k_1) \geq 0$. This means, using eq.(7.2.2), that k_1 is bounded from below. In the particular case of initial state radiation only, this restriction is not very severe, namely $k_1 \gtrsim 10^{-4}E$. If one includes final state radiation and the interference between initial state and final state radiation, the restriction becomes more severe, $k_1 \gtrsim 10^{-2}E$. The k_0 -problem now is the fact that for these latter k_1 -values, the second line of eq.(5.1.1) may give a non-negligible contribution. But since this term itself is the difference of two cross sections, it will in general have parts in phase space where it is negative, and hence it cannot be treated in a probabilistic way either. In other words, the k_0 -problem is caused by the fact that one does not know of a way to split the total cross section into parts that all are non-negative everywhere in phase space.

There is one obvious and simple solution to this problem: avoid having to decide in a probabilistic way whether the next event will have a hard photon or not. The price one has to pay when doing so, is that one ends up with two sets of events, one corresponding to the cross section σ_{VS} and one corresponding to the cross section σ_H , instead of having one set of events, corresponding to the total cross section. This means that the events will always have a weight $\neq 1$. In fact, the sign of the weight of events corresponding to σ_{VS} can become negative and hence opposite to the sign of the weight of events corresponding to σ_H . It is the difference in sign that is the inhibition for applying a weight rejection procedure in order to give all events unity weight. However it should be stressed that there is nothing wrong in working with two sets of events, having different weights, even

when those weights have opposite sign.

In practice, though, working with several sets of events is not preferable, nor is it an aesthetically satisfying solution to work with. Therefore people have tried to find other solutions, all of which use the notion of exponentiation of a part of the QED corrections. Section 7.3 and 7.4 describe two such efforts.

7.3 YFS exponentiation

7.3.1 Introduction

In this section it is discussed how one can exponentiate soft photon corrections from the initial state in a Monte Carlo program. It should be stressed that there may be many ways to do this, but that the method described here, which is due to Jadach and Ward [2], is particularly fit for Z physics at LEP1. The method incorporates the QED corrections in two different phases. Firstly the infra-red (IR) divergent corrections are taken into account to all orders in α by exponentiation along the lines of the work of Yennie, Frautschi and Suura [3]. The hard multi-photon distribution one then has to generate is a difficult one and will be treated in subsection 7.3.3. Secondly the higher order IR finite corrections are included by introducing Monte Carlo weights. This is done order by order, up to $\mathcal{O}(\alpha^2)$ corrections. The definition of these weights involves some technicalities, which are discussed in subsection 7.3.4. First however it is explained in more detail what the aim of the method is, i.e. what distribution one wants to have in the end.

7.3.2 The distribution that has to be generated

In this subsection we will present the multi-photon distribution that has to be generated. Using a number of approximations the phase space integral over this distribution will be calculated. This integral is needed in the following subsections and also gives some insight in the correspondence with semi-analytical methods like those discussed in chapter 2.

Consider the process

$$e^+(p_+) + e^-(p_-) \rightarrow \bar{f}(q_+) + f(q_-) + \gamma(k_1) + \dots + \gamma(k_n), \quad (7.3.1)$$

summed over the photon multiplicity n . The differential cross section for this process is given by

$$\begin{aligned} d\sigma = & \frac{1}{2s} \frac{1}{(2\pi)^2} F_{YFS}(\varepsilon) \sum_{n=0}^{\infty} \frac{1}{n!} d^4q_+ \delta^+(q_+^2 - m_f^2) d^4q_- \delta^+(q_-^2 - m_f^2) \quad (7.3.2) \\ & \times \prod_{i=1}^n \left[d^4k_i \delta^+(k_i^2) S(k_i) \vartheta(k_i^0 - \varepsilon E) \right] \delta^{(4)} \left(p_+ + p_- - q_+ - q_- - \sum_{j=1}^n k_j \right) \\ & \times \left\{ b_0(p_+, p_-, q_+, q_-) + \sum_{l=1}^n b_1(p_+, p_-, q_+, q_-, k_l) + \sum_{l \neq m} b_2(p_+, p_-, q_+, q_-, k_l, k_m) \right\}. \end{aligned}$$

The factor in front is the so-called Yennie-Frautschi-Suura (YFS) factor

$$F_{YFS}(\varepsilon) = \exp \left\{ \beta \log \varepsilon + \frac{\alpha}{\pi} \left[\frac{1}{2} \log \frac{s}{m_e^2} - 1 + 2 \zeta(2) \right] \right\}, \quad (7.3.3)$$

with $\beta = (2\alpha/\pi)(\log(s/m_e^2) - 1)$. In writing down this expression for F_{YFS} it is already assumed that all photons are connected with the initial state fermion current only. That is, we restrict ourselves to initial state corrections. It will become clear that the YFS factor cancels the ε -dependence of the integral over the rest of the distribution (7.3.2).

The function $S(k)$ is the soft photon bremsstrahlung distribution, which for initial state bremsstrahlung reads

$$S(k) = \frac{\alpha}{\pi} \frac{1}{2\pi} \left[\frac{2(p_+ \cdot p_-)}{(p_+ \cdot k)(p_- \cdot k)} - \frac{m_e^2}{(p_+ \cdot k)^2} - \frac{m_e^2}{(p_- \cdot k)^2} \right]. \quad (7.3.4)$$

The functions b_i incorporate the lowest order $e^+e^- \rightarrow \bar{f}f$ scattering (b_0), the IR finite virtual and soft photon corrections to that (b_0) and the IR finite hard photon corrections (b_1, b_2). The definitions of the b_i are given in subsection 7.3.4. In the way eq.(7.3.2) is written down the IR finite corrections are taken into account up to and including $\mathcal{O}(\alpha^2)$. The IR divergent corrections are resummed to all orders, which is apparent for the virtual and soft photon parts because they appear in the exponent in the YFS factor and for the hard photon part because eq.(7.3.2) contains an explicit summation over the photon multiplicity n from 0 to ∞ .

Most of the terms in eq.(7.3.2) are written in a Lorentz invariant way. An exception is $\vartheta(k_i^0 - \varepsilon E)$, where the $p_+ + p_-$ CM frame is chosen. The variable E stands for the beam energy in this frame. In the following we will work in this frame, unless a variable is denoted with a \star , in which case it is evaluated in the $q_+ + q_-$ CM frame.

In the remainder of this subsection the integral over $d\sigma$ is calculated in the case where all higher order IR finite corrections are neglected. That is we take

$$\begin{aligned} b_0(p_+, p_-, q_+, q_-) &= |\mathcal{M}_0|^2, \\ b_1(p_+, p_-, q_+, q_-, k_l) &= 0, \\ b_2(p_+, p_-, q_+, q_-, k_l, k_m) &= 0. \end{aligned} \quad (7.3.5)$$

The idea behind this simplification is that the IR finite corrections can be included in the final result by defining appropriate Monte Carlo weights. This will be the topic of subsection 7.3.4. In eq.(7.3.5) $|\mathcal{M}_0|^2$ is the Born matrix element squared for the process $e^+e^- \rightarrow \bar{f}f$. The result for the distribution $d\sigma$ after the simplifications (7.3.5) will be called the 0-th order exponentiated distribution.

It is convenient to introduce the momentum $Q^\mu = q_+^\mu + q_-^\mu$. In terms of the momentum Q^μ the integral over $d\sigma$ can be written as

$$\int d\sigma = \frac{1}{2s} \frac{1}{(2\pi)^2} F_{YFS}(\varepsilon) \int \sum_{n=0}^{\infty} \frac{1}{n!} d^4Q \frac{1}{8} \sqrt{1 - \frac{4m_f^2}{s'}} d\Omega_f^* d\sigma_0 \quad (7.3.6)$$

$$\times \delta^{(4)}\left(p_+ + p_- - Q - \sum_{j=1}^n k_j\right) \prod_{i=1}^n \left[d^4 k_i \delta^+(k_i^2) S(k_i) \vartheta(k_i^0 - \varepsilon E) \right] .$$

Ω_f^* stands for the solid angle of say q_+ in the $q_+ + q_-$ CM frame. For the reduced energy Q^2 the notation s' is often used. The Born matrix element squared $|\mathcal{M}_0|^2$ depends only on the variables Ω_f^* and s' . Therefore the integration over Q^μ can be performed, keeping s' fixed for the moment:

$$\int d\sigma = \frac{1}{2s} \frac{1}{(2\pi)^2} F_{YFS}(\varepsilon) \int \sum_{n=0}^{\infty} \frac{1}{n!} \frac{1}{8} \sqrt{1 - \frac{4m_f^2}{s'}} ds' d\Omega_f^* d\sigma_0 \quad (7.3.7)$$

$$\times \delta\left(s' - \left(p_+ + p_- - \sum_{j=1}^n k_j\right)^2\right) \prod_{i=1}^n \left[d^4 k_i \delta^+(k_i^2) S(k_i) \vartheta(k_i^0 - \varepsilon E) \right] .$$

Since $|\mathcal{M}_0|^2$ is the only term depending on Ω_f^* one can also carry out the integration over Ω_f^* . The result depends on the specific Born differential cross section under consideration. We will denote in general

$$\sigma_0(s') = \frac{1}{2s} \frac{1}{(2\pi)^2} \frac{1}{8} \sqrt{1 - \frac{4m_f^2}{s'}} \int d\Omega_f^* |\mathcal{M}_0|^2 . \quad (7.3.8)$$

For the integral of the 0-th order exponentiated distribution one then gets

$$\int d\sigma = F_{YFS}(\varepsilon) \int \sum_{n=0}^{\infty} \frac{1}{n!} \delta\left(s' - \left(p_+ + p_- - \sum_{j=1}^n k_j\right)^2\right) ds' \sigma_0(s')$$

$$\times \prod_{i=1}^n \left[d^4 k_i \delta^+(k_i^2) S(k_i) \vartheta(k_i^0 - \varepsilon E) \right] . \quad (7.3.9)$$

At this point we want to integrate over the photon momenta. The restriction on these momenta due to the δ -function involving s' is however a considerable problem. Therefore a crude approximation will be made. Again the underlying idea is that for the final result the exact answer can be obtained by introducing appropriate Monte Carlo weights. This will be the topic of the next subsection. The integral we will calculate here is

$$\int d\sigma = F_{YFS}(\varepsilon) \int ds' \sigma_0(s') \left\{ \delta(s - s') \right. \quad (7.3.10)$$

$$\left. + \sum_{n=1}^{\infty} \frac{n}{n!} \delta\left(s' - (p_+ + p_- - k_1)^2\right) \prod_{i=1}^n \left[\int_{\varepsilon E}^{k_{max} E} d k_i^0 \frac{1}{2} k_i^0 \int_{4\pi} d\Omega_{k_i} S(k_i) \right] \right\} .$$

The approximations that have been made are that all photon energies can be integrated over independently up to the energy $k_{max} E$ and that the energy loss $s \rightarrow s'$ is due to

photon 1 only. Because of the latter the energy of photon 1 is fixed by the δ -function for s' . Hence we have to assume that $(1 - s'/s) \in [\varepsilon, k_{max}]$. For the case $n = 0$ this is of course somewhat different, so that will have to treat $n = 0$ separately for a short while. Note furthermore that because one photon is given a special rôle, one has to compensate for the decrease of the number of permutations by multiplying by a factor n (for $n > 0$).

The approximations now lead to an integral that is easy to calculate and that will be the basis for an event generating algorithm (next subsection). The integral of the soft photon distribution $S(k)$ over the solid angle is

$$\int_{4\pi} d\Omega_k S(k) = \frac{2\alpha}{\pi} \left(\log \frac{s}{m_e^2} - 1 \right) \frac{1}{k^0} = \frac{\beta}{k^0}. \quad (7.3.11)$$

Using this and integrating over the photon energies one gets

$$\int d\sigma = F_{YFS}(\varepsilon) \int ds' \sigma_0(s') \left[\delta(s - s') + \frac{\vartheta(1 - s'/s - \varepsilon)}{(s - s')} \sum_{n=1}^{\infty} \frac{\beta^n}{(n-1)!} \log^{(n-1)} \frac{k_{max}}{\varepsilon} \right]. \quad (7.3.12)$$

The $n = 0$ term and the sum over the other terms can be merged into one term, yielding

$$\int d\sigma = F_{YFS}(\varepsilon) \int ds' \sigma_0(s') \frac{\beta^j}{s - s'} \exp \left(\beta \log \frac{k_{max}}{\varepsilon} \right). \quad (7.3.13)$$

From this expression it is clear that the ε -dependence is cancelled after integration over the photon momenta. What remains is a complicated s' -integral, which we will not calculate here.

The correspondence with semi-analytical approaches can be made more explicit by choosing a specific value for k_{max} . A possible choice is $k_{max} = (1 - s'/s)E$. It is easy to check that for given s' the value $(1 - s'/s)E$ is the maximum energy any photon can have. Therefore all of phase space is covered when using this choice. On the other hand the approximation that all photon energies can be integrated over independently is not a particularly good one for such values of k_{max} , but the Monte Carlo weights will correct this.

For this particular k_{max} value the integral over the 0-th order exponentiated distribution becomes

$$\int d\sigma = F_{YFS}(\varepsilon) \varepsilon^{-\beta} \int \frac{ds'}{s} \beta \left(1 - \frac{s'}{s} \right)^{-1 + \beta} \sigma_0(s'). \quad (7.3.14)$$

This can be compared to eq.(2.3.6) using the flux function (2.3.12). The differences that occur are higher order IR finite QED corrections.

In this subsection we have calculated the integral over the distribution (7.3.2). Two approximations have been made: eq.(7.3.5) and the approximation leading to eq.(7.3.10). In subsection 7.3.3 a method is discussed to generate the approximated distribution and at the same time define Monte Carlo weights to correct for the latter approximation. In subsection 7.3.4 Monte Carlo weights to correct for the former approximation are introduced.

7.3.3 Generating the 0-th order exponentiated distribution

An elegant method is discussed to generate the distribution (7.3.6). The method was introduced and implemented in a Monte Carlo program in [2]. Define the following notations:

$$P = p_+ + p_- , \quad K = \sum_{n=1}^n k_i , \quad \hat{K} = \sum_{n=1}^n \hat{k}_i , \quad v = 1 - s'/s . \quad (7.3.15)$$

A basic quantity for the method we want to describe is

$$\begin{aligned} I_n(s') = & \prod_{i=1}^n \left[d^4 \hat{k}_i \delta^+(\hat{k}_i^2) \vartheta(\hat{k}_i^0 - \varepsilon E) S(\hat{k}_i) \right] \delta(s' - (p_+ + p_- - k_1)^2) \\ & \times \prod_{j=1}^n d^4 k_j \delta^{(4)}(k_j - \lambda \hat{k}_j) \\ & \times d\lambda \delta(\lambda - f(P, \hat{K}, v)) w , \end{aligned} \quad (7.3.16)$$

where

$$f(P, \hat{K}, v) = \frac{P^2}{(P \cdot \hat{K})^2} \frac{v}{1 + \sqrt{1 - v P^2 \hat{K}^2 / (P \cdot \hat{K})^2}} \quad (7.3.17)$$

and

$$w = 2v P^2 \frac{\prod_{i=1}^n \vartheta(k_i^0 - \varepsilon)}{(P \cdot K) - K^2} . \quad (7.3.18)$$

The maximum value for w , for constant v , can be determined to be

$$w_{max} = \frac{1}{2} \left(1 + \frac{1}{\sqrt{1-v}} \right) . \quad (7.3.19)$$

Before evaluating $I_n(s')$, let us discuss eq.(7.3.16). The method first generates a value for s' and pretends there is only one photon responsible for the energy loss $(1 - s'/s)E$ (the δ -function on the first line). If $(1 - s'/s) \leq \varepsilon$ no photons are generated, but here only the case $(1 - s'/s) > \varepsilon$ is considered. As a second step it generates a number n to determine how many photons are to be generated on top of the first one. These extra photons are generated according to $S(k)$, as is the angular distribution of the first one (the rest of the first line). The third step is to scale all photons, so that afterwards the energy loss, now due to all photons, is $(1 - s'/s)E$ once again. The scaling is described by the second line, the scale factor is determined in the third line of eq.(7.3.16). The whole procedure is made exact by defining the weight w . Having generated all photons, the problem is brought down to the level of generating a fermion pair at energy s' . Since this can be done without much problems this is not discussed here.

The quantity $I_n(s')$ can be evaluated in a few steps. Firstly note that the combination

$$d^4 k_i \delta^+(k_i^2) S(k_i) \quad (7.3.20)$$

is invariant under $k_i \rightarrow a k_i$. Using this the integration over \hat{k}_i can be carried out. Next one can solve two of the δ -functions for v and λ using

$$\delta\left(\lambda - f(P, \hat{K}, v)\right) \delta\left(\frac{1}{\lambda} k_1^0 - vE\right) = \quad (7.3.21)$$

$$\frac{1}{E} \left| \frac{(P \cdot K) - K^2}{(P \cdot K) - \frac{1}{2} K^2} \right| \delta\left(\lambda - \frac{k_1^0}{vE}\right) \delta\left(v - \frac{2(P \cdot K) - K^2}{P^2}\right).$$

Using the definition of w and the specific form of v following from the δ -function, one gets

$$I_n(s') = \prod_{i=1}^n \left[d^4 k_i \delta(k_i^2) \vartheta(k_i^0 - \varepsilon E) \vartheta\left(\frac{1}{\lambda} k_i^0 - \varepsilon E\right) S(k_i) \right] \delta\left(s' - (P - K)^2\right). \quad (7.3.22)$$

Notice that there are two ϑ -functions for the lower bound on k_i^0 . Due to the specifics of the procedure one has $\lambda \leq 1$, i.e. the photons are always scaled *down* in energy. This is ensured by first pretending that one photon is responsible for the energy loss vE and then generating the rest of the photons. Because the rest of the photons will be responsible for some extra loss of energy, all photons will have to be scaled down, in order to stay at the pre-determined energy loss vE . Therefore the factor $\vartheta(k_i^0/\lambda - \varepsilon E)$ can be left out, as the other bound on k_i^0 is always more strict.

With the second ϑ -function left out $I_n(s')$ has exactly the desired form. It is precisely a part of the distribution (7.3.9). In the previous subsection this distribution could not be integrated over and therefore approximations were introduced. In fact the integration was done over the distribution where $I_n(s')$ was replaced by the first line of eq.(7.3.16) only. Now we are able to give an algorithm to generate this distribution and correct for the approximation. First the algorithm is given, then a number of points is discussed.

1. Generate s' in the interval $[s'_{min}, s]$ according to

$$\frac{d\sigma}{ds'} = \beta \left(1 - \frac{s'}{s}\right)^{-1 + \beta} \frac{1}{2} \left(1 + \sqrt{\frac{s}{s'}}\right) \sigma_0(s'). \quad (7.3.23)$$

2. If $(1 - s'/s) \leq \varepsilon$ then

Generate a fermion pair in the $p_+ + p_-$ CM frame with a total energy squared s .
Else

- 2.1. Set the energy of photon 1 equal to $k_1^0 = (1 - s'/s)E$.

- 2.2. Generate the photon multiplicity n between 1 and ∞ according to the distribution

$$P_n(n-1) = e^{-\bar{n}} \frac{\bar{n}^{(n-1)}}{(n-1)!}, \quad \bar{n} = \beta \log \frac{1 - s'/s}{\varepsilon}. \quad (7.3.24)$$

This is a Poisson distribution for $(n-1)$ with average \bar{n} .

- 2.3. Generate the energies of photons $2, \dots, n$ in $[\varepsilon E, (1 - s'/s)E]$ according to $1/k_i^0$.
 - 2.4. Generate the solid angle of all photons according to $S(k)$, i.e.
 - 2.4.1. Generate $c_i = \cos \vartheta_{k_i}$ as $1/(p + c_i) + 1/(p - c_i)$ in the interval $[-1, 1]$. Here ϑ_{k_i} is the polar angle of photon i with respect to the beam axis and $p = 1/\sqrt{1 - 4m_e^2/s}$.
 - 2.4.2. Apply weight rejection with the weight $1 - \frac{m_e^2}{2(p_+ \cdot p_-)} \left(\frac{p + c_i}{p - c_i} + \frac{p - c_i}{p + c_i} \right)$.
 - 2.4.3. Generate the azimuthal angle φ_{k_i} of photon i uniform in $[0, 2\pi]$.
 - 2.5. Calculate $\lambda = f(P, \sum_{i=1}^n k_i, v)$ using eq.(7.3.17).
 - 2.6. Scale all photons: $k_i^\mu \leftarrow \lambda k_i^\mu$.
 - 2.7. Generate a fermion pair in its rest frame with a total energy squared s' .
 - 2.8. Boost the fermion pair to the $p_+ + p_-$ CM frame using the vector $P^\mu - \sum_{i=1}^n k_i^\mu$.
3. Apply weight rejection with the weight $\frac{w}{w_{max}}$

A number of remarks should be made concerning this algorithm.

- The distribution (7.3.23) basically is the same as eq.(7.3.14), but there is one difference. The distribution (7.3.23) is multiplied by w_{max} , which is necessary because of the weight rejection 3.
- For the s' -distribution ε -regularization is not needed any more, due to the exponentiation. The variable ε now only plays the rôle of the parameter that determines the average hard photon multiplicity, as is described by eq.(7.3.24). Therefore the value of ε can formally be taken in the limit $\varepsilon \rightarrow 0$, thereby letting the average photon multiplicity go to infinity. However for practical purposes a finite photon multiplicity is needed and hence a finite value for ε is still required.
- The s' distribution (7.3.23) is a complicated one to generate. Probably the best way to do it is to use a general purpose routine.
- The weight rejection procedure 3 has a very low efficiency if $1 - v = s'/s \ll 1$, as can be seen from the form of w_{max} , eq.(7.3.19). Hence, if the lower bound on s' is very small, the efficiency of the whole procedure described here is rather low.
- The weight occurring in step 2.4.2 vanishes for $c_i = \pm 1$. Therefore the probability to generate a photon close to the beam is zero. However, including the full hard bremsstrahlung matrix element squared there is a non-zero probability for a photon along the beam axis. This implies that for an event with a photon close to the

beam the final weight w_{IR} (see eq.(7.3.32)) will become arbitrarily high. To avoid such arbitrarily high weights, it is best to leave out the weight rejection procedure 2.4.2. This has an effect on most of the rest of the algorithm, in particular on the value to be used for β , due to the effect on eq.(7.3.11) when omitting the mass terms in $S(k)$. For the precise effects of this we refer to [2]. It should be noted that in this case the cancellation of the ε -dependence is achieved only after inclusion of the weight w_{IR} .

7.3.4 The IR finite QED corrections

Let \mathcal{M}_i denote the Born amplitude for the process $e^+e^- \rightarrow \bar{f}f + i\gamma$, i.e. fermion pair production plus i photons. The expressions for these amplitudes are well known and will therefore not be given here. The b_i appearing in eq.(7.3.2) are defined in terms of these amplitudes as

$$b_0^{(2)}(p_+, p_-, q_+, q_-) = (1 + \delta_0^{(1)} + \delta_0^{(2)}) |\mathcal{M}_0|^2(p_+, p_-, q_+, q_-), \quad (7.3.25)$$

$$b_1^{(1)}(p_+, p_-, q_+, q_-, k_l) = (1 + \delta_1^{(1)}) |\mathcal{M}_1|^2(p_+, p_-, q_+, q_-, k_l) - S(p_+, p_-, k_l) b_0^{(1)}(\mathcal{R}p_+, \mathcal{R}p_-, \mathcal{R}q_+, \mathcal{R}q_-), \quad (7.3.26)$$

$$b_2^{(0)}(p_+, p_-, q_+, q_-, k_l, k_m) = |\mathcal{M}_2|^2(p_+, p_-, q_+, q_-, k_l, k_m) - S(p_+, p_-, k_l) b_1^{(0)}(\mathcal{R}p_+, \mathcal{R}p_-, \mathcal{R}q_+, \mathcal{R}q_-, \mathcal{R}k_m) - S(p_+, p_-, k_m) b_1^{(0)}(\mathcal{R}p_+, \mathcal{R}p_-, \mathcal{R}q_+, \mathcal{R}q_-, \mathcal{R}k_l) - S(p_+, p_-, k_l) S(p_+, p_-, k_m) b_0^{(0)}(\mathcal{R}p_+, \mathcal{R}p_-, \mathcal{R}q_+, \mathcal{R}q_-). \quad (7.3.27)$$

The indices $^{(i)}$ determine to which order the IR finite virtual and soft photon corrections are incorporated, so that $b_0^{(1)}$ is obtained from $b_0^{(2)}$ by omitting $\delta_0^{(2)}$, and likewise for $b_0^{(0)}$ and $b_1^{(0)}$. The function S is the soft photon bremsstrahlung distribution (7.3.4), where now all relevant momenta are explicitly listed as arguments. The $\delta^{(i)}$ are given by

$$\begin{aligned} \delta_0^{(1)} &= \frac{\alpha}{\pi} (L_e - 1), \\ \delta_0^{(2)} &= \frac{1}{2} \left(\frac{\alpha}{\pi} \right)^2 L_e^2, \end{aligned} \quad (7.3.28)$$

where $L_e = \log(s/m_e^2)$. Note that $\delta_0^{(2)}$ is taken in the leading logarithm approximation. The $\delta_1^{(1)}$ is more complicated, but can be approximated by $\delta_1^{(1)} = \delta_0^{(1)}$. A better approximation is given in [2].

The main point that has to be discussed is the so-called \mathcal{R} procedure. Let us take as an example the last term in the expression for $b_1^{(1)}$. We have a set of momenta p_+, p_-, q_+, q_-, k_l , obeying energy-momentum conservation: $(p_+ + p_- - q_+ - q_- - k_l)^\mu = 0^\mu$. The last term in (7.3.26) is the soft photon factor S times the b -function with one photon

less. This means that if simply the momenta p_+, p_-, q_+, q_- are taken as arguments for b_0 in this case, the set of momenta going into b_0 would not satisfy energy-momentum conservation. This gives rise to the following remarks.

- The violation of energy-momentum conservation is large if the photon k_i is energetic. There will always be such cases in a Monte Carlo calculation.
- The difficulties arise because of the event by event treatment. The problem can be seen as the lack of an algorithm that describes the influence of neglecting a photon momentum on the rest of the event.
- The violation of energy-momentum conservation need not be a problem; see the discussion of the *robustness* of matrix element calculations in [6].
- In [2] a procedure is proposed to transform the momenta such that they obey energy-momentum conservation. This transformation is called the reduction (\mathcal{R}) procedure.
- There does not seem to be any theoretical necessity to introduce such a procedure; its main value should lie in the fact that problems with matrix element calculations are avoided when using it.
- Since the procedure is not necessitated by theory, there is some freedom in defining it. If different definitions would lead to different answers, the whole method of generating events and defining the weights this way would not be trustworthy.

The \mathcal{R} procedure differs for each different set of momenta that it has to be applied to. In particular the procedure for the set of momenta p_+, p_-, q_+, q_-, k_l differs from the one for the set $p_+, p_-, q_+, q_-, k_l, k_m$. In general the following conditions are imposed on the \mathcal{R} procedure (the index i runs over those photons that are included in the set of momenta that the procedure has to be applied to):

$$\begin{aligned}
 (\mathcal{R}p_+ + \mathcal{R}p_- - \mathcal{R}q_+ - \mathcal{R}q_- - \sum_i \mathcal{R}k_i)^\mu &= 0^\mu & (7.3.29) \\
 \mathcal{R}k_i^\mu &= k_i^\mu \\
 (\mathcal{R}q_+ + \mathcal{R}q_-)^2 &= (q_+ + q_-)^2
 \end{aligned}$$

The first condition is of course the prime objective of introducing the procedure. The second condition ensures the cancellation of IR divergences. The third condition is imposed because the matrix elements depend strongly on s' , due to the presence of the Z resonance. Demanding that s' does not change under \mathcal{R} improves the soft photon approximation.

Furthermore it is reasonable to require that the sum of the reduced final state momenta are at rest in the LAB frame and that the reduced beam momenta are still along the z-axis

$$\begin{aligned}
 \mathcal{R}\vec{p}_+ + \mathcal{R}\vec{p}_- &= \mathcal{R}\vec{q}_+ + \mathcal{R}\vec{q}_- + \sum_i \mathcal{R}\vec{k}_i = \vec{0}, & (7.3.30) \\
 \mathcal{R}p_{+,x} &= \mathcal{R}p_{+,y} = \mathcal{R}p_{-,x} = \mathcal{R}p_{-,y} = 0.
 \end{aligned}$$

From this it follows that

$$\begin{aligned}\mathcal{R}p_+^0 &= \frac{1}{2}\sum_i k_i^0 + \frac{1}{2}\sqrt{s' + (\sum_i k_i^0)^2 - (\sum_i k_i)^2}, \\ \mathcal{R}(q_+ + q_-)^0 &= \sqrt{s' + (\sum_i \vec{k}_i)^2}.\end{aligned}\tag{7.3.31}$$

Although the momenta $\mathcal{R}p_+$, $\mathcal{R}p_-$, $\mathcal{R}k_i$ and $\mathcal{R}(q_+ + q_-)$ are fixed now, there is still freedom to choose the directions of $\mathcal{R}q_+$ and $\mathcal{R}q_-$. A natural choice is to maintain the angular distribution the fermion pair has in its CM frame. The momenta $\mathcal{R}q_\pm$ can then be obtained by boosting q_\pm^* (the result of step 2.7 of the algorithm in the previous subsection) with the boost vector $\mathcal{R}p_+ + \mathcal{R}p_- - \sum_i k_i$. Note that i still only runs over those photons that are included in the set of momenta that the procedure has to be applied to.

In words the \mathcal{R} procedure can be described as follows. The photons are not changed. The energy of the incoming momenta (the beam energy) is reduced to match the total energy of the final state where a number of photons have been neglected. The momenta of the fermion pair are determined analogously to step 2.8 of the previous subsection, where in the expression for the boost vector only the remaining photons are taken into account.

Having defined the b_i and the reduction procedure, the Monte Carlo weight to include up to second order IR finite photonic corrections can be written as

$$\begin{aligned}w_{IR} &= \frac{1}{B} \left\{ b_0^{(2)}(\mathcal{R}p_+, \mathcal{R}p_-, \mathcal{R}q_+, \mathcal{R}q_-) \right. \\ &\quad + \sum_{l=1}^n \frac{b_1^{(1)}(\mathcal{R}p_+, \mathcal{R}p_-, \mathcal{R}q_+, \mathcal{R}q_-, \mathcal{R}k_l)}{S(p_+, p_-, k_l)} \\ &\quad \left. + \sum_{l \neq m} \frac{b_2^{(0)}(\mathcal{R}p_+, \mathcal{R}p_-, \mathcal{R}q_+, \mathcal{R}q_-, \mathcal{R}k_l, \mathcal{R}k_m)}{S(p_+, p_-, k_l)S(p_+, p_-, k_m)} \right\}.\end{aligned}\tag{7.3.32}$$

The term B in the denominator corresponds to the distribution that was generated. If e.g. the fermion pair was generated in its CM frame according to the exact Born $e^+e^- \rightarrow \bar{f}f$ amplitude squared $|\mathcal{M}_0|^2$, then $B = b_0^{(0)}(\mathcal{R}p_+, \mathcal{R}p_-, \mathcal{R}q_+, \mathcal{R}q_-)$. If however one generates an approximation of $|\mathcal{M}_0|^2$ one has to redefine $\sigma_0(s')$, see eq.(7.3.8), and also B .

7.4 The structure function based approach

In this section a method is presented to generate events for the process $e^+e^- \rightarrow \bar{f}f + n\gamma$, based on the structure function approach. In [4] such a method is presented and implemented in a Monte Carlo program. The algorithm outlined in this section does not follow [4] in all details, but the general structure is the same. The notation is not taken

over from [4], but rather sticks as closely as possible to the notations used elsewhere in this thesis.

The starting point is the mass factorization formula for the total cross section, the equivalent of eq.(3.2.13):

$$\sigma(s) = \int dx_1 \int dx_2 \Gamma(x_1)\Gamma(x_2) \hat{\sigma}(x_1 x_2 s). \quad (7.4.1)$$

Only the leading log diagonal splitting functions are considered here, which corresponds to only taking photon radiation in the collinear limit into account. The splitting function $\Gamma(x)$ can then be written as

$$\Gamma(x) = \delta(1-x) + \left(\frac{\alpha L}{2\pi}\right) P_{ee}(x) + \frac{1}{2} \left(\frac{\alpha L}{2\pi}\right)^2 (P_{ee} \otimes P_{ee})(x) + \dots, \quad (7.4.2)$$

where

$$L = \log \frac{Q^2}{m_e^2}. \quad (7.4.3)$$

Because it is applied to s-channel processes, for which explicit calculations have been performed up to and including $\mathcal{O}(\alpha^2)$, we will choose $Q^2 = s$. The Altarelli-Parisi splitting function P_{ee} is given by (see also chapter 3)

$$P_{ee}(x) = \delta(1-x) \left[\frac{3}{2} + 2 \log \varepsilon \right] + \vartheta(1-x-\varepsilon) \frac{1+x^2}{1-x} \quad (7.4.4)$$

and determines the fraction $1-x$ of the energy that is carried away by a photon. In [4] this is generalized to describe also the transverse energy distribution of the photon, and hence of the fermion. Here we will formulate the generalization in terms of the emission angles $\Omega = (\vartheta, \varphi)$ of the photon, rather than in terms of p_T . The generalization reads

$$L P_{ee}(x) = \int_{4\pi} d\Omega \mathcal{P}(x, \Omega), \quad (7.4.5)$$

where

$$\mathcal{P}(x, \Omega) = P_{ee}(x) \frac{1}{2\pi} \frac{1}{1 - \sqrt{1 - 4m_e^2/Q^2} \cos \vartheta}. \quad (7.4.6)$$

This generalization is only valid if $m_e^2 \ll Q^2$. It is clear that in writing $\mathcal{P}(x, \Omega)$ the dependence on m_e^2 and Q^2 is suppressed. However from eqs.(7.4.1) and (7.4.2) one sees that for the distribution of $\cos \vartheta$ one has to take the value of Q^2 that one wants to have in the expression for the total cross section. Since the explicit calculation of [7] shows that for the total cross section the choice $Q^2 = s$ is appropriate up to and including $\mathcal{O}(\alpha^2)$, we have to fix Q^2 in our algorithm, even if eq.(7.4.6) is used iteratively. Further, the fact that m_e^2 in eq.(7.4.6) is taken to be the physical mass squared of the radiating fermion, and *not* p^2 of that fermion, being either on-shell or off-shell, is imperative, for otherwise the resulting logarithms would not even contain the correct mass.

With the ingredients described so far one can construct an algorithm to generate events. Firstly note that eq.(7.4.2) implies that the number of hard photons radiated off one particular fermion is distributed as a Poisson distribution with the average

$$\bar{n} = \frac{\alpha L}{2\pi} \left(-2 \log \varepsilon - \frac{3}{2} \right). \quad (7.4.7)$$

A photon is called hard in this context if it carries more than a fraction ε of the energy of the radiating fermion. One can use this to start the algorithm by generating n_+ and n_- , being the number of photons radiated off the incoming e^+ and e^- respectively. For each photon one then generates the fraction x and the angles ϑ and φ according to $\mathcal{P}(x, \Omega)$ in eq.(7.4.6). For n_{\pm} photons one takes the angles with respect to e^{\pm} . One has to bear in mind, though, that after emission of each photon, the fermion momentum changes. After emission of all photons the incoming e^{\pm} have momenta \hat{p}_{\pm} . The final step is then to generate a pair of fermion momenta in their CM frame, having an invariant mass squared of $(\hat{p}_+ + \hat{p}_-)^2$, and to boost them to the LAB frame. The distribution of fermion momenta is given by the Born matrix element squared.

More specifically the algorithm is as follows:

1. Generate n_+ and n_- according to a Poisson distribution

$$P_{\bar{n}}(n) = e^{-\bar{n}} \frac{\bar{n}^n}{n!}, \quad \bar{n} = \frac{\alpha L}{2\pi} \left(-2 \log \varepsilon - \frac{3}{2} \right). \quad (7.4.8)$$

2. Define $\hat{p}_{\pm}^{\mu} = p_{\pm}^{\mu}$.

3. Do for i from 1 to n_+

- 3.1. Define ϑ_+ , φ_+ as the polar and azimuthal angle of $\vec{\hat{p}}_+$ with respect to \vec{p}_+ .

- 3.2. Generate x_i , ϑ_i , φ_i according to $\mathcal{P}(x_i, \Omega_i)$.

- 3.3. The momenta of photon i and of the fermion after the emission of that photon are given by

$$\begin{aligned} k_i^{\mu} &= (1 - x_i) \hat{p}_+^0 (1, \sin \vartheta_i \cos \varphi_i, \sin \vartheta_i \sin \varphi_i, \cos \vartheta_i) \\ \hat{p}_+^{\mu} &\leftarrow \hat{p}_+^0 \left(x_i, -(1 - x_i) \sin \vartheta_i \cos \varphi_i, -(1 - x_i) \sin \vartheta_i \sin \varphi_i, \right. \\ &\quad \left. \sqrt{1 - \hat{p}_+^2 / (\hat{p}_+^0)^2} - (1 - x_i) \cos \vartheta_i \right) \end{aligned}$$

- 3.4. Rotate \vec{k} and $\vec{\hat{p}}_+$ by $-\varphi_+$ around \vec{p}_+ and then by $-\vartheta_+$ around the $\varphi_+ = \frac{\pi}{2}$ -axis.

4. Repeat the previous step with all indices "+" replaced by "-".

5. Set $s' = (\hat{p}_+ + \hat{p}_-)^2$ and generate a fermion pair in their CM frame according to $d\hat{\sigma}/d\Omega_f(s', \Omega_f)$. Then boost the fermion momenta to the LAB frame.

There is a number of points concerning this algorithm that are worth mentioning here:

- Since n_+ and n_- both are Poisson distributed variables, with averages \bar{n}_+ and \bar{n}_- respectively, the total photon multiplicity $n = n_+ + n_-$ is also Poisson distributed, with average $\bar{n}_+ + \bar{n}_-$. One can compare this with eq.(7.3.24). Note however that there $n - 1$ is Poisson distributed. The differences at this level are not meaningful; only after inclusion of all Monte Carlo weights the two methods can be compared.
- The variable ε can be set arbitrarily low, as long as it is non-zero. As in the method of section 7.3, the variable ε determines the average multiplicity of 'hard photons'. An important difference, though, is hidden in the definition of 'hard photon', see below eq.(7.4.7).
- The total cross section is calculated by averaging the values of $w = d\hat{\sigma}/d\Omega_f$. To get events with unity weight one has to apply the weight rejection procedure with this weight. Since $d\hat{\sigma}/d\Omega_f$ varies steeply with s' , this can become very inefficient.
- This method only yields the leading log (LL) QED corrections. Including the non-log terms, or even only a part of them, is quite tricky. E.g. replacing $L \rightarrow L - 1$ in eqs.(7.4.2) and (7.4.5), without altering the angular distribution (7.4.6) is not correct. However, in principle the first order initial state QED corrections can be written in a factorized form, evaluating a correction factor and, separately, the lowest order cross section for reduced beam momenta. In higher order this can still be done for the LL and the next-to-leading terms, but not for the non-log terms [8]
- This technique exponentiates the QED corrections per incoming fermion. For the LL terms this seems to amount to the same as exponentiating per fermion current. For the non-LL terms it is not so obvious that this is still true.

7.5 Advantages and drawbacks

For the straightforward method of fixed order Monte Carlo, the situation is transparent. The big advantage is that it is clear what one has to do in order to improve on a given calculation, although it may be tedious to do it. The one important drawback is the k_0 -problem. For the other methods one can make more comments. The advantages of the YFS method are, in a nutshell:

- A1. The k_0 -problem is avoided.
- A2. The exponentiation of soft photon corrections is theoretically well founded.
- A3. There is an elegant solution to make the generation of s' efficient, even in the presence of a resonance.

A4. Inclusion of yet higher order IR finite corrections can be done according to a well defined procedure.

The drawbacks are:

D1. It is not obvious that negative weights cannot occur here. A proof that the weight w_{IR} is positive definite would be very welcome indeed.

D2. The dependence on the \mathcal{R} -procedure has not been studied. It would be of great interest to know that the results are independent of the \mathcal{R} -procedure.

D3. At the moment this method for the initial state corrections can only be combined with a fixed order calculation for the final state corrections. Inclusion of the interference between initial state and final state corrections is not possible at present. Exponentiation of the final state corrections is prohibited at the moment due to the absence of an event generating algorithm. Once such an algorithm is constructed, it will probably be possible to include the interference between initial state and final state corrections.

D4. The efficiency of the method drops dramatically if $s'_{min} \ll s$.

For the structure function based method the advantages are:

A1. The k_0 -problem is avoided.

A2. The method is conceptually simple and easy to implement.

A3. It is easy to adapt the method for final state corrections.

The drawbacks are:

D1. The efficiency of the generation of s' is very low, especially in the presence of a resonance.

D2. Although possible, it is very difficult to include initial state non-log terms in first order, leave alone the higher order non-LL terms.

D3. It is not clear how to include interference effects between initial state and final state corrections.

D4. Due to the entanglement of initial and final state corrections for Bhabha scattering, it may prove impossible to include non-LL terms there.

References

- [1] W. Beenakker, F.A. Berends and S.C. van der Marck, "Small angle Bhabha scattering", to be published in Nucl. Phys. B, see also chapter 5
- [2] S. Jadach and B.F.L. Ward, Phys. Rev. D38 (1988) 2897 (E:D39 (1989) 1471); Contr. to Proceedings of the Workshop on "electroweak Radiative Corrections", Ringberg Castle (FRG), 1989, ed. J. H. Kühn; Contr. to Proceedings of the NATO Conference on Radiative Corrections, Brighton, 1989, to be published; preprint SLAC-PUB-4834.
- [3] D.R. Yennie, S.C. Frautschi and H. Suura, Ann. Phys. 13 (1961) 379.
- [4] G. Bonvicini and L. Trentadue, Nucl. Phys. B323 (1989) 253.
- [5] R. Kleiss et al. in "Z Physics at LEP 1", CERN 89-08, vol. 3, p.1, eds. G. Altarelli, C. Verzegnassi and R. Kleiss.
- [6] R. Kleiss and S.C. van der Marck, Nucl. Phys. B342 (1990) 61, see also chapter 6 of this thesis.
- [7] F.A. Berends, G. Burgers and W.L. van Neerven, Nucl. Phys. B297 (1988) 429; E Nucl. Phys. B304 (1988) 921.
- [8] R. Kleiss, Nucl. Phys. B347 (1990) 67.

Samenvatting

De studie van processen die plaatsvinden bij botsingen van een electron met zijn anti-deeltje, het positron, is reeds lange tijd een van de belangrijkste onderzoeksgebieden van de hoge-energiefysica, ook wel elementaire-deeltjesfysica genoemd. Tot 1989 zijn experimenten aan e^+e^- -botsingen gedaan bij energieën van ongeveer 40 GeV (Petra, Duitsland) tot ongeveer 60 GeV (Tristan, Japan). Deze experimenten werden lange tijd beschreven door quantumelectrodynamica (QED), de theorie van electromagnetische interacties tussen elementaire deeltjes. Gezien de nauwkeurigheid van de experimenten moest niet alleen de laagste-ordeterm in storingstheorie worden meegenomen, maar ook de eerste-ordecorrectie hierop. De storingsparameter is hierbij overigens de koppelingsconstante van QED, de fijnstructuurconstante α .

Bij energieën van rond 60 GeV begon men echter de invloed te merken van de zwakke interactie, aangezien men niet ver meer verwijderd was van de typische energieschaal voor zwakke interacties. Deze typische schaal wordt gegeven door de massa van de deeltjes die de zwakke kracht overbrengen, de zogenaamde W- en Z-bosonen. De massa van deze deeltjes is ruwweg $80 \text{ GeV}/c^2$ voor de W bosonen en $90 \text{ GeV}/c^2$ voor het Z boson. Daarom moest men bij de theoretische beschrijving van de processen bij 60 GeV de laagste-ordetermen ten gevolge van de zwakke interactie in rekening brengen.

In 1989 kon men SLC (Stanford Linear Collider te Stanford, Verenigde Staten) en LEP (Large Electron Positron collider te Genève, Zwitserland) in gebruik nemen. Beide machines kunnen e^+e^- -botsingen produceren bij energieën rond 90 GeV. Alhoewel dit ten opzichte van 60 GeV op het eerste gezicht geen grote stap voorwaarts lijkt, betekende dit toch dat er een fundamenteel nieuwe situatie ontstond. Voor het eerst in de e^+e^- -fysica was er nu een situatie waarbij voor sommige processen niet de quantumelectrodynamica, maar de zwakke kracht dominant was. Het dominante proces is, om precies te zijn, dat proces waarbij het electron en het positron annihileren en een Z-boson vormen. Dit annihilatie-proces is resonant bij een energie die overeenkomt met de massa van de Z, rond de 90 GeV. Het Z-boson is echter een instabiel deeltje en vervalt dus vrijwel meteen. Niettemin kan men, door de vervalproducten waar te nemen, de eigenschappen van het Z-deeltje nauwkeurig bestuderen. Met name met LEP heeft men dan ook al precieze bepalingen gedaan van de massa en de vervalbreedte van de Z. Deze tak van onderzoek heeft, om duidelijke redenen, de naam Z-fysica gekregen.

Ook voor de theoretische beschrijving van deze experimenten was een nieuwe situatie ontstaan. Om met de theoretische voorspellingen de nauwkeurigheid van de experimenten

op zijn minst te evenaren, moesten er drie berekeningen gedaan worden.

Ten eerste moesten de eerste-ordecorrecties ten gevolge van de zwakke interactie berekend worden. Immers, aangezien in laagste orde de zwakke interactie dominant is, kan men niet volstaan met slechts die laagste orde. De 'zwakke correcties' van de eerste orde zijn in de afgelopen jaren door verschillende groepen uitgerekend. Omdat deze bijdragen niet groot bleken te zijn, kon geconcludeerd worden dat zwakke correcties van hogere orde niet uitgerekend hoefden te worden.

Ten tweede moesten de QED-correcties berekend worden. De eerste-ordecorrecties zijn geheel analoog aan de QED-correcties voor processen die in laagste orde door QED beschreven worden. Deze QED-correcties van de eerste orde waren al berekend en konden met enkele wijzigingen worden toegepast op Z -productie en ν -verval. Het bleek echter dat deze correcties voor deze toepassing erg groot zijn: ongeveer -35% . Dit in tegenstelling tot vorige toepassingen, waarbij deze correcties doorgaans minder dan 10% bedroegen. Dit betekende dan ook dat de QED-correcties van hogere orde uitgerekend moesten worden.

Ten derde was de precisie die men bij de experimenten bij LEP dacht te zullen bereiken, en die men in sommige gevallen zelfs al bereikt heeft, hoger dan men tot dan toe gepresteerd had. In het bijzonder is de bepaling van de totale werkzame doorsnede nu al zeer nauwkeurig. Oorzaak hiervan is voornamelijk de hoge statistiek. Er is echter een heikel punt in deze experimentele bepaling: men moet de zogeheten luminositeit van de versneller weten, dat wil zeggen, men moet weten hoeveel e^+ - en e^- -deeltjes men op elkaar heeft afgevuurd. Deze luminositeit is niet op voorhand bekend en wordt daarom experimenteel bepaald door theorie en experiment te vergelijken voor één specifiek proces. Men neemt hiervoor altijd $e^+e^- \rightarrow e^+e^-$, ook wel Bhabha-verstrooiing genoemd, en wel bij kleine verstrooiingshoeken. De twee belangrijkste redenen om Bhabha-verstrooiing te nemen zijn, ten eerste, dat dit proces bij kleine hoeken sterk gedomineerd wordt door de quantumelectrodynamica, en, ten tweede, dat de werkzame doorsnede ervan groot is, resulterend in hoge statistiek. Het feit dat de experimenten bij LEP de totale werkzame doorsnede meten met een onnauwkeurigheid die kleiner is dan 1% , houdt in dat voor de theoretische beschrijving, die even nauwkeurig moet zijn, de QED-correcties van de tweede orde nodig zijn. Ook voor Bhabha-verstrooiing was dus een verbetering van de bestaande theoretische beschrijving nodig.

Kortom, de QED-correcties van hogere orde moesten uitgerekend worden, zowel voor Z -productie als voor Bhabha-verstrooiing.

In de afgelopen jaren hebben veel groepen gewerkt aan de berekening van hogere-orde-QED-correcties voor Z -productie en Bhabha-verstrooiing. In dit proefschrift wordt verslag gedaan van een van de bijdragen op dit gebied. De inhoud valt ruwweg te verdelen in twee delen die van elkaar verschillen in de manier waarop de QED-correcties worden uitgerekend. In het ene deel, hoofdstuk 2 tot en met 5, wordt de zogeheten semi-analytische methode gebruikt. Hier worden zo veel mogelijk integraties analytisch uitgewerkt en wordt alleen voor de laatste integratiestap of -stappen de numerieke uitweg gezocht. In het andere

deel, hoofdstuk 6 en 7, worden Monte Carlo-technieken toegepast. Dat wil zeggen, hier worden alle integraties van begin tot eind numeriek gedaan.

De inhoud van de hoofdstukken is als volgt. Na de inleiding (hoofdstuk 1) worden in hoofdstuk 2 op semi-analytische wijze de processen $e^+e^- \rightarrow ff$ behandeld, onder uitsluiting van $f = e^-, \nu_e$. Dit zijn de 'typische LEP-processen', gedomineerd door de zwakke interactie. In hoofdstuk 3 wordt het geval $f = e^-$, Bhabha-verstrooiing, behandeld, eveneens semi-analytisch. Dit gebeurt door te eisen dat zowel e^+ als e^- over grote hoeken verstrooien, waardoor ook dit proces nog gedomineerd wordt door de zwakke interactie. De mogelijkheden om dergelijke sneden op de verstrooiingshoeken op te leggen worden in hoofdstuk 4 uitgebreid, waarmee dan het verschil tussen voorwaartse en achterwaartse verstrooiing semi-analytisch kan worden uitgerekend. In hoofdstuk 5 worden deze technieken wederom toegepast, nu op Bhabha-verstrooiing bij lage hoeken. Hier wordt ook een afweging gemaakt van het belang van een groot aantal correcties van verschillende herkomst.

Hoofdstuk 6 behandelt opnieuw de gevallen $f \neq e^-, \nu_e$, maar nu met behulp van Monte Carlo-technieken. De resultaten hiervan voor de totale werkzame doorsnede kunnen vergeleken worden met die van hoofdstuk 2. Ten slotte wordt in hoofdstuk 7 een overzicht gegeven van de belangrijkste implementaties van Monte Carlo-technieken, zoals deze zijn toegepast voor $f \neq e^-, \nu_e$. De voor- en nadelen van ieder van deze methodes worden behandeld.

Curriculum vitae

Na het behalen van het diploma gymnasium- β aan het Barlaeus-gymnasium te Amsterdam, begon ik aan mijn studie natuurkunde aan de Rijksuniversiteit Leiden. Het prope-
deutisch examen natuurkunde heb ik in augustus 1983 afgelegd. Gedurende de experi-
mentele stage heb ik gewerkt in de groep Magnetische Resonantie en Relaxatie o.l.v.
prof.dr. W.Th. Wenckebach. In de zomer van 1986 was ik zomerstudent bij CERN
te Genève, Zwitserland. In maart 1987 volgde het doctoraal examen in de theoretische
natuurkunde. Het doctoraal onderzoek heb ik verricht o.l.v. prof.dr. F.A. Berends aan het
onderwerp "Niet-lineaire representaties van de Poincaré-algebra." Direct na het doctoraal
examen begon ik aan mijn promotie-onderzoek, eveneens o.l.v. prof.dr. F.A. Berends. In
het kader van dit onderzoek werden reizen gemaakt naar Chapel Hill (Verenigde Staten),
Genève (Zwitserland, 2x) en Brighton (Engeland). In september 1987 nam ik deel aan
de Herbstschule te Maria Laach (Duitsland) en in augustus 1990 aan de zomerschool te
Cargèse (Corsica).

In de nabije toekomst hoop ik mijn militaire dienstplicht te vervullen bij de Koninklijke
Marine, gedetacheerd bij het Fysisch en Elektronisch Laboratorium TNO te Den Haag.

List of publications

1. T. Matsuura, S.C. van der Marck and W.L. van Neerven, The calculation of the second order soft and virtual contributions to the Drell-Yan cross section, Phys. Lett. B211 (1988) 171.
2. T. Matsuura, S.C. van der Marck and W.L. van Neerven, The order α_s^2 Drell-Yan K-factor, Nucl. Phys. B (Proc. Suppl.) 7B (1989) 80.
3. T. Matsuura, S.C. van der Marck and W.L. van Neerven, The calculation of the second order soft and virtual contributions to the Drell-Yan cross section, Nucl. Phys. B319 (1989) 570.
4. F.A. Berends et al., Z line shape, in: Z physics at LEP 1, CERN 89-08, vol.1, p.89, eds. G. Altarelli, R. Kleiss and C. Verzegnassi.
5. R. Kleiss et al., Monte Carlos for electroweak physics, in: Z physics at LEP 1, CERN 89-08, vol.3, p.1, eds. G. Altarelli, R. Kleiss and C. Verzegnassi.
6. W. Beenakker, F.A. Berends and S.C. van der Marck, Rules of thumb for the Z line shape, Z. f. Phys. C46 (1990) 687.
7. R. Kleiss and S.C. van der Marck, Two photon bremsstrahlung, Nucl. Phys. B342 (1990) 61.
8. W. Beenakker, F.A. Berends and S.C. van der Marck, Higher order corrections to the forward backward asymmetry, Phys. Lett. B251 (1990) 299.
9. W. Beenakker, F.A. Berends and S.C. van der Marck, Large angle Bhabha scattering, Nucl. Phys. B349 (1991) 323.
10. W. Beenakker, F.A. Berends and S.C. van der Marck, Small angle Bhabha scattering, to be published in Nucl. Phys. B.

STELLINGEN

1. De kwestie van vrijwillige euthanasie toont aan dat de parlementaire democratie in Nederland niet optimaal functioneert.

Opinieonderzoek Lagendijk in opdracht van de NVVE, 1980

Enquête Lagendijk in opdracht van de AVRO, 1984

Enquête Intomart in opdracht van de KRO, 1985

Enquête NIPO in opdracht van de AVRO, 1986

Opinieonderzoek Intomart in opdracht van de NVVE, 1988

2. De door Bengtsson et al. afgeleide interactie tussen drie massaloze bosonen met willekeurige maar gelijke spin, kan niet alleen uitgebreid worden naar interacties tussen drie massaloze bosonen met alle drie verschillende spin, maar ook naar interacties tussen twee massaloze fermionen en een massalooz boson met alle drie verschillende spin. De vorm van de interactie-term in de lagrangiaan is in de lichtkegel-ijk

$$\mathcal{L} = \sum_{n=0}^{s_2+s_3-s_1} (-1)^n \binom{s_2+s_3-s_1}{n} \bar{\varphi}_1 \times (\partial_+)^{s_1} \left[\frac{\bar{\partial}^n}{\partial_+^{(n+s_1-s_3+1/2)}} \varphi_2 \frac{\bar{\partial}^{(s_2+s_3-s_1-n)}}{\partial_+^{(s_3+1/2-n)}} \varphi_3 \right] + c.c.$$

Hierin zijn φ_i de velden corresponderend met de deeltjes met spin s_i . De bovenstaande vorm geldt wanneer s_2 en s_3 halftallig zijn en s_1 heeltallig, waarbij $s_1 \leq s_{2,3}$. De vorm voor het geval waar het boson niet de laagste spin heeft kan hieruit verkregen worden door middel van de substitutie $s_{1,2} \rightarrow s_{1,2} - \frac{1}{2}$. Het boson heeft dan het label 2, terwijl nog steeds moet gelden $s_1 \leq s_{2,3}$. De massadimensie van de koppelingsconstante die met deze interacties geassocieerd kan worden is $-(s_2 + s_3 - s_1 - 1)$.

A.K.H. Bengtsson, I. Bengtsson en L. Brink, Nucl.Phys. B227 (1983) 31

A.K.H. Bengtsson, I. Bengtsson en N. Linden, Class.Qu.Grav. 4 (1987) 1333

3. De manier waarop door Jegerlehner de hadronische vacuümpolarisatie is geprogrammeerd als dispersie-integraal over de hadronische werkzame doorsnede in e^+e^- -botsingen is onzinnig, aangezien voorbij wordt gegaan aan de statistische fluctuatie van de metingen.

H. Burkhardt et al., Z.f.Phys. C43 (1989) 497

4. Stel, men doorloopt op willekeurige wijze een rij van N verschillende getallen, totdat men een getal tegenkomt dat al eerder was voorgekomen. Het p -de moment van de kansverdeling om l stappen te hebben gemaakt is, voor grote N

$$\langle l^p \rangle = N^{\frac{1}{2}p} p!! \begin{cases} \sqrt{\frac{\pi}{2}} & , \quad p \text{ oneven,} \\ 1 & , \quad p \text{ even.} \end{cases}$$

Voor $p = 1, 2$ levert dit het bekende resultaat op dat de gemiddelde lengte van zo'n wandeling $\sqrt{\frac{\pi}{2}N}$ is, met een standaarddeviatie van $\sqrt{(2 - \frac{\pi}{2})N}$.

5. Door Bengtsson et al. wordt in *Class.Qu.Grav.* 4 (1987) 1333 een foutieve definitie van het begrip veldherdefinitie gehanteerd. Dit leidt ertoe dat bepaalde niet-triviale interacties door hen niet beschreven kunnen worden.
6. In het computerprogramma VEGAS worden verschillende Monte Carlo-schatters voor dezelfde grootheid gecombineerd tot een 'cumulatieve' schatter voor die grootheid. De schatter voor de standaarddeviatie behorende bij deze cumulatieve schatter, wordt door VEGAS niet correct berekend.

G.P. Lepage, J.Comp.Phys. 27 (1978) 192

7. Wanneer men de belangrijkste logaritmische bijdragen van fermionpaar-remstraling van de begintoestand meeneemt in de berekening van de resonantiecurve van het Z-boson, dan geeft dit een extra bijdrage aan de zogeheten schijnbare breedte van het Z-boson van

$$\Delta\Gamma_Z = \frac{1}{24} \left(\frac{\pi}{2} + \log 2 \right) \left[\frac{2\alpha}{\pi} \left(\log \frac{M_Z^2}{m_e^2} - 1 \right) \right]^2 \Gamma_Z .$$

Hierin zijn M_Z en Γ_Z de massa en de breedte van het Z-boson en is m_e de massa van het electron. De numerieke bijdrage van $\Delta\Gamma_Z$ is ongeveer 2 à 3 MeV.

V. Gribov en L. Lipatov, Sov.J.Nucl.Phys. 15 (1972) 438 en 675
Dit proefschrift, hoofdstuk 2

8. Beschouw de QED-correcties op de werkzame doorsnede van een proces waarin de massa's van de inkomende en uitgaande deeltjes klein zijn en dat kan plaatsvinden via uitwisseling van een (vrijwel) massaloos deeltje in het zogeheten t-kanaal. De '1-deeltjes inclusieve berekening' hiervan zal in het algemeen deze correcties zwaar overschatten (naar de positieve kant).

Dit proefschrift, hoofdstuk 3

9. Beschouw de totale werkzame doorsnede voor $e^+e^- \rightarrow e^+e^-\bar{f}f$. Wanneer zowel het e^+ als het e^- onder kleine hoeken verstrooien, vormt dit proces een achtergrond voor het proces waarbij alleen een $\bar{f}f$ -paar gecreëerd wordt. Als we nu bovendien eisen dat zowel f als \bar{f} verstrooien over hoeken tussen ϑ_{min} en $\pi-\vartheta_{min}$, is de totale werkzame doorsnede voor $e^+e^- \rightarrow e^+e^-\bar{f}f$ in grove benadering gegeven door

$$\sigma = \frac{2\alpha^4 Q_f^4}{\pi s'_{min}} \frac{1}{s'_{min}} \left[\log^2 \eta + 2 \log \frac{4\eta}{(1+\eta)^2} \right] \log^2 \frac{\frac{1}{2}s(1-c_m)}{m_e^2}.$$

Hierin is $c_m = \cos \vartheta_{min}$, $\eta = (1-c_m)/(1+c_m)$, s'_{min} de ondergrens op de invariante massa van het $\bar{f}f$ -paar, m_e de massa van het electron en s het kwadraat van de totale energie in het massamiddelpuntssysteem. Voor het bovenstaande resultaat is aangenomen dat $s'_{min}/s \leq \eta$ en dat $s'_{min} \ll s$. Verder is de massa van f en \bar{f} verwaarloosd. De generalisatie naar een asymmetrisch hoekbereik is eenvoudig.

10. Wanneer bij de QED-correcties van de eerste orde voor een grootheid de zacht-fotoncorrecties niet dominant zijn, is er geen reden om aan te nemen dat het exponentiëren van de zacht-fotoncorrecties tot een beter resultaat leidt dan het eerste-orderresultaat.

11. Door Ruijgrok en Cohen zijn de gesloten banen op een rooster met spiegels niet correct geteld.

Th.W. Ruijgrok en E.G.D. Cohen, Phys. Lett. A133 (1988) 415

12. De methode van hoofdstuk 3 en 4 van dit proefschrift kan generaliseerd worden, zodat ook productie van massieve deeltjes beschreven kan worden. De vergelijkingen (3.2.18) en (3.3.9) blijven ongewijzigd geldig, wanneer men $t_1 = (p_1 - p_3)^2 - m_f^2$ en analoog voor t_2 , u_1 en u_2 definieert. Hierin is m_f de massa van de deeltjes in de eindtoestand. Wanneer men de notaties

$$T(c) = \frac{-x_1^2 x_2 s}{(x_1 + x_2)^2 - c^2(x_1 - x_2)^2} \left[x_1 + x_2 + c^2(x_2 - x_1) - 2x_2 c R(c) \right],$$

$$R(c) = \left\{ 1 - \frac{m_f^2}{x_1^2 x_2^2 s} \left[(x_1 + x_2)^2 - c^2(x_1 - x_2)^2 \right] \right\}^{\frac{1}{2}},$$

$$x_0(x, c) = \frac{x m_f}{x^2 s - m_f^2(1 - c^2)} \left[m_f(1 + c^2) + \sqrt{x^2 s(1 - c^2) + 4m_f^2 c^2} \right]$$

introduceert, worden de grenzen op de integratie-variabele \hat{t}_1 , ten gevolge van de hoeksnedes, verkregen door de integrand te vermenigvuldigen met de factor

$$\begin{aligned}
& \vartheta(x_2 - x_0(x_1, 0)) \vartheta(\hat{t}_1 - T(c_{m+})) \vartheta(-\hat{t}_1 + T(c_{M+})) \\
& + \left[\vartheta(c_{M+}) \vartheta(x_1 - x_2) \vartheta(x_2 - x_0(x_1, c_{M+})) \vartheta(-x_2 + x_0(x_1, 0)) \right. \\
& \quad \times \vartheta(\hat{t}_1 - T(-c_{M+})) \vartheta(-\hat{t}_1 + T(c_{M+})) \\
& \quad - \vartheta(-c_{M+}) \vartheta(x_2 - x_1) \vartheta(x_1 - x_0(x_2, -c_{M+})) \vartheta(-x_1 + x_0(x_2, 0)) \\
& \quad \times \vartheta(\hat{t}_1 - T(c_{M+})) \vartheta(-\hat{t}_1 + T(-c_{M+})) \\
& \quad \left. - \left\{ c_{M+} \rightarrow c_{m+} \right\} \right].
\end{aligned}$$

en analoog voor c_{M-} , c_{m-} , met $x_1 \leftrightarrow x_2$. De grenzen op \hat{t}_1 ten gevolge van de energie-sneden blijven ongewijzigd. Voor $m_f \rightarrow 0$ blijft alleen de eerste regel over en reduceert deze regel tot het resultaat (4.9). Door op geschikte wijze de hoeksnedes te combineren kan uit het bovenstaande, voor een willekeurige massa m_f , de differentiële werkzame doorsnede $d\sigma/dc$ afgeleid worden. Het resultaat voor $d\sigma/dc$ is in overeenstemming met dat van W. Beenakker et al. in Proc. Workshop on electroweak radiative corrections, Ringberg (1989), ed. J.H. Kühn.

S.C. van der Marck, april 1991